Spectroscopic Studies of Rare Earth Ions Doped Lithium Bismuth Alumino Borosilicate Glasses for Photonic Applications

THESIS

Submitted to

Delhi Technological University

in partial fulfillment of the requirements for the degree of

DOCTOR OF PHILOSOPHY

in

APPLIED PHYSICS

Submitted By

MOHIT KUMAR

Reg.Number:2K17/PHDAP/11

Under the Supervision of

Prof. A.S. Rao

Department of Applied Physics
Delhi Technological University
Delhi -110042

May, 2023

Dedicated

To

My Grandfather

DELHI TECHNOLOGICAL UNIVERSITY
Formerly Delhi College of Engineering
(Under Delhi Act 6 of 2009, Govt. of NCT of Delhi)
Shahbad Daulatpur, Bawana Road, Delhi-110042

CERTIFICATE

This is to certify that the thesis titled *"**Spectroscopic Studies of Rare Earth Ions Doped Lithium Bismuth Alumino Borosilicate Glasses for Photonic Applications**"* is being submitted by ***Mr. Mohit Kumar*** with registration number ***2K17/PHDAP/11*** to the Delhi Technological University for the award of the degree of Doctor of Philosophy in Applied Physics. The work embodied in this thesis is a record of bonafide research work carried out by me in the Department of Applied Physics, Delhi Technological University (Formerly Delhi College of Engineering), New Delhi under the guidance of ***Prof. A. S. Rao***. It is further certified that this work is original and has not been submitted in part or fully to any other University or Institute for the award of any degree or diploma.

Mohit Kumar
Research Scholar
Roll No. 2K17/PHDAP/11

This is to certify that the above statement made by the candidate is correct to the best of our knowledge.

Prof. A.S. Rao
Supervisor
Department of Applied Physics
Delhi Technological University
Delhi, India

Prof. A.S. Rao
Head,
Department of Applied Physics
Delhi Technological University
Delhi, India

Acknowledgements

I feel highly grateful to acknowledge all those who have made their contributions and helped me directly or indirectly with the completion of my thesis work. First and foremost, I must acknowledge and express thanks to the ***Almighty****, for his blessing, throughout my life.*

At the outset, I would like to my profound sense of thankfulness, indebtedness and respect to my supervisor, ***Prof. A. S. Rao****, Head, Department of Applied Physics, Delhi Technological University, Delhi who cultivated my research capabilities for a successful scientific career. It has been an honor to work under an excellent, enthusiastic and eminent supervisor. I am grateful for all his contributions of time, suggestions, constructive criticism and facilities to make my PhD experience productive and stimulating His immense knowledge of the subject, analytic gaze, farsightedness and perseverance were a constant source of motivation during this thesis work and writing of this thesis.*

I am deeply grateful to ***Prof. S.C. Sharma****, former HOD, Department of Applied Physics, DTU, for his constant blessings and suggestions throughout this degree. I wish to thank the* ***Prof. Rinku Sharma, Dean Academic (PG)*** *for always being a pillar of support during my pursuit of the Ph.D. degree. I express my sincere gratitude especially to* ***Prof. G. Vijaya Prakash****, Indian Institute of Technology (IIT) Delhi, and* ***Dr. M. Jayasimhadri*** *DTU for their timely advice and experimental support as SRC members. I should not forget to acknowledge all the faculty members of the Department of Applied Physics for their continuous encouragement and help during my research work.*

I sincerely thank my seniors ***Dr. Nisha Deopa****,* ***Dr. Sumandeep Kaur****,* ***Dr. Ritu Sharma****,* ***Dr. Kanika****,* ***Dr. Arti****,* ***Dr. Amit Vishwakarma****,* ***Dr. Kaushal Jha****,* ***Dr. Aman Prasad, Dr. Harpreet Kaur, Dr. Yasha Tayal*** *and fellow research scholars,* ***Mr. Rajat Bajaj****,* ***Mrs. Kartika, Dr. Ravita Pilania****,* ***Ms. Pooja Rohilla****,* ***Ms. Anu****,* ***Ms Sheetal, Ms. Deepali, Mr. Indrajeet Maurya****,* ***Mr. Videsh, Mrs. Vertika*** *for their*

valuable suggestions and support during my PhD. I am especially thankful to my dear friends and fellow researchers ***Dr. Mukesh K. Sahu*** *and* ***Mr. Vikas Sangwan*** *for their help during my entire research tenure. I wish to acknowledge the enjoyable company and suitable help rendered by my dear friends,* ***Dr. S. Shankar Dr. Prateek, and Dr. Vijay Meena****, for their help and support during this tenure.*

Finally, I thank my joint family and teachers for their support and motivation, every moment of my research period. I thank my grandfather ***Late Bharat Singh Tyagi*** *for his guidance and blessing in my life. I am very grateful to my parents* ***Mr. Bresh Chand Tyagi*** *and* ***Mrs. Munni Devi*** *Uncle* ***Mr. Umesh Tyagi, Late Adesh Tyagi*** *and* ***Mr. Yogesh Tyagi,*** *Aunty* ***Mrs. Bala Devi, Mrs. Amrita Devi*** *and* ***Mrs. Manju Devi****, sisters and brothers who have always been my pillars of strength and they enabled me to maintain a positive attitude throughout my studies. I am thankful to my sweet wife* ***Nidhi Tyagi*** *for her endless support and continuous encouragement. My heartfelt acknowledgement to my loving children* ***Vamika*** *and* ***Varnit*** *who always make me smile before going to work.*

This endeavor would not have been a success without the persistent support and encouragement of my dearest friends ***Dr. Kulveer Singh, Deepak Choudhary, Dr. Manish, Dr. Anuj Panwar, Dr. Ajay Panwar, Dr. Ashish, Sunil, Dr. Pawan Tyagi, Ajay Gochar, Dr. Teerthraj, Dr. Ranjeet, Dr. Saurabh Raut and Dr. Anakj.***

I extend my gratitude to Delhi Technological University, Department of Applied Physics and staff in Administration, Accounts, Store & Purchase, Library and Computer Centre for all the necessary facilities help and services.

Finally, I wish to thank one and all for their timely interference in my life making it happier and more meaningful.

Thank you all!!!

Mohit Kumar

2K17/PHDAP/11

List of publications

1. **Mohit Kumar** and A.S. Rao. "Concentration-dependent reddish-orange photoluminescence studies of Sm^{3+} ions in borosilicate glasses."
   Optical Materials 109 (2020): 110356 **(Impact factor = 3.9)**

2. **Mohit Kumar** and A.S. Rao. "Influence of Tb^{3+} ions concentration and temperature on lithium bismuth alumino borosilicate glasses for green photonic device applications."
   Optical Materials 120 (2021): 111439 **(Impact factor = 3.9).**

3. **Mohit Kumar,** A.S. Rao and Sumandeep Kaur. "Downshifting analysis of Sm^{3+}/Eu^{3+} co-doped LiBiAlBSi glasses for red emission element for white LEDs."
   Chemical Physics Letters 788 (2022) 139303 **(Impact factor = 2.8).**

4. **Mohit Kumar,** Mukesh K. Sahu, Sumandeep Kaur, Aman Prasad, Rajat Bajaj, Rupesh A. Talewar, Yasha Tayal and A.S. Rao. "Visible and NIR spectral analysis of Er^{3+} doped LiBiAlBSi glasses for laser applications."
   Laser Physics (2023) (communicated) **(Impact factor = 1.6).**

Abstract

Lithium bismuth alumino borosilicate (LiBiAlBSi) glasses were successfully prepared by melt quenching procedure using single and codoped RE ions such as samarium (Sm^{3+}), terbium (Tb^{3+}), europium (Eu^{3+}) and erbium (Er^{3+}). The structural, physical, absorption, photoluminescence (PL), decay spectral profiles and time-dependent PL studies of the prepared glasses have been performed to understand the suitability of these glasses for various photonic applications. The XRD and FT-IR studies are used for structural characterization. XRD patterns were recorded for un-doped and RE-doped glasses and all showed non-appearance of intense sharp peaks which confirms the amorphous nature of our glasses. FT-IR spectrum identified the different functional groups in the un-doped glass. For physical characterization, the density and refractive index of the as-prepared glass have been measured using well-known methods. Various other physical quantities such as dielectric constant, reflection losses, molar refraction, polaron radius, dielectric constant and electronic polarizability were assessed using density and refractive index by the recognized methods available in the literature.

From the absorption spectra, the energies of the absorption bands termed oscillator strengths were measured to evaluate the Judd-Ofelt (J-O) parameters using the least square fitting procedure. The J-O parameters and emission spectra were used for finding numerous radiative parameters such as emission cross-section, transition probability, radiative lifetimes, total transition probability, branching ratios, gain bandwidths and optical gain for the noticeable transitions of the RE^{3+} doped LiBiAlBSi glasses. A Time-dependent PL study showed our glass system has good thermal stability. The aforesaid parameters are very much vital for various photonic applications such as solid-state lasers, white LEDs in solid-state lighting, PV cells and fiber amplifiers. The emission spectra of co-doped Sm^{3+}/Eu^{3+} LiBiAlBSi glasses obtained the down-conversion ability of the n-UV and blue wavelength photons and ET process found from Sm^{3+} ions to Eu^{3+} ions in our glass system. The quantum efficiency of the obtained glasses was evaluated by correlating experimental decay times with radiative lifetimes. Moreover, CIE chromaticity coordinates were assessed to understand the appropriateness of prepared glasses for several visible emission applications.

List of Figures

List of Tables

Table of Contents

CHAPTER 1

General Introduction

Rare-earth doped glasses have attracted researchers across the globe as they possess applications in diversified fields such as solid-state lasers, lighting, flat-panel displays, optical fiber, light-emitting diodes (LEDs), solar cells, and optical fiber amplifiers. This chapter provides the basic details of the spectroscopy of RE-doped materials, different types of glasses, components involved in the glass formation, and their specific important properties. A brief description of the rare earth elements with their importance has been provided. This chapter also explains different types of luminescence with a main focus on photoluminescence and energy transfer properties. Furthermore, the properties of "Lithium Bismuth Alumino Borosilicate (LiBiAlBSi)" glass doped with RE ions have been discussed in this chapter. The significance and motivation of selecting LiBiAlBSi glass as a host system and the objectives of the present work are highlighted.

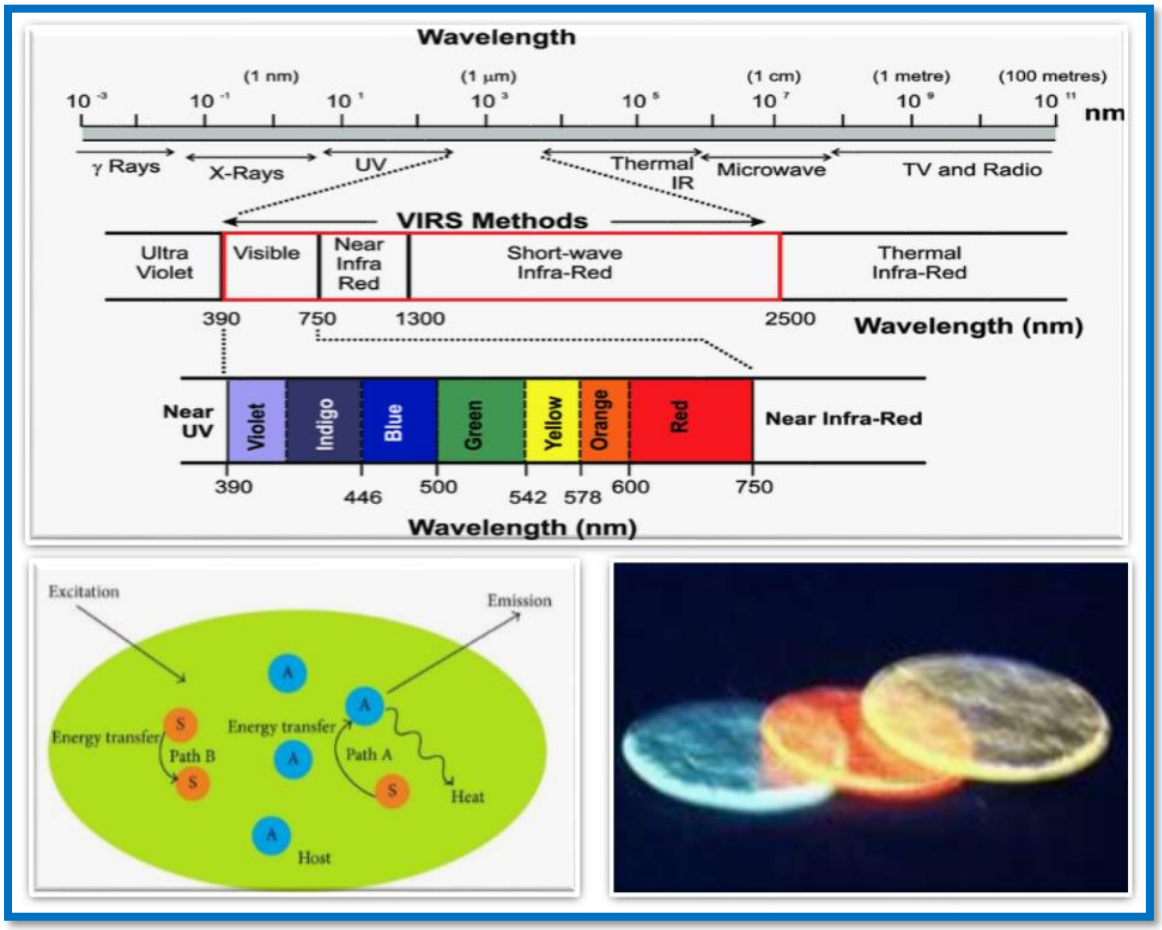

1.1. Introduction

Spectroscopy is a branch of physics which is concerned with the measurement and investigation of the spectra produced when electromagnetic (EM) radiation interacts with a substance. The EM radiation spectrum covers a wide wavelength range from gamma rays to radio waves. The definite interaction of the matter and the EM radiation is used to characterize the matter on various levels, such as molecular, atomic and nuclear scales [1,2]. Most of the information the about the atoms & molecules and the environment around them are investigated by spectroscopy. The spectroscopic study is very valuable and widely used for qualitative and quantitative analysis [3,4]. Optical spectroscopy, an experimental subject is a significant tool in the field of physics, material science and chemistry. Optical spectroscopy is based on the excitation of the valence electron in a wavelength range of 200-3000 nm and deals with the absorption, reflection, emission and scattering after the interaction of suitable UV (ultraviolet), VIS (visible) and near-infrared (IR) radiation with matter. Many lanthanide elements have been discovered by optical spectroscopy. In absorption spectroscopy, the molecules or atoms are excited from the lower energy state to a higher energy state whereas in emission spectroscopy higher energy level to lower energy level transitions take place and energy is emitted in the form of photons [2,5,6].

Over the last few decades, researchers working in material science had shown great interest in the studies of luminescent properties of crystalline as well as amorphous materials doped with transition metals (TM) or rare-earth (RE) elements due to their potential application in various fields such as chemistry, biology, physics, agriculture, optical communication, defence, geology, forensic, medicine, agriculture etc. A luminescent material has the property to convert certain types of energy into the UV, VIS and IR spectral regions. Recent growth and forthcoming scenarios illustrate that luminescent materials have a lot of potential from a technical point of view as well as a scientific [2,7–12].

In recent years, worldwide researchers have conducted extensive studies on materials doped with RE elements as activators as their emission covers a wide spectral range from IR to UV spectral regions. RE doped materials as luminescent materials have various photonic applications such as solid-state lighting (SSL), modern display devices, optical fibre amplifiers, solid-state lasers, waveguides, scintillators, photovoltaic (PV) cells, optical converters, optical information processing and sensors. Photonics supports the technology of day-to-day life from

lighting technology to smartphones to laptops to the internet to security and entertainment [8,13–15].

1.2. Scope of the present work

Over the few decades, RE-doped materials are enhancing technological developments and inventions for diversified applications of photonics such as white light-emitting diodes (w-LEDs), solid-state lasers (SSL), flat-panel displays, optical fibre amplifiers and solar cells as shown in Fig 1.1. Particularly, glasses doped with RE ions have fascinating properties such as good thermal stability, acceptance for relatively high RE ion doping capacity, broad inhomogeneous bandwidths, good thermal stability, low production cost, and easy manufacturing procedure [5,14–21].

Fig. 1.1. Some applications of RE-doped glasses.

It is well known that crystals have good optical properties but are hard to synthesize and not easily to made into the required shape. On the other hand, glasses are inexpensive and easy to synthesize in to a required shape for photonic device applications. For photonic applications, glasses should be optically transparent, electrically resistive, mechanically strong, chemically inactive and thermally non-conductive [5,13–16,21]. To find out glass hosts with these features, researchers are putting their efforts with several chemical compositions. Ideal glasses

should have relatively low phonon energy for doping with RE ions. Relatively less phonon energy of a glass can reduces non-radiative relaxations and increase the radiative emissions and thereby quantum efficiency. Such relatively less phonon energies of glass systems are quite suitable for various photonic device applications [22,23]. The objective of the present research work is to prepare host glass having relatively less phonon energy for better luminescence when doped with certain RE ions for a wide range of photonic applications. Among numerous host glass matrixes, a suitable mixture of borate (B_2O_3) and silicate (SiO_2) forms a network of borosilicate glass with vital beneficial features such as good mechanical strength, high thermal stability, lower melting and resistance to corrosion. These beneficial features have sustained the appropriateness and usefulness of borosilicate glass systems for numerous applications in the field of photonics. Borosilicate glasses have relatively high phonon energy due to the stretching vibration of network-forming oxides which is the cause of non-radiative losses [21,24,25]. Such relatively high phonon energies can be efficiently reduced by adding heavy metal oxides (HMOs) into the glass host matrix. For this purpose, investigators generally choose to add HMOs like lead oxides (PbO) and bismuth trioxide (Bi_2O_3) to the host glass having relatively high phonon energies. HMOs have high atomic numbers and density which make the glass helpful to act as shielding material from radioactive radiation [8,26–28]. The Borosilicate glasses network can be modified by adding a low concentration of PbO due to its lead structural unit [PbO_4]. At relatively higher concentrations PbO also works as a glass former. Therefore, lead oxides play a dual role such as glass former and an improviser useful in improving the radiative properties of the host glass in which it is added. But hazardous effects of lead on the environment and health produce several issues [27, 29]. Bi_2O_3 plays an important role in glass hosts similar to that of PbO because of their similar electronic structure. Glasses with Bi_2O_3 have several useful properties such as a large dielectric constant, higher infrared transparency, high density and a large index of refraction. The host materials containing bismuth are important in the luminescence process as they possess relatively high refractive index. It is well known that the spontaneous emission transition probability increases with the refractive index. Bi_2O_3 cannot perform as the network former stand-alone because Bi^{3+} ions have small field strength. However, with the existence of B_2O_3 in borosilicate glasses, Bi_2O_3 may perform as a glass former. Bismuth-containing glasses are also appropriate for radiation shielding because of their high atomic number [30–33]. The addition of aluminium trioxide (Al_2O_3) to the borosilicate glass network improves the emission properties of this glass host due to Al^{3+} ions structural units present in Al_2O_3 as tetrahedral and octahedral. Moreover,

in a glass host matrix, Al_2O_3 can play the role of a network modifier which helps to enhance the thermo-mechanical and chemical stability of the host matrix [21, 34]. Lithium oxide (Li_2O) added to a glass network can increase the transition temperature and reduce the thermal expansion coefficient. Also, Li_2O can enhance the stability of the glass host matrix by removing air bubbles by producing moisture resistance. Li_2O can act as a network modifier and interrupt the B–O–B and Si–O–Si linkages which produce non-bridging oxygen's (NBOs) along with coordinated defects in the borosilicate glass system. The different structural units are produced due to the formation of NBOs which change the structural and optical features of the glass host matrix [23,35,36]. All the aforesaid scientific patronages offered by the chemicals such as Bi_2O_3, B_2O_3, Al_2O_3, SiO_2, and Li_2O encouraged us to synthesize a host glass with the following chemical composition (in mol%).

$$20Li_2O + 7.5Bi_2O_3 + 7.5Al_2O_3 + 45H_3BO_3 + 20Si_2O_3$$

As per the chemical elements present in the composition mentioned above, the glass system is prepared properly and titled as "Lithium Bismuth Alumino Borosilicate (LiBiAlBSi)" glass. The as-prepared LiBiAlBSi glass doped with different RE ions has been characterized via various spectroscopic tools to understand its suitability in various photonic device applications. Scientists working in material science have a special interest in RE elements due to the diverse spectroscopic characteristic features influenced by electrons occurring in 5f and 4d orbitals. This unique feature makes them auspicious candidates in solid-state lighting, laser, optical communication and electronic industries [24,37–41]. The Judd-Ofelt (J-O) theory has been employed in the RE ions doped host glasses to understand the radiative potentiality of the titled glasses [42,43]. The RE ions used for doping in the present thesis work are:

i. Samarium (Sm): Samarium ions (Sm^{3+}) produce strong reddish-orange emission of the visible part of the electromagnetic spectrum as they are capable of absorbing UV light more efficiently and have applications in visible solid-state lasers, lighting devices, communications, display devices high-density data storage devices and remote sensing. These optical properties of Sm^{3+} ions doped glasses are due to its prominent emission transitions $^4G_{5/2} \rightarrow {}^6H_{J= 5/2, 7/2, 9/2 \text{ and } 11/2}$ in all host matrices [13,44–46].

ii. Terbium (Tb): Terbium ions (Tb^{3+}) are most capable of giving strong visible green emissions via its transition $^5D_4 \rightarrow {}^7F_5$. Various applications of Tb^{3+} doped luminescent materials

are in solid-state lasers, w-LEDs, light converters, thermo-luminescent dosimeters and in as green color component in display devices [47–49].

iii. Europium (Eu): Europium has variable valence states Eu^{2+} and Eu^{3+}. Eu^{3+} is stable and has its energy-level pattern with high emission efficiency of the transition $^5D_0 \rightarrow {}^7F_2$. This is the very sensitive transition to minor deviations in the chemical adjoining the Eu^{3+} ions. The Eu^{3+} doped luminescent materials have applications in biomedical engineering and w-LEDs as red component emitters [50–53].

iv. Erbium (Er): Erbium (Er^{3+}) shows useful laser transitions such as

(a) $^4S_{3/2} \rightarrow {}^4I1_{3/2}$ at ≈ 0.8 μm, which used for S-I photo-emissive surfaces

(b). $^4I_{13/2} \rightarrow {}^4I_{15/2}$, at ≈ 1.54 μm which is absorbed by the ocular media of the eye and offers protection for the retina. Also, the 1.6 μm wavelength is extensively used in optical communication applications. Moreover, the studies in different mediums of Up-conversion emission of Er^{3+} ions have been improved due to its visible red and green emissions [54–58].

1.3. Classification of solids

Based on the atomic arrangement, generally solid materials are divided into two basic categories crystalline and amorphous (non-crystalline) which are characterized by the X-ray diffraction (XRD) technique. The crystalline materials show sharp peaks in XRD patterns which indicate a long-range regular arrangement of the atoms in the materials. On the other hand, XRD patterns of amorphous materials give the absence of sharp peaks and show broad humps indicating the short-range order with no regular structural arrangement of the atoms. The molecular arrangements in crystalline (left) and glass (right) are shown in Fig.1.2. The crystalline and amorphous materials show the properties of anisotropy and isotropy respectively. Amorphous materials do not show sharp boiling and melting points. They have a wide range of temperatures for melting. Some examples of crystalline materials are quartz, sugar, calcite etc. and amorphous solids are glass, plastic, rubber etc. [9,34,59,60].

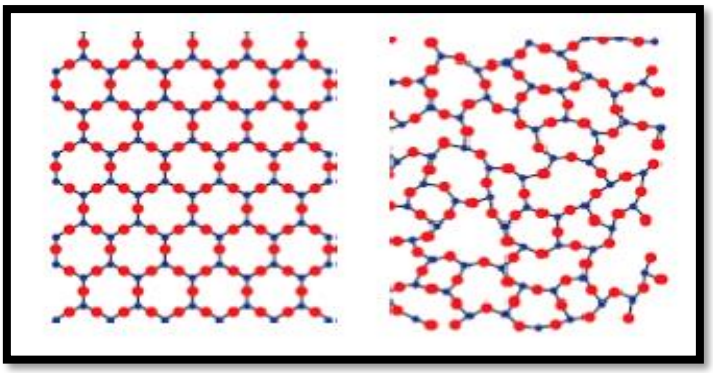

Fig. 1.2. Molecular arrangements in crystalline (left) and glass (right) materials.

1.3.1. Glass: An overview

Glass has an important role in our day-to-day life in the form of water glass, water glass bottles, Television screens, computer & mobile screens, window glass, lighting glass, watch dials, and headlights of vehicles. A glass has lot of scientific uses such as solid-state lasers, LEDs, optical fiber amplifiers, telecommunication, etc. The word, glass has been derived from the Latin word “glaseum” which has the meaning of translucent and shiny. The word "glass" is usually used for a fusion product obtained when an inorganic material is cooled to a solid-state fusion product without crystallizing. Glass is the best example of an amorphous solid-state material which is brittle, hard and usually radiant with different colours. From ancient times, people had used glass without knowing the method of production of glass. They used naturally produced glass, particularly from the volcano (obsidian). Obsidian was used for making arrowheads, knives, money and jewellery. As per archaeological evidence, glass existed in Egypt and eastern Mesopotamia around 3500 BC. In the beginning, glass manufacturing was slow because it was a tedious process [8,18,34,59,61]. With time, the application of glass is explored to vessels, construction, lighting, transportation, chemical and telecommunication industry etc. Innovation in the glass industry with doping of RE & TM elements explore new solutions in the fields of lighting, lasers, energy transformation, optical amplifier, optical fibre communications, medicine and optoelectronics. Some unique properties of glasses which are given below make the glasses important solid-state materials having applications in science and technology [5,8–11,60–64].

1. Glass is a non-crystalline transparent material with the absence of long-range atomic order.
2. Glasses do not show any definite melting point, unlike crystals.
3. Glass is a good thermally and electrically insulator at normal temperatures; while the temperature is upsurging, it converts into conducting nature.

4. Glass has always greater internal energy than the crystalline state of similar composition.
5. Glass show an isotropic nature i.e., physical properties are uniform in all direction of glasses which is very vital and typical for optical applications.
6. The coefficient of thermal expansion of glasses depends on the chemical constitution and is constant in the temperature range 400-600 °C.
7. Glass can be formed by various techniques and becomes softened before melting.
8. Glass materials are less affected by chemicals.
9. The glass viscosity decreases continuously as the temperature increases
10. Glass follows Hook's law firmly until enough stress for fracture.

1.3.2. Glass transition

The glass transformation behaviour is time-dependent as shown by every glass and arises in a range of temperatures called the glass transformation region. Therefore, we can define glass as "an amorphous solid material that has the absence of long-range atomic order and shows a section of the behaviour of glass transformation." Any substance, inorganic, organic, or metallic, prepared by any procedure, which shows the behaviour of glass transformation is called glass. Glass was formed by the procedure which avoids the crystallization development of material in a molten state. Basically, all substances are capable of making amorphous solid materials by rapid cooling. For the formation of glass, the cooling rate is mainly subject to the glass composition. To prepare the amorphous substance, the melt state of the material should be cooled below a certain critical temperature which is called glass-transition temperature. After this point of critical temperature, the material atoms-molecular movement are slow to set down resulting in the formation of amorphous glass. This formed glass is not as ordered as compared to the crystalline materials but is more systematized as compared to the liquid [10,34,65].

The behaviour of glass transition can be described by the thermodynamic quantity that is either volume or enthalpy with temperature variation. To understand this thought, we can imagine a liquid with a small volume at a higher temperature than the melting temperature. As this liquid is cooling, the possibilities of any one of the following phenomena or both may take place:

(a) Change of the substance to the crystalline state with the creation of long-range order and periodic arrangement at the melting point (T_m). If this happens, the enthalpy will decline sharply to the value suitable for the crystalline state.

(b) If the cooling of liquid is less than the melting temperature without crystallization, the obtained liquid is called a supercooled liquid. As the temperature is decreased, the liquid structure continues to reorder, but enthalpy does not show a rapid decrease due to irregular structural reordering. Viscosity increases with further cooling of the liquid. The rise in viscosity finally becomes so high that atoms cannot be able to rearrange themselves to an equilibrium liquid structure during the experiment time. The structure initiates to drop behind and the enthalpy starts to diverge from the line of equilibrium by reducing the slope of the curve such that viscosity rises too high so that the liquid achieves a fixed structure i.e., frozen liquid and becomes temperature-independent. The temperature range occurs between the limits where the enthalpy of the frozen solid and the equilibrium liquid is recognized as the glass transformation region. The frozen liquid is known as glass.

Fig.1.3 denotes the variation curve of temperature and the enthalpy of glass formation. From this diagram, it is clear that the glass transformation cannot be specified by any single point temperature, it is rather happening over a range of temperatures. However, for convenience, a single point temperature is just used as an indication of the glass transformation region during the glass heating which is called the *glass transition temperature (T_g) or glass transformation temperature.* The T_g value is a function of the rate of heating and is used to draw these curves [34,59,60].

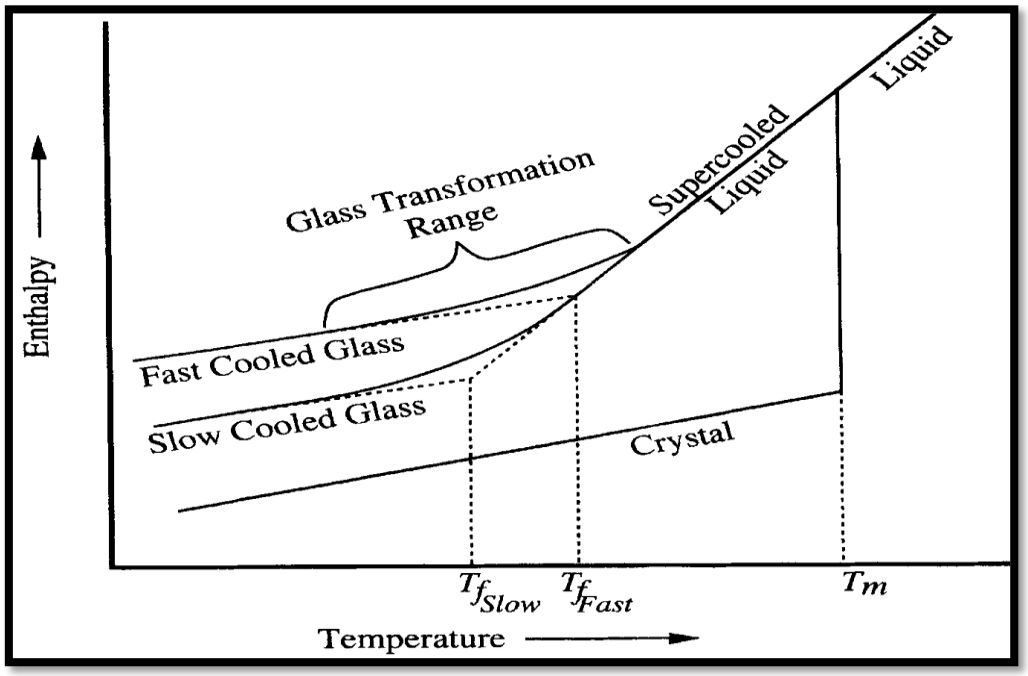

Fig. 1.3. Temperature effect on the enthalpy of a glass-forming melt

1.3.3. Components of glass

Glass components play an important role in the functions and characteristics of glass. The glass shows a random network dislike crystal. Glass components are categorized into three classes such as glass network formers, network modifiers and intermediates having different bond strengths [34,59,66,67].

1.3.3.1. Glass network formers

Oxides work as glass network formers with a single bond strength of more than 334 kJ-mol^{-1} (~ 80 kcal/mol). Some frequently used and important glass formers are SiO_2, B_2O_3, P_2O_5, V_2O_5, As_2O_3, PO_4, GeO_2, Sb_2O_5 etc. These oxides on their own are capable of forming the glass skeleton and the coordination number of cations-oxygen in glass network formers is commonly four.

1.3.3.2. Network modifiers

The oxides which break up the glass network called glass network modifiers have a single bond strength of less than 60 kcal/mol and these oxides are not a part of the glass network former. The glass properties are modified by the network modifiers and alkali oxides usually use glass network modifiers. The oxides Li_2O, K_2O, Na_2O, BaO, ZnO, CaO, MgO, and SrO are examples of a few important network modifiers. The most current applications of glasses, such as a bioactive material, sensor and optoelectronic, laser and lighting devices require a proper selection of a cation-oxide modifier. Therefore, the selection of a modifier is a significant job in the research of a specific type of glass material for particular applications.

1.3.3.3. Intermediates

The oxides, single bond strength values of oxides exist between 60 and 80 kcal/mol are play the role of intermediates. Intermediates exist among the glass formers and the modifiers as a sandwiched. The oxides Al_2O_3, CdO, PbO, BeO and ZnO are some important examples of intermediates. In a glass host system with multi-component, terms such as glass formers, intermediates and modifiers are usually used to define the part of the particular oxides. The glass intermediate oxides may act as network modifiers and the network formers of the glass depend on the composition of the glass host matrix.

1.3.4. Different types of glasses

Glasses are amorphous and hard solids which have structural disorders analogous to liquids, but their mechanical properties are unlike. Commonly, glasses are broadly separated into two classes. The first type of glass is produced by nature so-called natural glasses and the second class is artificial glass made by man.

1.3.4.1. Natural glasses

Natural glasses, for example, obsidians, pumice, pechsteins etc., can be obtained when molten lava is cooled speedily and reaches the surface of the earth's crust. They can also be obtained from the rapid surge in temperature by strong shock waves e.g., tektites. In some rare events, the biological process can also form glass. The energy of the intense heat of meteoritic influences in the Libyan Desert also causes the formation of glassy rock.

1.3.4.2. Artificial glasses

The glasses are formed by artificial methods and have widely extensive classes of materials. Although numerous materials are used to make the glasses, only a few of them are significant for practical purposes. A brief discussion of the different structural features and properties of the few glasses is presented in the subsequent sections.

i. Oxide glasses: Oxide glasses are the much-diversified class and play a significant part amid the inorganic glasses. The key oxide glass formers are silicate (SiO_2), phosphates (P_2O_5), borate (B_2O_3), and germinate (GeO_2). Oxide glasses have feasible optical and photonic utilizations e.g., lasing, lighting and core materials for optical fiber. Oxide glasses have been systematically analyzed and practically applied for a long time.

ii. Chalcogenide glasses: The elements (O, S, Se, Te, and Po) related to group VI A of the periodic table are known as chalcogenide. The term chalcogenide glass refers to only the composition holding the elements S, Se, and/or Te. Several other elements from groups IV A (Si, Ge, Sn) and V (P, As, Sb, Bi) can be mixed into these glasses. The glasses which do not have oxygen are so fascinating due to their appropriate applications for infrared optical transmission, opto-acoustic, and electrical switching. These glasses are also used as detectors and modulators for infrared rays.

iii. Metallic glasses: Metallic glasses are formed by ultrafast quenching of liquid metal alloys. Their interesting properties are the cause for their very rapid development. In the USA, they are known as "materials of the century" and in Japan "dream materials." They can be classified into two types, one is metal-metal alloy and the second is metal-metalloid. These glasses show the properties of resistance against radiation, low magnetic loss, zero magnetization, very high mechanical strength, zero magnetization, hardness, and high resistance against chemical corrosion. These materials have applications in high frequency-based power transformers, and recording cartridges in magnetic cores.

iv. Halide glasses: Halide glasses are transparent from UV to IR region. The halide glasses are suitable applicants for thermonuclear fusions and high-power lasers. Among the halide compounds, BeF_2, PbF_2, GaF_3 and AlF_3 are network formers. The structure of BeF_2 is very similar to the vitreous silica (SiO_2) and performs as a weak model of SiO_2. Another halide glass is $ZnCl_2$, but it does not easily produce glasses like BeF_2.

v. Organic glasses: Organic glasses contain carbon-carbon chains which are so tangled that quick cooling of the melt avoids rearrangement into crystalline regions. The glass transformation temperature of various organic glasses happens below room temperature.

1.3.5. Properties of glass

Glass has a liquid-like structure and has transparency, which is a major property. Glasses have structural disorders or the absence of integral grain boundaries. Glasses possess some special properties as given below [9,10,15,59,67–69].

1.3.5.1 Optical properties

The optical properties of glasses are related its refractive index and transparency. The refractive index and transparency depend on the composition of the host glass. The rate of cooling also affects the refractive index of glass. The relatively high transparency property of glasses is used in fabricating light bulbs, glass windows, vision lenses and optical fibre. Optical fibres are used for fast and enhanced communication.

1.3.5.2. Electrical properties

The electrical and electronic properties of glass depend on the composition of the host glasses. The electrical conductivity is interconnected with the resistivity of substances which varies with the glass host composition. Glasses are categorized into three different types based on electrical conductivity as follows (i) small conductive glasses which have high resistivity (ii) Glass with low electronic conductivity along with very high ionic conductivity and (iii) Only electronic conductive glasses.

1.4. Rare earth elements

RE elements activated luminescent and photonic materials are widely used in numerous applications such as lighting, optical fiber amplifiers, solid-state lasers and compact microchip lasers due to their vital properties of 4f–4f electronic transitions. The *lanthanide* group elements of the periodic table are called rare earth elements as they exist intermittently in nature. The RE elements are the group of 15 elements from lanthanum to lutetium with atomic numbers Z = 57 to 71. Yttrium and Scandium elements are also considered in the group of RE

elements because of their similar properties. RE elements have extensive applications almost in all disciplines of science and technology. Generally, RE elements occur in the form of RE_2O_3 oxide having the trivalent state (RE^{3+}), but very few can occur in the divalent state (RE^{2+}). RE elements have the electronic configuration $[Xe]4f^n$ (n = 0 – 14) where [Xe] is xenon configuration. The electronic configuration of RE elements in different excited states with the ground state is presented in Table 1.1. Various energy levels are obtained from these configurations which are specified by the spectral term ($^{2S+1}L_J$), where L, S, and J are three quantum numbers and these values ensue from the spin-orbit coupling. These energy levels have definite energy and are very well defined by Dieke's energy level diagram which is presented in Fig.1.4 for trivalent RE ions. The electrons of 4f are much less affected by the surrounding ligand atoms and do not show a significant part in the chemical bonding due to protective shielding to 4f electrons by $5s^2$ and $5p^6$ orbitals. Due to this shielding, RE ions have unique optical properties. RE ions can work either as an activator (A), sensitizer (S), or co-activator based on oxidation state, ionic radii, and solubility in the different host matrices. [70–79].

Trivalent RE ions have been the broadly used activator-doped ions for numerous fluorescent photonic applications. RE ions have some unique properties given below which are different from other optically active ions

- The revealed luminescence from RE ions occurs in several spectral regions of the electromagnetic spectrum such as visible and NIR.
- They have numerous energy levels appropriate for optical pumping.
- The $4f^n$ transitions of RE ions show small homogeneous line widths.
- These ions have quite long emission lifetimes and show narrow spectral lines.
- Well-developed theoretical models exist for systematically investigating energy levels, excited state dynamics and transition intensities.

The abovementioned attractive properties of trivalent RE ions expedite their usefulness in innumerable applications in solid-state laser, lighting, display, optical amplifiers in telecommunication fields etc.

Table 1.1. The outer electronic configuration in different ionic states of the ground states of rare earth (RE) ions.

Symbol (Atomic Number)	Configuration (Ground state)			
	RE^0	RE^+	RE^{2+}	RE^{3+}
La (57)	$5d^1\ 6s^2\ (^2D_{3/2})$	$5d^1\ 6s^1\ (^7F_2)$	$5d^1\ (^2D_{3/2})$	$4f^0\ (^1S_0)$
Ce (58)	$4f^1\ 5d^1\ 6s^2\ (^1G_4)$	$4f^{15}d^16s^1(^2G_{7/2})$	$4f^2\ (^3H_4)$	$4f^1\ (^2F_{3/2})$
Pr (59)	$4f^3\ 6s^2\ (^4I_{3/2})$	$4f^3\ 6s^1(^5I_4)$	$4f^3\ (^4I_{9/2})$	$4f^2\ (^3H_4)$
Nd (60)	$4f^4\ 6s^2\ (^3I_4)$	$4f^4\ 6s^1\ (^6I_{7/2})$	$4f^4\ (^3I_4)$	$4f^3\ (^4I_{9/2})$
Pm (61)	$4f^5\ 6s^2\ (^6H_{5/2})$	$4f^5\ 6s^1\ (^7H_2)$	$4f^5\ (^6H_{5/2})$	$4f^4\ (^3I_4)$
Sm (62)	$4f^6\ 6s^2(^7F_0)$	$4f^6\ 6s^1\ (^4F_{3/2})$	$4f^6\ (^7F_0)$	$4f^5\ (^6H_{5/2})$
Eu (63)	$4f^7\ 6s^2\ (^8S_{3/2})$	$4f^7\ 6s^1\ (^9S_4)$	$4f^7\ (^8S_{7/2})$	$4f^6\ (^7F_0)$
Gd (64)	$4f^75d^16s^2\ (^9D_2)$	$4f^75d^16s^1\ (^{10}D_{5/2})$	$4f^75d^1\ (^9D_2)$	$4f^7\ (^8S_{7/2})$
Tb (65)	$4f^9\ 6s^2\ (^6H_{15/2})$	$4f^9\ 6s^1\ (^7H_8)$	$4f^9\ (^6H_{15/2})$	$4f^8\ (^7F_6)$
Dy (66)	$4f^{10}\ 6s^2\ (^5I_8)$	$4f^{10}\ 6s^1\ (^6I_{17/2})$	$4f^{10}\ (^5I_8)$	$4f^9\ (^6H_{15/2})$
Ho (67)	$4f^{11}\ 6s^2\ (^4I_{15/2})$	$4f^{11}\ 6s^1\ (^5I_8)$	$4f^{11}\ (^4I_{15/2})$	$4f^{10}\ (^5I_8)$
Er (68)	$4f^{12}\ 6s^2\ (^3H_6)$	$4f^{12}\ 6s^1\ (^4H_{13/2})$	$4f^{12}\ (^3H_6)$	$4f^{11}\ (^4I_{15/2})$
Tm (69)	$4f^{13}\ 6s^2\ (^2F_{7/2})$	$4f^{13}\ 6s^1\ (^3F_4)$	$4f^{13}\ (^2F_{7/2})$	$4f^{12}\ (^3H_6)$
Yb (70)	$4f^{14}\ 6s^2\ (^1S_0)$	$4f^{14}\ 6s^1\ (^2S_{1/2})$	$4f^{14}\ (^1S_0)$	$4f^{13}\ (^2F_{7/2})$
Lu (71)	$4f^{15}d^16s^2\ (^2D_{3/2})$	$4f^{14}\ 6s^2\ (^1S_0)$	$4f^{14}\ 6s^1\ (^2S_{1/2})$	$4f^{14}\ (^1S_0)$

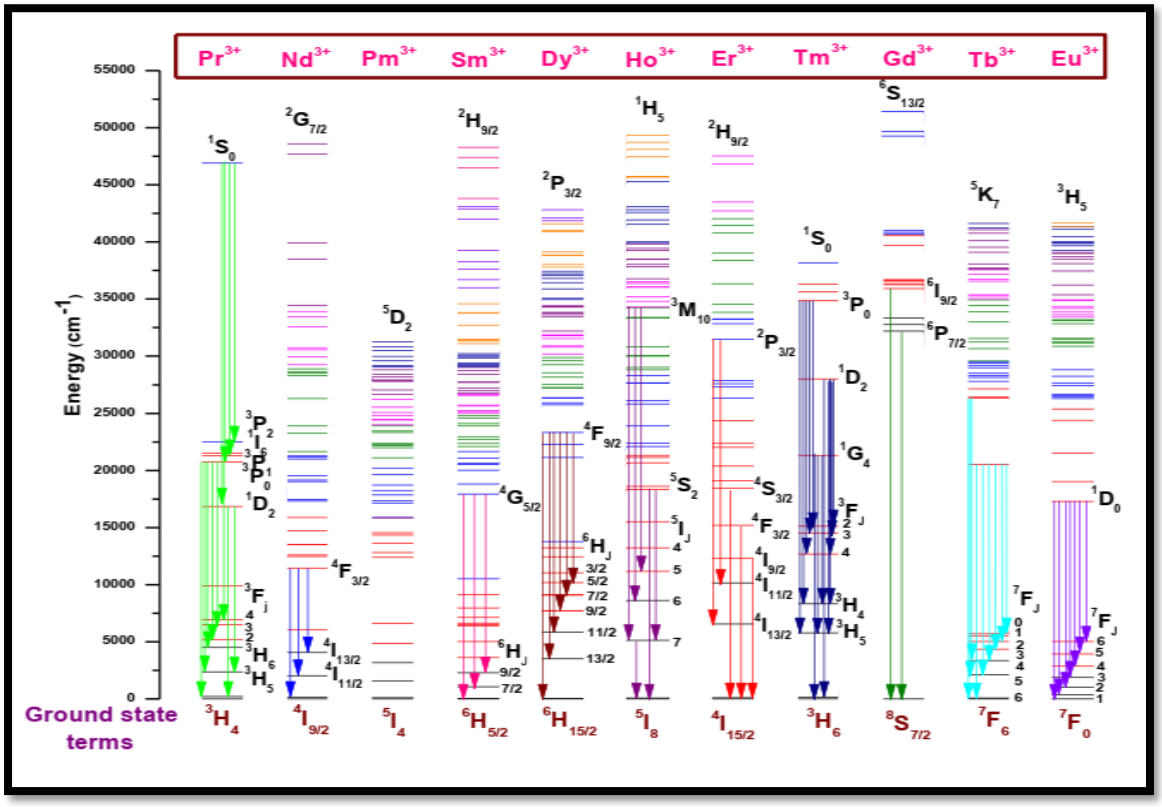

Fig. 1.4. Dieke's energy level diagram for RE^{3+} ions. The configurations range from $f^1(Ce^{3+})$ to f^{13} (Yb^{3+}).

1.4.1. Categories of interactions in RE ions

Generally, the interaction among the different levels of RE ions is classified based on three types of optical transitions such as characteristic transitions between numerous 4f levels, transitions $4f^{n-1}5d^1$ -$4f^n5d^0$ and charge transfer transitions, these all transitions are discussed as follows [12,43,80,81]:

1.4.1.1. Intra-configurational (f-f) transitions

To understand the transitions of the lanthanides, absorption and PL spectroscopy are the most significant tools. The absorption spectra exhibit broad bands or a group of sharp peaks for the case of the solution, crystal, and glasses. These bands and peaks are attributed to the electronic transitions in the 4f subshell. Each band and peak are a consequence of different transitions happening between $^{2S+1}L_J$ (or J-manifolds) to free ion level and are because of intra-configurational f-f transition. These transitions are spin forbidden. Excitation and emission energies in the f-f transition are independent of the host system incorporated with activator ions because they are excellently shielded from 5s and 5p orbitals. In the host, interaction among the RE ions with the light occurs through different kinds of transitions as stated below:

i. Electric dipole transition: An electric dipole (ED) transition occurs when the RE ions interact with the incident EM radiation component of the electric field via an electric dipole. The electric dipole outcomes are mainly due to charge linear movement. It is observed from the literature review that mostly induced transitions in RE ions have the nature of electric dipole type. As the start and end states of the $4f^n$ transition show the same parity, intra-configurational ED transitions are forbidden in RE ions doped materials. Henceforth, these transitions are limited by Laporte's selection rule ($|\Delta s| = 0$, $|\Delta l| = \pm 1$, $|\Delta L| \leq 6$, $|\Delta J| \leq 6$). However, the ED transitions are induced by non-centro symmetrical interactions of the electronic levels of opposite parity and are known as induced ED transitions. The intensities of the order 10^{-6} of the induced ED transitions are comparatively much lesser than the ordinary ED transitions.

ii. Magnetic dipole transitions: The incident EM radiation magnetic field component interacts through a magnetic dipole with the active RE ions and outcome of this, a weak intense transition occurs which is called magnetic dipole (MD) transition. The MD transition intensity is of the order of 10^{-8} which is much lesser than the induced electric dipole transition. The MD transition shows even parity and allows transition among the states that possess the same parity. Therefore, an MD transition is permitted by Laporte's selection rule ($|\Delta s| = 0$, $|\Delta l| = \pm 1$, $|\Delta L| \leq 0$, $|\Delta J| = 0$; $J = 0 \leftrightarrow 0$ transition is forbidden).

iii. Electric quadrupole transitions: The electric quadrupole (EQ) transitions have a quadrupole nature and outcome from the displacement of charges. An EQ is the combination of two dipoles or four-point charges with a net-zero charge and organized as their net dipole moments are zero. EQ has even parity. The EQ transitions have very weak intensities compared with the induced ED and MD transitions.

iv. Hypersensitive transition: The intensity of certain induced electric-dipole transitions is more sensitive to the ligand field environment around the RE ions. The intensities variation of these transitions shows the peculiar nature and therefore these transitions are called "hypersensitive transitions" which follow the selection rules ($|\Delta L| \leq 6$, $|\Delta S| = 0$, $|\Delta J| \leq 6$). The hypersensitive transitions are also called pseudo quadrupole transitions as they follow the same selection rules as obeyed by quadrupole transitions but the magnitude of the intensities of hypersensitive transitions are much higher. Hypersensitive transitions are the outcome of an asymmetrical distribution of dipoles developed by the EM radiation in the neighbouring RE ions. These transition intensities depend on the inhomogeneity in the dielectric medium and the local field symmetry around RE ions.

1.4.1.2. Inter-configurational (4fn5d0 - 4fn-15d1) transitions

The d orbitals get prominently influenced by the effect of the ligand field, hence 4f electrons transfer into 5d subshell is parity allowed. The intensity of such transitions is highly susceptible to the ligand environment around the RE ions. The transitions between 4f-4f levels give rise to very narrow peaks whereas transitions between the $4f^n5d^0$ and $4f^{n-1}5d^1$ levels give an upsurge to a wide range for the wavelength of excitation and emission. The wide range of f-d transitions can be explained with two principles: the Franck-Condon principle and the 4f ground state degeneracy breaks. As per the Franck-Condon principle, two rotational states have different vibrational states, that outcome in transitions with different energies. Additionally, the 4f degeneracy breaks into multiple levels due to spin-orbit coupling and activator ions in a host may undergo crystal field splitting and /or centroid shift.

1.4.1.3. Charge transfer transitions

The charge transfer transitions can affect excitation and emission spectra occurring in the dopant or host matrix. This type of transition can easily show the f-f absorption of the activator and generally, they are very intense. These types of transitions can happen in the host such as tungstate or vanadate; and also, in the activator itself e.g., the charge transfer from $O^{2-} \rightarrow RE^{3+}$.

1.5. Luminescence

Luminescence initiates from the Latin word “lumen” which means light and was given by historian and physicist Eilhardt Wiedemann in the year 1888. The emission of EM radiation involves generally absorption of invisible EM radiation energy and succeeding emission of visible and IR radiation which is classified basically under the term luminescence. Luminescence comes into the picture when the atoms of a substance are excited from the ground level to a higher excited level and emit excess energy while coming from higher states to the ground state in the form of UV, visible or infrared radiation. The materials that can convert absorbed EM radiation into visible light/IR radiation are recognized as luminescent Materials. Luminescent materials can be amorphous or crystalline [7,12,82,83]. Generally, luminescent glass materials are a good choice under the amorphous.

There are several approaches to excitation and depending on the excitation, luminescence can be categorized into several types as tabulated in Table 1.2 along with their source of the excitation and application.

Table 1.2. Luminescence phenomena with their source of excitation and application.

Phenomena	**Excitation Source**	**Application**
Photoluminescence	Photon	• Light sources • Photography and Fluorescent Lamps • Highlighting Ink and Paints • Display Devices • Laser • Sensor • Photovoltaic (PV) cells
Electroluminescent	Electric field	• Laser Diodes • TFEL Lamps and Dislpay • LED
Cathodoluminescence	Electron beam	• CRO • TV screen
Thermoluminescence	Heat	• Dosimetry of ionizing radiation • Geological and Archaeological dating • Environmental monitoring
Radioluminescence	γ /X-rays	• X-ray Screen and Scintillators
Chemiluminescence	Chemical reaction	• Chemical Analysis • Glow-in dark tubes
Bioluminescence	Bio-chemical reaction	• Analytical Chemistry

Among the different types of luminescence as tabulated above, the work embedded in the present thesis is focused on photoluminescence.

1.5.1. Photoluminescence (PL)

The absorption of the energy of EM radiation in the form of photons by the activator and then succeeding emission in the visible/NIR range is recognised as photoluminescence. The ions that act as the luminescence centre in the host matrix are called activators. Usually, the photoluminescence happens by these steps: -

- the activator being excited from the ground to a higher energy state;
- the activator relaxation to the lowermost energy state of the excited state;
- photons emission during the transition of the activator ions from the excited level to the ground level.

Photoluminescence is classified into two categories **fluorescence** and **phosphorescence** as per the emission. The emission during the time of excitation ($<10^{-8}$ s) is known as fluorescence while delayed emission ($>10^{-8}$ s) is called phosphorescence. In other words, fluorescence is prompt emission from the luminescent material when radiation falls on it through excitation, whereas in phosphorescence the emission is delayed for a second to hours. The excited ions return from the excited level to ground level via the non-radiative and radiative processes. In the radiative process, light is emitted in the visible region whereas the non-radiative process does not produce any emission in the visible region. The non-radiative energy is either the form of energy transfer (cross-relaxation, resonant energy transfer) of electronic states of atoms and/or in the form of phonons (lattice vibrations of solid). In the process of photoluminescence, energy loss is involved due to an emitted photon having lower energy in comparison to the incident photon which is called the Stokes emission whereas this process is known as down-conversion. The excitation and emission photons energy gap are called the Stokes shift. Furthermore, there is another probability in which a substance could absorb more than one photon (two or several) at once and promote the emission of a higher energy photon. This procedure is called an up-conversion process and such type of emission is termed anti-Stokes emission [83–85]. These both processes are shown in Fig.1.5 (i) and (ii).

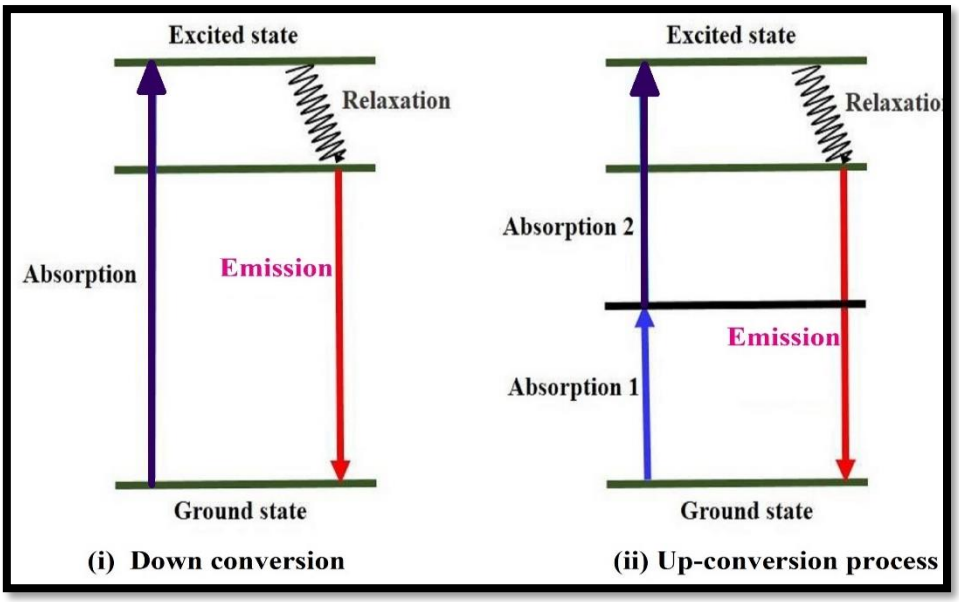

Fig. 1.5. Schematic representation of **(i)** down-conversion and **(ii)** up-conversion process

1.6. Spectroscopic study of RE ions doped materials

1.6.1. Nephelauxetic effect and evaluation of bonding parameter

The covalence of RE ions and the oxygen bond of ligand in the host matrix is evaluated with the help of the Nephelauxetic effect which appears due to a partly filled f-orbital. It is investigated that the influence of the nephelauxetic effect can deform the 4f orbitals associated with RE ions when RE ions are doped in any host matrix. The energy level structure of RE ions becomes constriction due to the overlapping shapes among its oxygen orbits and 4f orbitals. Consequently, they will possess a wavelength shift. The Nephelauxetic ratio (β) and bonding parameters (δ) were estimated to know the nature of bonding among RE ions and oxygen ligands [86,87].

The value of "β" can be found by using the equation

$$\beta = \frac{\nu_c}{\nu_a} \tag{1.1}$$

In the above equation, υ_C and υ_a are the wavenumbers relating to RE and aqua ions respectively for the particular transition. Further, δ can be assessed using the below equation

$$\delta = \frac{1 - \bar{\beta}}{\bar{\beta}} \tag{1.2}$$

where, $\bar{\beta}$ represents the average value of β. The bonding nature either ionic or covalent between RE ions and the ligand field environment is based on the obtained value of δ either negative or positive respectively.

1.6.2. Energy band gap

The optical energy band gap (E_{opt}) values for the as-prepared glasses were evaluated using the fundamental absorption edge of absorption spectra using the relation of Davis and Mott [88,89]

$$\alpha h\nu = B\left(h\nu - E_{opt}\right)^{m} \tag{1.3}$$

Where α is the absorption coefficient, B is the bond trailing parameter, ν is frequency, and m is the number that helps to choose the nature of the inter-energy band electronic transition due to absorption. For direct and indirect allowed transitions, the values of m can be 1/2 and 2 respectively. The coefficient of absorption can be estimated by the following equation

$$\alpha(\nu) = \frac{1}{d} ln\left(\frac{I_0}{I_t}\right) \tag{1.4}$$

here, d is the thickness of glass samples, I_0 and I_t denotes the intensity of incident radiation and transmitted radiation, respectively. The value of E_{opt} can be assessed by extrapolating the liner section of Tauc's plot which is drawn for $(\alpha h\upsilon)^{1/2}$ versus hυ.

1.6.3. The intensity of absorption bands-oscillator strengths

In an amorphous material, the energy of an absorption band of RE ions can be assessed by considering the area under the absorption plot which is termed oscillator strength. Ladenburg [90] introduced the concept of oscillator strength which can be estimated by using the ratio of actual intensity to radiated intensity by a harmonically oscillating electron in 3 dimensions. The experimental oscillator strengths which denoted by f_{exp} is estimated by the following equation [91]

$$f_{exp} = \frac{2.303\mathrm{m}c^2}{\mathrm{N}\pi e^2} = 4.318\ x\ 10^{-9} \int \varepsilon\ (\upsilon) d\upsilon \tag{1.5}$$

Where the terms ε(υ), e, m, N and c represent the molar extinction coefficient in cm^{-1} relating to an absorption band, charge of the electron, the mass of the electron, Avagadro number and speed of light respectively. It is observed that the order of oscillator strengths is 10^{-6} for induced electric-dipole transitions of RE ions.

1.7. Judd-Ofelt (J-O) theory

J-O theory was introduced in 1962 by Judd and Ofelt [42,43]. They individually derived methods for estimating the oscillator strength (*f*) related to induce ED transitions of RE ions for f-f configuration [42,43,83]. J-O theory states that the intensity of forbidden f-f electric-dipole transition can arise from the mixture of $4f^n$ as well as excited state configurations such as $4f^{n-1}5d$ which have opposite parity. The f_{exp} parameter of RE ions can be assessed by the given equation

$$f_{exp} = f_{ED} + f_{MD} \tag{1.6}$$

Where, $f_{ED}\ and\ f_{MD}$ represent the electric and magnetic dipole oscillator strength respectively. This equation specifies that when the RE ion interacts with EM radiation, the experimental oscillator strength of the RE ion includes the $f_{ED}\ and\ f_{MD}$. The total oscillator is represented for an absorption band with energy ν (cm^{-1}) by the following equation

$$f_{exp}(\psi_j, \psi_{j'}) = \left[\frac{8\pi^2 mc\nu}{3h(2J+1)}\right]\left[\frac{(n^2+2)^2}{9n} S_{ED}(\psi_j, \psi_{j'}) + nS_{MD}(\psi_j, \psi_{j'})\right] \tag{1.7}$$

Where h and n are Planck's constant and refractive index respectively. The term $\frac{n(n^2+2)^2}{9n}$ is the Lorentz local field correction which clarifies the dipole-dipole correction. The J parameter denotes total angular momentum and (2J+1) is the ground state degeneracy. S_{ED} and S_{ED} are electric and magnetic line strengths respectively. The magnetic dipole transition intensities are very weak and around 1% of f_{ED}. Thus, the electric dipole oscillator strengths nearly represent the total experimental oscillator strength

$$f_{exp} = f_{ED} \tag{1.8}$$

Therefore, the experimental oscillator strengths can be related to the calculated oscillator strengths $f_{cal}(\psi_j, \psi_{j'})$ of an induced electric-dipole transition from the ground (ψ_j) to an excited level ($\psi_{j'}$) by the J-O theory as

$$f_{exp}(\psi_j, \psi_{j'}) = f_{cal}(\psi_j, \psi_{j'}) = \left[\frac{8\pi^2 mc\nu}{3h(2J+1)}\right]\left[\frac{(n^2+2)^2}{9n} S_{ED}(\psi_j, \psi_{j'})\right] \tag{1.9}$$

Hence, the oscillator strengths are assessed by the above-stated equations. The goodness of fit between f_{exp} and f_{cal} is assessed by the least square fitting procedure. In this way, root mean square (r.m.s.) deviations can be assessed by the expression

$$\delta_{rms} = \left[\frac{\Sigma\left(f_{exp} - f_{cal}\right)^2}{p}\right]^{\frac{1}{2}} \quad (1.10)$$

Where p denotes the total number of energy levels that occur in the fitting method. By applying the J-O theory, the J-O intensity three parameters (Ω_2, Ω_4, and Ω_6) of RE ions have been assessed. To reveal information about the performance and the efficiency of the luminescent material, J-O intensity parameters play a vital role. The J-O intensity parameters are also an enormous concern in finding the covalence between RE ions and oxygen ions and also the symmetry in the host around the RE ions. The Ω_2 parameter is connected to covalence and it is related to structural changes and the ligand field symmetry around the RE ion site. The Ω_4 and Ω_6 intensity parameters are related to the bulk properties such as viscosity and rigidity of the host environment in which RE ions are present [17,92].

1.7.2. Radiative properties of RE ions

The J-O theory is used to estimate the radiative parameters by combining the absorption and emission spectral data. The radiative transition rate (A) means the intensity of f-f transition of RE ions of any given excited state $\psi_{j'}$ is assessed by the following equation [83,93,94]

$$A\left(\psi_j, \psi_{j'}\right) = \left[\frac{64\pi^4\nu^3}{3h(2J+1)}\right]\left[\frac{(n^2+2)^2}{9n} S_{ED}\left(\psi_j, \psi_{j'}\right) + nS_{MD}\left(\psi_j, \psi_{j'}\right)\right] \quad (1.11)$$

The radiative transition rate is also called the probability of spontaneous emission.

The summation of the A calculated over all the excited states is called the total radiative transition probability (A_T) and can be assessed by the given equation

$$A_T = \Sigma_{\psi_{j'}} \mathrm{A}\left(\psi_j, \psi_{j'}\right) \quad (1.12)$$

The radiative lifetime in the excited state of the RE ion is denoted by τ_R and it is estimated by the following equation

$$\tau_R\left(\psi_j, \psi_{j'}\right) = \frac{1}{A_T} \quad (1.13)$$

The branching ratio (fluorescence) is represented by β_R and is related to the relative intensities of the emission lines from the excited state to a lesser-lying state. The equation for β_R from the relaxing state to a lower-lying state is as follows

$$\beta_R(\psi_j, \psi_{j'}) = \Sigma A_R(\psi_j, \psi_{j'}) \tau_R(\psi_j, \psi_{j'}) \quad (1.14)$$

For a potential lasing transition, the value of the branching ratio should be higher than 0.5.

The peak stimulated emission cross-section is a very significant parameter for explaining the rate of energy extraction from the host matrix doped with RE ions for lasing action and is denoted as $\sigma_{se}(\psi_j, \psi_{j'})$. It can be expressed between the states ψj and $\psi j'$ as

$$\sigma_{se}(\psi_j, \psi_{j'}) = \left[\frac{\lambda_p^4}{8\pi c n^2 \Delta\lambda_p}\right] A(\psi_j, \psi_{j'}) \quad (1.15)$$

Where λp is peak wavelength and $\Delta\lambda p$ is effective emission line width which can be assessed by using the equation

$$\Delta\lambda_p = \frac{1}{I_{max}} \int I(\lambda) d\lambda \quad (1.16)$$

Here, $I(\lambda)$ represents the intensity for a band at a particular wavelength (λ) and I_{max} is the maximum intensity.

Additional parameters such as gain bandwidth ($\sigma_{se}\, x\, \tau_R$) and optical gain ($\sigma_{se}\, x\, \Delta\lambda_p$) are calculated to identify the appropriateness of the material for fiber lasers.

1.8. Excited-state dynamics of RE ions

When a sufficient amount of energy is used for excitation to a RE ion, excitation along with de-excitation processes starts due to RE ion Intra *4f-4f* electronic transitions [21,63,95–97]. A time-resolved intensity spectrum shown in Fig.1.6 explains the mechanism of excitation and de-excitation.

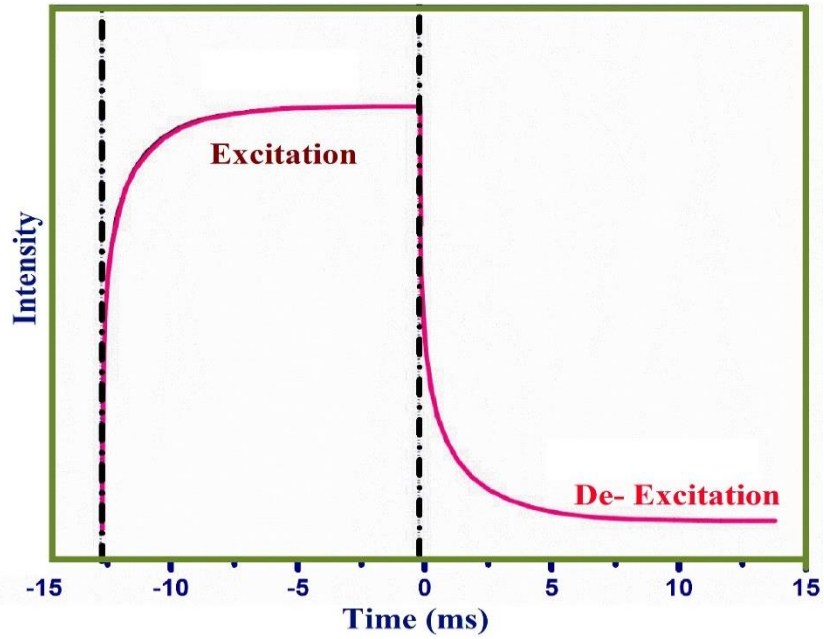

Fig. 1.6. Excitation and de-excitation process as a function of time for RE ions

The RE ion may de-excite from the excited state to the ground state through the process of energy transfer of radiative transition between adjacent RE ions or by cross-relaxation (CR) channels. At a small concentration of RE ions, interaction among RE ions is very less, hence PL decay profile can be fitted with a single exponential function for intensity versus time. The PL intensity can be stated by using the expression

$$I_t = I_o + A \exp\left(-\frac{t}{\tau}\right) \tag{1.17}$$

Here, I_o and I_t are the PL intensities at time t=0 and t = t respectively. A denotes the fitting constant. τ represents the lifetime in the excited state of the RE ion and it can be assessed by the intensity logarithmic plot with time. It is observed from Fig.1.6 that the excited state intensity declines after a time τ as $1/e$.

In an excited state, the experimental lifetime of the RE ion can be assessed by using the following equation

$$\tau_{exp} = \frac{\int t\ I(t)dt}{\int I(t)dt} \tag{1.18}$$

In some cases, RE ions decay curves are well fitted with the bi-exponential expression. The bi-exponential fit curves PL intensity can be shown by using the expression

$$I = I_0 + A_1\, exp(-t/\tau_1) + A_2\, exp(-t/\tau_2) \quad (1.19)$$

Where PL intensities I_0 and I are at time t = 0 and t = t respectively. τ_1 and τ_2 are the exponential portions of the lifetime. The A_1 and A_2 represent the fitting constants.

The average lifetime, in this case, is estimated by the expression

$$\tau_{avg} = \frac{A_1\tau_1^2 + A_2\tau_2^2}{A\tau_1 + A_2\tau_2} \quad (1.20)$$

Another significant parameter is quantum efficiency (η) which can be assessed by associating radiative (τ_R) and experimental lifetime (τ_{exp})

$$\eta = \frac{\tau_{exp}}{\tau_R} \times 100 \quad (1.21)$$

The value of η depends on the lifetimes of the excited states, emission cross-section, radiative transition probabilities, RE ions concentration and ligand fields produced by network modifiers.

The radiative (τ_R) and experimental lifetime (τ_{exp}) encountered the discrepancy due to the presence of non-radiative (W_{NR}) processes. The non-radiative relaxation rate can be estimated by the equation

$$W_{NR} = \frac{1}{\tau_{exp}} - \frac{1}{\tau_R} \quad (1.22)$$

1.9. Energy transfer

To discuss the process involved in the energy transfer (ET), firstly we will understand the meaning of these words such as sensitizer/donor and activator/acceptor. A sensitizer is a species which offers energy viz. electron, proton, etc. whereas an acceptor accepts them. In the present discussion, the energy is absorbed by the donor in the form of light and that energy provides to the acceptor. In the host lattice, the luminescent centres or ions are called activators/acceptors. The sensitizer acts to sensitize the activator in the ET process which outcome gives the emission. A small amount of additives or impurities doped into a host material are known as activators or dopants. The energy absorption happens either by activators or host lattices. Mostly, the emission takes place only at the activator sites. To improve the absorption, sensitizers are added to the host lattice. In the process of ET, a donor sensitizes the activator and the light emission is done by the activator or acceptor. In some cases, the host

(ion or molecule) can also work as a sensitizer and transfer its energy to the activator; this process is known as host sensitization. Although, some portion of the excitation energy can be conveyed from one luminescent centre to another centre. After absorbing excitation energy, electrons in the luminescent centres transit to excited states and excited states energy of an electron can generally be distributed in the following manner: as shown in Fig.1.7 (i) the emission of light through direct excitation of the acceptor and (b) as shown in Fig.1.7 (ii) indirect excitation from the sensitizer to the acceptor [98–100]. Generally, luminescence from inorganic glasses/phosphors has three main processes excitation, ET, and emission as represented in Fig.1.7 (ii) [101,102]. In the emission from the luminescent centre, two primary processes are involved. In the first process, the energy of the emitted photons is not more than the energy of the incident photon which is called Stokes emission. The reason for energy loss is lattice relaxation due to an alteration in the strength of the chemical bond. The energy difference between absorption and emission energy is called a Stokes shift. There is also the possibility of a second process where the energy of the excitation photon is less and phosphor might absorb two (or more) photons at once and release a higher energy photon than the incident photon. This emission is known as anti-Stokes emission and the process is named up-conversion. [103].

Four fundamental mechanisms occur in ET procedures among ions other than the ET by the movement of electron transfer (i) Resonant radiative ET via emission of sensitizer and this emission re-absorbed by the activator (ii) non-radiative ET related with resonance (iii) multi-photon related ET and (iv) cross-relaxation ET between two similar ions.

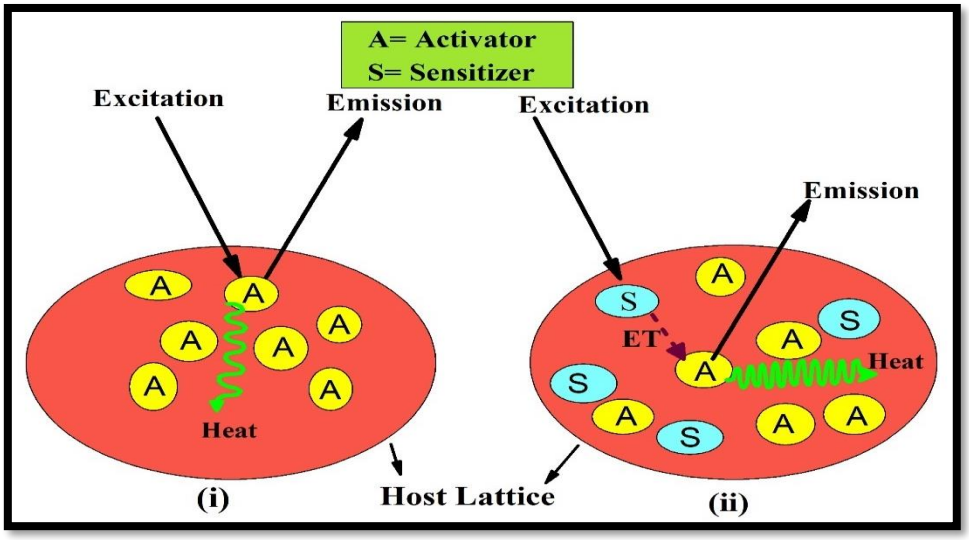

Fig. 1.7. Sketch of (i) excitation and emission and (ii) excitation, ET and emission in the host lattice.

The efficiency of radiative ET is related to activator excitation efficiency by the sensitizer emission as shown in Fig.1.8 (a). The excitation spectrum of the activator and the emission spectrum of the sensitizer should have a significant overlap. If ET occurs predominantly through radiative, then sensitizer fluorescence lifetime does not vary with activator concentration. In Fig.1.8 (b), the non-radiative ET is shown because the fluorescence decay time of the sensitizer significantly decreases with the activator content. The ET mechanism occurrence increases when the energy difference is equal among the exciting levels of the sensitizer and the activator. The large energy gap between the ground and excited levels of sensitizer and activator can lead to non-resonant ET with the aid of a phonon. The probability of radiative ET is negligible when the two ions have different excited states and non-radiative transitions occur between the ions which are assisted by phonon as shown in Fig.1.8 (c). The cross-relaxation process happens when a portion of the energy of an ion in the excited state transfers to another ion in the ground state which does not yield any radiative emission because they both lie in an intermediate state. For all types of down conversion, ET among two similar adjacent ions or luminescent centres occurs is termed as cross-relaxation. Fig.1.8 (d) depicts a simple cross-relaxation possible energy level system in which initially the first ion in a higher state exchanges energy with another ground state ion; subsequently, both ions concurrently shift to some intermediate states in the range of energy between their initial states [73,98].

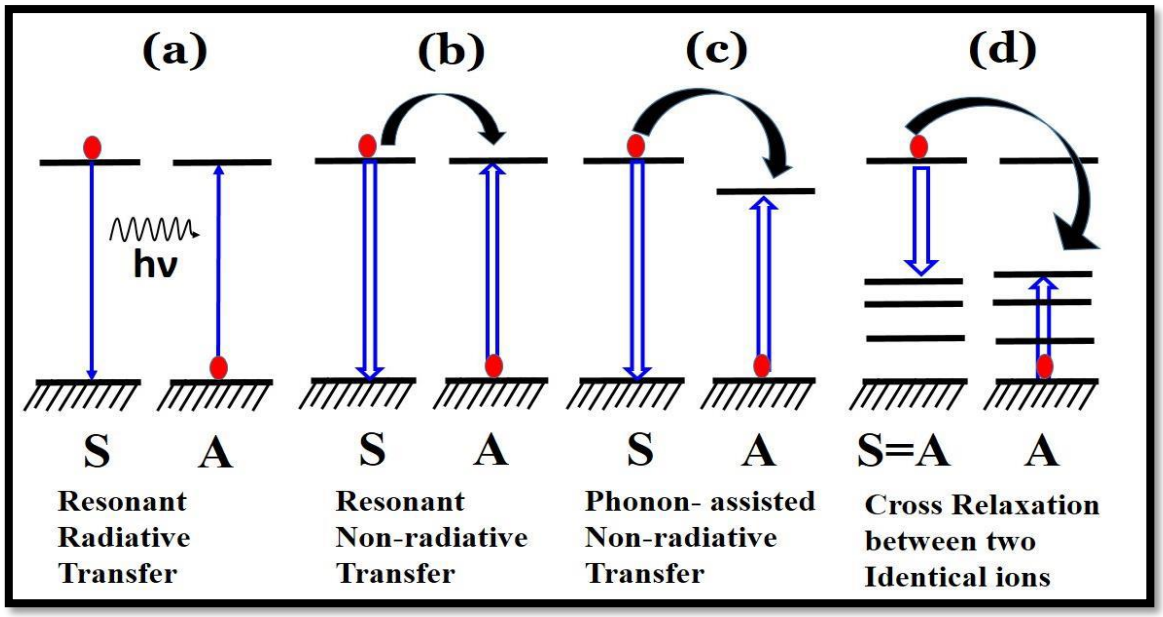

Fig. 1.8. The diagram illustration between the two ions for different ET processes.

1.9.1. Non-radiative relaxation

When RE ion is exposed to a sufficient amount of energy, it gets an excited state and returns to the ground state via non-radiative relaxations such as cross-relaxation. The non-radiative decay rate (W_{NR}) plays a significant role in quenching the lifetime. W_{NR} is the combination of the following non-radiative decay processes such as non-radiative rates for multi-phonon relaxation (W_{MPR}), ET between donor and acceptor (W_{ET}), concentration quenching (W_{CQ}) and hydroxyl group (W_{OH}) as given in the below equation and these processes can decrease the lifetime of an excited RE ion.

$$W_{NR} = W_{MPR} + W_{ET} + W_{CQ} + W_{OH} \tag{1.23}$$

1.9.2. Multi-phonon relaxations

Multi-phonon relaxation occurs due to the local vibrations of surrounding atoms which are called phonons. The multi-phonon relaxation process is dominant when the cross-relaxation and the ET processes are negligible. In such case, the de-excitation mechanism is given by the equation [104]

$$W_{MPR} = \beta\, e^{(-\alpha \Delta E)} \tag{1.24}$$

Where β is the host-dependent parameter and independent of RE ion concentration. ΔE is the energy gap between the excited state J and the next nearest lower-level J′

If the states J and J′ have a higher energy gap than the phonon energy, then various phonon emissions occur to fill the energy gap. It is noticed that the highly energetic vibrations keep non-radiative decay because of the conversion of energy in the lowest order. Usually, glass network stretching vibrations are the most energetic vibrations. In multi-phonon processes, several energetic vibrations are active. It is noticed that the logarithm of the multi-phonon decay rate declines linearly with the energy gap. The phonon energy of some basic network formers is presented in Table 1.3.

Table 1.3. Phonon energy of some glasses.

S. No	Glass system	Phonon energy (cm^{-1})
1	Borate glass	1300
2	Phosphate glass	1200
3	Silicate glass	1100
4	Germinate glass	900
5	Tellurite glass	700

1.9.3. Concentration quenching

Generally, the luminescence intensity in RE-doped materials increases up to a definite concentration of RE ions doped in the materials and decreases beyond that. This process is known as concentration quenching. The occurrence rises the luminescent intensity due to an increase in absorption efficiency and remains maximum up to a certain concentration of RE ion called critical concentration [2,105].

The ET among the luminescent centers is the main reason for concentration quenching in a host matrix. As the concentration of RE ions upsurges, the distance between acceptor and donor atoms decreases which leads to luminescent concentration quenching due to ET between the atoms.

The concentration quenching process can be explained in two different ways.

i. In one type of mechanism, the excitation energy can be distributed into several luminescent centers before being emitted due to proficient ET. By the emission of infrared or multi-photon relaxation, these exciting luminescent centers relax to their ground state. In the ET chain, these centers can also act as energy sinks and result in the quenching of luminescent intensity.

ii. In another type of mechanism, the excitation energy cannot be distributed to luminescent centers but energy will lose from the emitted state via a cross-relaxation process that occurs by resonant ET between the two nearby luminescent centers. The cross-relaxation is shown in the energy level diagram in Fig.1.9. If one luminescent center (donor) has the energy E_3-

E_2 which is equal to energy E_0-E_1 of another nearby center (acceptor), the resonance ET occurs and which intensely depends upon the nature of energy levels. In a cross-relaxation mechanism, the E_2 excited state has a donor center and the acceptor center will go to the E_1 excited state that outcomes in either non-radiative relaxation or emission of a photon of energy other than E_3-E_2. This further promotes the quenching of emission intensity.

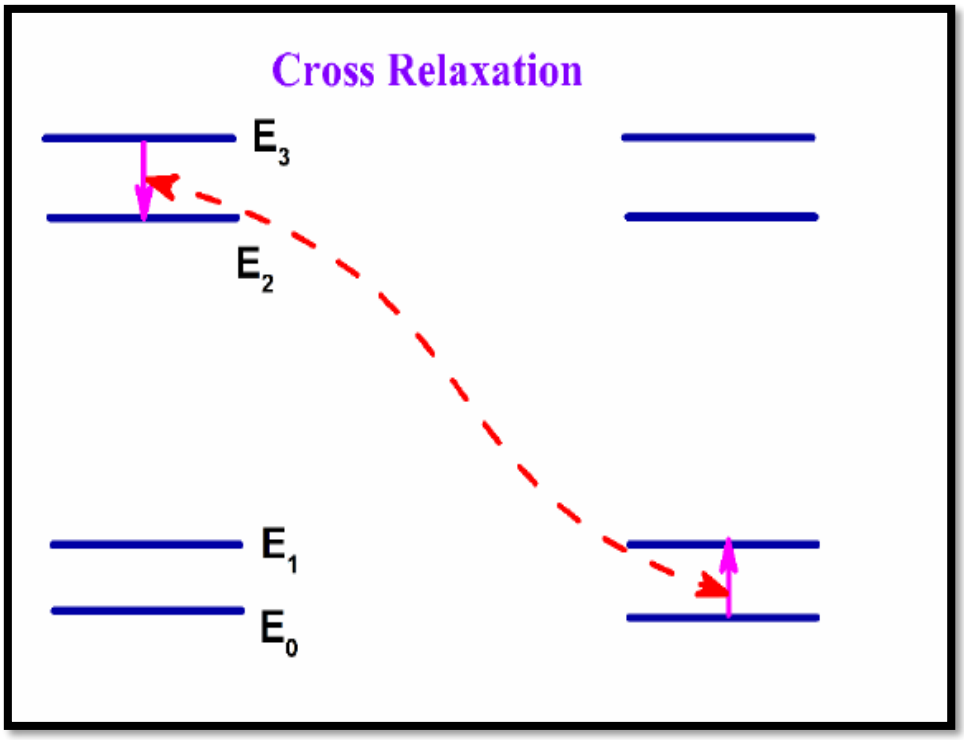

Fig. 1.9. Cross-relaxation between pairs of centers.

1.10. CIE chromaticity coordinates

CIE (Commission Internationale de l'Eclairage) is the utmost extensively used system to investigate color from PL spectra of RE-doped materials by describing the composition of any color in terms of three primary colors (red, green and blue).

CIE color coordinates assessed by PL spectra and standard equal energy points can be compared for analyzing different colors in the visible region. The specified power spectral density P (λ) which is the degree of stimulation desired to match the color is assessed by the set of three equations.

$$X = \int \bar{x}(\lambda)P(\lambda)d\lambda \qquad (1.25)$$

$$Y = \int \bar{y}(\lambda)P(\lambda)d\lambda \qquad (1.26)$$

$$Z = \int \bar{z}(\lambda)P(\lambda)d\lambda \qquad (1.27)$$

Where, X, Y and Z are the tristimulus values that provide the value of stimulation for each primary (red, green, blue) color to match the color of P(λ) whereas $\bar{x}$, $\bar{y}$ and $\bar{z}$ are matching functions defined in the CIE diagram. Today, the most commonly used tool to describe color in spectroscopy is CIE 1931 *chromatic* diagram. The CIE coordinates (x, y) can be evaluated with the tristimulus values (X, Y and Z) by using these two equations

$$x = \frac{X}{X + Y + Z} \qquad (1.28)$$

$$y = \frac{Y}{X + Y + Z} \qquad (1.29)$$

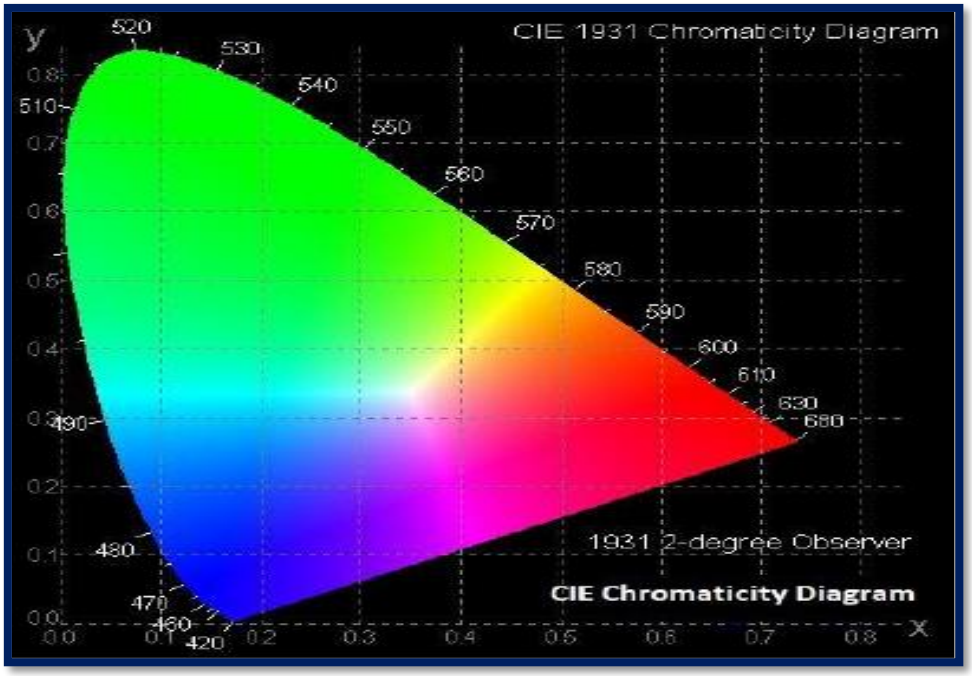

Fig. 1.10. CIE chromaticity diagram.

According to the chromaticity diagram, CIE chromaticity coordinates (0.67, 0.33), (0.14, 0.08) and (0.21, 0.71) represent the primary colors red, blue and green respectively. The CIE color coordinate represented by pure white light is (0.33, 0.33) [96,106].

The correlated colour temperature (CCT) is another significant tool and can be estimated using the following equation proposed by McCamy [107]

$$CCT = -449v^3 + 3525v^2 - 6823.2\,v + 5520.3 \quad (1.30)$$

Where $v = \frac{(x-0.332)}{(y-0{\cdot}186)}$. The higher the value of CCT, the better will be the visual insight with high brightness perception. The CIE chromaticity diagram showing different color corresponding to different wavelengths can be seen in Fig.1.10.

1.11. Thermal stability by using temperature-dependent PL (TD-PL):

At higher temperatures such as 423 K, the sustainability of the emission intensity of glasses/phosphors materials is a major essential requirement for LED applications. The effect of temperature on PL properties has been taken up by recording the TD-PL studies. Usually, the reducing tendency of intensity in emission spectra with a temperature rise is noticed due to the thermal quenching phenomenon. The thermal quenching phenomenon occurs due to non-radiative relaxations.

TD-PL studies have been performed and it is suitable to know the thermal stability of glass substance under examination by an Arrhenius equation [50,108] as given below

$$I_T = \frac{I_o}{1 + C\,\exp\left(-\frac{\Delta E}{K_B T}\right)} \quad (1.31)$$

Where I_o is the PL intensity at room temperature (RT= 300 K) and I_T represents the PL intensity at temperature T (K). C is an arbitrary constant; ΔE denotes the activation energy and K_B stands for Boltzmann's constant with its value 8.67×10^{-5} eV/K. For the most intense emission peak, the graph between $\ln[(I_o/I_T)-1]$ and $(1/K_BT)$ is a linear graph with some slope and the value of ΔE is estimated from this graph. The estimated value of ΔE in eV establishes the thermal stability of the luminescent material and a relatively high value of ΔE is better for the thermal stability of the luminescent material.

1.12. Objectives of the present work

1. To optimize the conditions of production of a good optical glass doped with certain RE ions for a wide range of photonic applications.
2. Extensive physical characterization of as-prepared glasses by measuring properties such as refractive index, density, etc. The structural and functional group identification of the titled glasses by using techniques such as XRD and FT-IR.
3. To study absorption, excitation, and emission spectral features of the RE ions doped LiBiAlBSi glasses to understand the effect of glass host as well as the concentration of RE ion.
4. Evaluation of emission cross-section and quantum efficiency of the as-prepared glasses by correlating the absorption spectral data with the emission and decay spectral measurements. RE ion concentration optimization of the as-prepared glassy systems for lasing potentialities, fiber amplifiers, and light-emitting diodes.
5. RE ion concentration optimization and by doping with suitable RE (single or double) ions of the as-prepared glassy systems for better luminescence efficiency.

CHAPTER 2

Glass Preparation and Characterization Techniques

To develop the high-grade glassy materials requires a deep understanding of the experimental procedure. In the present chapter, the conventional melt-quenching procedure used for the preparation of glassy materials is discussed in detail. The prepared glassy materials have been characterized for structural and PL properties by using several analytical techniques such as X-ray diffraction (XRD), Fourier transforms infrared (FT-IR) and UV-VIS-NIR spectroscopy. This chapter explains thoroughly all the experimental techniques employed in the present thesis work including the method used for the preparation of glasses.

2.1. Glass sample preparation procedures

Amorphous/Non-crystalline materials can be synthesized by employing different techniques such as[109]

- Sudden melt quench
- Vapour quenching sputtering (evaporation, sputtering and reactive deposition)
- Solid state methods (Radiation damage, intense shock-waves, diffusion effects)
- Electrochemical methods
- Prolysis
- Sol-gel method

Among all the listed techniques, melt quenching is the oldest and easiest technique used for the preparation of amorphous materials. This technique is also widely used commercially.

2.1.1. Melt quenching technique

In the melt-quenching process, amorphous materials are prepared in the desired shape by suddenly cooling the molten form of precursor materials. The amorphous solids are formed through the continuous hardening of the uniformly melted material, which is the distinguishing property of the melt-quenching procedure. For glassy-state formation, the required cooling rate varies for various host glass systems. Essential cooling can be attained by quenching the melt rapidly after taking it away from the temperature-controlled electric furnace and then pouring it in between two pre-heated conductive materials like copper plates or brass plates [110].

The formation procedure of the glass host matrix through the melt quenching method is illustrated in Fig.2.1. The obtained glasses have been annealed below glass transition temperature for 3 to 4 h in a muffle furnace to remove air bubbles, thermal shocks, and cracks in the as-prepared glasses. Finally, transparent or air bubble-free glasses have been obtained along with proper thickness. The prepared glasses are used for further characterization such as X-ray diffraction (XRD), FT-IR, optical absorption, PL excitation, PL emission, PL decay measurements and temperature-dependent PL spectral analysis.

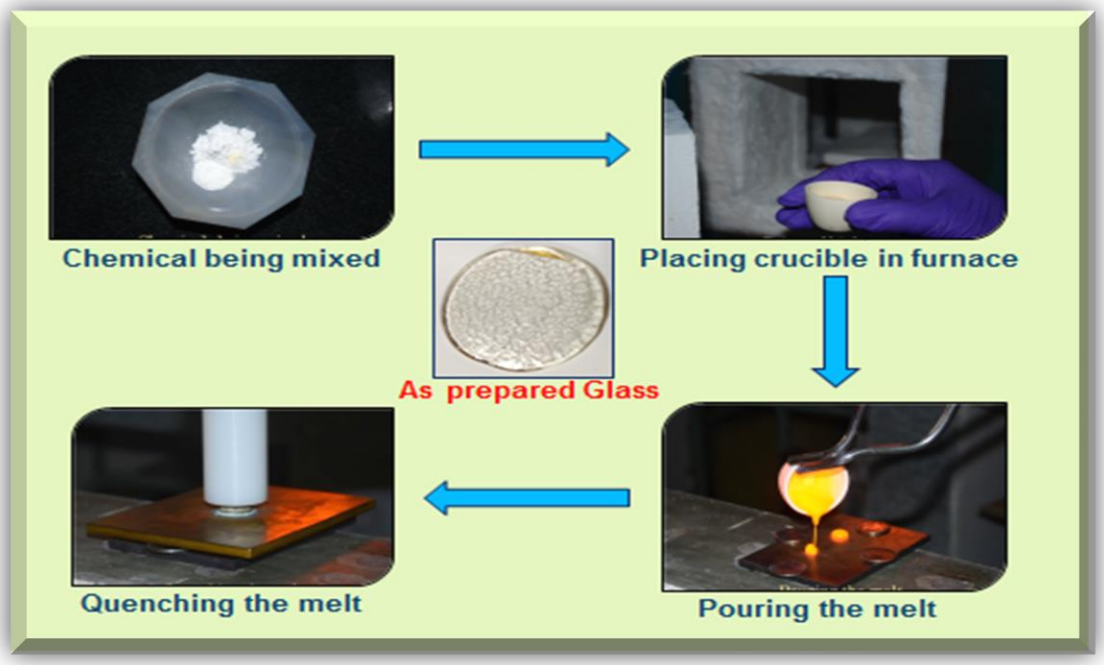

Fig. 2.1. Melt Quench procedure used for the preparation of the glasses.

2.2. Glass composition calculations and their preparation

2.2.1. Raw materials

The oxide raw ingredients have been acquired from different companies along with high A. R. grade (≥ 99.99%) primarily for dopant RE^{3+} ions. The used raw ingredients in our research along with the purity and company details are tabulated in Table 2.1. A transparent series of LiBiAlBSi glasses doped with different RE^{3+} ions such as Sm^{3+}, Tb^{3+}, $Sm^{3+}/Eu^{3+,}$ and Er^{3+} has been successfully synthesized via using the following molar composition in mol% below:

$$20.0\ Li_2CO_3 – 7.5\ Bi_2O_3 – (7.5 - x)\ Al_2O_3 – 45.0\ H_3BO_3 – 20.0\ SiO_2 – x\ RE^{3+}$$

The aforementioned raw ingredients have been weighted using a digital balance (Shimadzu modal: ATX244) as per the stoichiometric proportion at ambient temperature. About 7 gm of raw ingredients are mixed and crushed in an agate mortar along with acetone used as a wetting medium until smooth and homogenous mixture is acquired.

Table 2.1. The list of raw ingredients, A. R. purity (%), and company details.

S. No.	Name of raw ingredients	A.R. Purity (%)	Company Details
1.	H_3BO_3	99.00	Fisher scientific
2.	SiO_2	99.00	Fisher scientific
3.	Bi_2O_3	99.00	Fisher scientific
4.	Al_2O_3	99.00	Fisher scientific
5.	Li_2CO_3	99.00	Fisher scientific
6.	Sm_2O_3	99.99	Sigma Aldrich
7.	Tb_4O_7	99.99	Sigma Aldrich
8.	Eu_2O_3	99.99	Sigma Aldrich
9.	Er_2O_3	99.99	Sigma Aldrich

2.2.2. Glass melting and annealing

The homogenous mixture has been taken in an alumina crucible and kept in a programmable electric furnace at around 1100°C for 30 min to get the desired melt. To get the same thickness to the glass LiBiAlBSi samples, the melts were quenched quickly by pouring the melts in between the pre-heated smooth brass molds. Then, the prepared LiBiAlBSi glass samples have been annealing at 350 °C for 4 h to make them free from air bubbles and stress. Finally, RE^{3+} doped LiBiAlBSi glasses have been obtained for their further characterization using various spectroscopic techniques.

2.3. Characterization techniques

The as-prepared LiBiAlBSi glasses were characterized via various tools to explore the various characterizations like physical, structural, optical, photoluminescent, etc. The discussions on the several characterization tools are illustrated in the following section.

2.3.1. X-ray Diffraction (XRD)

X-ray crystallography is the most essential non-destructive and standard procedure that is used to understand the atomic structure of crystals and measure the crystallite size, phase and internal stress of the tiny crystalline sections. One can recognize structural characteristics such as preferred orientation, lattice points, and contraction. X-rays are part of electromagnetic spectrum of short wavelength varying in a few angstroms, which is analogous to the interplanar spacing of atoms in a material. The XRD technique was first discovered in 1912 when a CuS crystal was exposed to a beam of X-rays and the results have been measured on photographic

plates. Mr W. L. Bragg and his son outlined the governing rule of the diffraction pattern and solved the first-ever crystal structure [111]. This technique performs the best for crystalline materials or partially crystalline but is also used in the study of amorphous/non-crystalline materials.

2.3.1.1. X-ray diffractometer:

X-ray diffractometer is the instrument of XRD and it has three important parts such as an X-ray tube to generate the X-ray and emit a collimated X-ray beam, a goniometer to offer a place for the sample holding and arranging, and an array of X-ray detector that measured the intensity of X-rays diffracted from within the crystal. The schematic diagram of collecting data in the XRD is shown in Fig.2.2. As shown in the schematic diagram, the incident collimated beam that comes from the X-ray tube varies in the crystallographic plane of the used sample during irradiation. The diffracted X-rays from the sample converged on receiving slit which compiled these X-rays and sends them to the detector. Data is measured in *theta-2 theta* mode in the XRD operation. The sample holder and the detector are fitted at the θ axis and 2θ axis. XRD data is explained by the graph between intensities from various crystals and corresponding 2θ values which is referred to as a diffractogram [112].

In the present studies, the XRD data have been measured on an X-ray diffractometer model Bruker D8 Advance with Ni-filtered X-rays (CuK_{α} radiation) as presented in Fig.2.3. The XRD measurements have been performed in the 2θ range along with a step size of 0.02^{o}. The current and tube voltage has been kept at 40 mA and 40 kV respectively.

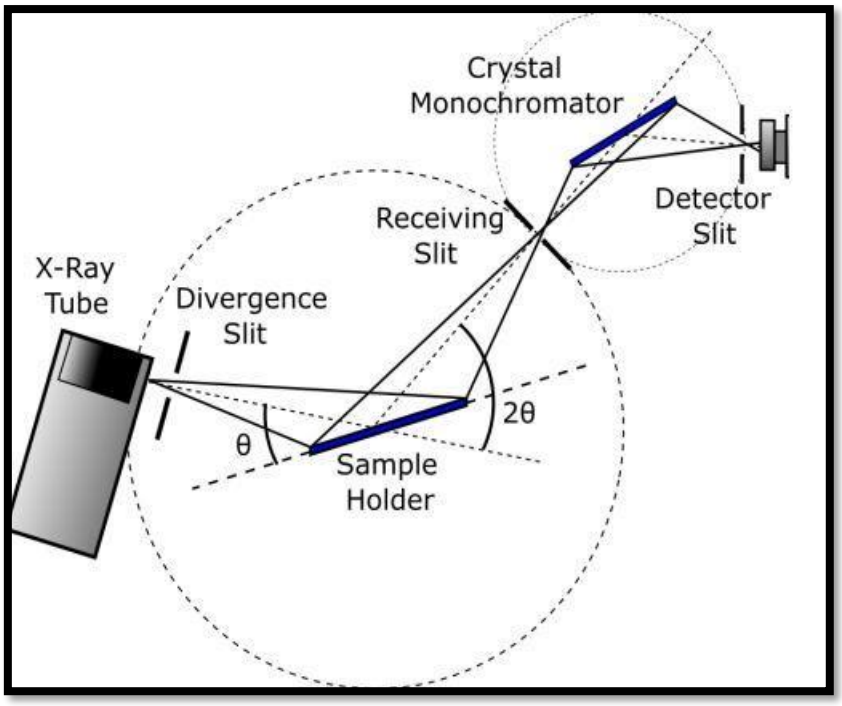

Fig. 2.2. The schematic diagram of collecting data in the XRD.

Fig. 2.3. Bruker D8 Advance X-ray diffraction machine.

2.3.2. Fourier transform infrared spectroscopy (FT-IR)

FT-IR spectroscopy is a tool that finds the absorption bands in the near-infrared (NIR) to far-infrared (FIR) spectral range. FT-IR spectroscopic analysis is one of the most complex types of spectroscopic methods, which compiles all wavelengths simultaneously. This method is used extensively for identifying vibrational and bonding groups in inorganic and organic materials. It might also categorize the atomic conformations of glass-forming network structures. The two types of vibrations that can exist in the molecules such as stretching and bending can be detected. The separation between two consecutive atoms changes in the stretching, whereas the angle among them remains unchanged. Nevertheless, the bending position of the atoms changes regarding the bond axis. As infrared radiation incident on the molecule, the vibration amplitude of a certain frequency has gone up correspondingly. Therefore, Infrared (IR) spectroscopy offers a way of finding the functional groups such as OH, NH_2, and C=O and NO_2 present them with the molecules. FT-IR instrument generally works on the Michelson Interferometer technique [113]. The schematic diagram that represents the first working of the FT-IR instrument is presented in Fig.2.4.

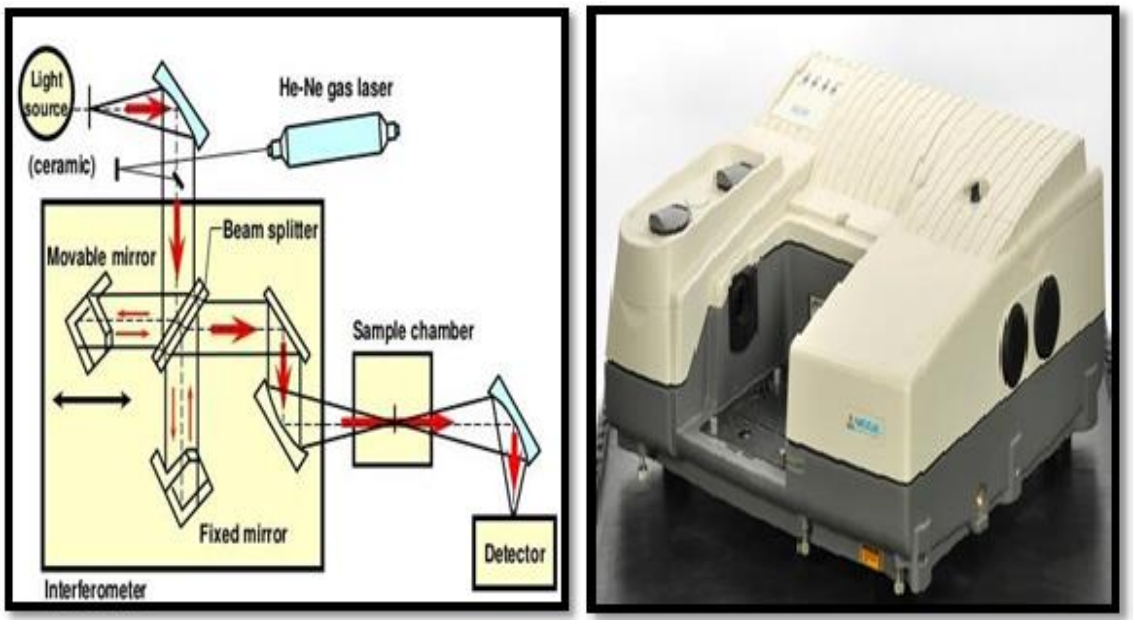

Fig. 2.4. Schematic representation of typical FT-IR setup and the instrument.

The interferometer technique consists of two mirrors, which are located at right angles to each other through the beam splitter. One of the mirrors is moving its position to a particular distance and the other is fixed, and the output beam turns into a result of the interference of the reflected beam from both mirrors. On passing the beam by the sample, it generates an interference pattern and via employing the Fourier transform method, the IR spectrum of the material has

been acquired. The FT-IR has been recorded via employing a Thermo Nicolet Nexus FT-IR spectrometer. For which the pellet was prepared by mixing an un-doped LiBiAlBSi glass in powder along with KBr and then compressed. The FT-IR Spectrometer for measurement is presented in Fig.2.4.

2.3.3. UV-VIS-NIR Spectroscopy

When EM radiation or light strikes any object, it experiences three different phenomena, i.e., reflection, absorption, and transmission of the EM radiation. In UV-VIS-NIR spectroscopy, the light source is excited on the sample in the UV to NIR range and the transmitted light is detected at the other end of the test sample. The radiation through the sample of fixed thickness provides information about the test sample because it is changed after interaction with the test sample. UV-VIS-NIR spectroscopy is a commonly existing non-destructive technique for measuring the optical characteristics of organic and inorganic materials. The Beer-Lambert law follows in this spectroscopy and this law states that "when a beam of monochromatic light passes through a solution of absorbing materials, the rate of reduction of the intensity of radiation with a thickness of the absorbing solution is directly proportional to the intensity of the incident radiation and the concentration of the solution." The expression for the absorbance (A) is as follows [2,6]:

$$A = log_{10}\left(\frac{I_t}{I_0}\right) \qquad (2.1)$$

in the above expression, I_t represents the transmitted light intensity and I_0 denotes the incident light intensity, respectively. The transmittance is denoted by T and defined as, $T=I/I_0$. When monochromatic light passes through a uniform sample, the intensity of transmitted light depends on the thickness of the sample. From the transmittance spectra, the value of the absorbance (A) may be evaluated by using the given relation below:

$$A = log_{10}\left(\frac{I}{I_0}\right) = log_{10}\left(\frac{1}{T}\right) \qquad (2.2)$$

In this case, the value of absorption coefficient $\alpha(\vartheta)$ under study has been estimated from the absorption data by the following equation [114]:

$$\alpha(\vartheta) = \frac{1}{d} ln\left(\frac{I_t}{I_0}\right) \qquad (2.3)$$

Where, d denotes the thickness of the test sample, factor $ln\left(\frac{I_t}{I_0}\right)$ signifies the absorbance and $\alpha(\vartheta)$ represents the absorption coefficient, respectively. In the present work, the optical absorption spectrum has been measured by employing the Jasco-770 spectrophotometer which has a spectral resolution of 0.2 nm. This instrument is fitted with a tungsten lamp for the VIS to NIR range and a deuterium lamp for the UV spectral range. The spectrophotometer is used to analyze the percentage of EM radiation being absorbed or transmitted in the UV-VIS-NIR spectral range.

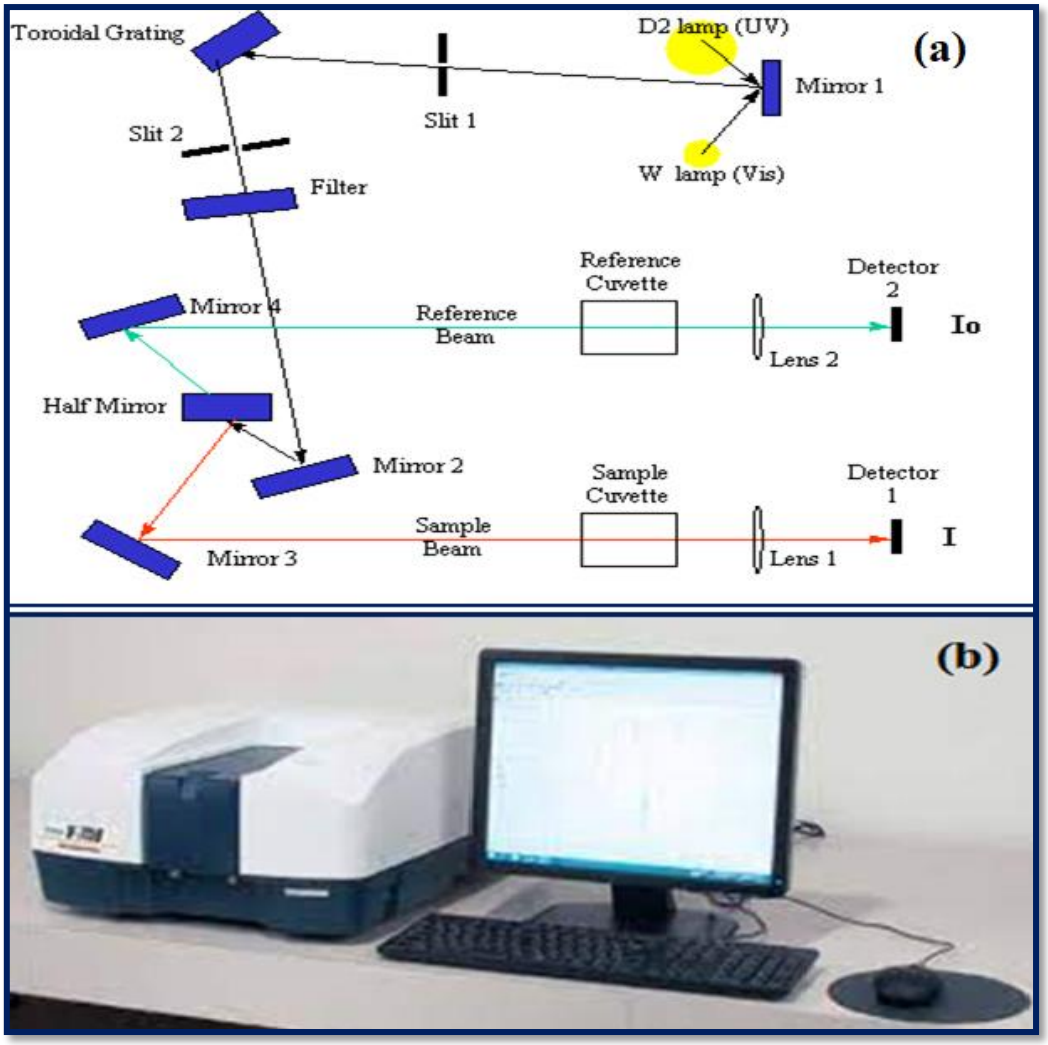

Fig. 2.5. (a) Schematic working diagram of UV-Vis spectrophotometer, (b) UV-VIS-NIR spectrometer (Jasco model V-770 instrument).

The schematic diagram of the UV-VIS-NIR spectrophotometer is presented in Fig.2.5(a). The monochromators transform the broad signals into separate wavelengths and optical filters are used to prevent the intersecting of various orders of the diffracted lines. The primary function of this tool was based on the double-beam method where one of the beams goes through the

sample and a second through the reference before it reaches the detector. Two detector photomultiplier tubes and lead sulphide (PbS) photoconductive cells are being employed for spectral measurement. Finally, the measured spectrum has been examined via the software to obtain the spectrum on a wavelength scale. The various RE^{3+} ions doped LiBiAlBSi glasses having suitable thicknesses have been taken for spectroscopic analysis. Fig. 2.5 (b) shows a UV-VIS-NIR spectrophotometer (Jasco V-770) used for recording the absorption spectral features related to the present thesis work.

2.3.4. Photoluminescence (PL) spectroscopy

PL spectroscopy is a powerful analytical and non-destructive method used for investigating the luminescent characteristics of inorganic and organic materials. The study of luminescent-based materials is characterized by their emission spectra, decay time measurement, and confocal images. PL spectroscopy explains the spontaneous emission of light from any substance when monitored with the appropriate excitation. This is a substantial contactless method used for explaining the electronic structure of the used materials. The incident light of a certain wavelength is targeted on the test sample, where it has been absorbed, and because of this, the electrons get excited at a higher level from the ground levels. When these electrons return to the ground level, the energy is released either in the form of heat recognized as the non-radiative process or in the form of light called the radiative process. The schematic diagram associated with the configuration of the spectrometer is illustrated in Fig.2.6.

i. Instrumentation and procedure: The PL spectrophotometer is mainly composed of three main parts, a sample holder, an excitation source and a detector. The excitation source must emit a continuous spectrum within the place of line spectra. Normally, Xenon (Xe) lamped is used as an excitation source because it is the source of relative continuum light output of intense intensity beyond 220 nm wavelength. The excitation monochromator is linked along with an assembly that permits only the designated wavelength of light which comprises the diffraction gratings with the greater aperture value to accumulate the most luminous excitation light, contributing to the greater sensitivity of the spectrofluorometer.

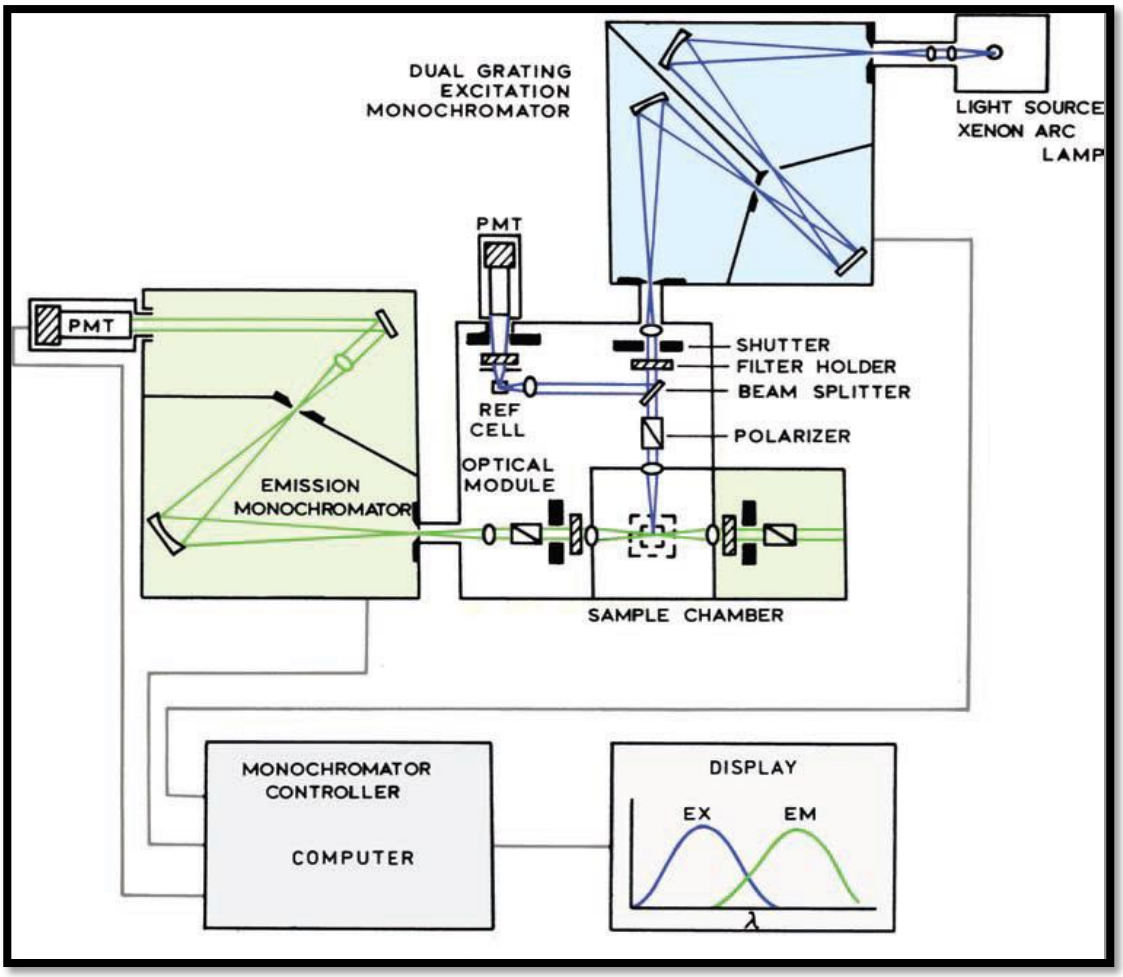

Fig. 2.6. Schematic diagram of a spectrofluorometer.

The specimen holder is placed with glass or phosphor samples that are being exposed with a light beam from the excitation monochromator and selectively emission monochromator brings together fluorescent light from the specimen and thereafter uses a photodetector as a photomultiplier tube (PMT) to assess the intensity of fluorescence. The PMT plays an important role in a significant spectral response. The non-uniformity in the radiation spectral of light from Xe-lamps and volatility of light emission lead to signal distortion and greater noise. To overcome this issue, a light-source compensation scheme is being employed. A PMT along with reference cells has been mounted in addition to the excitation monochromator to observe and modify that part of the excitation light and send the consequent signal return to the detector [6,95]. The PL (excitation and emission) spectra have been measured at ambient temperature with excitation and emission slit width of 0.1 nm and high-voltage PMT setup via choosing the appropriate wavelength scanning mode at a low, medium and high scanning speed. The decay analysis is conducted in time scanning mode and the pulsed excitation source

is used. For TD-PL studies, the sample temperature has been increased by a homemade heating device, and after that, PL spectral studies are carried out at numerous higher temperatures.

ii. Data analysis: Regarding the luminous materials, if an incident photon energy is equal to or more than that of the energy bandgap of the material which generates the excited charged carriers. During the relaxation, these excited carriers emit radiative photons. The obtained PL spectrum may be accumulated and evaluated which offers information on the optical transitions of electron states and recombination processes that involve radiative and non-radiative transitions inside the light-emitting materials. While PL spectral measurements, we may also modify additional external parameters such as the excitation power, pressure, temperature, and external perturbation like a magnetic or electric field. So, we might have more facts on the electronic bands and states.

When fitting the TR-PL data along with single, bi- or tri-exponential expression, we will be able to understand certain detailed information on the non-radiative relaxations. Therefore, TR-PL is an extremely powerful tool for analysing the non-radiative process in luminescent materials. For illumination applications, the thermal stability of the luminescent materials is a prerequisite which may be achieved by recording PL spectra at a higher temperature. Then, the setup is named TD-PL. Generally, the PL spectrum was not expected to vary at higher temperatures, but its intensity may be reduced owing to thermal quenching phenomena. For better luminescent material, the thermal quenching is supposed to be the minimum that represents the luminescent material has higher thermal stability at higher temperatures. In this work, the luminescent characteristics of the prepared luminescent material such as glasses are registered via using different spectrofluorophotometers as presented in Fig. 2.7 (a-c).

(a) JASCO FP 8300 spectrofluorophotometer

(b) Edinburgh FLSP920 Fluorescence lifetime spectrometer

(c) Ocean optics FLAME-S-XR1-ES spectrometer (for measuring the TD-PL)

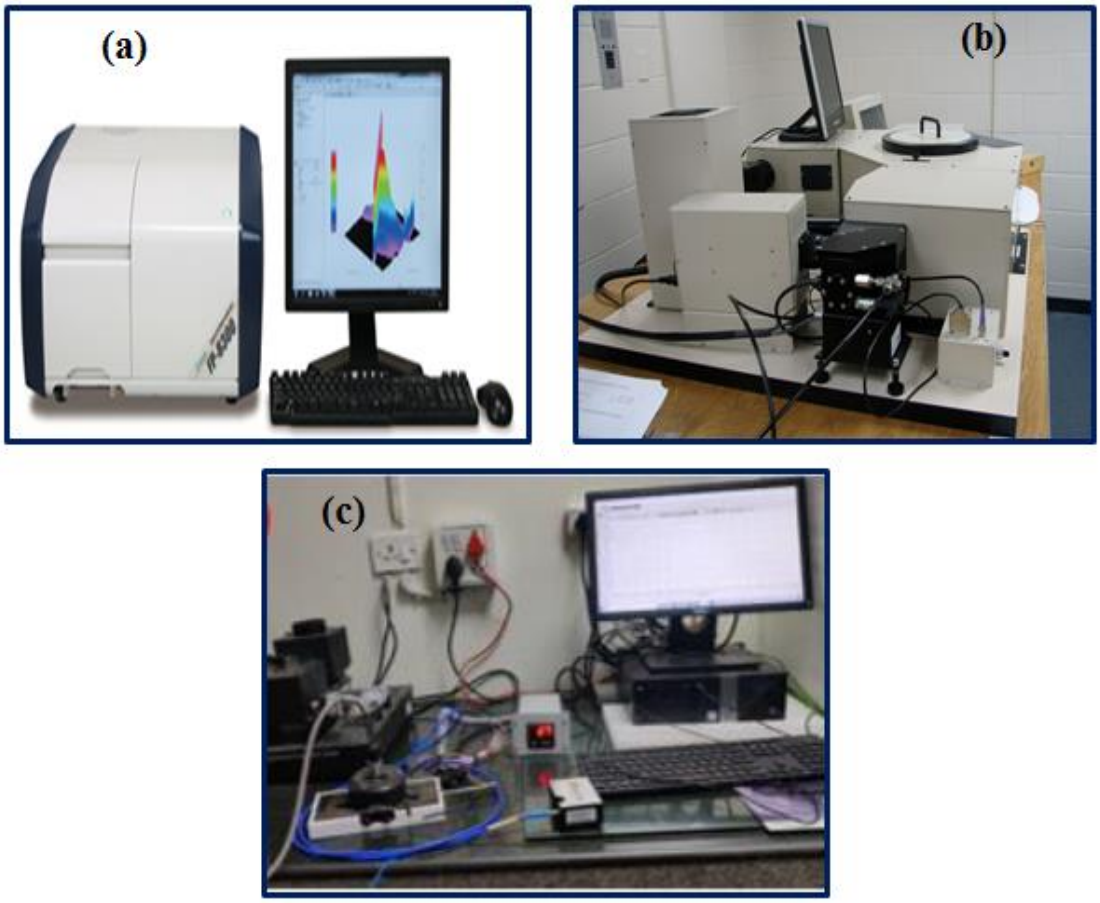

Fig. 2.7. (a) JASCO FP 8300 Spectrofluorophotometer (b) Edinburgh FLSP920 Fluorescence lifetime spectrometer and (c) Ocean optics FLAME-S-XR1-ES spectrometer (for measuring the TD-PL).

CHAPTER 3

Concentration-dependent reddish-orange photoluminescence studies of Sm^{3+} ions in borosilicate glasses

(The content of this chapter has been published in **"Optical Materials, 109 (2020) 110356")**

This chapter elucidates the concentration-dependent PL properties of samarium ions in LiBiAlBSi glasses using XRD, FT-IR, absorption, PL excitation, PL emission & PL decay to quantify the luminescence properties of the titled glasses. XRD and FT-IR spectral data ascertain the non-crystalline nature and vibrational energies in host glass respectively. The intense excitation band observed at 400 nm in the near UV region (under λ_{em}=600 nm) is employed to read the emission spectra. Under 400 nm intense excitation wavelength, the titled glasses show intense visible reddish-orange emission at 600 nm. From the emission spectra, it is observed that 0.5 mol% of Sm^{3+} ions in LiBiAlBSi glass is optimum for reddish-orange emission. The CIE coordinates estimated for LiBiAlBSi glasses are in good proximity with the reddish-orange emission coordinates specified by Nichia Corporation. Branching ratios, emission cross-sections, quantum efficiency, and CIE coordinates estimated finally reveal the aptness of the LiBiAlBSi glasses for reddish-orange optoelectronic device applications.

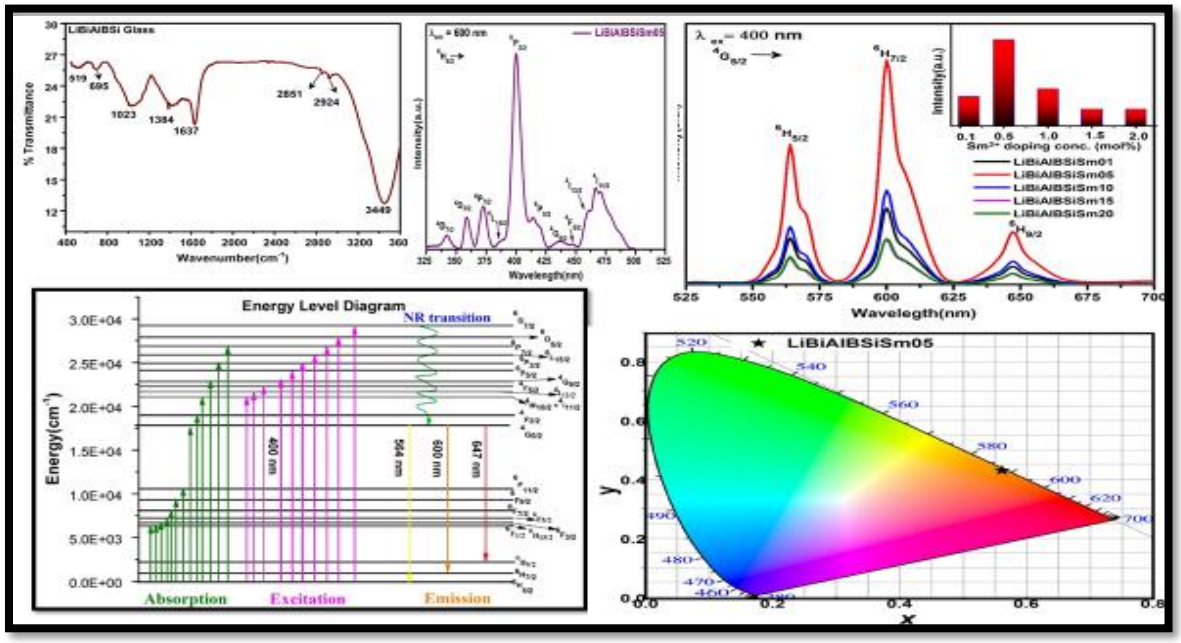

3.1. Introduction

The steady growth in the field of luminescence exhibited by RE-activated materials fascinated scientists because of their remarkable applications in up & down-converting lasers and photonics devices. The intra-transitions produced between 4f electronic states of RE ions in the host matrix play a substantial role in the aforementioned applications. Especially, RE-doped glasses have certain interesting features like broad inhomogeneous bandwidths, the capacity to accept high concentrations of RE ions, low production cost, good thermal stability and easy manufacturing process [40,63,87,115–119]. Glass lasers have high fluorescence lifetimes, high gain and can be easily made into the required shape. A host matrix with relatively low phonon energy can give high quantum efficiency by reducing the non-radiative relaxation process. Materials with low phonon energies are very much needed to design optical fiber amplifiers and lasers [63,110,120]. Borates and silicates are two well-known glass formers with scientific merits such as low melting point, a high degree of transparency, good RE ions solubility, high thermal stability, high field strength, less cation size, and high chemical durability. A combination of B_2O_3 and SiO_2 produces a significant glass network known as borosilicate glasses which have a lower thermal expansion coefficient, less melting temperatures, high softening temperature, good mechanical strength, high thermal stability, and are highly resistant to corrosion. Such characteristic features of borosilicate glasses may be helpful for many industrial applications like photovoltaic cells, displays, MEMs, etc. Borosilicate glasses possess relatively high phonon energy and cannot reduce non-radiative decay losses [22,30,52,59,121]. Nevertheless, such redundant and unwanted high phonon energies existing in borosilicate glasses can be curbed effectively by supplementing them suitably with heavy metal oxides (HMOs) such as bismuth oxide (Bi_2O_3) and lead oxide (PbO). High density & atomic numbers of HMOs added to a glass help them to act robustly in providing shielding to the radioactive radiations. A low concentration of PbO amends the network of borosilicate glasses due to lead structural unit [PbO_4] can interact strongly with the borate and silicate structural units. Further, increase in PbO content can make it partially play the role of a glass former. This dual role of lead can also enhance the radiative emission property of the host glass. At the same time, the use of lead creates several issues due to hazardous effects on the environment and health. Bi_2O_3 plays a similar kind of role in glasses hosts as PbO due to their identical electronic properties without hazardous effects. Glasses containing bismuth have higher infrared transparency, a large index of refraction, a large dielectric constant, and high density. As Bi^{3+} ions are prone to give low field strengths, stand-

alone, Bi_2O_3 can't portrait the role of network former. However, in the presence of B_2O_3, it may act as a glass former in borosilicate glasses and enhance the glass-forming ability [27,31,122,123]. Bismuth-containing glasses are also suitable for radiation shielding due to the high atomic number of bismuth [28]. Hence, borosilicate glasses containing bismuth may be considered the best choice to fabricate innovative photonic materials. In addition to the aforesaid HMO, aluminum trioxide (Al_2O_3) is also added to a borosilicate glass network as the tetrahedral and octahedral structural units of Al^{3+} ions present in Al_2O_3 help in enhancing the emission properties of borosilicate glass. Besides this, Al_2O_3 can act as a network modifier and improve the thermo-mechanical and chemical stability of the host glass to which it is added [34,124]. Lithium oxide (Li_2O) added to a borate network reduces the thermal expansion coefficient and increases the transition temperature. In the borosilicate glass system, the addition of Li_2O breaks B–O–B and Si-O-Si linkages and creates coordinated defects along with non-bridging oxygens (NBOs) ions and acts as a network modifier. The different structural units created due to the formation of NBOs in the parent glass network, therefore, the structural and optical properties being altered [35,36,40,125].

Several RE ions like Pr^{3+}, Eu^{3+}, Tb^{3+}, $Dy^{3+,}$ and Sm^{3+} have different energy states within the ultraviolet & visible part of the electromagnetic spectrum and can provide a wide spectrum of options for producing visible lasers and other optoelectronic devices. The shielding provided by $5s^2$ and $5p^6$ orbitals to the partially filled 4f shells makes the f-f electronic transitions of RE ions give sharp absorption as well as emission transitions. The line type of emission spectra produced by f-f transitions is solely responsible for the high luminescence efficiency possessed by RE ions doped into different host materials. Among many RE ions, Sm^{3+} ions can absorb ultraviolet light more efficiently and produce strong fluorescence in the visible reddish-orange region of the electromagnetic spectrum with relatively high quantum efficiency and emission cross-section.

Among all the visible fluorescence bands of samarium ions, the one pertaining to $^4G_{5/2} \rightarrow {}^6H_{7/2}$ transition mostly observed in the reddish-orange region (approximately at 600 nm) is relatively more intense with good emission cross-section. In fact, Sm^{3+} ions are important activators for different hosts owing to their capability to give reddish-orange emission having fantastic utility in lighting devices, high-density data storage devices, telecommunications, remote sensing, display devices, and in medical fields for the treatment of cancer [46,92,110,126–129]. In the present investigation, LiBiAlBSi glasses activated with samarium ions in different

concentrations were fabricated and dealt with absorption, emission, and decay studies to accord their prospective usage in optoelectronic devices.

3.2. Experimental

LiBiAlBSi glasses activated with Sm^{3+} ions with chemical composition $20Li_2CO_3$ -$7.5Bi_2O_3$ -(7.5-x) Al_2O_3 -$45H_3BO_3$ – $20SiO_2$: x Sm_2O_3 (where, x = 0.1, 0.5, 1.0, 1.5 and 2.0 mol %) were prepared by engaging melt quench method. For convenience, these glasses are abbreviated as LiBiAlBSiSm01, LiBiAlBSiSm05, LiBiAlBSiSm10, LiBiAlBSiSm15, and LiBiAlBSiSm20 according to Sm^{3+} ions concentration ranging from 0.1, 0.5, 1.0, 1.5 and 2.0 mol% respectively. The aforementioned constituent chemicals analar in grade are weighed as per the stoichiometric proportions mentioned above in batches of 7g each and ground until to get a smooth and homogeneous powder using agate mortar. Such smooth powders were heated at 1050 °C for 30 min in a silica crucible to get uniform melt. To get the same thickness as the glass samples, the melts were quenched by pouring the melts in between the pre-heated smooth brass molds. The as-prepared glasses were then annealed at 350 °C for 4 h to make them free from certain flaws like cracks and air bubbles.

The X-ray diffraction (XRD) spectrum was recorded by Bruker-Model D8 advance X-ray diffractometer of anode Cu (λ=1.5406 Å). The density for the titled glasses was measured by the Archimedes principle with water as an immersion liquid using a weighing balance equipped with specific gravity measurement (Shimadzu, AUW220) having the accuracy of ±0.01. The refractive index of the titled glasses was measured at λ = 650 nm (He–Ne laser) by using Brewster's method with an accuracy of ±0.01. The FT-IR spectrum was recorded with the help of a Thermo Nicolet Nexus FT-IR spectrometer. The necessary optical absorption spectral measurements were taken by a JASCO model V-670 UV-VIS-NIR spectrophotometer. The PL excitation & PL emission spectral readings were taken on Shimadzu RF-5301-PC spectrofluorophotometer having a Xenon lamp as a source of excitation. The PL decay spectral measurements were taken on Edinburgh FLSP900 having a Xenon flash lamp facility for excitation.

3.3. Results and discussion

3.3.1. X-ray diffraction spectral analysis

The XRD pattern recorded for LiBiAlBSi glass is depicted in Fig 3.1. It is not showing any sharp peaks indicating the absence of long-range order. The presence of short-range order (absence of long-range order) is one of the prime characteristic features of a non-crystalline material. A wide hump observed in the XRD spectrum supports the existence of shows short-range structural order, which is a characteristic feature of an amorphous/glassy material [130].

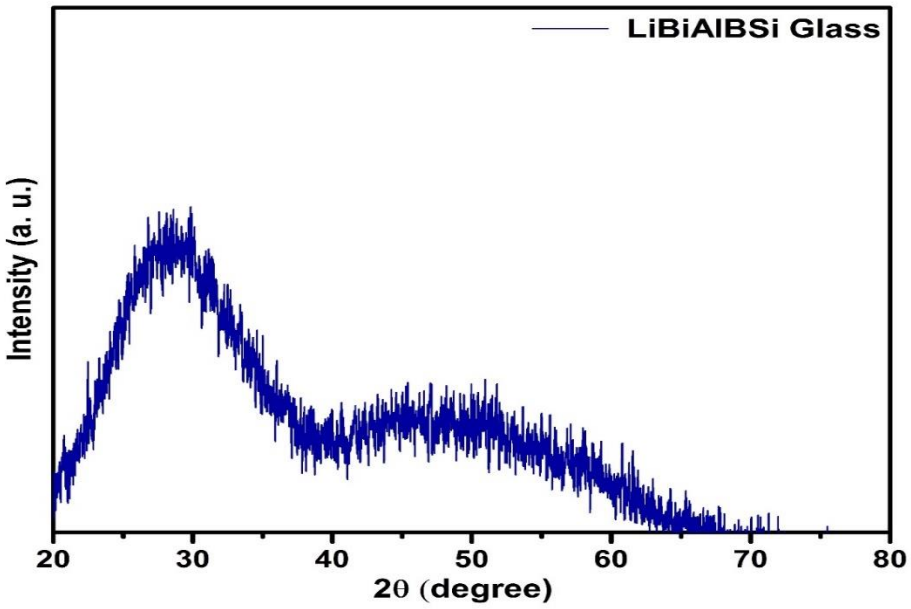

Fig. 3.1. XRD spectrum of an un-doped LiBiAlBSi glass.

3.3.2. Physical properties

Table 3.1 depicts different physical properties of the titled glasses evaluated by involving experimentally measured refractive index & densities by using appropriate equations available in the literature [91]. As per the data appearing in Table 3.1, it is conspicuous that, the physical properties are not the same for all the glasses under investigation. The variation observed in physical properties with Sm^{3+} ion content clearly indicates the change in the ligand environmental around Sm^{3+} ions. Refractive index and density are increasing with Sm^{3+} ions content in the titled glasses. The density value increasing with Sm^{3+} ions in the titled glasses may be due to the restoration of some of the Al^{3+} sites with Sm^{3+} sites. As per the data presented in Table 3.1, one set of properties such as average molecular weight, molar volume, mean atomic volume, field strengths, reflection losses, molar refraction, and optical dielectric constant are escalating their values in contrast to the other set of physical properties such as

inter-atomic distance, polaron radius and molecular electronic polarizability (α) with enhancement in Sm^{3+} ion content in them as prepared glasses.

Table 3.1. Physical properties of the Sm^{3+} doped LiBiAlBSi glasses.

Physical properties	**LiBiAlBSi Sm01**	**LiBiAlBSi Sm05**	**LiBiAlBSi Sm10**	**LiBiAlBSi Sm15**	**LiBiAlBSi Sm20**
Density, d ($g.cm^{-3}$)	2.2876	2.3021	2.3203	2.3384	2.3566
Refractive index, n	1.50336	1.50416	1.50516	1.50616	1.50716
Average molecular weight, M (g)	97.458	98.445	99.679	100.913	102.147
Molar volume, V_m (cm^3/mol)	40.60	42.76	42.95	43.15	43.45
Sm^{3+} ion concentration ($\times 10^{22}$ ions/cm^3)	0.141	0.704	1.401	2.0931	2.778
Mean atomic volume (g/cm^3/atom)	7.47	7.50	7.54	7.57	7.60
Dielectric constant(ϵ)	2.260	2.262	2.265	2.2685	2.272
Optical Dielectric constant (ϵ-1)	1.260	1.262	1.265	1.2685	1.272
Reflection losses, R (%)	4.043	4.053	4.066	4.079	4.091
Molar refraction, Rm (cm^{-3})	12.60	12.66	12.75	12.82	12.90
Polaron radius, r_p (Å)	3.59	2.10	1.67	1.46	1.33
Inter-atomic distance, r_i (Å)	8.910	5.217	4.147	3.628	3.301
Molecular electronic polarisability α (10^{-23} cm^3)	4.998	1.004	0.5055	0.3391	0.2559
Field Strength, F (10^{15} cm^{-2})	2.327	6.788	10.742	14.035	16.952

An increase in density and thereby increase in molar volume with Sm^{3+} ions content is an indication for the production of non-bridging oxygen (NBOs) content in the titled glasses. The reason for the production of NBOs with Sm^{3+} ions content in the titled glasses may be due to the occupancy of interstitial spaces with Sm_2O_3 content and glass network expansion produced thereby [131]. Molecular electronic polarizability of a material plays a vital role in deciding the optical & dielectric properties and chemical stability as well. The chemical stability of material will be more if molecular electronic polarizability is less and vice versa. As shown in Table 3.1, it is evident that the glasses prepared for the present investigation are chemically more stable as they are showing relatively lesser molecular electronic polarizability values. Another interesting physical property of a glassy material which decides the RE ions solubility is field strength values. Relatively less field strengths indicate a high capacity of RE ions solubility in the titled glasses [87].

3.3.3. FT-IR spectral analysis

In the process of knowing the network structural units and vibrational energies present in the LiBiAlBSi glass, the FT-IR spectrograph has been recorded in the spectral range of 400-3600 cm^{-1} and is shown in Fig. 3.2. Different functional groups along with their vibrational energies witnessed in Fig. 3.2 are given in Table 3.2. As shown in Fig. 3.2, the host glass is having eight infrared functional groups located at 519, 695, 1023, 1384, 1637, 2851, 2924, and 3449 cm^{-1}. The broadness observed in bands may be due to the combination of a high degree of degeneracy produced in vibrational states, along with mechanical scattering and thermal broadening [127]. A broad band observed at wavenumber 3449 cm^{-1} may be due to the stretching vibration of O-H produced by hydroxyl groups. Another band reported at around 2924 cm^{-1} may be because of hydrogen bonding in the titled glass. A band detected at 2851 cm^{-1} shows the existence of organic contaminants [132]. The bands observed at around 1637 and 1384 cm^{-1} may be due to stretching vibrations of the B–O bond produced by BO_3 borate group units [127]. A band positioned at 1023 cm^{-1} maybe because of the stretching vibration produced by BO_4 di-borate groups network [133]. The bands at wavenumbers 695 cm^{-1} and 519 cm^{-1} indicating bending of B-O-B linkages in borate network groups and Bi-O bending of BiO_6 units respectively [134].

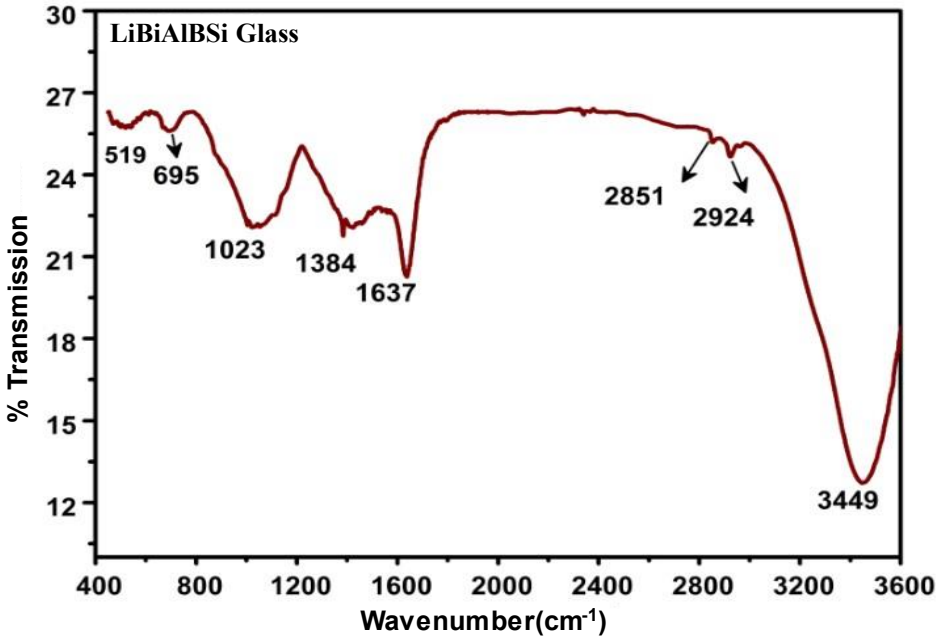

Fig. 3.2. FT-IR spectrum of an un-doped LiBiAlBSi glass.

Table 3.2. The FT-IR band positions and their assignments in an un-doped LiBiAlBSi glass.

Band Positions (cm^{-1})	Assignments
519	Bi-O bending vibrations in the BiO_6 units
695	Bending B-O-B linkages in borate network
1023	Stretching of various borate rings in BO_4 groups
1384	B–O stretching containing planar 6-member borate groups
1637	Stretching vibrations of BO_3 triangles
2851	Existence of organic contaminants
2924	Hydrogen bonding
3449	Hydroxyl groups of O–H stretching vibrations

3.3.4. Absorption spectral analysis

Absorption spectra for Sm^{3+} ions in LiBiAlBSi glasses were recorded at ambient temperature in the wavelength range from 350 to 1800 nm. Fig. 3.3 shows the absorption spectrum recorded for 2.0 mol% Sm^{3+} ions in LiBiAlBSi glass. All the titled glasses are showing 13 bands observed in UV, Visible, and NIR regions at 372, 400, 437, 474, 527, 562, 942, 1077, 1225, 1371, 1472, 1525, and 1587 nm pertaining to the transitions observed from $^6H_{5/2}$ ground state to different excited states as shown in Fig. 3.3. Strong absorption caused by the host glass in UV & visible regions resulted in missing few absorption peaks in the as investigated glasses. Spectral identification in the present work has been done as per the literature protocols [135]. In the present investigation, the absorption transitions observed due to electric dipole and magnetic dipole-induced interactions are in accordance with the selection rules $|\Delta J| \leq 6$ & $|\Delta J| = 0, \pm 1$ respectively [40]. The shielding produced by 5s & 5p shells to 4f electrons results in sharp and intense absorption bands in the NIR region in all the titled glasses. On the other hand, the overlap produced between $^{2S+1}L_J$ levels in UV & Vis region results in less intensity for the absorption peaks in that region.

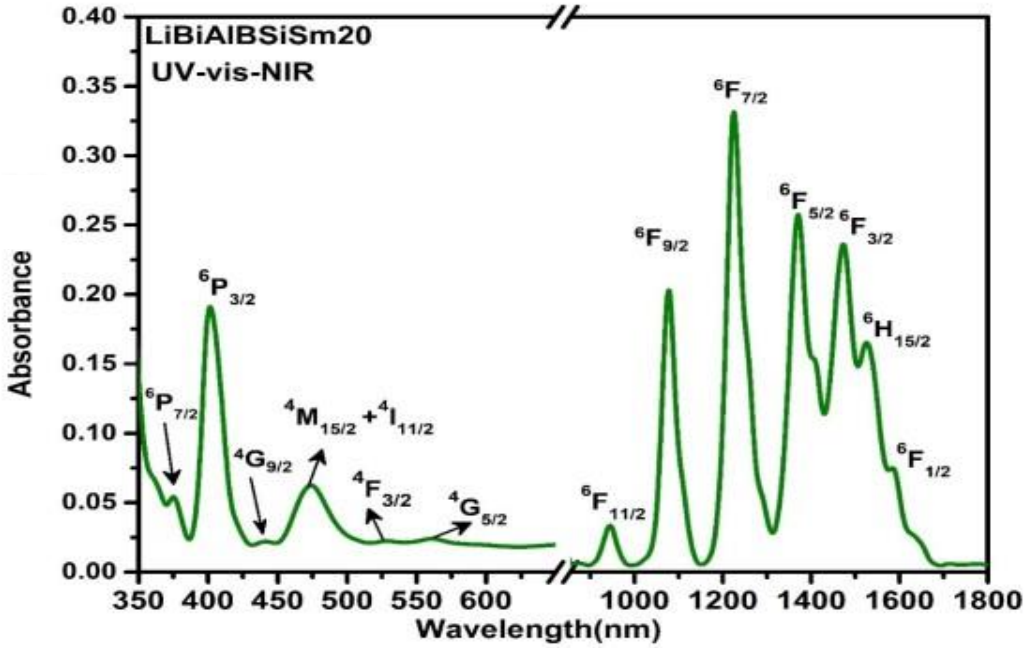

Fig. 3.3. The absorption spectrum of 2.0 mol% of Sm^{3+} ions doped LiBiAlBSi glass.

The partly filled f-shells present in RE ions cause an effect called the nephelauxetic effect, useful to get the information pertaining to the covalency existing between RE ions and oxygen ligands. The ligand field environment existing in the host matrix deforms the 4f electronic orbits of the doped RE ions. The energy level structure of RE ions gets contracts because of the overlapping produced between its 4f orbits and oxygen orbits. As a consequence, there will be a wavelength shift. The nephelauxetic ratio (β) and bonding parameters (δ) are mainly estimated to understand the bonding nature existing between RE ions doped in the host matrix and oxygen ligands present in the same host. β and δ were evaluated by using the given Eqn. no. 1.1, and 1.2 in chapter 1 [91]. The β values estimated for all the LiBiAlBSi glasses having Sm^{3+} ions concentration from 0.1 to 2.0 mol% are 0.993375, 1.01001, 1.010235, 1.010247 and 1.01093 respectively. The estimated values of "δ" for glasses LiBiAlBSiSm01 to LiBiAlBSiSm20 are 0.6669, -0.9918, -1.0131, -1.0143 and -1.0188 respectively. A gradual increase in negative values obtained in the present work indicates the increasing ionic nature of bonding between Sm^{3+} ions and oxygen ligands.

3.3.5. Oscillator strengths and Judd-Ofelt analysis

The values of f_{exp}, f_{cal} and δ_{rms} were estimated by using the given equation in chapter 1 and presented in Table 3.3. Relatively less δ_{rms} values appearing in Table 3.3 sounds the validity and aptness of J-O theory and subsequently evaluated J-O parameters essential to estimate various radiative properties of the titled glasses. According to Jorgensen and Judd [42,81], the

intensity of few absorption bands is the host environment-sensitive and are called hypersensitive transitions that follow the selection rules $|\Delta S| = 0$, $|\Delta L| \leq 2$, $|\Delta J| \leq 2$ [81,93]. According to Judd [40], among the three square reduced matrix elements, hypersensitive transitions mainly depend on $||U^2||$ and correspondingly Ω_2 parameter only plays a pivotal role in fixing the radiative properties of the host matrix. As shown in Fig. 3.3 and data given in Table 3.3, it is conspicuous that, the intensity (Fig.3.3) and oscillator strength (Table 3.3) values pertaining to $^6H_{5/2} \rightarrow {}^6P_{3/2}$ and $^6H_{5/2} \rightarrow {}^6F_{7/2}$ transitions are maximum as they are hypersensitive in nature. The quantum efficiency of a luminescent material mainly depends on the excited-state dynamics process involved in the energy states of doped RE ions. The excited-state dynamic process in turn depends on the J-O intensity parameters of RE ions.

Table 3.3. Experimental (f_{exp} x 10^{-6}), calculated (f_{cal} x 10^{-6}) oscillator strengths and r.m.s deviation (δ_{rms} x10^{-6}) of Sm^{3+} ions in LiBiAlBSi glasses.

Transition from $^6H_{5/2}$	**LiBiAlBSiSm01**		**LiBiAlBSiSm05**		**LiBiAlBSiSm10**		**LiBiAlBSiSm15**		**LiBiAlBSiSm20**	
Peaks	f_{exp}	f_{cal}	f_{exp}	f_{cal}	f_{exp}	f_{cal}	f_{exp}	f_{cal}	f_{exp}	f_{cal}
$^6P_{7/2}$	0.88	3.48	0.66	4.23	0.95	3.21	0.07	2.73	0.31	2.69
$^6P_{3/2}$	1.54	6.34	8.10	5.05	6.58	3.89	3.04	2.55	10.43	3.74
$^4G_{9/2}$	5.36	0.15	0.12	0.16	0.21	0.12	0.77	0.10	0.07	0.10
$^4M_{15/2}$ $+^4I_{11/2}$	0.91	0.76	3.15	0.90	2.95	0.68	2.98	0.59	2.49	0.58
$^4F_{3/2}$	0.70	-0.0002	0.79	0.00	0.11	0.0001	0.04	-0.0001	0.08	-0.001
$^4G_{5/2}$	1.91	0.02	0.28	0.02	0.16	0.012	0.06	0.008	0.07	0.11
$^6F_{11/2}$	1.81	0.96	0.68	1.13	1.91	0.86	0.87	0.74	0.61	0.73
$^6F_{9/2}$	3.87	5.80	6.49	6.74	4.91	5.13	4.13	4.39	4.8	4.39
$^6F_{7/2}$	9.27	7.88	8.99	8.63	6.7	6.57	5.74	5.47	5.52	5.71
$^6F_{5/2}$	3.6	3.14	1.80	2.51	1.39	1.95	1.09	1.27	0.79	1.81
$^6F_{3/2}$	1.09	1.37	1.19	1.12	0.98	0.89	0.52	0.55	0.47	0.63
$^6H_{15/2}$	0.24	0.05	0.21	0.05	0.17	0.044	0.09	0.04	0.07	0.04
$^6F_{1/2}$	0.05	-0.04	0.50	-0.004	0.05	0.03	0.02	-0.02	0.01	-0.25
δ_{rms} x 10^{-6}	±2.286		±1.488		±1.21		±1.025		±2.04	

Table 3.4 gives the J-O intensity parameters along with the published data for other glasses. As per the data given in Table 3.4, all the investigated glasses are following the same trend in J-O parameters ($\Omega_6 > \Omega_4 > \Omega_2$) and are in consistent with literature values [136,137]. The Ω_2 parameter reveals the information pertaining to the covalency of the metal-ligand (Sm-O) bond [40,94]. As given in Table 3.4, an increase in Sm^{3+} ions concentration in LiBiAlBSi glass changes the Ω_2 value. In the present investigation, Ω_2 getting lower values indicates the asymmetric nature of ion sites produced because of the predominant ionic bonding nature between metal and ligand (Sm-O). This is in consonance with the bonding nature estimated by the nephelauxetic effect.

Table 3.4. Judd-Ofelt Parameters (Ω_λ x $10^{-20}cm^2$) of Sm^{3+} ions in LiBiAlBSi glasses along with reported values in literature.

Glass System	Ω_2	Ω_4	Ω_6	Trend	References
LiBiAlBSiSm01	0.14	6.26	7.17	$\Omega_6 > \Omega_4 > \Omega_2$	present work
LiBiAlBSiSm05	-0.13	5.00	8.47	$\Omega_6 > \Omega_4 > \Omega_2$	present work
LiBiAlBSiSm10	0.09	3.85	6.42	$\Omega_6 > \Omega_4 > \Omega_2$	present work
LiBiAlBSiSm15	-0.08	2.52	5.56	$\Omega_6 > \Omega_4 > \Omega_2$	present work
LiBiAlBSiSm20	-0.08	3.70	5.46	$\Omega_6 > \Omega_4 > \Omega_2$	present work
PPfKANSm1.0	1.60	5.20	5.81	$\Omega_6 > \Omega_4 > \Omega_2$	[93]
NaZnBS	0.55	9.68	9.77	$\Omega_6 > \Omega_4 > \Omega_2$	[136]

3.3.6. Excitation and emission spectral analysis

The excitation spectrum recorded for 0.5 mol% of Sm^{3+} ions doped LiBiAlBSi glass is shown in Fig. 3.4. It shows 10 sharp peaks at 342, 358, 372, 386, 400, 414, 437, 448, 460, and 467 nm pertaining to various excited states arising from $^6H_{5/2}$ ground state as shown in Fig.3.4 [110]. It can be noticed that, among all the 10 excitation peaks, the one observed at 400 nm is relatively more intense and is employed to read the emission data from the titled glasses. Under 400 nm excitation, all the glasses under investigation show emission spectra with three peaks at 564 (yellow), 600 (reddish-orange), and 647 nm (red) as shown in Fig. 3.5. Among the three emission transitions, one observed at 600 nm is relatively more intense. The intensity of emission peaks is increasing with Sm^{3+} ions content up to 0.5 mol % and beyond diminishing showing concentration quenching produced by the cross-relaxation energy transfer process between one activator center to another [87]. The inset in Fig. 3.5 shows how the intensity of the reddish-orange emission peak changes with Sm^{3+} ions concentration in the titled glass.

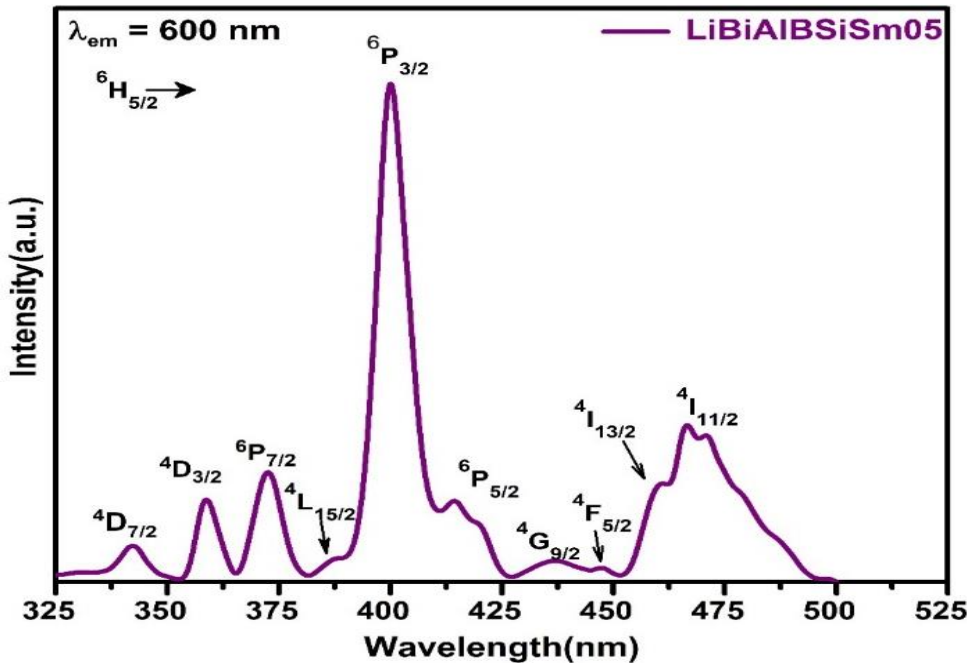

Fig. 3.4. Excitation spectrum of 0.5 mol% of Sm^{3+} ions doped LiBiAlBSi glass.

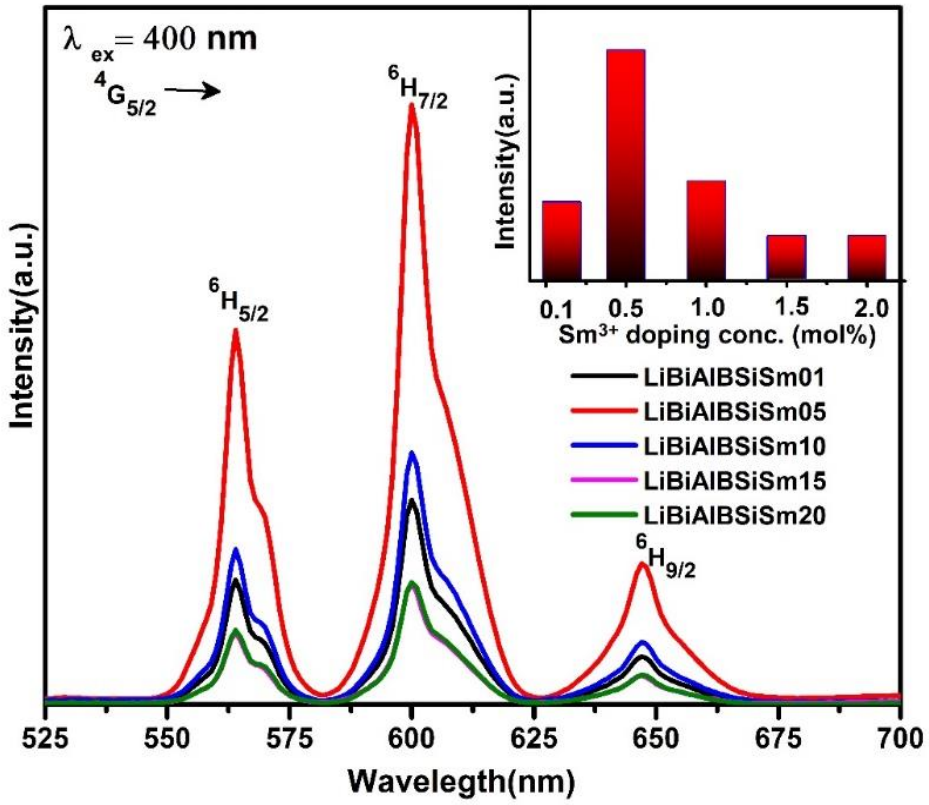

Fig. 3.5. Emission spectra of Sm^{3+} ions doped LiBiAlBSi glasses.

The symmetry nature of 4f ions situated in a local environment can be understood by taking the ratio for magnetic dipole ($^4G_{5/2} \rightarrow {}^6H_{5/2}$) to electric dipole ($^4G_{5/2} \rightarrow {}^6H_{9/2}$) transitions. In the present investigation, the intensity of $^4G_{5/2} \rightarrow {}^6H_{5/2}$ transition is more than the third transition peak $^4G_{5/2} \rightarrow {}^6H_{9/2}$ indicating lower asymmetric for 4f ions situated in the as-prepared glasses [138,139].

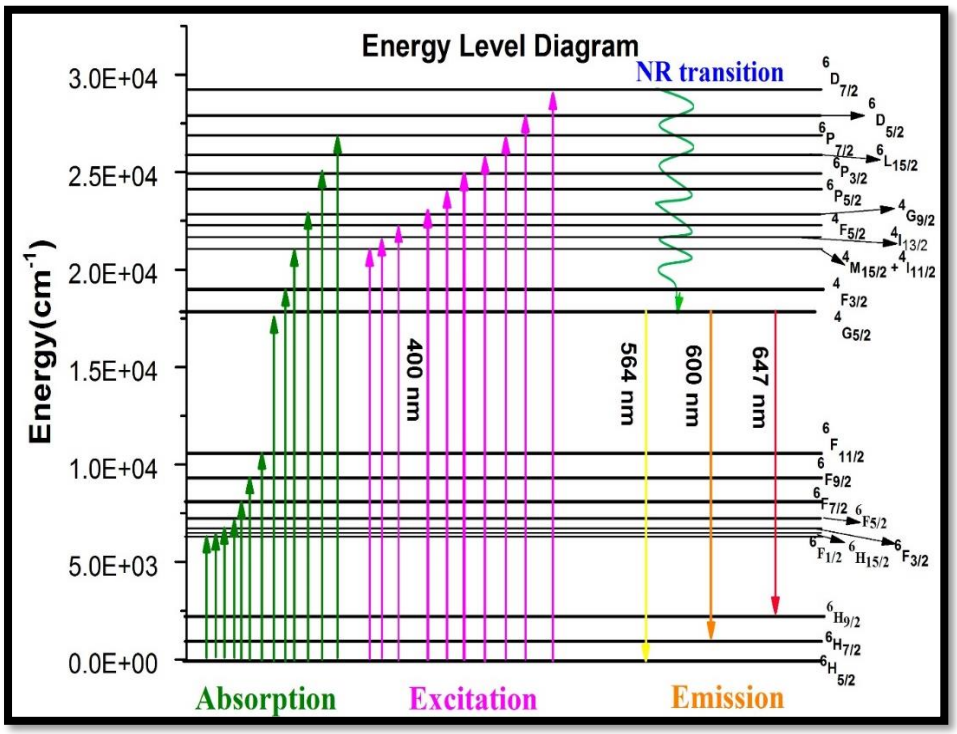

Fig. 3.6. Energy level diagram of Sm^{3+} ions doped LiBiAlBSi glasses with absorption, excitation and emission mechanisms.

Fig. 3.6 clearly shows the absorption, excitation, and emission process involved in the investigated glasses. When 400 nm photons have impinged on the glasses, the Sm^{3+} ions residing in the $^6H_{5/2}$ ground state absorb it and get stimulated to reach several higher energy states above the $^4G_{5/2}$ meta-stable state of Sm^{3+} ions as shown in Fig.3.6. As the energy gap existing between higher energy states above $^4G_{5/2}$ state of Sm^{3+} ions are very small, such exciting Sm^{3+} ions de-excites immediately to $^4G_{5/2}$ energy state through non-radiative decay process as shown in Fig.3.6. On the other hand, since the energy gap existing between $^4G_{5/2}$ & $^6F_{11/2}$ levels is large enough, the multi-photon relaxation process cannot be initiated between them. This ultimately leads to radiative emission from the $^4G_{5/2}$ meta-stable state to $^6H_{5/2}$, $^6H_{7/2}$ and $^6H_{9/2}$ lower levels resulting in the emission spectra shown in Fig.3.5.

3.3.7. Radiative properties

In the backdrop of J-O theory, the synergy of absorption & emission spectral data facilitates the estimation of various radiative properties such as A_R, A_T, τ_R and β_R by using the Eqn. no. 1.11 to 1.14 that are given in chapter 1 for Sm^{3+} ions in LiBiAlBSi glasses and are depicted in Table 3.5 [140]. From Table 3.5, it can be noticed that the A_R value is relatively higher for the $^4G_{5/2} \rightarrow {}^6H_{7/2}$ transition than other the remaining two. The value of β_R should be ≥ 0.5 for a potential laser transition [141]. The β_R value calculated for $^4G_{5/2} \rightarrow {}^6H_{7/2}$ transition for all the titled glasses is greater than 0.50 indicating the richness of the as-prepared glasses for laser applications. Among all, the one with 0.5mol% of Sm^{3+} ions show the relatively highest β_R value (56.59%) indicating its superiority for laser applications. It is well known that the σ_{se} at the desired wavelength should be relatively high for high gain laser applications and estimated using the eqn. no. 1.15 given in chapter 1. The vital radiative parameters such as $\Delta\lambda_P$, σ_{se}, optical gain parameters (σ_{se} x τ_R), and gain band widths (σ_{se} x $\Delta\lambda_P$) calculated for the observed emission transitions $^4G_{5/2} \rightarrow {}^6H_J$ (J= 5/2, 7/2, 9/2) are given in Tables 3.6. The β_{exp} values are estimated using the areas of Sm^{3+} emission bands are also given in Table 3.6 along with β_R values. The β_{exp} values are in consonance with β_R values as shown in Table 3.6. From the data appearing in Table 3.6, it is conspicuous that, all the aforementioned radiative properties are relatively high for LiBiAlBSiSm05 glass pertaining to $^4G_{5/2} \rightarrow {}^6H_{7/2}$ reddish-orange transition. This allows us to contemplate that, LiBiAlBSiSm05 glass is the most suitable candidate to fabricate reddish-orange lasers as well as visible fiber amplifiers.

Table 3.5. Transition probability (A_R) (s^{-1}), radiative branching ratio (β_R), total transition probability (A_T) (s^{-1}) and radiative lifetime (τ_R) (μs) for the observed emission transitions of Sm^{3+} ions in LiBiAlBSi glasses.

Transition	A_R	β_R	A_T	τ_R
LiBiAlBSiSm01				
$^4G_{5/2} \rightarrow {}^6H_{5/2}$	20.75	0.0539	385.37	2594
$^4G_{5/2} \rightarrow {}^6H_{7/2}$	208.72	0.5416		
$^4G_{5/2} \rightarrow {}^6H_{9/2}$	77.46	0 .2010		
LiBiAlBSiSm05				
$^4G_{5/2} \rightarrow {}^6H_{5/2}$	19.26	0.0517	372.38	2685
$^4G_{5/2} \rightarrow {}^6H_{7/2}$	210.74	0.5659		
$^4G_{5/2} \rightarrow {}^6H_{9/2}$	67.99	0.1826		
LiBiAlBSiSm10				
$^4G_{5/2} \rightarrow {}^6H_{5/2}$	17.98	0.0610	294.69	3393
$^4G_{5/2} \rightarrow {}^6H_{7/2}$	163.71	0.5555		
$^4G_{5/2} \rightarrow {}^6H_{9/2}$	53.56	0.1817		
LiBiAlBSiSm15				
$^4G_{5/2} \rightarrow {}^6H_{5/2}$	16.40	0.0700	285.67	3500
$^4G_{5/2} \rightarrow {}^6H_{7/2}$	131.71	0.5622		
$^4G_{5/2} \rightarrow {}^6H_{9/2}$	39.03	0.1666		
LiBiAlBSiSm20				
$^4G_{5/2} \rightarrow {}^6H_{5/2}$	18.28	0.0640	234.28	4268
$^4G_{5/2} \rightarrow {}^6H_{7/2}$	147.73	0.5171		
$^4G_{5/2} \rightarrow {}^6H_{9/2}$	61.21	0.2143		

Table 3.6. Emission peak wavelength λ_p (nm), effective bandwidths ($\Delta\lambda_p$) (nm), measured and experimental branching ratios (β_R & βexp), stimulated emission cross-sections (σ_{sc}) (cm^2), gain bandwidth (σ_{sc} x $\Delta\lambda$p) (cm^3) and optical gain parameter (σ_{sc} x τ_R) (cm^2 s) for the emission transitions of Sm^{3+} ions in LiBiAlBSi glasses.

Spectral parameters	LiBiAlBSiSm01	LiBiAlBSiSm05	LiBiAlBSiSm10	LiBiAlBSiSm15	LiBiAlBSiSm20
λ_p = 564 nm	$^4G_{5/2}$ → $^6H_{5/2}$				
$\Delta\lambda$p	9.90	9.68	9.83	10.49	10.14
β_R	0.0539	0.0517	0.061	0.070	0.064
β_{exp}	0.272	0.266	0.273	0.268	0.272
σ_{se}(x 10^{-22})	1.25	1.18	1.09	0.929	1.07
σ_{se} x $\Delta\lambda$p (x 10^{-28})	1.237	1.147	1.069	0.974	0.108
σ_{se} x τ_R (x 10^{-25})	3.355	3.077	3.688	3.250	4.562
λ_p = 600 nm	$^4G_{5/2}$ → $^6H_{7/2}$				
$\Delta\lambda$p	12.66	12.76	12.50	13.73	12.92
β_R	0.5416	0.5659	0.5555	0.5622	0.5171
β_{exp}	0.572	0.5763	0.5682	0.563	0.571
σ_{se}(x 10^{-22})	12.26	12.60	9.97	7.63	8.69
σ_{se} x $\Delta\lambda$p (x 10^{-28})	15.942	16.075	12.471	10.020	11.224
σ_{se} x τ_R (x 10^{-25})	33.804	32.672	33.842	26.711	37.078
λ_p = 647 nm	$^4G_{5/2}$ → $^6H_{7/2}$				
$\Delta\lambda$p	14.76	14.91	14.44	16.039	14.588
β_R	0.2010	0.1826	0.1817	0.1666	0.2143
β_{exp}	0.155	0.157	0.158	0.168	0.157
σ_{se}(x 10^{-22})	5.42	4.76	3.82	2.50	4.31
σ_{se} x $\Delta\lambda$p (x 10^{-28})	7.999	7.012	5.517	4.015	6.288
σ_{se} x τ_R (x 10^{-25})	14.551	12.208	12.963	8.761	18.397

3.3.8. Decay analysis and energy transfer mechanism

The PL decay curves give the information pertaining to the excited states dynamics and facilitate getting the experimental lifetime values of excited states of RE ions in a host matrix [110]. Under 400 nm excitation wavelength, the PL decay curves recorded for the intense visible reddish- orange emission (600 nm) for all the titled glasses are shown in Fig. 3.7. All the decay curves are showing single exponential nature and the experimental lifetimes (τ_{exp}) estimated using a single exponential function are given in Table 3.7 along with radiative

lifetimes (τ_R). The τ_{exp} and τ_R (shown in parenthesis) values are found to be 2521μs (2695μs), 2026 μs (2685μs,) 1770 μs (3393 μs), 1225 μs (3500 μs), and 1185μs (4268 μs) for LiBiAlBSiSm01, LiBiAlBSiSm05, LiBiAlBSiSm10, LiBiAlBSiSm15, and LiBiAlBSiSm20 glasses respectively. As Sm^{3+} ion content increases, the τ_{exp} values for the $^4G_{5/2}$ level are decreasing because of the concentration quenching phenomenon. This is also in consonance with the emission spectra shown in Fig.3.5. The quenching effect with an increase in Sm^{3+} ion content in the present investigation is because of the cross-relaxation energy transfer process (but not through multi-photon relaxation) produced between Sm^{3+} ions through non-radiative emission process [132,142]. The best possible cross-relaxation (CR) channels responsible for the quenching phenomenon are depicted in Fig. 3.8. The same cross-relaxation energy transfer process shown in Fig. 3.8 is also responsible for getting lower values for τ_{exp} than τ_R shown in Table 3.7.

Correspondingly, the non-radiative decay rate (W_{NR}) that is linked with the radiative and experimental lifetimes can be estimated by using the eqn. no. 1.22 given in chapter 1. The W_{NR} (s^{-1}) values calculated for the $^4G_{5/2}$ level are found to be 24, 108, 269, 530 and 608 for LiBiAlBSiSm01, LiBiAlBSiSm05, LiBiAlBSiSm10, LiBiAlBSiSm15, and LiBiAlBSiSm20 glasses respectively. The difference between τ_{exp} and τ_R is responsible for getting relatively higher W_{NR} values.

The ratio for light intensity emitted to the light intensity absorbed by a luminescent material is customarily called quantum efficiency (η) of that material and can be assessed by using the eqn. no. 1.21 given in chapter 1. The η depends on the concentration of RE ions, radiative transition probabilities, emission cross-section, ligand fields generated by network modifiers, and lifetimes of the excited states. Table 3.7 shows the values of τ_{exp}, τ_R, W_{NR}, and η obtained for the $^4G_{5/2} \rightarrow {}^6H_{7/2}$ transition of Sm^{3+} ions in the titled glasses [143,144]. The quantum efficiency also gets reduced because of the cross-relaxation energy transfer process initiated between the donors (excited Sm^{3+} ions) and acceptors (ground state Sm^{3+} ions). The values of σ_{se} and η obtained for LiBiAlBSiSm05 glass have been compared with other reported values in literature in Table 3.8 [17,46,90,92,143].

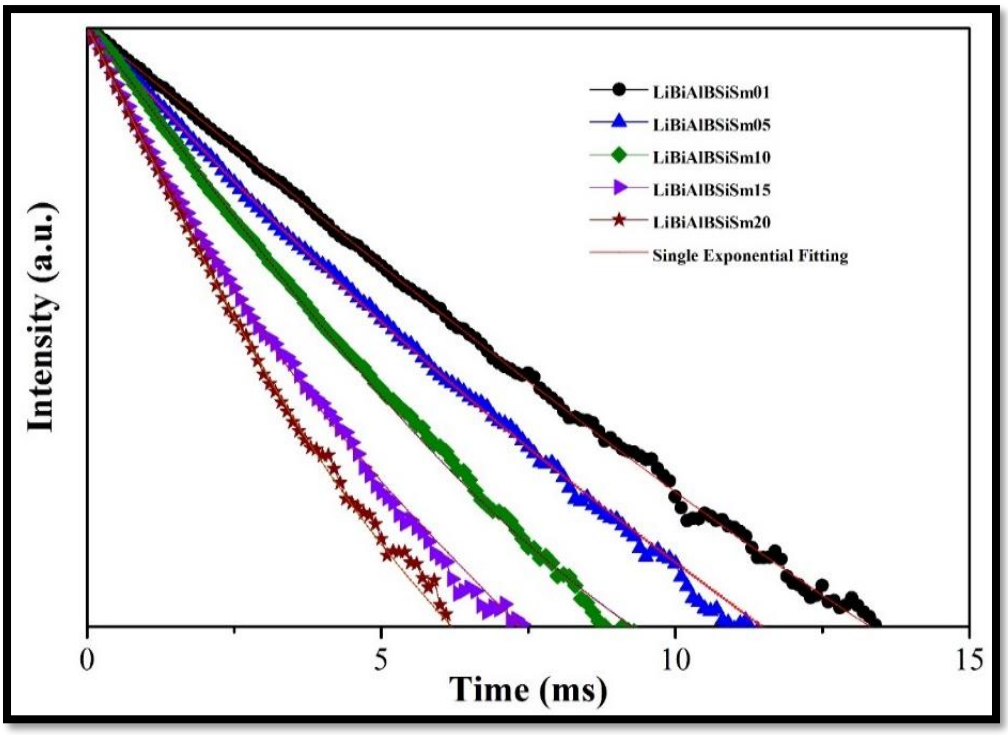

Fig. 3.7. Single exponential decay produced for $^4G_{5/2} \rightarrow {}^6H_{7/2}$ (600nm) emission transition of Sm^{3+} ions in LiBiAlBSi glasses under 400nm excitation.

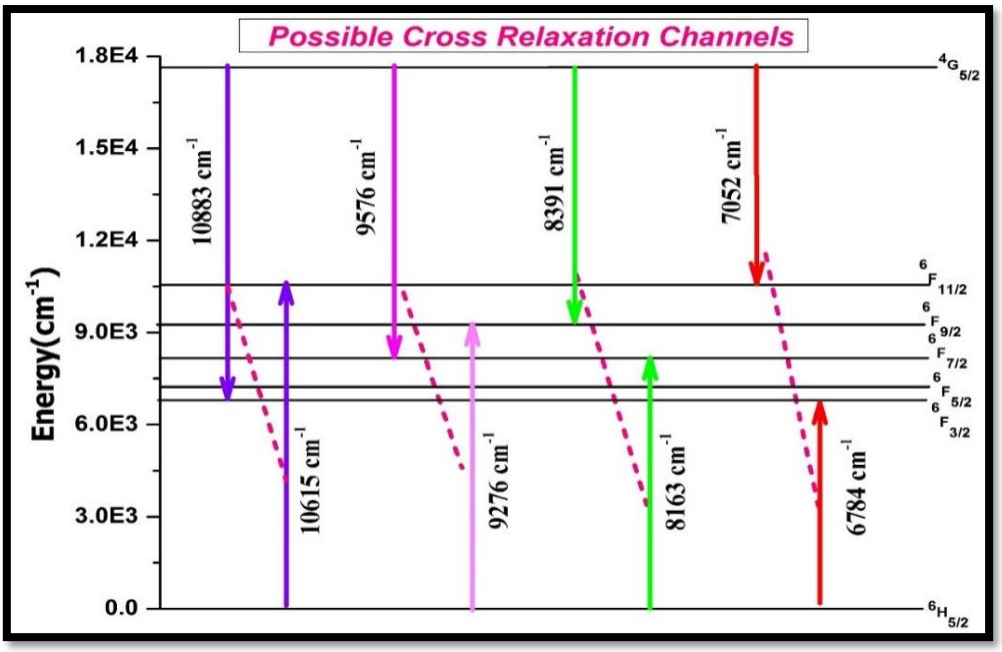

Fig. 3.8. Cross-relaxation channels involved in Sm^{3+} ions in LiBiAlBSi glasses.

Table 3.7. τ_{exp} (μs), τ_R (μs), η, and W_{NR} for $^4G_{5/2} \rightarrow {}^6H_{7/2}$ (600 nm) transition of Sm^{3+} ions in LiBiAlBSi glasses.

Name of sample	τ_{exp}	τ_R	η (%)	W_{NR}
LiBiAlBSiSm01	2521	2594	93.89	24
LiBiAlBSiSm05	2026	2685	78.11	108
LiBiAlBSiSm10	1770	3393	52.19	269
LiBiAlBSiSm15	1225	3500	35.02	530
LiBiAlBSiSm20	1185	4268	27.79	608

Table 3.8. Comparison of σ_{se} and η of LiBiAlBSiSm05 glass for the prominent emission $^4G_{5/2} \rightarrow {}^6H_{7/2}$ (λ_P =600 nm) with other Sm^{3+} ions doped glasses reported in the literature.

Name of the Glass	$\sigma_{se}(10^{-22}$ cm$^2)$	η (%)	Ref.
LiBiAlBSiSm05	12.60	78.11	present work
TMZNB	11.70	26	[143]
BNL0.5Sm	7.26	42	[17]
PNZSm1	4.65	79.28	[17]
PNZSm0.5	4.15	81.20	[17]
SLfSfASm1	9.23	-	[92]
MgAS	6.57	93.70	[90]
CaAS	7.89	82.43	[90]

3.3.9. CIE chromaticity co-ordinates

The Commission Internationale de L'Eclairage (CIE) color coordinates system [145] and CIE diagram are important to represent the exact emission color using the emission spectrum of the as-prepared glasses. The tristimulus values X, Y, and Z are considered to stimulate the value for red, green, and blue (RGB) color to match the color of specified power spectral density P(λ). CIE chromaticity coordinates and correlated color temperature (CCT) were evaluated by using using the Eqn. no. 1.28, 1.29 and 1.30 that are given in chapter 1 [30,130]. The CIE and CCT values evaluated from PL spectra of Sm^{3+} ions for LiBiAlBSi glasses are given in Table 3.9.

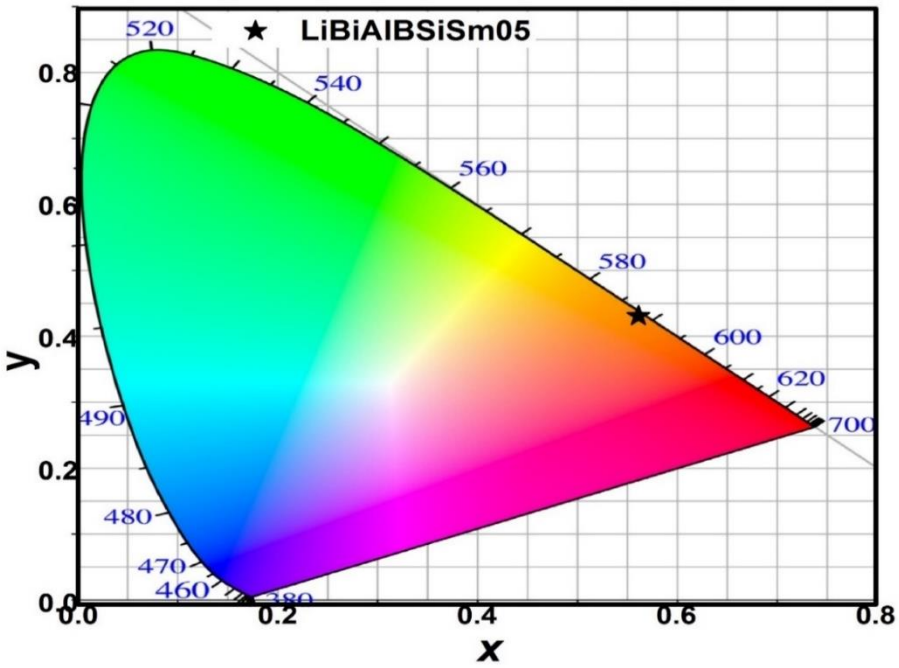

Fig. 3.9. CIE chromaticity coordinates of 0.5 mol% of Sm^{3+} ions in LiBiAlBSi glass.

The CIE coordinates estimated for an optimized LiBiAlBSSm05 glass (0.562, 0.436) are falling in the reddish-orange region as shown in Fig. 3.9. This result is in consonance with the emission data shown in Fig. 3.5. The PL spectra of Sm^{3+} ions in LiBiAlBSi glasses (shown in Fig.3.5) has three portions; the first and third portions fall in green and red regions respectively. The second portion falls in the reddish-orange region. Among all the three peaks observed in three different regions, the second part observed in the reddish-orange region is relatively more intense.

Table 3.9. CIE chromaticity coordinates of Sm^{3+} ions in LiBiAlBSi glasses under 400 nm excitation wavelength

Glass samples	x-coordinate	y-coordinate	CCT (K)
LiBiAlBSiSm01	0.557	0.437	1958
LiBiAlBSiSm05	0.562	0.436	1919
LiBiAlBSiSm10	0.559	0.438	1947
LiBiAlBSiSm15	0.570	0.429	1848
LiBiAlBSiSm20	0.562	0.436	1920

3.4. Summary

Sm^{3+} doped LiBiAlBSi glasses were prepared via the melt quenching technique. Morphological studies like XRD and FT-IR were carried out on the as-prepared undoped glass to confirm the amorphous nature and vibrational energies present in the host lattice. The luminescence properties of the as-prepared glasses were thoroughly investigated using absorption spectra and their correlation with emission and decay spectral data. The bonding parameter estimated from the nephelauxetic ratio reveals the nature of bonding existing between Sm^{3+} ions and oxygen ligands as ionic and as such the ionic nature of bonding increases with an increase in Sm^{3+} ions content in the as-prepared glasses. This result is in consonance with the bonding nature estimated by J-O analysis. The intensity of emission peaks is increasing with Sm^{3+} ions up to 0.5 mol% of Sm^{3+} ions and beyond diminishes due to the quenching effect. The decay curves are showing single exponential nature for all the glasses and the experimental lifetimes are decreasing with an increase in Sm^{3+} ion content. The non-radiative cross-relaxation energy transfer process is responsible for the quenching phenomenon observed. The branching ratios, emission cross-sections, quantum efficiency, and CIE coordinates estimated for the as-prepared glasses finally reveals their suitability for fabricating yellow lasers and w-LEDs.

CHAPTER 4

Influence of Tb^{3+} ions concentration and temperature on lithium bismuth alumino borosilicate glasses for green photonic device applications

(The content of this chapter has been published in **"Optical Materials, 120 (2021), 111439"**)

LiBiAlBSi glasses doped with various concentrations of Tb^{3+} ions were prepared to explore their physical, optical, and PL characteristics features. The indirect optical band gap for Tb^{3+} doped LiBiAlBSi glasses was found in the 3.16-3.46 eV range. PL measurements such as emission (under 378 nm excitation) and excitation (under 542 nm emission) were recorded to study the usage of the as-prepared glasses for green photonic device applications. The intensity of the emission peak observed in the green region at 542 nm ($^5D_4 \rightarrow {}^7F_5$) escalates up to 1.5 mol% of Tb^{3+} ion concentration and declines beyond due to concentration quenching. The CIE coordinates and CCT values calculated for the as-prepared glasses are closure to the values of intense green emission given by the European Broadcasting Union illuminant. The PL studies along with colorimetric studies confirm the aptness of the LBiAlBSiTb15 glass for photonic applications such as laser and tricolor w-LEDs as a green emitting component.

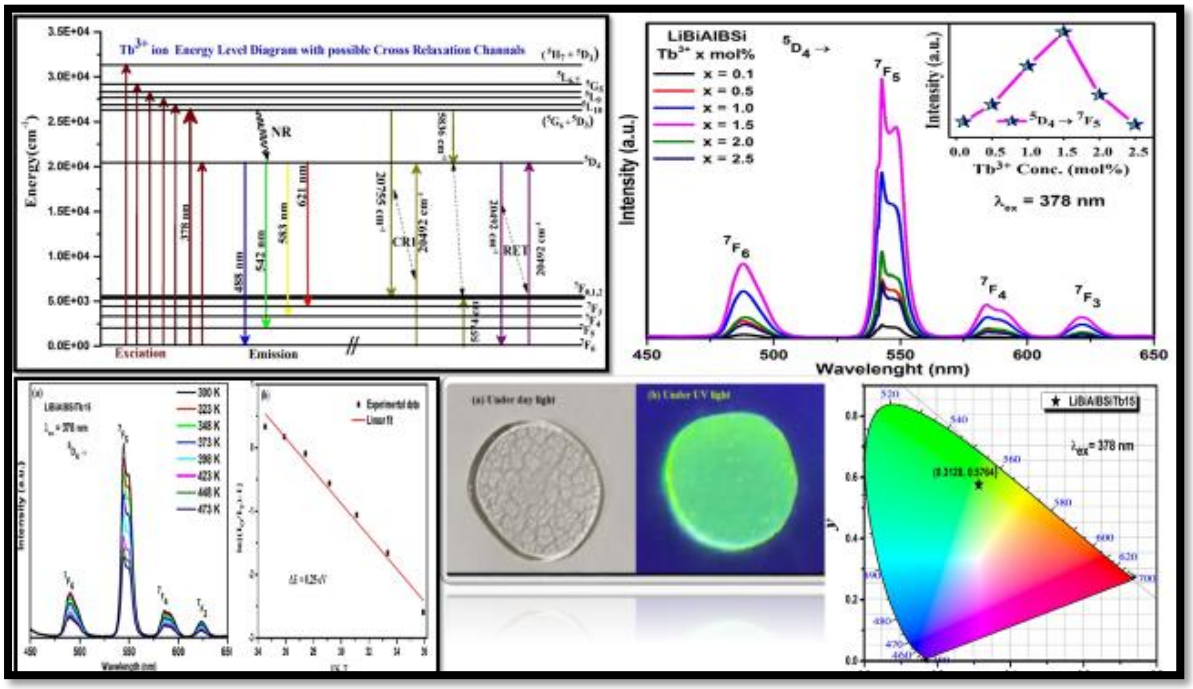

4.1. Introduction

In recent years, the scientific community has made a great effort in exploring the spectral behavior of RE ions doped glasses for various photonic device applications. The unique spectroscopic features such as narrow emission bands, possessing many fluorescing states, relatively longer lifetimes, and a large number of excited states for optical pumping of RE ions prompted the scientists to explore the applications of RE-doped materials in solid-state lasers, LEDs, flat-panel displays, optical amplifiers, solar cells, and optical fibre amplifiers [47,146–148]. For the fabrication of advanced optical devices, the knowledge of the optical characteristics of RE ions activated materials such as transition positions, transition probabilities, quantum efficiency, branching ratios, non-radiative and radiative decay rates are required [148,149]. The outcome of the visible emission transitions of RE ions was noticed within their 4f shells. These transitions were unresponsive to the surrounding environment owing to the shielding outcome of outer electrons of 5s and 5p orbitals. Due to the special property, RE ions doped glasses have been preferred as significant luminescent materials and found to be employed for the aforesaid applications. The RE ions activated luminescent glass materials possess several remarkable characteristics such as relatively easy fabrication with low cost, longer lifetime, environmental friendliness and higher reliability [21,42,43,47,150]. Nowadays, LEDs are replacing conventional light sources in the lighting industry. The RE ions doped glasses are the most appropriate candidates for w-LEDs fabrication because of the prime reason for the non-usage of epoxy resin while constructing an LED. This automatically results in no ageing effects and subsequently a longer life span when compared with LEDs prepared by using crystalline phosphors in which epoxy is a must [23,151]. In addition to the above, an inhomogeneous broadening of emission of RE ions in the glass medium is the result of the characteristic dispersal of RE ions in local sites of the crystal field. The host matrix induced the crystal field which influences the luminescence characteristics of RE ions doped host matrix [148,152,153].

Amongst the different RE ions, Tb^{3+} is considered as most competent to give visible green emission through its $^5D_4 \rightarrow {}^7F_5$ transition. The emission intensity of Tb^{3+} ions in a host matrix is governed by the host matrix composition, radiative and non-radiative transitions, and the concentration of Tb^{3+} ions entering the host matrix. A large energy gap (~ 14918 cm^{-1}) existing between the $^5D_4$ meta-stable state to different ^7F_J (J = 0 to 6) multiplet states gives the information pertaining to the energy level structure of Tb^{3+} ions in the host glass and thereby the observed luminescence phenomenon. Owing to the advantages and direct usage of Tb^{3+}

ions doped glassy systems in many variegated areas, a large number of Tb^{3+} doped glasses have been synthesized and characterized using various spectroscopic tools. The diversified applications of Tb^{3+} doped luminescent materials in w-LEDs, the green color component in displays, light converters, sensors, solid-state lasers, thermo-luminescent dosimeters field emission displays, optoelectronic, etc. were attractive to researchers [47,49,154–156].

In this chapter, a series of Tb^{3+} ions doped LiBiAlBSi glasses were prepared and an effort has been made towards understanding the luminescent features of the as-synthesized glasses using various spectroscopic techniques such as absorption, excitation, emission, and decay spectral features along with XRD. The spectral information obtained is analyzed and compared with the literature values to have a better understanding of the relative performance of the as-prepared glasses and their applications in tricolor w-LEDs and green lasers.

4.2. Experimental

Tb^{3+} doped LiBiAlBSi glasses with its composition (20-x) Li_2CO_3-7.5Bi_2O_3-7.5Al_2O_3 - 45H_3BO_3 - 20SiO_2 - x Tb_4O_7 (where x = 0.1 to 2.5 mol%) have been synthesized via conventional melt quenching procedure. For convenience, the glasses are labelled as LiBiAlBSiTb01, LiBiAlBSiTb05, LiBiAlBSiTb10, LiBiAlBSiTb15, LiBiAlBSiTb20 and LiBiAlBSiTb25 based on Tb^{3+} ions concentration of 0.1, 0.5, 1.0, 1.5, 2.0 and 2.5 mol%, correspondingly. In the present work, highly pure precursor chemicals such as Li_2CO_3, Bi_2O_3, Al_2O_3, H_3BO_3, SiO_2, and Tb_4O_7 were weighed in the stoichiometric proportions and crushed using agate mortar until to get a homogeneous powder. The precursor chemical powders collected into an alumina crucible turned into uniform liquid when heated at 1150°C for half an hour in a furnace. The melts were quenched in between two smooth brass plates (pre-heated) to obtain glasses of the same thickness. Subsequently, the glasses so prepared are annealed at 350°C for 4 h to make them free from thermal shocks such as air gaps and cracks. The XRD patterns required to understand the amorphous nature of the titled glasses were done by employing an X-ray diffractometer (Bruker-Model D8). The density of the titled glasses was measured using the Archimedes method employing water as an immersion liquid. A JASCO-made V-770 UV–VIS spectrophotometer was employed to measure the absorption spectra of the titled glasses. PL spectral features were recorded by employing a JASCO-made FP-8300 spectrofluorometer having a Xenon lamp as an excitation source. The fluorescence decay curves were recorded on an Edinburgh FL920 fluorescence spectrometer having a Xenon flash lamp as an excitation source.

4.3. Result and discussion

4.3.1. XRD patterns analysis

XRD patterns of an un-doped, as well as 1.5 mol% Tb^{3+} ions doped LiBiAlBSi glasses, are depicted in Fig. 4.1. Both the XRD patterns depicted in Fig. 4.1 are exhibiting a broad hump (absence of intense sharp peaks) indicates the presence of short-range order and endorses the non-crystalline or amorphous nature of the present glass system [59,157].

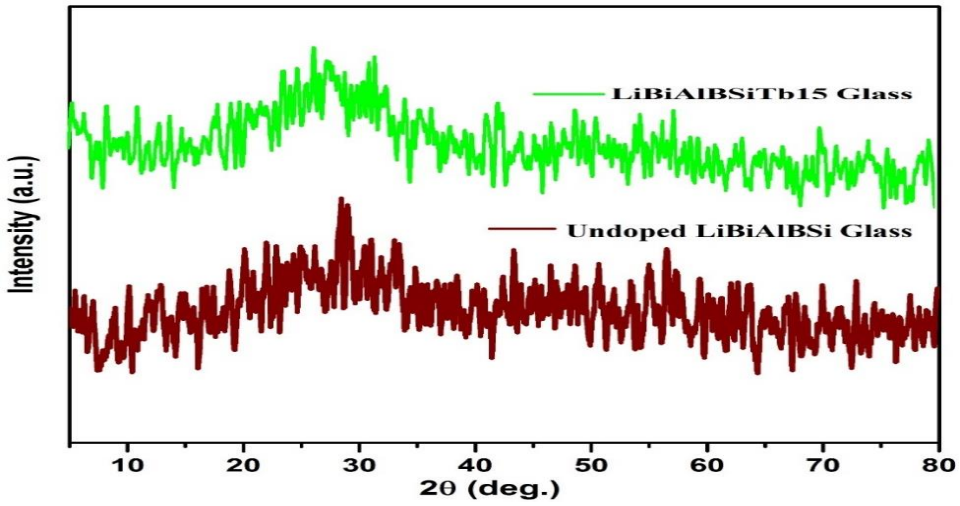

Fig. 4.1. XRD patterns of an un-doped LiBiAlBSi and 1.5 mol% Tb^{3+} doped glasses.

4.3.2. Absorption spectral analysis

An UV-VIS spectrum has been recorded for all the Tb^{3+} ions doped LiBiAlBSi glasses from 350 to 500 nm wavelength range. Fig. 4.2 depicts the absorption spectral profiles obtained for 1.5 mol % Tb^{3+} doped LiBiAlBSi glasses. The absorption spectral profiles for the remaining glasses are quite similar in-band positions except for some variation in the intensity of individual peaks and hence they were not shown in Fig. 4.2. The absorption profile consists of the transition of Tb^{3+} ions starting from its ground state ($^7F_6$) to $^5D_3$ and $^5D_4$, higher levels at 378 nm and 484 nm respectively. In the current analysis, these two absorption bands are induced as a result of dipole-dipole transitions of electric in nature, which obeys the selection rules $|\Delta J| \leq 6$, $|\Delta L| \leq 6$, and $\Delta S = 0$ [23,26,158]. The absorption bands of Tb^{3+} ions in LiBiAlBSi glasses in n-UV and blue regions are very weak due to the forbidden character of the 4f-4f transitions.

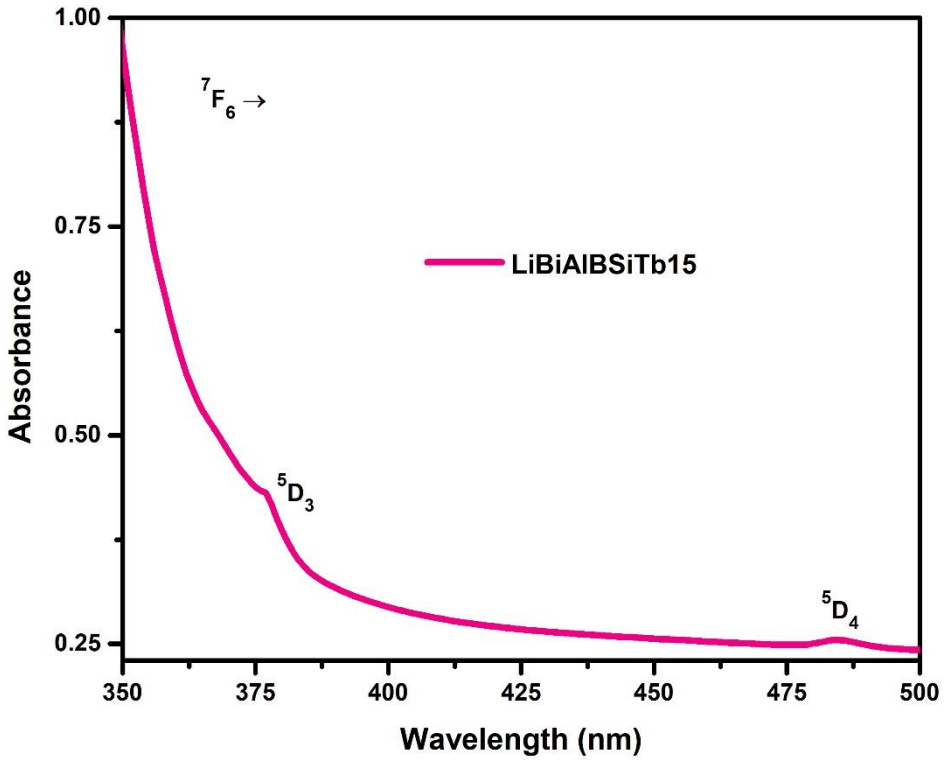

Fig. 4.2. The absorption spectrum of 1.5 mol% of Tb^{3+} ions doped LiBiAlBSi glass.

4.3.2.1. Energy band gap, refractive index, and physical properties

In the UV region, the fundamental absorption edge gives information pertaining to the optical transitions and electronic band structure for amorphous as well as crystalline materials. So, the indirect optical energy band gap energy values (E_{opt}) pertaining to Tb^{3+} in LiBiAlBSi glasses were estimated using the absorption spectra. The absorption edges are not sharp because of the amorphous nature of the present glasses. The E_{opt} for Tb^{3+} doped LiBiAlBSi glasses were estimated from the relation of Davis and Mott given Equ.no. 1.3 in chapter 1 [49,88]. In general, the indirect bandgap is evaluated for oxide glasses. The indirect E_{opt} values were estimated by extrapolating the linear section of the curves of Tauc's plot as depicted in Fig. 4.3. The indirect energy band gap values for the allowed transitions are presented in Table 4.1. It was noticed the values of band gap values decrease with Tb_2O_3 content. The indirect band gap values are 3.46 to 3.16 eV with Tb_2O_3 content in the as-prepared glasses. This declination noticed in band gap values may be ascribed to the creation of non-bridging oxygen (NBOs) due to oxygen bonding variation in the glass matrix. As a result of the addition of Tb_2O_3 content, maximum NBOs created in the valence band and NBOs shifts increasing towards conduction band due to that the values of E_{opt} is decreased [23,32,159,160].

The refractive index (n) for Tb^{3+} doped LiBiAlBSi glasses was calculated on the basis of indirect E_{opt} by using the relation[49,160–162]:

$$\frac{n^2-1}{n^2+2} = 1 - \sqrt{\frac{E_{opt}}{20}} \qquad (4.1)$$

The n value for all the glasses is listed in Table 4.1. Based on the refractive index (n), the other physical properties were evaluated for the LiBiAlBSiTb15 glass by using the appropriate equation given in the literature [91]. These physical properties are represented in Table 4.2 and compared with other reported glasses like ZnAlBiBTb1.5 [26] and zinc boro-silicate Tb^{3+} doped glass [163]. The physical properties of Tb^{3+} doped LiBiAlBSiTb15 glass are comparable to these reported glasses.

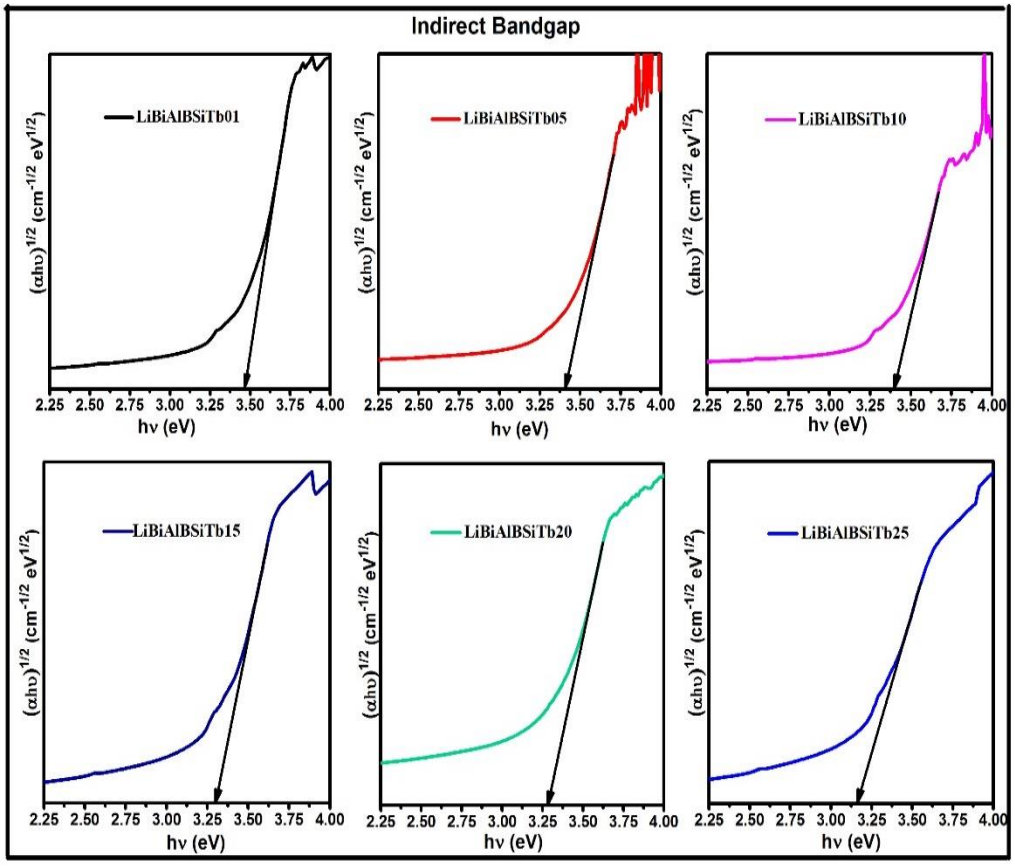

Fig. 4.3. Indirect bandgap plot of Tb^{3+} ions doped LiBiAlBSi glasses.

Table 4.1. The optical band gap (E_{opt}), for indirect allowed transitions along with the refractive index of Tb^{3+} ions in LiBiAlBSi glasses.

Glass samples	Indirect E_{opt} (eV)	Refractive Index(n)
LiBiAlBSiTb01	3.46	2.283
LiBiAlBSiTb05	3.41	2.295
LiBiAlBSiTb10	3.38	2.302
LiBiAlBSiTb15	3.30	2.321
LiBiAlBSiTb20	3.28	2.326
LiBiAlBSiTb25	3.16	2.355

Table 4.2. Physical properties of the 1.5 mol% of Tb^{3+} ions doped LiBiAlBSi glasses along with other reported glasses

Physical properties	LiBiAlBSiTb15	ZnAlBiBTb15 [26]	Tb^{3+} doped Zinc Boro-Silicate Glass [163]
Density, d (g/cm^3)	3.425	3.868	4.031
Refractive index, n	2.321	1.793	1.78
Average molecular weight(g)	107.32	113.19	76.261
Dielectric constant(ϵ)	5.38	3.124	3.173
Optical dielectric constant (ϵ-1)	4.38	2.214	-
Polaron radius, r_p (Å)	1.31	1.307	1.27
Inter-atomic distance,r_i (Å)	3.26	3.243	3.15
Molecular electronic polarizability α (10^{-23} cm^3)	0.491	0.328	0.315
Field Strength, F (10^{15} cm^{-2})	17.37	17.56	1.85

4.3.3. PL excitation and emission spectral analysis

The PL excitation spectra for all the as-prepared glasses have been recorded at an ambient temperature. The PL excitation spectrum of 1.0 mol% of Tb^{3+} ions in LiBiAlBSi glass from 300 to 500 nm wavelength range under 542 nm emission wavelength is shown in Fig. 4.4. The excitation spectra for the remaining LiBiAlBSi glasses are quite similar in-band positions with

slight variation in their intensities and hence they were not shown in Fig.4.4. The excitation spectrum for LiBiAlBSiTb10 glass exhibits several excitation peaks in UV, n-UV, and the blue region as shown in Fig. 4.4. The PL excitation peaks observed at 318, 342, 352, 359, 370, 378, and 485 nm are attributed to the transitions from ground level ($^7F_6$) to $^5H_7$ + $^5D_1$, $^5L_{6,7}$, $^5G_5$, $^5L_9$, $^5L_{10}$, $^5G_6$ +$^5D_3$, and $^5D_4$ excited states, respectively [79]. From Fig. 4.4, it can be perceived that the excitation peaks pertaining to the $^7F_6 \rightarrow {}^5D_3$ (378 nm) transition is relatively more intense and is useful as an excitation wavelength (λ_{ex}=378 nm) to record PL emission spectral features of the as prepared glasses.

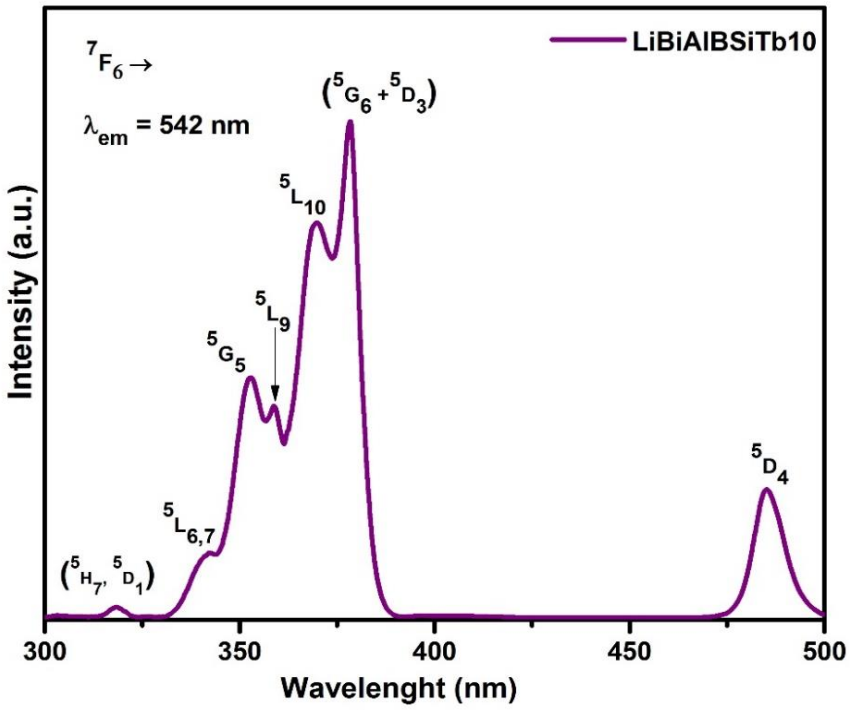

Fig. 4.4. The excitation spectrum of 1.0 mol% of Tb^{3+} ions doped LiBiAlBSi glass.

The PL emission spectra of Tb^{3+} ions doped LiBiAlBSi glasses under 378 nm excitation wavelength is depicted in Fig.4.5. The PL emission spectra show four visible peaks in blue (488 nm), strong green (542 nm), yellow (584 nm), and red (622 nm) regions related to the transitions $^5D_4 \rightarrow {}^7F_J$, where J = 6, 5, 4 and 3 of Tb^{3+} ions respectively. The blue peaks at 488 due to the $^5D_4 \rightarrow {}^7F_6$ transition, follow the selection rule for magnetic dipole transition (ΔJ = ±1). The strong green peak at 542 nm due to the $^5D_4 \rightarrow {}^7F_5$ transition follows the Laporte-forbidden selection rule. A minor splitting observed in the center of the peak at 542 nm ($^5D_4 \rightarrow {}^7F_5$) is due to the effect of distortion created by the host system network on Tb^{3+} ions called stark splitting [23,164]. From Fig. 4.5 it is evident that the intensity of emission peaks increases gradually up to 1.5 mol% of Tb^{3+} ions and beyond decreases due to the quenching

effect. The reasons for quenching with the growing concentration of Tb^{3+} ions may be attributed to the non-radiative multipole-multipole interaction among Tb^{3+} (activators) ions and cross-relaxation (CR) process via energy transfer (ET) mechanism between Tb^{3+} ions [23,26,148].

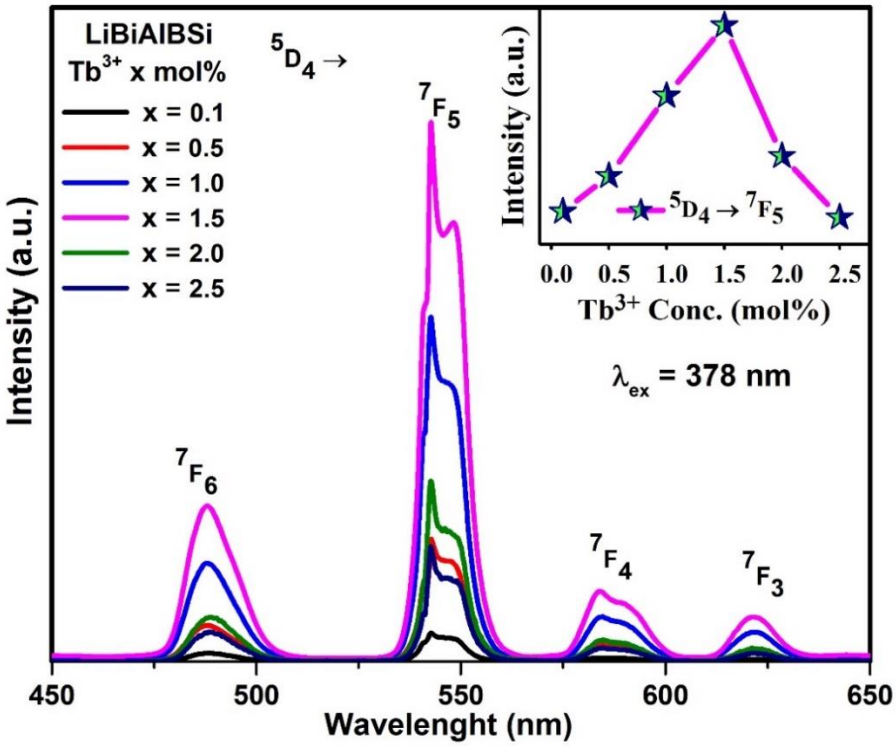

Fig. 4.5. The emission spectra of Tb^{3+} ions doped LiBiAlBSi glasses.

Dexter's theory has been applied to the PL emission spectra to assess the type of interaction mechanism involved among the doped Tb^{3+} ions and responsible for the observed quenching phenomenon. This theory has predicted three mechanisms accountable for the inter-ionic interaction type by the equation between the PL intensity (I) and the activator concentration (x) given below

$$\log\left(\frac{I}{x}\right) = c - \frac{s}{3}\log(x) \tag{4.2}$$

where I is the PL intensity of transition $^5D_4 \rightarrow {}^7F_5$, x is the Tb^{3+} ions concentration in mol% and "s" is fitting parameters [s = 6, 8, and 10 for d–d (dipole-dipole), d–q (dipole-quadrupole), and q–q (quadrupole-quadrupole) interactions respectively] [151].

The graph plotted based on equation (4.2) has been displayed in Fig.4.6. The experimental data can be fitted into a straight line with a slope of -1.641. This yields the value for s equal to 4.923,

which is close to 6. This declares that the interaction responsible for the non-radiative energy transfer between Tb^{3+} ions is dipole-dipole in nature. Further such non-radiative energy transfer results in the concentration quenching phenomenon observed in PL emission spectra.

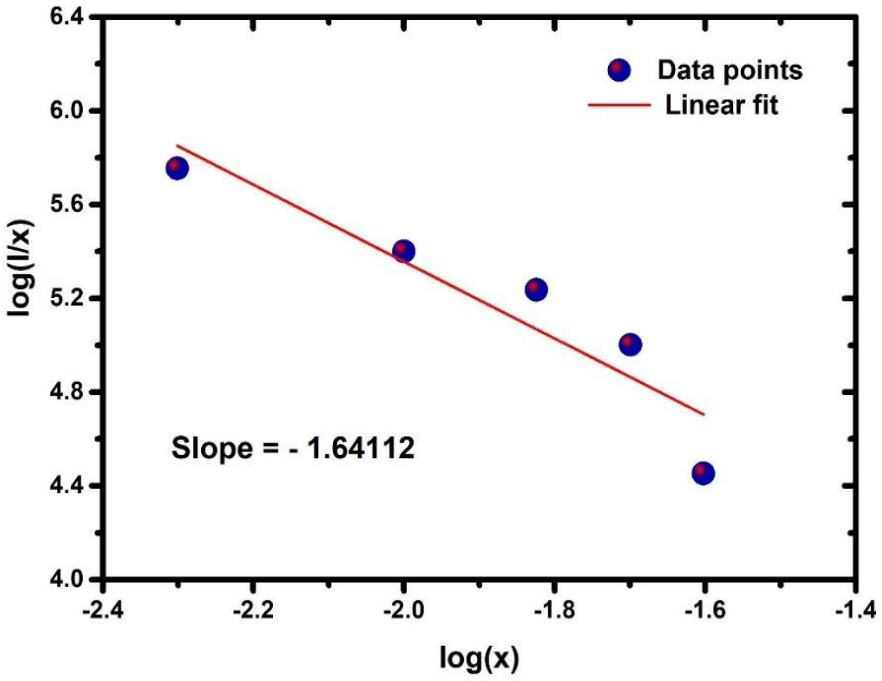

Fig. 4.6. Relation between log (I/x) and log (x) for different concentrations of Tb^{3+} ions in LiBiAlBSi glass. Dexter model fitting is shown by the solid line.

The partial energy level diagram for Tb^{3+} ions doped LiBiAlBSi glasses is shown in Fig. 4.7, which explains the PL excitation, PL emission, probable cross-relaxation (CR) channels with resonant energy transfer (RET) mechanisms involved in the as-prepared glass. As represented in Fig. 4.7, under 378 nm excitation wavelength, the Tb^{3+} ions are excited from the $^7F_6$ ground (lowest) state to the $^5D_3$ higher energy state. The occupied $^5D_3$ excited states of Tb^{3+} ions may undertake two main courses [148,165,166],

1. $^5D_4$ or $^7F_0$ levels the non-radiative (NR) transition through CR energy transfers, and
2. The radiative transitions to numerous lower-lying levels.

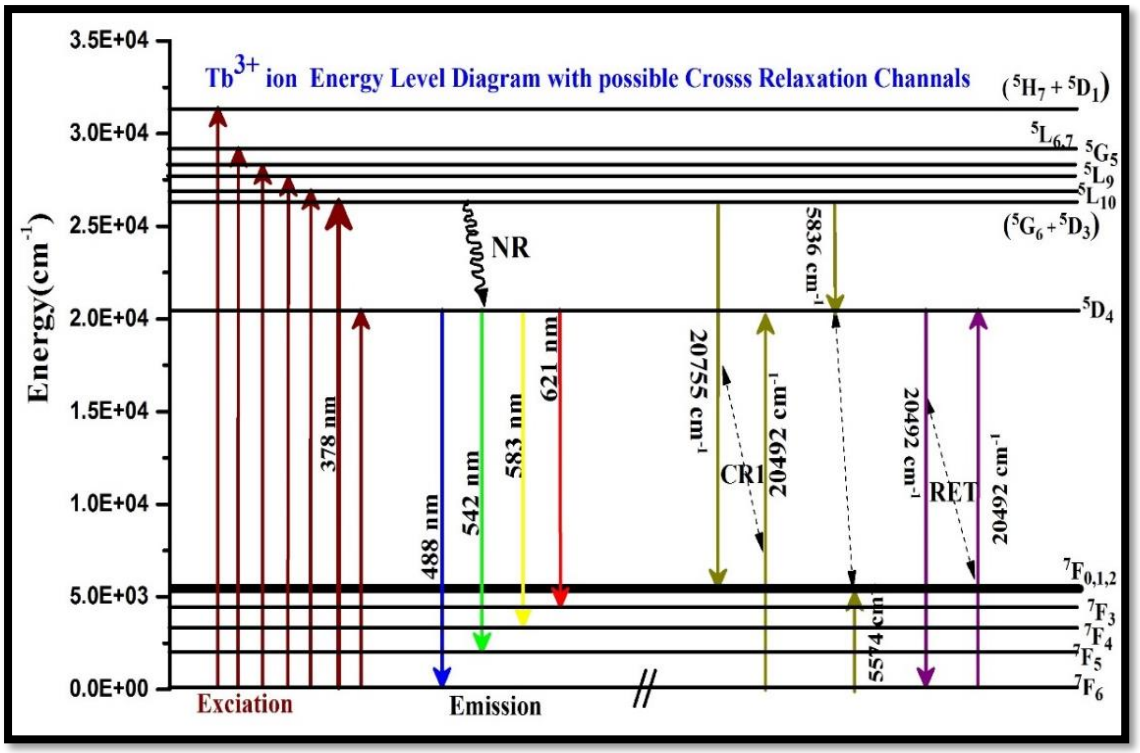

Fig. 4.7. Energy level diagram of 1.5 mol% Tb^{3+} ions doped LiBiAlBSi glasses with possible cross-relaxation channels.

The possible CR channels for Tb^{3+} ions doped LiBiAlBSi glasses are as follows:

$$CR1: {}^5D_3/{}^7F_6 \rightarrow {}^7F_0/{}^5D_4$$

$$CR2: {}^5D_3/{}^7F_6 \rightarrow {}^5D_4/{}^7F_0$$

$$RET: {}^5D_4/{}^7F_6 \rightarrow {}^7F_6/{}^5D_4$$

The weak emission from the $^5D_3$ excited level is not observed in the present work as the emission due to the $^5D_4$ level is strong. The $^5D_3$ transition weak intensity attentions the noticeable energy transfer by CR to the $^5D_4$ state. It is well-identified that, the CR procedure arises whenever the absorption and emission transitions encounter each other. The quenching of the $^5D_4$ level at higher concentrations of Tb^{3+} ions (> 1.5 mol%) may be due to the cooperative energy transfer and energy migration among the nearest Tb^{3+} ions. From the PL emission spectral studies, it is conspicuous that, 1.5 mol% of Tb^{3+} ions concentration in the titled glasses is optimum for emitting relatively intense green emission.

4.3.3.1. Chromaticity color coordinates

The CIE chromaticity coordinates and CCT values for all the Tb^{3+} ions doped LiBiAlBSi glasses have been estimated from emission spectra recorded under 378 nm excitation. Chromaticity coordinates are evaluated by employing the method proposed by Commission International de I'Eclairage (CIE). The evaluated chromaticity coordinates are shown in Table 4.3. For all the LiBiAlBSi glasses, the CIE coordinates fall in the visible green region. Especially, the CIE coordinates of the optimized glass (0.3128, 0.5764) show good proximity with the intense green light coordinates (0.29, 0.60) specified by the European Broadcasting Union (EBU) [21,23]. The CCT values calculated under 378 nm excitation for all the titled glasses are in the green light zone (5700–5900 K). A relatively higher CCT value obtained for the titled glasses indicates clearly the improved visual perception along with relatively high brightness. Image of optimized LiBiAlBSiTb15 glass under (a) daylight and (b) UV light is shown in Fig. 4.9. From the above calculated colorimetric values, it is finally declared that LiBiAlBSiTb15 glass is a potential candidate for the fabrication of green solid-state lasers and a green component of tricolor w-LEDs.

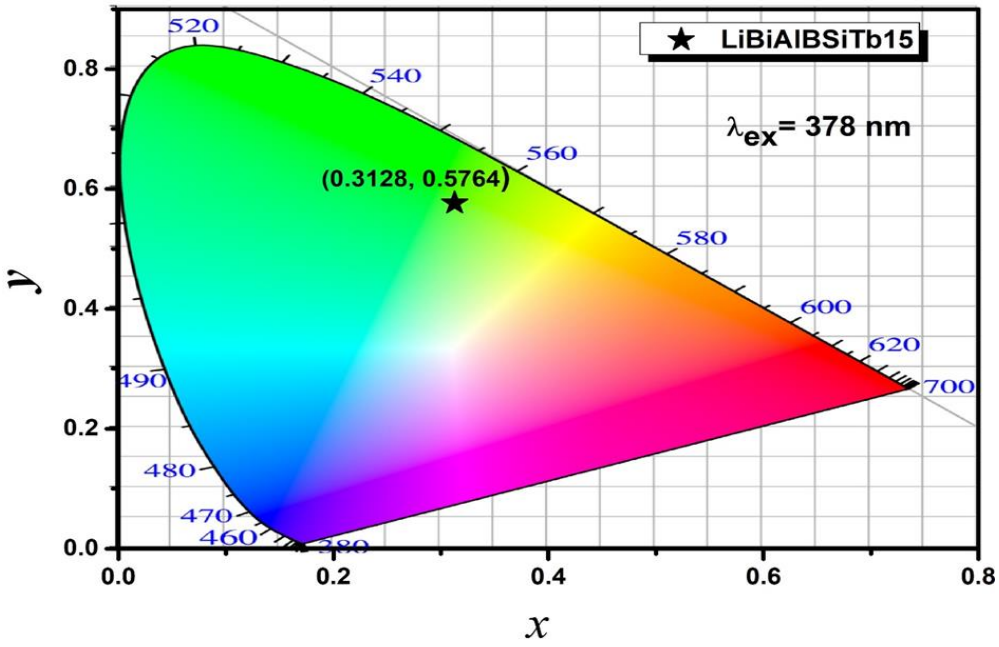

Fig. 4.8. CIE chromaticity coordinates of 1.5 mol% of Tb^{3+} ions doped LiBiAlBSi glass.

Table 4.3. CIE chromaticity coordinates and CCT (K) of Tb^{3+} ions in LiBiAlBSi glasses under 378 nm excitation wavelength

Glass sample	x-coordinate	y-coordinate	CCT (K)
LiBiAlBSiTb01	0.3102	0.5816	5912
LiBiAlBSiTb05	0.3152	0.5829	5820
LiBiAlBSiTb10	0.3138	0.5776	5849
LiBiAlBSiTb15	0.3128	0.5764	5869
LiBiAlBSiTb20	0.3182	0.5910	5760
LiBiAlBSiTb25	0.3194	0.5909	5740

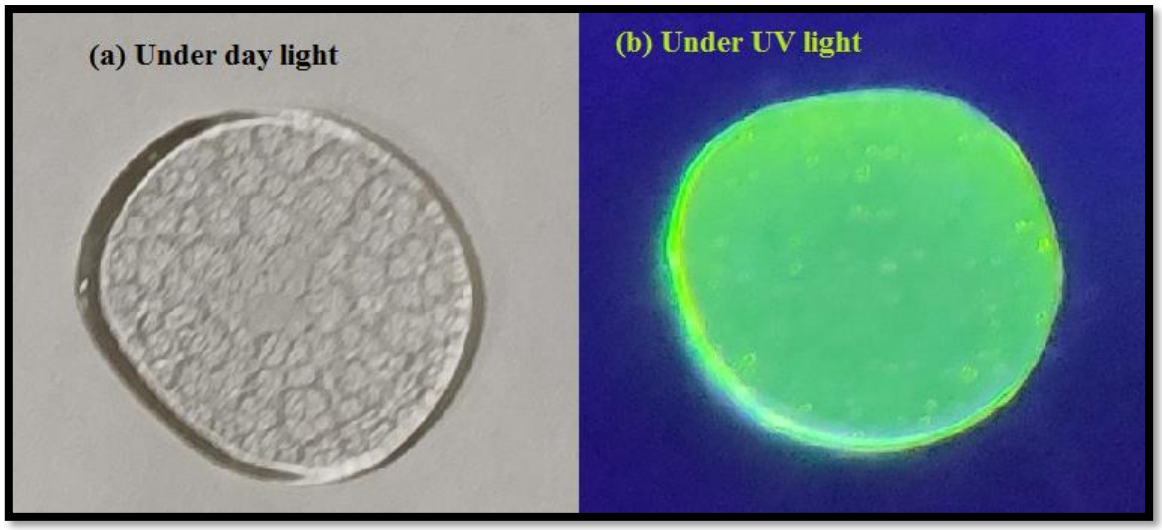

Fig. 4.9. Image of 1.5 mol% of Tb^{3+} ions doped LiBiAlBSi glass under (a) daylight and (b) UV light.

4.3.4. Fluorescence decay analysis

The PL decay plot reveals the information of excited states and experimental lifetime (τ_{exp}) values and the dynamics of the excited level of RE ions in a host matrix. The PL decay curves of the as-prepared glasses were recorded for 542 nm emission under 378 nm excitation. This green emission initiates from a radiative transition of $^5D_4$ excited level to $^7F_5$ lower level. For all the as-prepared glasses, the experimental decay plots are well fitted through a bi-exponential function as shown in Fig. 4.10. The reason for the bi-exponential nature of decay plots may be due to the excited donor ions transfer the energy to the unexcited acceptor ions. In the case of

the bi-exponential fitting, the intensity of emission (I) and the average values of decay lifetime (τ_{avg}) can be expressed by the Eqn. no. 1.19 & 1.20 given in chapter 1 [23,167]

The order of τ_{avg} values of Tb^{3+} ions doped LiBiAlBSi glasses are in milliseconds (ms) and τ_{avg} values are presented in Table 4.4 as τ_{exp}. Table 4.4 depicts τ_{exp} values obtained for the as-prepared glasses, which are descending from 2.13 to 1.34 ms with Tb^{3+} ions concentration ranging from 0.1 to 2.5 mol%. With an increase in Tb^{3+} ions concentration, the distance of separation among Tb^{3+} ions decreases incredibly and this leads to an energy transfer from excited Tb^{3+} ions (donors) to un-excited Tb^{3+} ions (acceptors). This kind of non-radiative energy transfer that took place between the doped RE ions at their higher concentration levels decreases the experimental lifetimes. This declining behavior in the decay lifetime of the $^5D_4$ excited level is also because of its large population, which enhances the probability of energy migration.

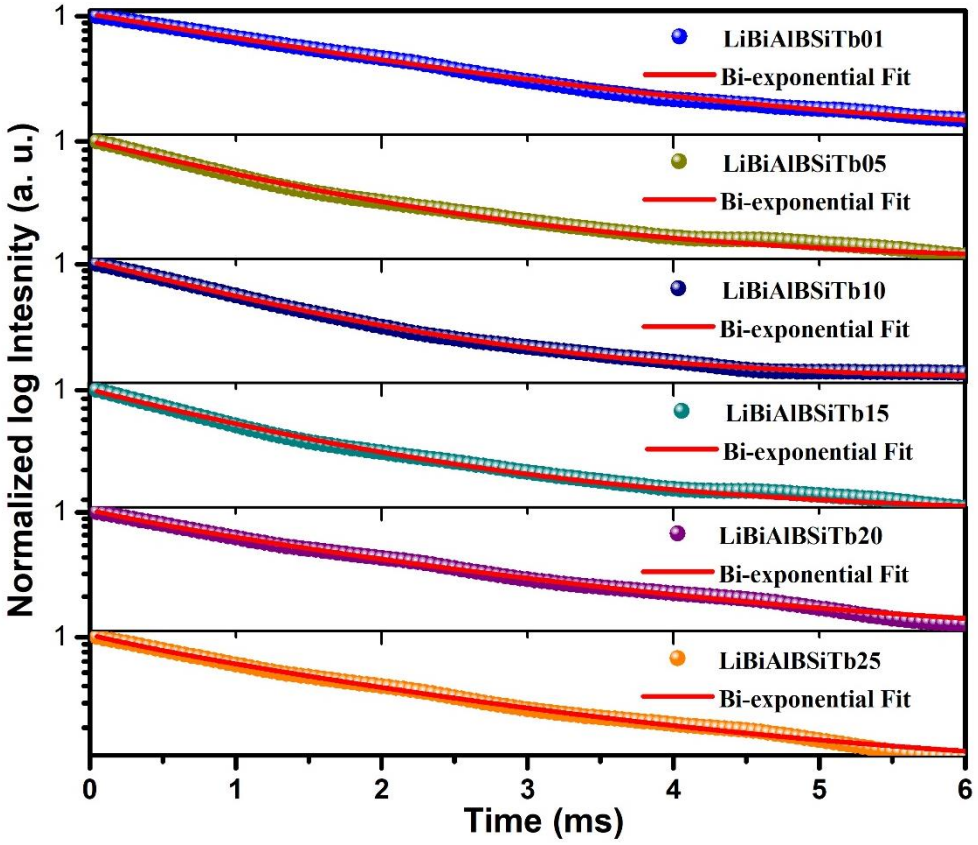

Fig. 4.10. Bi-exponential decay produced for $^5D_4 \rightarrow {}^7F_5$ (542 nm) emission transition of Tb^{3+} ions doped LiBiAlBSi glasses under 378 nm excitation.

Table 4.4. Experimental lifetimes (τ_{exp}) (ms), energy transfer efficiency (η_{ETE}) and total transition probability (A_T) (s^{-1}) for $^5D_4 \rightarrow {}^7F_5$ (542 nm) transition of Tb^{3+} ions in LiBiAlBSi glasses.

Name of sample	τ_{exp}	η_{ETE} (%)	A_T
LiBiAlBSiTb01	2.13	0	469.48
LiBiAlBSiTb05	2.06	3	485.44
LiBiAlBSiTb10	1.87	12	534.76
LiBiAlBSiTb15	1.64	23	609.76
LiBiAlBSiTb20	1.49	30	671.15
LiBiAlBSiTb25	1.34	37	746.27

The energy transfer efficiency (η_{ETE}) among the Tb^{3+} ions in the LiBiAlBSi glasses can be estimated via the equation [110]

$$\eta_{ETE} = \left(1 - \frac{\tau_x}{\tau_0}\right) X\ 100 \tag{4.3}$$

where τ_o is the experimental lifetime of the Tb^{3+}in the as-prepared glasses at 0.1 mol% of the dopant ion concentration and τ_x is the experimental lifetime of Tb^{3+} ions in the same host glass for concentrations ranging from 0.5 - 2.5 mol%. The experimental decay lifetimes with varying concentrations of Tb^{3+} ions doped LiBiAlBSi glasses are presented in Table 4.4 along with energy transfer efficiency.

The data appearing in Table 4.4 clearly demonstrates that Tb^{3+} ions in the as-prepared glasses are showing relatively longer luminescence experimental lifetimes useful for producing high population inversion necessary to produce efficient lasing action in the green region.

4.3.5. Radiative properties analysis

Judd-Ofelt theory (J-O) is mostly used to estimate the spectroscopic quantities of RE ions in doped materials. By using absorption & emission spectral data, this theory facilitates the evaluation of the numerous radiative properties such as namely radiative transition probability (A), branching ratio (β_R) and intrinsic lifetimes (τ_R) of the exciting levels of RE ions, based on

the determination of the J-O intensity parameters (Ω_λ; where λ= 2,4,6). The J-O intensity parameters are determined by using many standard equations given in the literature [42,43]. Li et al. presented an alternate procedure i.e., a reverse J-O calculation based on the emission spectra analysis and not on absorption spectra [168]. A similar procedure has been followed by many researchers to estimate the radiative properties of RE-doped materials [53,148,155]. In this method, the experimental lifetime value (τ_{exp}) is used to determine the total transition probability (A_T) from the relation $A_T = 1/\tau_{exp}$ and presented in Table 4.4, supposing that it resembles the radiative lifetime ($\tau_{rad} = \tau_{exp}$) value. This estimation can be considered because the energy gap between $^5D_4$ excited level to the next lower level $^7F_0$ is large (~15000 cm^{-1}); this makes highly improbable restricted non-radiative transitions from the higher level $^5D_4$ to lower levels.

The transition probability A for each transition is related to radiative branching ratios (β_R) and the total radiative transition probability (A_T) through the following relation [35]:

$$\beta_R = \frac{A}{A_T} \tag{4.4}$$

Where the values β_R (= β_{exp} experimental branching ratios) can be estimated from the emission spectrum. For potential lasing transition, the branching ratios value should be relatively larger than 0.5. The stimulated emission cross-section is denoted by σ_{se} is another proficient factor useful in understanding the efficiency of the host matrix doped with RE ions for lasing action and estimated by the eqn.no. 1.15 given in chapter 1 [21,148]

For LiBiAlBSiTb15 optimized glass, the values of λ_p β_{exp}, A, $\Delta\lambda_p$, σ_{se} , gain bandwidth and optical gain parameters are given in Table 4.5. Table 4.6 shows the comparison of radiative properties obtained for the $^5D_4 \rightarrow {}^7F_5$ green emission of the LiBiAlBSiTb15 optimized glass with the other Tb^{3+}-doped glasses [23,148]. In glasses doped with RE ions, the optical gain is one of the significant factors in estimating glass medium amplification. From Tables 4.5 and 4.6, it is conspicuous that, for $^5D_4 \rightarrow {}^7F_5$ green transition the radiative properties such as $\beta_{exp}, \sigma_{se}, (\sigma_{se}\ x\ \Delta\lambda_p)$, and $(\sigma_{se}, x\ \tau_{exp})$ are relatively high for LiBiAlBSiTb15 optimized glass. These parameters indicate that the optimized LiBiAlBSiTb15 glass is an incredible candidate for fabricating green lasers and green components in w-LEDs.

Table 4.5. Emission peak wavelength λp (nm), experimental branching ratios (β_{exp}), Transition probability (A) (s^{-1}), effective bandwidths ($\Delta\lambda p$) (nm), stimulated emission cross-sections (σ_{se} x 10^{-22}) (cm^2), gain bandwidth ($\sigma_{se} \times \Delta\lambda p$ x 10^{-28}) (cm^3) and optical gain parameter ($\sigma_{se} \times \tau_{exp}$ x 10^{-25}) (cm^2 s) for the emission transitions of 1.5 mol% Tb^{3+} ions in LiBiAlBSi glasses.

Transition	λp	β_{exp}	A	$\Delta\lambda p$	σ_{se}	$\sigma_{se} \times \Delta\lambda p$	$\sigma_{se} \times \tau_{exp}$
LiBiAlBSiTb15							
$^5D_4 \rightarrow {}^7F_6$	488	0.22	136.37	13.88	2.76	3.83	4.52
$^5D_4 \rightarrow {}^7F_5$	542	0.62	379.69	10.79	15.02	16.22	24.63
$^5D_4 \rightarrow {}^7F_4$	584	0.10	63.66	14.78	2.48	3.66	4.07
$^5D_4 \rightarrow {}^7F_3$	622	0.05	30.04	11.58	1.92	2.23	3.15

4.3.6. Temperature-dependent PL (TD-PL) studies

In the process of understanding the thermal stability of the optimized LiBiAlBSiTb15 glass, the effect of temperature on PL properties has been taken up by recording the TD- PL studies under 378 nm excitation wavelength in the temperature range from 300 to 473 K and is depicted in Fig. 4.11 (a). From Fig. 4.11 (a), it is evident that the PL intensity gradually reduces with temperature showing relatively high at room temperature (300 K). An increase in thermal energy with temperature forces the electrons to undergo emission through the non-radiative (NR) decay process.

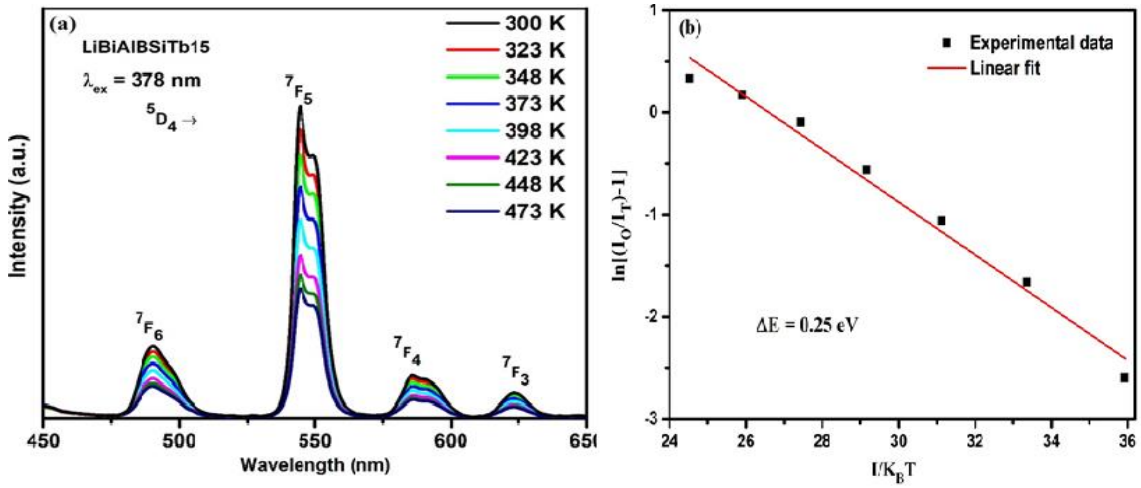

Fig. 4.11. (a) TD-PL spectra for 1.5 mol% Tb^{3+} ions doped LiBiAlBSi glasses, (b) Graph between $\ln[(I_o/I_T)-1]$ and $(1/K_BT)$ for 1.5 mol% Tb^{3+} ions doped LiBiAlBSi glasses.

From the TD-PL studies, it is possible to estimate activation energy, which is useful to understand the thermal stability of the material under investigation using the Arrhenius equation given in Chapter 1 (Equ. no. 1.31) [169–172]. The graph between $\ln[(I_o/I_T)-1]$ and $(1/K_BT)$ is a linear fitted one as shown in Fig. 4.11(b) and the slope of this graph gives activation energy equal to 0.25eV. This relatively high activation energy value suggests that the optimized LiBiAlBSiTb15 glass has good thermal stability and is quite useful for its utility as a new potential candidate for emitting green color useful for fabricating tricolor w-LEDs and green lasers.

4.4 Summary

LiBiAlBSi glasses activated with Tb^{3+} ions were prepared by engaging the melt quench process to understand their suitability for visible green photonic device applications. A broad hump shown by the XRD spectrum recorded for an un-doped LiBiAlBSi glass confirms the amorphous nature. The PL excitation spectrum recorded for LiBiAlBSiTb10 glass under 542 nm excitation wavelength shows an intense peak at 378 nm. The PL measurements recorded under 378 nm UV excitation wavelength for all the as-prepared glasses show four emission bands of which an emission band centered at 542 nm (green region) is more intense relatively. The intensity of PL emission increases with Tb^{3+} ions concentration up to 1.5 mol% and declines beyond depicting the effect of concentration quenching. The Dexter model applied to the emission spectral data reveals the underlying mechanism responsible for quenching as dipole-dipole interaction among Tb^{3+} ions. The CIE and CCT values estimated from the emission spectral features are in consonance with the bright green emission shown by the PL spectra of the as-synthesized glasses. The PL decay curves measured for the as-synthesized glasses show bi-exponential behavior with the decrease in τ_{exp} values with Tb^{3+} ions concentration. Correlation of τ_{exp} values with emission spectral features of the titled glasses result in the estimation of its radiative properties. The activation energy estimated from the TD-PL spectra recorded for LiBiAlBSiTb15 glass reveals its thermal stability. The radiative properties, CIE coordinates, CCT values, and TD-PL studies allow us to contemplate that 1.5 mol% of Tb^{3+} ions concentration is optimum in LiBiAlBSi glasses for intense green photonic device applications.

CHAPTER 5

Downshifting analysis of Sm^{3+}/Eu^{3+} co-doped LiBiAlBSi glasses for red emission element of white LEDs

(The content of this chapter has been published in **"Chemical Physics Letters 788 (2022)139303"**)

The Sm^{3+}, Eu^{3+} single-doped, and Sm^{3+}/Eu^{3+} co-doped LiBiAlBSi glasses were prepared and studied PL excitation, PL emission, and PL decay to have a better insight into their utility as red emission element for white LEDs. Sm^{3+}/Eu^{3+} co-doped LiBiAlBSi glasses can be adeptly excited by the blue and n-UV region which is confirmed from the excitation spectrum. In the Sm^{3+}/Eu^{3+} co-doped LiBiAlBSi glasses, the PL decay lifetime for the Sm^{3+} emitting level $^4G_{5/2}$ declines and the energy transfer efficiency increases with an upsurge Eu^{3+} content, which suggests the energy transfer (ET) process occurs from Sm^{3+} to Eu^{3+} ions. The calculated values of CIE chromaticity coordinate for the as-prepared glasses under n-UV excitation shifted from reddish-orange to the red spectral part with the upsurge in Eu^{3+} concentration. All the results obtained finally suggest that LiBiAlBSi glass with 0.5 mol% of Sm^{3+} ions and 1.0 mol% of Eu^{3+} ions is thermally stable to produce the intense red color needed to fabricate white LEDs under n-UV and blue excitation.

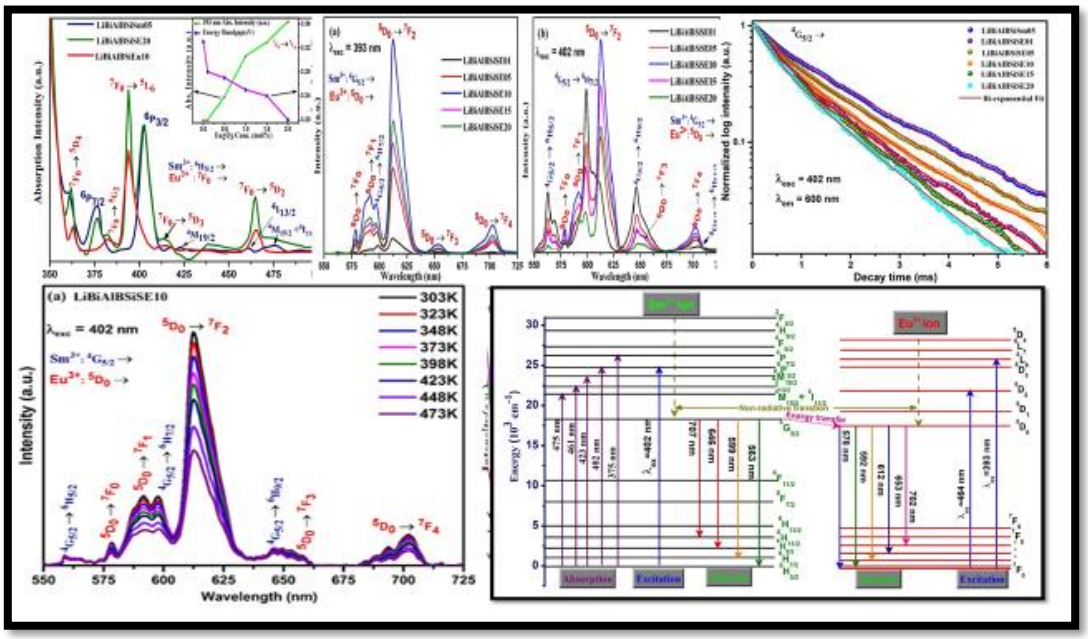

5.1. Introduction

Over the years, the assimilation of RE ions into glass systems have revolutionary changes in diverse fields such as solid-state lighting (SSL), waveguides, optical fiber, flat-panel display, optical converters, solid-state lasers, optical information processing, and photovoltaic (PV) cells [97,173–175]. In the field of SSL, white LEDs show recognized remarkable attention as compared to conventional sources of light and their several uses are flat-panel display, cellular phone illumination, automotive displays, traffic signals, etc. White LEDs have numerous prominent characteristics such as a long-serving lifetime, high luminous efficiency, small size, energy conservation, high brightness, fast switching, and being environmentally friendly. Despite these advantages, white LEDs have some weaknesses in practical applications, such as high color temperature because of the deficiency in red emission characteristics [172,173,176]. Presently, two diverse approaches have been purposeful in acquiring white light using LED chips. The first method is a combination of separate red, green and blue-releasing LED sources to attain white light and is called the RGB method. In the second method, the fabrication of white LEDs, single(yellow)/multiple (RGB) phosphor materials are used with n-UV/blue sources of excitation [41,177]. The first commercial technique to fabricate the phosphor-converted white LEDs uses the yellow emitting phosphor which is basically cerium-doped yttrium aluminium garnet (YAG: Ce^{3+}) with a blue LED chip. This method has numerous drawbacks like poor color rendering index, thermal quenching, and halo effect because of the separation of yellow-blue color. For better white light attainment with an improved color rendering index, a combination of RGB phosphors and an excitation source n-UV LED chip is required. Nonetheless, in this method, red phosphor shows very weak efficiency as compared to blue and green phosphors [97,178,179]. In both methods, phosphor is used in the form of powder and encapsulated in an epoxy resin. This epoxy resin deteriorates at high energy light sources of excitations, high power, and high temperatures which affects the luminous efficacy of phosphor. Therefore, RE ions doped glasses are preferred over phosphor because they satisfy the both purposes of the wavelength converter and epoxy resin-free encapsulation. Moreover, RE-doped glasses have the benefits of a low-cost simple fabrication procedure, excellent thermal-mechanical stability, homogeneous light emission, and high durability compared with conventional phosphors [173,180].

Among the RE ions, the Sm^{3+} ion is a vital RE ion, as its emitting level $^4G_{5/2}$ shows an efficient emission in NIR and visible regions. Visible emission is the result of UV excitation and Sm^{3+} ions can perform as a down-converter and luminescence down conversion is an excellent

approach for improving the efficacy of PV devices because these devices show the weak response to UV light. The emission properties of Sm^{3+} ions find a broad range of applications in several areas such as lighting devices, display devices, high-density optical storage, remote sensing and undersea communication, etc. [92,174,181]. Another special RE ion is Eu^{3+} owing to its energy-level pattern and high emission efficiency of the $^5D_0 \rightarrow {}^7F_2$ transition. It is found that this transition is very sensitive to minor variations in the chemical neighbouring of the Eu^{3+} ion [37,182]. The ionic radius of the Sm^{3+} ion is very much comparable to the Eu^{3+} ions. Under the n-UV and blue excitations, Sm^{3+} ions energy levels are close to Eu^{3+} ions energy levels such that Sm^{3+} ions perform as a sensitizer whereas Eu^{3+} perform as an activator in the same host [37,174,176,182,183]. Therefore, Sm^{3+} and Eu^{3+} are the appropriate candidates for co-doping into glasses to achieve the appropriate spectral conversion from UV to visible emission in the reddish-orange and red regions due to their characteristic energy- levels.

In this chapter, Sm^{3+}/Eu^{3+} co-doped with increasing Eu^{3+} ions content in LiBiAlBSi glasses formed with the melt quench process. The PL features and the process of energy transfer (ET) were explained in detail based on the results of numerous spectroscopic methods such as absorption, PL excitation, PL emission, and PL decay. The CIE chromaticity coordinates, energy transfer probability rate and efficiency of the ET process were also evaluated. The main objective of the present investigation is to have a better insight into the usage of Sm^{3+}/Eu^{3+} co-doped LiBiAlBSi glasses as a red emission element for white LEDs and other related visible red photonic devices.

5.2. Experimental method

The following glass systems Sm^{3+}, Eu^{3+} single doped and Sm^{3+}/Eu^{3+} co-doped with varying concentrations of Eu_2O_3 were prepared by the melt-quenching method for the investigation with molar composition:

i. 20 Li_2CO_3 -7.5Bi_2O_3 – 7.0 Al_2O_3 -45H_3BO_3 – 20SiO_2- 0.5Sm_2O_3 (LiBiAlBSiSm05)
ii. 20 Li_2CO_3 -7.5Bi_2O_3 – 6.5 Al_2O_3 -45H_3BO_3 – 20SiO_2- 1.0 Eu_2O_3 (LiBiAlBSiEu10)
iii. 20 Li_2CO_3 -7.5Bi_2O_3 – (7-y) Al_2O_3 -45H_3BO_3 – 20SiO_2- 0.5Sm_2O_3- yEu_2O_3 where y = 0.1, 0.5, 1.0, 1.5, and 2.0 mol% and for convenience, the glasses are named as LiBiAlBSiSE01, LiBiAlBSiSE05, LiBiAlBSiSE10, LiBiAlBSiSE15, and LiBiAlBSiSE20 depending on the concentration of the Eu ions concentration ranging from 0.1 to 2.0 mol% respectively.

All the preparatory chemicals (Li_2CO_3, Bi_2O_3, Al_2O_3, H_3BO_3, SiO_2, Sm_2O_3, and Eu_2O_3) used in the present work are Analytical reagents in grade. As per the stoichiometric proportions, these chemicals were weighed and crushed in an agate mortar. The obtained homogeneous mixture is collected into a silica crucible and kept in an electric furnace for about two hours at a heating temperature of 1150°C. At this temperature, the mixture melts uniformly and then two pre-heated plates of brass are used to quench this melt to obtain glasses of uniform thickness. Normally in the sudden melt quench method, glasses will form with air bubbles, thermal shocks, and cracks. To remove these defects, the as-prepared glasses were annealed for 4 h at 350°C by keeping them in another electrical furnace. After annealing, the obtained glass samples are used for further spectroscopic investigation.

The XRD patterns were recorded by employing Bruker- advance X-ray diffractometer Model D8 of anode Cu (λ = 1.5406 Å). The optical absorption spectra were recorded using a JASCO model V-670 UV-vis-NIR spectrophotometer. The PL excitation & PL emission spectral data were recorded using a JASCO model FP-8300 spectrofluorometer equipped with a Xenon lamp as a source of excitation. The PL decay spectral measurements were taken on the Edinburgh FL920 fluorescence spectrometer with a Xenon lamp as an excitation source. The TD-PL spectra have been recorded with an ocean optics spectrometer having an inbuilt heating unit.

5.3. Results and discussion

5.3.1. XRD pattern analysis

The XRD patterns of an undoped LiBiAlBSi, Sm^{3+} doped LiBiAlBSiSm05, Eu^{3+} doped LiBiAlBSiEu10 and Sm^{3+}/ Eu^{3+} co-doped LiBiAlBSiSE15 glasses are shown in Fig. 5.1. All the four XRD patterns shown in Fig. 5.1 are showing the non-appearance of intense sharp peaks and directs the occurrence of short-range order. Hence, this acclaims that the existing glass systems have an amorphous nature [184,185].

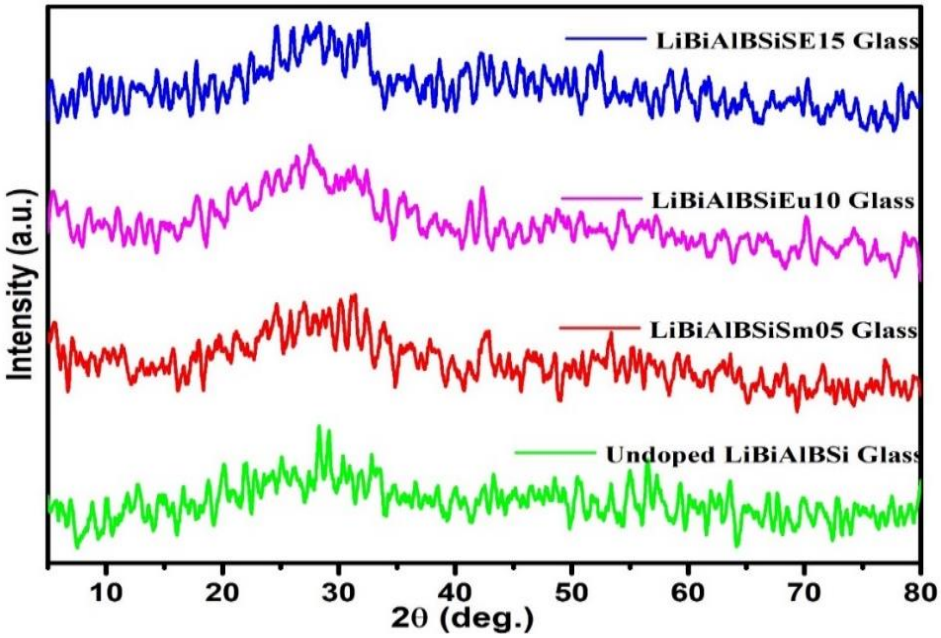

Fig. 5.1. XRD patterns of LiBiAlBSi, LiBiAlBSiSm05, LiBiAlBSiEu10 and LiBiAlBSiSE15 glasses.

5.3.2. Absorption analysis and band gap measurement

The absorption spectra were monitored in the range from 350 to 500 nm at ambient temperature for Sm^{3+}, Eu^{3+} single doped and Sm^{3+}/Eu^{3+} co-doped LiBiAlBSi glasses. The absorption spectra for LiBiAlBSiSm05, LiBiAlBSiEu10 and co-doped LiBiAlBSiSE20 glasses are shown in Fig. 5.2. Single Sm^{3+} ions doped LiBiAlBSiSm05 glass show five absorption peaks in the UV-visible region at 375, 402, 423, 461, and 475 nm with transitions from ground level ($^6H_{5/2}$) to higher excited levels $^6P_{7/2}$, $^6P_{3/2}$, $^4M_{19/2}$, $^4I_{13/2}$, and $^4M_{19/2}$ + $^4I_{11/2}$ respectively. Single Eu^{3+} ions doped LiBiAlBSiEu10 glass show five absorption bands in UV-visible region at 362, 383, 393, 415, and 464 nm with transitions from ground level ($^7F_0$) to higher levels $^5D_4$, $^5G_2$, $^5L_6$, $^5D_3$ and $^5D_2$ respectively.

The absorption spectrum of Sm^{3+}/Eu^{3+} co-doped LiBiAlBSiSE20 glass has also been displayed in Fig. 5.2, in which the eight absorption bands are obtained due to Sm^{3+} and Eu^{3+} ions at the same position as mentioned above. In the present work, the transition characteristics of Sm^{3+} and Eu^{3+} identification are done using the results of already published literature [78,135]. From the inset in Fig. 5.2, it can be noticed that the intensity of the Eu^{3+} ion absorption peak observed at 393 nm ($^7F_0 \rightarrow {}^5L_6$) is varying linearly with Eu_2O_3 concentration. This predicts that Eu^{3+} ions were proficiently incorporated into the glass system.

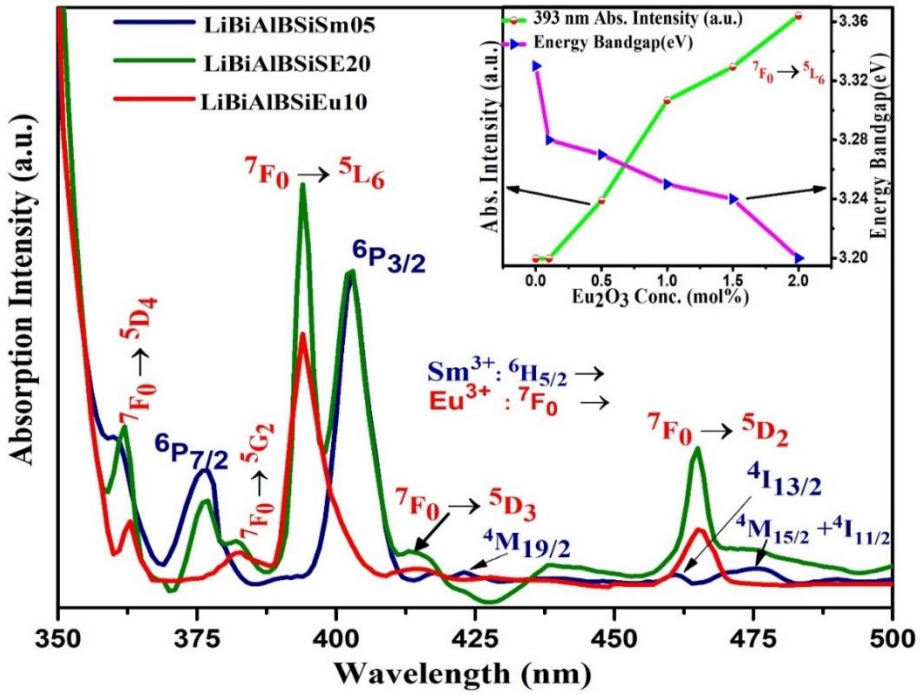

Fig. 5.2. The absorption spectra of LiBiAlBSiSm05, LiBiAlBSiEu10 and co-doped LiBiAlBSiSE20 glasses (Inset: Variation of absorption intensity of the transition $^7F_o \rightarrow {}^5L_6$ and energy bandgap (eV) with Eu^{3+} ion concentration).

In the UV region, the electronic band structure and optical transitions for solid-state materials are attained from the fundamental absorption edge. The fundamental absorption edge is the speedy rise in the absorption coefficient. The optical band gap is a vital parameter for amorphous and crystalline materials. Usually, the fundamental absorption edge for amorphous materials is described for optical band gap in terms of indirect transitions. Therefore, the absorption spectra were used for the estimation of the indirect optical energy band gap (E_{opt}) values for Sm^{3+}, Eu^{3+} single-doped, Sm^{3+}/Eu^{3+} co-doped LiBiAlBSi glasses by using the relation of Davis and Mott gave in chapter 1(Equ. no.1.3) [88,151] :

The E_{opt} values were assessed by extrapolating from the linear part of plots of $(\alpha h\nu)^{1/2}$ verses $h\nu$(eV) as shown in Fig. 5.3. The E_{opt} values of LiBiAlBSiSm05, LiBiAlBSiEu10 LiBiAlBSiSE01, LiBiAlBSiSE05, LiBiAlBSiSE10, LiBiAlBSiSE15 and LiBiAlBSiSE20 glasses are 3.33, 3.30, 3.28, 3.27, 3.25, 3.24 and 3.20 eV respectively. It is observed that the E_{opt} values are reducing with the increase in Eu_2O_3 content, and this variation is shown in the inset of Fig. 5.2. The reason for E_{opt} values reduction may be a variation of oxygen bonding in the glass environment due to non-bridging oxygens (NBOs) creation. These NBOs created

in the valance band and shifting towards the conduction band leads to the reduction of the optical band gap [159,160].

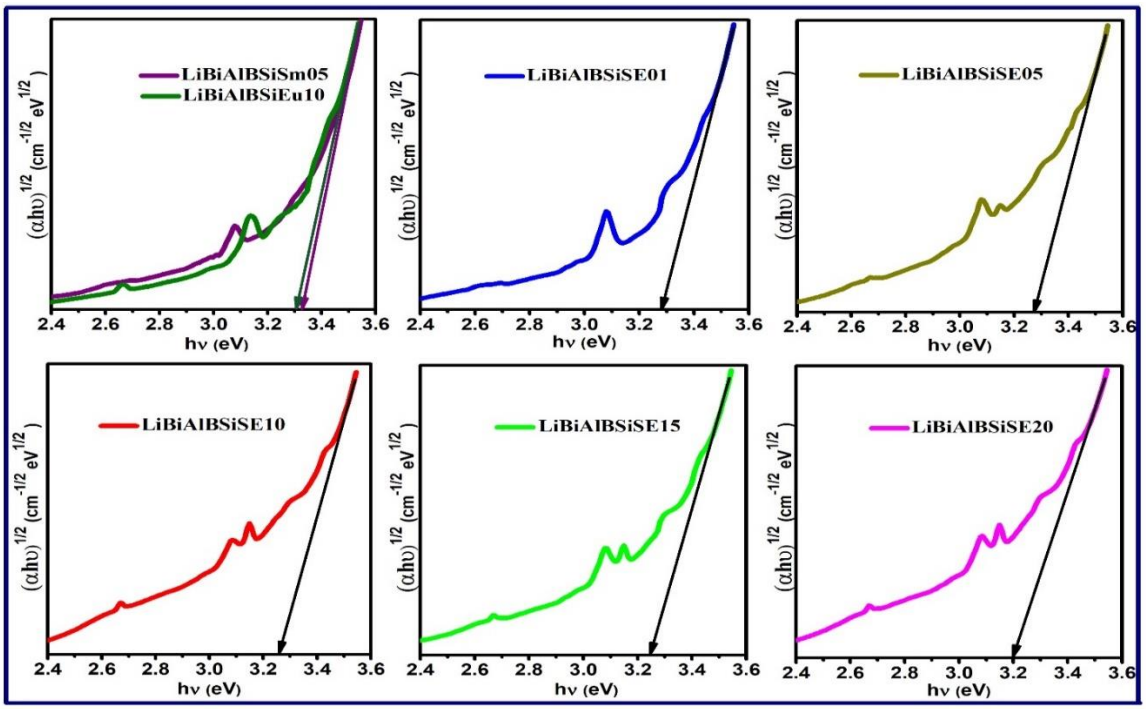

Fig. 5.3. Indirect bandgap plots of Sm^{3+}, Eu^{3+} and Sm^{3+}/Eu^{3+} co-doped LiBiAlBSi glasses.

5.3.3. Photoluminescence spectral analysis

5.3.3.1. PL properties of single Sm^{3+} and single Eu^{3+} ions doped LiBiAlBSi glasses

As reported in chapter 3, the optimum concentration of Sm^{3+} ions in LiBiAlBSi glasses was found to be at 0.5 mol% [13]. This made us fix the concentration of Sm^{3+} ions in LiBiAlBSi glasses at 0.5 mol% to study the PL excitation & PL emission spectral studies in the present work. The recorded PL excitation & PL emission spectra of 0.5 mol% Sm^{3+} ions (LiBiAlBSiSm05) and 1.0 mol% of Eu^{3+} ions (LiBiAlBSiEu10) doped glasses are depicted in Fig. 5.4(a) and 5.4(b) respectively. In Fig. 5.4(a) under 600 nm emission wavelength, the LiBiAlBSiSm05 glass show seven excitation peaks at 344, 362, 375, 402, 418, 461, and 475 nm corresponding to the transitions from the lowest level $^6H_{5/2}$ to the various excited levels $^4H_{9/2}$, $^4F_{9/2}$, $^6P_{7/2}$, $^6P_{3/2}$, $^4M_{19/2}$, $^4I_{13/2}$, and ($^4M_{15/2}$ + $^4I_{11/2}$) respectively [135]. Among the seven excitation peaks, the one observed at 402 nm ($^6H_{5/2} \rightarrow {}^6P_{3/2}$) is relatively more intense and is used to record the emission spectrum of LiBiAlBSiSm05 glass.

Under 402 nm intense excitation wavelength, the LiBiAlBSiSm05 glass shows four emission peaks at 562, 599, 646, and 707 nm corresponding to the transitions from $^4G_{5/2}$ level (excited)

of Sm^{3+} ions to various sublevels $^6H_{J/2}$ (J=5, 7, 9, and 11) respectively. Among the four emission peaks, the one observed at 599 nm pertaining to the $^4G_{5/2} \rightarrow {}^6H_{7/2}$ transition is relatively more intense. All the peaks show a broad shoulder and characteristic Stark splitting pattern to the longer wavelength region.

As shown in Fig. 5.4(b) under 612 nm emission wavelength, the LiBiAlBSiEu10 glass shows five excitation bands at 360 nm, 381 nm, 393 nm, 414 nm, and 464 nm with corresponding transition arising from $^7F_0$ ground level of Eu^{3+} ions to $^5D_4$,$^5G_2$, $^5L_6$, $^5D_3$, and $^5D_2$ higher levels respectively. Among the five excitation peaks, the one observed at 393 nm pertaining to $^7F_0 \rightarrow {}^5L_6$ transition is relatively more intense and is quite suitable to record the emission spectrum of LiBiAlBSiEu10 glass. Under 393 nm intense excitation wavelength, the LiBiAlBSiEu10 glass shows five emission peaks at 702 nm, 653 nm, 612 nm, 591 nm, and 579 nm corresponding to the transitions from $^5D_0$ level (excited) of Eu^{3+} ions to various lower levels $^7F_4$, $^7F_3$, $^7F_2$, $^7F_1$, and $^7F_0$ respectively. Among these five emission peaks, the one observed at 612 nm pertaining to the $^5D_0 \rightarrow {}^7F_2$ transition observed in the red region of the visible spectrum is relatively more intense and follows the selection rule $|\Delta J| \leq 6$. The $^5D_0 \rightarrow {}^7F_2$ transition of Eu^{3+} ions is forced electric dipole (ED) and hypersensitive in nature. It is well known that the intensity of such hypersensitive transitions is sensitive to the environment of the crystal field produced by ligands around the doped RE ions in a host matrix. While $^5D_0 \rightarrow {}^7F_1$ transition of Eu^{3+} ions is magnetic dipole (MD) and insensitive in nature by following the selection rules $\Delta J = 0, \pm 1$ [78,177,186].

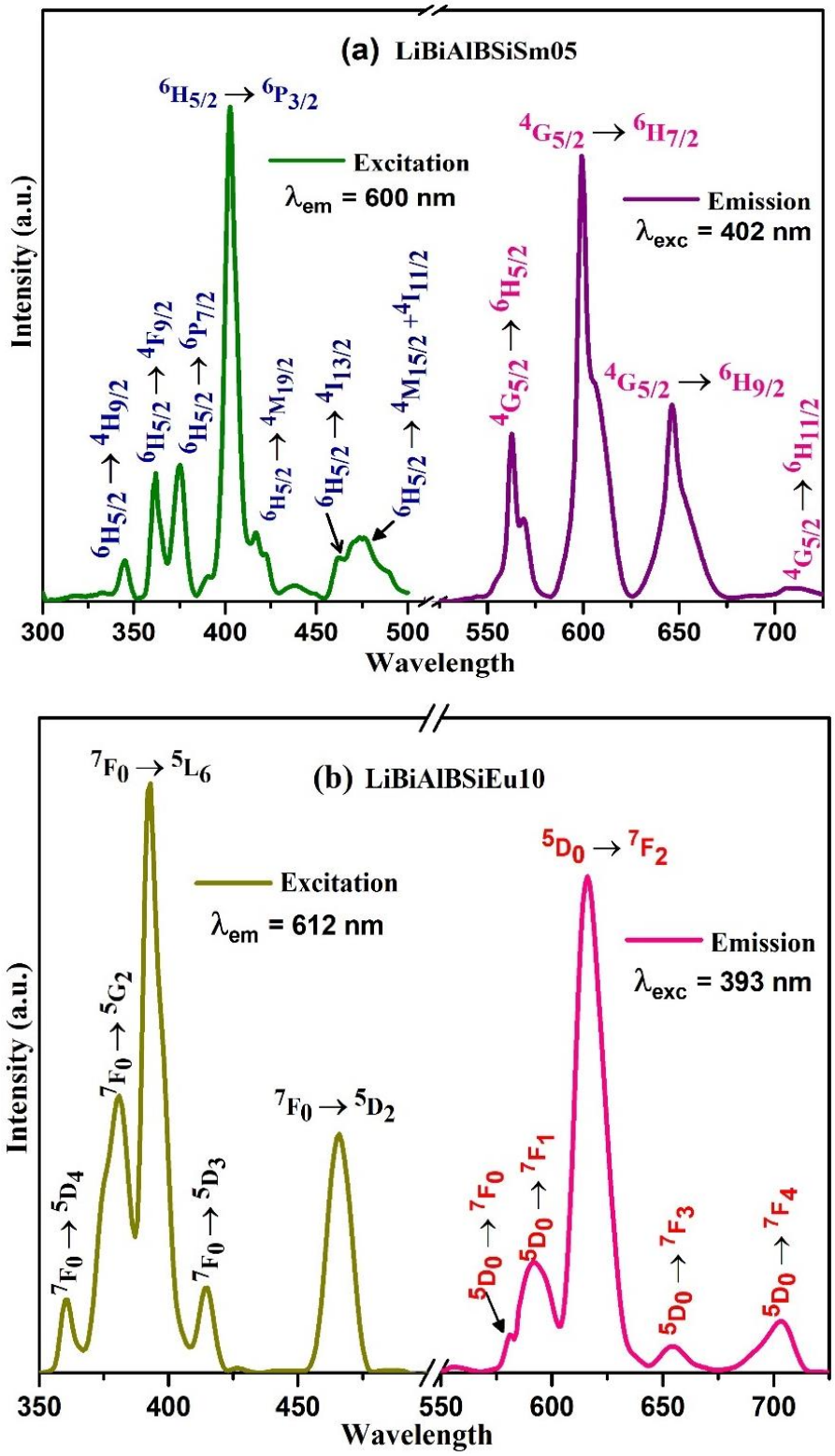

Fig. 5.4. The excitation and emission spectrum of (a) 0.5 mol% of Sm^{3+} ions in LiBiAlBSi glass and (b) 1.0 mol% of Eu^{3+} ions in LiBiAlBSi glass.

5.3.3.2. PL properties of Sm^{3+}/Eu^{3+} co-doped LiBiAlBSi glasses

Fig. 5.5 (a) and 5.5 (b), represent the excitation spectra of Sm^{3+}/Eu^{3+} co-doped LiBiAlBSi glasses under emission wavelength 600 nm and 612 nm respectively in the range 300-500 nm. For the diverse ions, the excitation spectra play an important role in finding the perfect excitation wavelength. Fig. 5.5(a) shows the excitation spectra of Sm^{3+}/Eu^{3+} co-doped LiBiAlBSi glasses monitored at 600 nm emission ($^4G_{5/2} \rightarrow {}^6H_{7/2}$) corresponds to Sm^{3+} ions. Fig. 5.5 (a) depicts the Sm^{3+} ions excitation bands ascribed to the transitions $^4H_{9/2}$ (344 nm), $^4F_{9/2}$ (362 nm), $^6P_{7/2}$ (375 nm), $^6P_{3/2}$ (402 nm), $^4M_{19/2}$ (418 nm), $^4I_{13/2}$ (461 nm), ($^4M_{15/2}$ + $^4I_{11/2}$)(475 nm) and Eu^{3+} ion excitation bands ascribed to the transitions $^7F_0 \rightarrow {}^5G_2$ (381 nm), $^7F_0 \rightarrow {}^5L_6$(393 nm) and $^7F_0 \rightarrow {}^5D_2$ (464 nm) [78,186].

Fig. 5.5 (b) shows the excitation spectra for Sm^{3+}/Eu^{3+} co-doped LiBiAlBSi glasses monitored at 612 nm emission ($^5D_0 \rightarrow {}^7F_2$) correspond to Eu^{3+} ions. Fig.5.5(b) depicts the Sm^{3+} ions excitation bands ascribed to the transitions $^6H_{5/2} \rightarrow {}^6P_{5/2}$ (304 nm), $^6H_{5/2} \rightarrow {}^4H_{9/2}$ (344 nm), $^6H_{5/2} \rightarrow {}^6P_{7/2}$ (375 nm), $^6H_{5/2} \rightarrow {}^6P_{3/2}$ (402 nm) and Eu^{3+} ion excitation bands ascribed to the transitions $^7F_0 \rightarrow {}^5H_4$ (318 nm), $^7F_0 \rightarrow {}^5D_4$ (360 nm), $^7F_0 \rightarrow {}^5G_2$ (381 nm), $^7F_0 \rightarrow {}^5L_6$ (393 nm), $^7F_0 \rightarrow {}^5D_3$ (414 nm), $^7F_0 \rightarrow {}^5D_2$ (464 nm). Fig. 5.5 (a) & (b) are recorded to study the co-doping effect of Sm^{3+} and Eu^{3+} and their ability to tune the widespread emission in the orange-red region as a function of Eu^{3+} ion content. From both the excitation spectra, it is observed that the peaks at 393, 402, and 464 nm are intense among all the excitation peaks and were fixed as excitation wavelengths to record the emission spectra of the as-prepared glasses. Intensities variation of Sm^{3+} excitation transition $^6H_{5/2} \rightarrow {}^6P_{3/2}$ (402 nm) under 600 nm emission and Eu^{3+} excitation transition $^7F_o \rightarrow {}^5L_6$ (393 nm) under 612 nm emission with Eu_2O_3 concentration are shown in Fig. 5.6. The excitation spectra under 612 nm emission wavelength of LiBiAlBSi glasses clearly show the occurrence of several Sm^{3+} excitation bands which suggests the existence of ET process from Sm^{3+} to Eu^{3+} ions. Thus, Sm^{3+} ions are performing a sensitizer role and Eu^{3+} ions are performing an activator role in Sm^{3+}/Eu^{3+} ions co-doped LiBiAlBSi glasses [37,174,177].

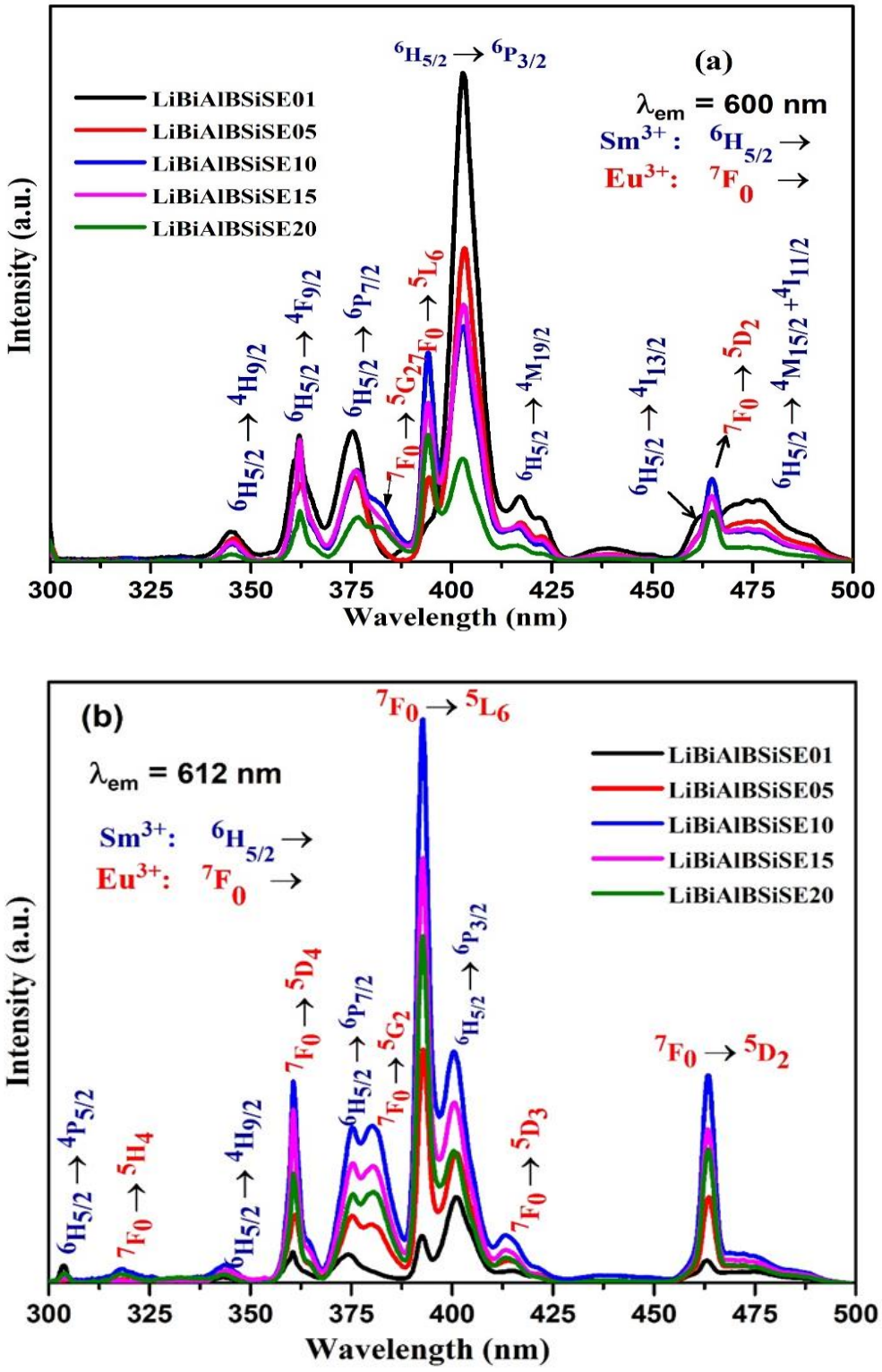

Fig. 5.5. The excitation spectra of Sm^{3+}/Eu^{3+} co-doped LiBiAlBSi glasses under different emission wavelengths (a) 600 nm and (b) 612 nm.

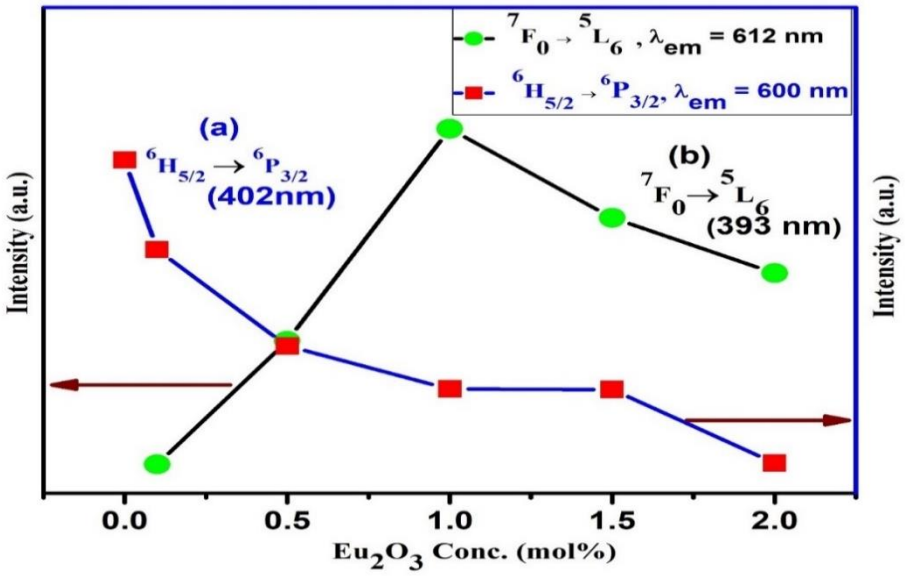

Fig. 5.6. Peak intensities variation of transitions (a) $^6H_{5/2} \rightarrow {}^6P_{3/2}$ (402 nm) at λ_{em} = 600 nm and (b) $^7F_o \rightarrow {}^5L_6$ (393 nm) at λ_{em} = 612 nm with Eu_2O_3 concentration

In the process of understanding the influence of Eu^{3+} ions concentration on Sm^{3+} ions in the co-doped LiBiAlBSi glasses, the PL emission spectra of Sm^{3+}/Eu^{3+} co-doped LiBiAlBSiSE glasses under three different exciting wavelengths i.e., 393, 402, and 464 nm have been recorded and are shown in Fig. 5.7 (a-c). The selection of three excitation wavelengths is based on their higher intensities in the excitation spectra as discussed above (Fig. 5.5). The excitation wavelengths 393 nm and 464 nm are efficiently exciting Eu^{3+} ions whereas 402 nm excitation wavelength efficiently exciting Sm^{3+} ions. The emission spectra recorded for Sm^{3+}/Eu^{3+} co-doped LiBiAlBSi glasses under 393 nm excitations wavelength of Eu^{3+} ions pertaining to its $^7F_0 \rightarrow {}^5L_6$ transition is shown in Fig. 5.7(a). From this figure, it is conspicuous that, Eu^{3+} ions show several emission peaks at 702 nm ($^5D_0 \rightarrow {}^7F_4$), 653 nm ($^5D_0 \rightarrow {}^7F_3$), 612 nm ($^5D_0 \rightarrow {}^7F_2$), 591 nm ($^5D_0 \rightarrow {}^7F_1$), and 579 nm ($^5D_0 \rightarrow {}^7F_0$) wherein possibly only one peak at 600 nm corresponds to $^4G_{5/2} \rightarrow {}^6H_{7/2}$ transition of Sm^{3+} ions is overlapping with $^5D_0 \rightarrow {}^7F_1$ transition of Eu^{3+} ions observed at 591 nm. From Fig. 5.7(a) it can also be observed that the intensity of the most intense emission transition ($^5D_0 \rightarrow {}^7F_2$) of Eu^{3+} ions is much stronger than the intensity of the most intense emission transition ($^4G_{5/2} \rightarrow {}^6H_{7/2}$) of Sm^{3+} ions indicating the possible ET from Sm^{3+} to Eu^{3+} in LiBiAlBSi glasses [97,175–177].

The emission spectra recorded for Sm^{3+}/Eu^{3+} co-doped LiBiAlBSi glasses under 402 nm ($^6H_{5/2} \rightarrow {}^6P_{3/2}$) excitations wavelength of Sm^{3+} ions show numerous emission peaks in visible range pertaining to the f–f transitions of Sm^{3+} and Eu^{3+} ions as shown in Fig. 5.7(b). From this figure,

it is conspicuous that, Eu^{3+} ions show several emission peaks observed at 579 nm ($^5D_0 \rightarrow {}^7F_0$), 591 nm ($^5D_0 \rightarrow {}^7F_1$), 612 nm ($^5D_0 \rightarrow {}^7F_2$), 653 nm ($^5D_0 \rightarrow {}^7F_3$), and 702 nm ($^5D_0 \rightarrow {}^7F_4$). The emission peaks observed at 646 nm and 653 nm are due to Sm^{3+} and Eu^{3+} ion transitions, respectively combined into one and becoming non-distinguishable as Eu^{3+} ion content increased. With the increase in Eu^{3+} ions content, the intensity of all the emission peaks pertaining to Sm^{3+} ions are continuously decreasing. The intensity of all the emission peaks pertaining to Eu^{3+} ions are growing with an increase in Eu^{3+} ions from 0.1 to 1.0 mol% and then decreasing beyond due to concentration quenching. Observing Eu^{3+} ions emission peaks in the co-doped LiBiAlBSi glasses under 402 nm excitation wavelength of Sm^{3+} ions and their upsurge with the increase in Eu^{3+} ions content at the expense of declination observed in the intensity of the emission peaks pertaining to Sm^{3+} ions indicate a clear possible ET process from Sm^{3+} ions to Eu^{3+} ions. These results predict that LiBiAlBSi glasses co-doped with Sm^{3+} ions and Eu^{3+} ions have a down-conversion ability of the photons to emit in orange and red regions of emission spectra which is the highest absorption range for copper phthalocyanine-based solar cells or PV cells [37,97,174,177,187].

Fig. 5.7(c) displays the emission spectra recorded under 464 nm excitation wavelength of Eu^{3+} ions pertaining to its $^7F_0 \rightarrow {}^5D_2$ transition for Sm^{3+}/Eu^{3+} co-doped LiBiAlBSi glasses. In this figure, the emission transition shown for Eu^{3+} and Sm^{3+} ions are $^5D_0 \rightarrow {}^7F_I$ (I = 0,1,2,3,4) and $^4G_{5/2} \rightarrow {}^6H_{J/2}$ (J = 5,7,9) respectively. It is observed that the intensity of Sm^{3+} ion emission transition declines with the upsurge of Eu^{3+} content. This outcome also acclaims the possible ET occurring from Sm^{3+} ions to Eu^{3+} ions and there is no back transfer of energy from Eu^{3+} ions to Sm^{3+} ions [97,183,188,189]. The outcome of all the emission spectra shown in Fig. 5.7 allows us to contemplate that, among all the Sm^{3+}/Eu^{3+} co-doped LiBiAlBSi glasses, the one containing 0.5 mol% of Sm^{3+} ions and 1.0 mol% of Eu^{3+} ions (LiBiAlBSiSE10 glass) is an optimized glass and a capable candidate to generate intense red color needed to fabricate white LEDs under n-UV & blue excitation wavelengths through a downshifting process.

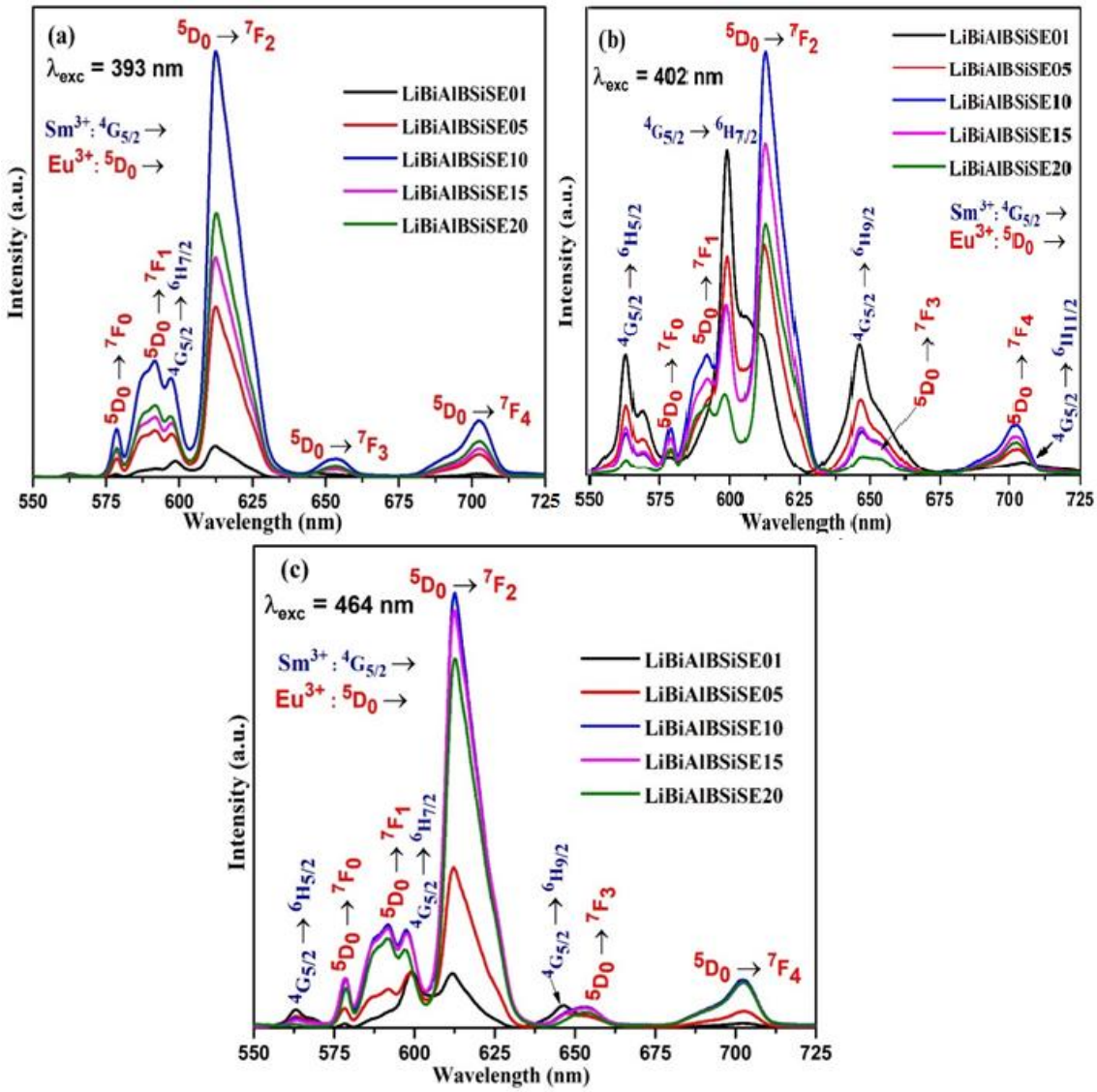

Fig. 5.7. The emission spectra of Sm^{3+}/Eu^{3+} co-doped LiBiAlBSi glasses under different excitation wavelengths (a) 393 nm (b) 402 nm and (c) 464 nm.

5.3.4. PL Decay analysis

PL decay analysis is an advantageous investigation to understand the process of luminescence quenching and to know the progression of the ET process among the RE ions. The decay time is a vital parameter for the studies of the ET process from Sm^{3+} to Eu^{3+} ions. The PL decay plots for the titled glasses were monitored for 600 nm emission wavelength attributed to the transition $^4G_{5/2} \rightarrow {}^6H_{7/2}$ under 402 nm excitation wavelength as shown in Fig. 5.8.

The decay profiles for the singly Sm^{3+} doped and Sm^{3+} co-doped with Eu^{3+} in LiBiAlBSi glasses were best fitted for bi-exponential equation and decay lifetimes average values (τ_{avg}) were estimated by using Equ.no.1.19 and 1.20 given in chapter 1 [97,177]. The τ_{avg} for singly

Sm^{3+} doped and Sm^{3+}/Eu^{3+} co-doped LiBiAlBSi glasses are presented in Table 5.1. From Table 5.1, it is observed that τ_{avg} values for $^4G_{5/2}$ state of the Sm^{3+} ions decline with the increase in Eu^{3+} ions concentration and this declination is a strong indication for ET from Sm^{3+} to Eu^{3+} ions.

The value of energy transfer efficiency (η_T) and the energy transfer probability rate (P_T) can be estimated using the following equation [37,177]:

$$\eta_T = \left(1 - \frac{\tau_d}{\tau_{do}}\right) X\ 100 \qquad (5.1)$$

$$P_T = \frac{1}{\tau_d} - \frac{1}{\tau_{do}} \qquad (5.2)$$

where, τ_{d0} and τ_d denote the decay time for the Sm^{3+} ions doped host glass without the Eu^{3+} ions and with the Eu^{3+} ions, respectively. The ET efficiencies (η_T) and ET probabilities (P_T) values are presented in Table 5.1. Both values of η_T and P_T upsurge with a rise in the Eu^{3+} ions concentration signifying that as Eu^{3+} ions concentration rises, the energy transfers from Sm^{3+} ions to Eu^{3+} ions may increase.

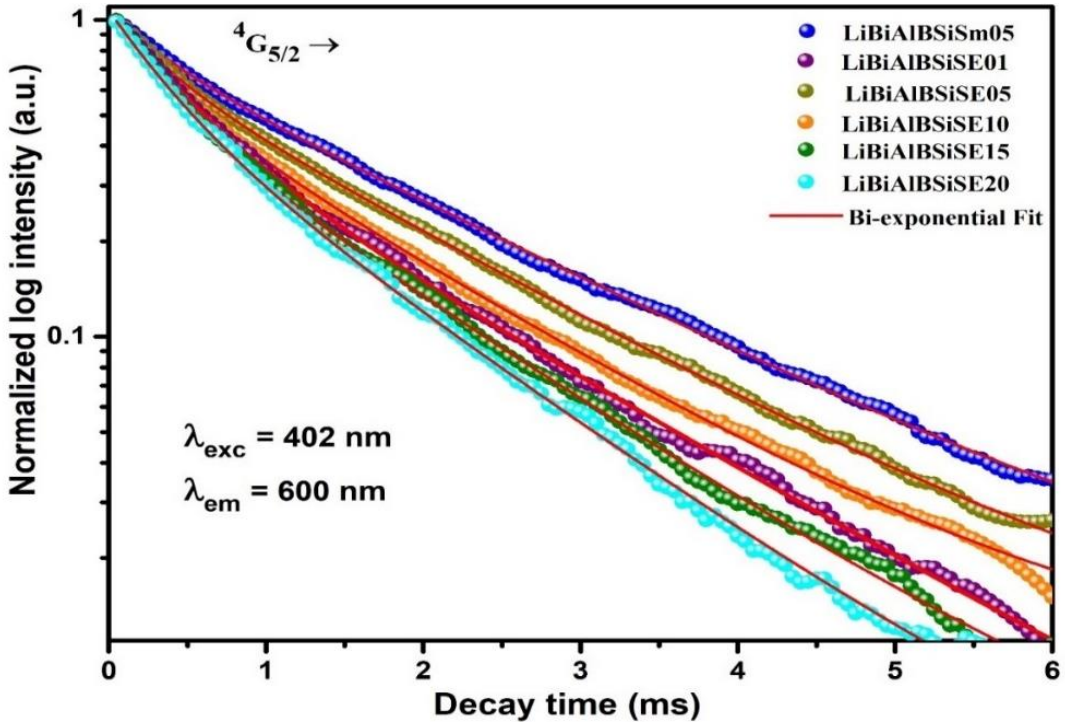

Fig. 5.8. Bi-exponential decay plots for Sm^{3+} and Sm^{3+}/Eu^{3+} co-doped LiBiAlBSi glasses.

Table 5.1. The average value of decay lifetime, energy transfer efficiency (η_T) and energy transfer probability rate (P_T) of Sm^{3+}/Eu^{3+} co-doped LiBiAlBSi glasses

Sample Name	Decay lifetime (ms)	Energy transfer efficiency η_T (%)	Energy transfer probability rate (P_T)
LiBiAlBSiSm05	1.656	--	--
LiBiAlBSiSE01	1.460	11.79	0.08
LiBiAlBSiSE05	1.354	18.23	0.13
LiBiAlBSiSE10	1.316	20.51	0.16
LiBiAlBSiSE15	1.283	22.53	0.18
LiBiAlBSiSE20	1.241	25.03	0.20

5.3.5. Energy transfer mechanism

The energy transfer amid the RE ions may occur via two different interactions such as exchange and multipolar interactions. The ET process from the Sm^{3+} ions to Eu^{3+} ions can arise through exchange or multipolar interactions. In Sm^{3+} and Eu^{3+} co-doped LiBiAlBSi glasses, the interaction emphasises the multipolar interaction process because exchange interaction arises only when both the sensitizer ions and the activator ions are present with appropriate distance at the adjacent neighbour sites.

The theory on multipolar interactions, Dexter's ET scheme, and Reisfeld's calculation have been usually applied to the study of ET interaction among Sm^{3+} and Eu^{3+} as per the following relation [37,177]:

$$\frac{\eta_0}{\eta} \propto C^{n/3} \qquad (5.3)$$

Where C represents the summation of the mole percentage of Sm^{3+} and Eu^{3+} ions concentration, η_0 and η are the quantum efficiencies of the sensitizer (Sm^{3+}) ions in the absence and occurrence of the activator (Eu^{3+}) ions respectively; n denotes the nature of multipolar interaction. The value of "n" for dipole-dipole (d-d) interaction, dipole-quadrupole (d-q) interaction, and quadrupole-quadrupole (q-q) interaction are 6, 8 and 10, respectively.

The $\frac{\eta_0}{\eta}$ value can be nearly assessed by the interrelated luminescence intensities ratio as [37,97]:

$$\frac{I_{so}}{I_s} \propto C^{n/3} \qquad (5.4)$$

where I_{so} is intrinsic intensity for emission of Sm^{3+} ion in the absence of Eu^{3+} ion and I_s is the emission intensity of Sm^{3+} in the presence of Eu^{3+}. The plots $\frac{I_{s0}}{I_s} \propto C^{n}/_{3}$ are shown in Fig. 5.9 and the best fit was achieved for n=6 under 402 nm excitation. This result proposes that the non-radiative d-d interaction is the basis for the energy transferred from the Sm^{3+} ions to Eu^{3+} ions.

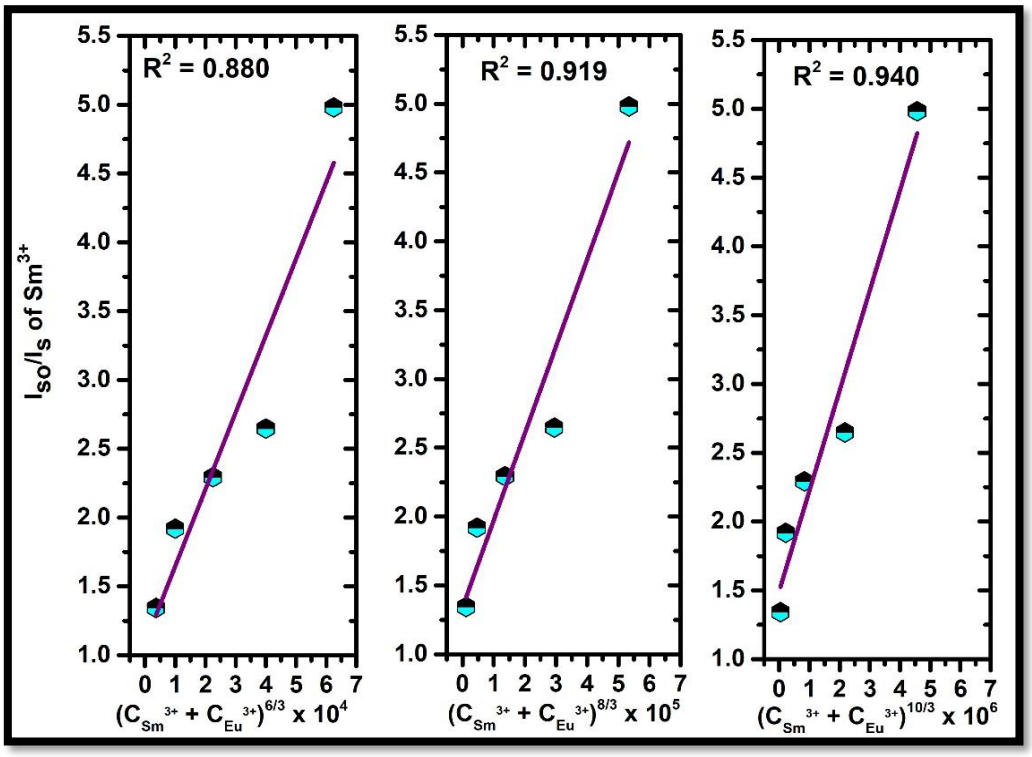

Fig. 5.9. Variation of I_{SO}/I_S of Sm^{3+} with (a) $(C_{Sm+Eu})^{6/3}$ (b) $(C_{Sm+Eu})^{8/3}$ and (c) $(C_{Sm+Eu})^{10/3}$ in the Sm^{3+}/ Eu^{3+} co-doped LiBiAlBSi glasses for 402 nm excitation.

The phenomenon of the ET mechanism along with absorption, excitation, and emission transitions of both Sm^{3+} and Eu^{3+} ions in LiBiAlBSi glasses is shown in Fig.5.10. From Fig. 5.10 it is conspicuous that, under 402 nm excitation the Sm^{3+} ions in Sm^{3+}/Eu^{3+} co-doped LiBiAlBSi glasses gets excited from its ground level ($^6H_{5/2}$) to numerous higher excited levels of Sm^{3+} ions. All such Sm^{3+} ions excited to numerous higher excited levels relaxes subsequently into the $^4G_{5/2}$ excited state of Sm^{3+} ions through the non-radiative process due to the small energy gap between the higher excited states. The Sm^{3+} ions may relax from its $^4G_{5/2}$ excited state to its lower levels ^6H_J (J = 5/2, 7/2, and 9/2) with visible emission (or) to the $^5D_0$ energy level of Eu^{3+} ions through the non-radiative energy transfer process. The energy

difference between the $^4G_{5/2}$ energy state of Sm^{3+} ions and the $^5D_0$ energy level of Eu^{3+} ions is 493 cm^{-1}. This small energy difference can be compensated by lattice vibration phonons and makes the possible non-radiative energy transfer process possible. This analysis proposes that Sm^{3+} performs as an effective sensitizer/donor for the Eu^{3+} ions in the titled glasses [177,187–190].

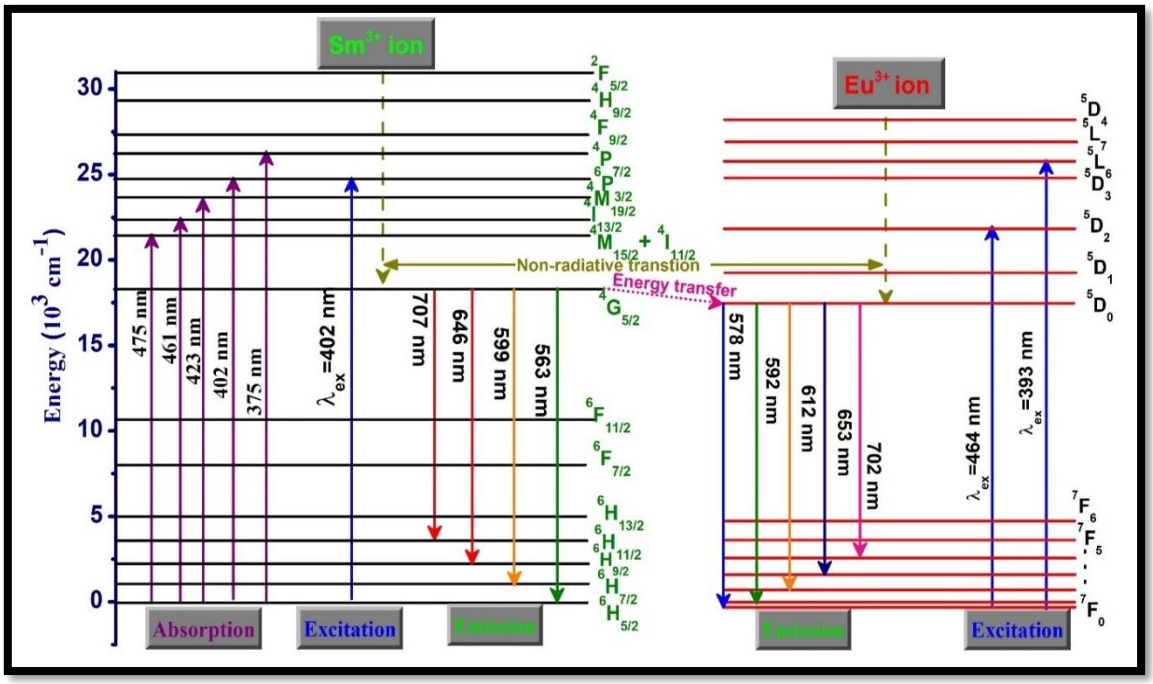

Fig. 5.10. Energy level diagram showing energy transfer involved in Sm^{3+}/Eu^{3+} ions co-doped LiBiAlBSi glasses.

5.3.6. CIE coordinates

The CIE chromaticity coordinates shown in the CIE1931 diagram of the overall emission for singly doped Sm^{3+} ion and co-doped Sm^{3+}/Eu^{3+} in LiBiAlBSi glasses under excitation at wavelengths (a) 393 nm, (b) 402 nm, and (c) 464 nm depicted in Fig. 5.11(a), 5.11(b), and 5.11(c) respectively and values of CIE coordinates are presented in Table 5.2. It is noticed from this table that the calculated CIE coordinate (0.5979, 0.4007) for LiBiAlBSiSm05 glass under 402 nm excitation is near to the coordinates for Nichia Corporation designed Amber LED (0.570, 0.420) NSPAR 70BS [97]. For overall emission, it is also remarked that with the increment of Eu^{3+} ions concentration, the CIE coordinates shift from the reddish-orange region to the red region because of the enrichment in the Eu^{3+} ions emission peak which is the possible reason is proficient ET procedure from Sm^{3+} to Eu^{3+} ions. For the glass LiBiAlBSiSE20, CIE coordinates for all three excited wavelengths are nearby to the commercially available Y_2O_2S: Eu^{3+} (0.647, 0.343) red phosphor [191].

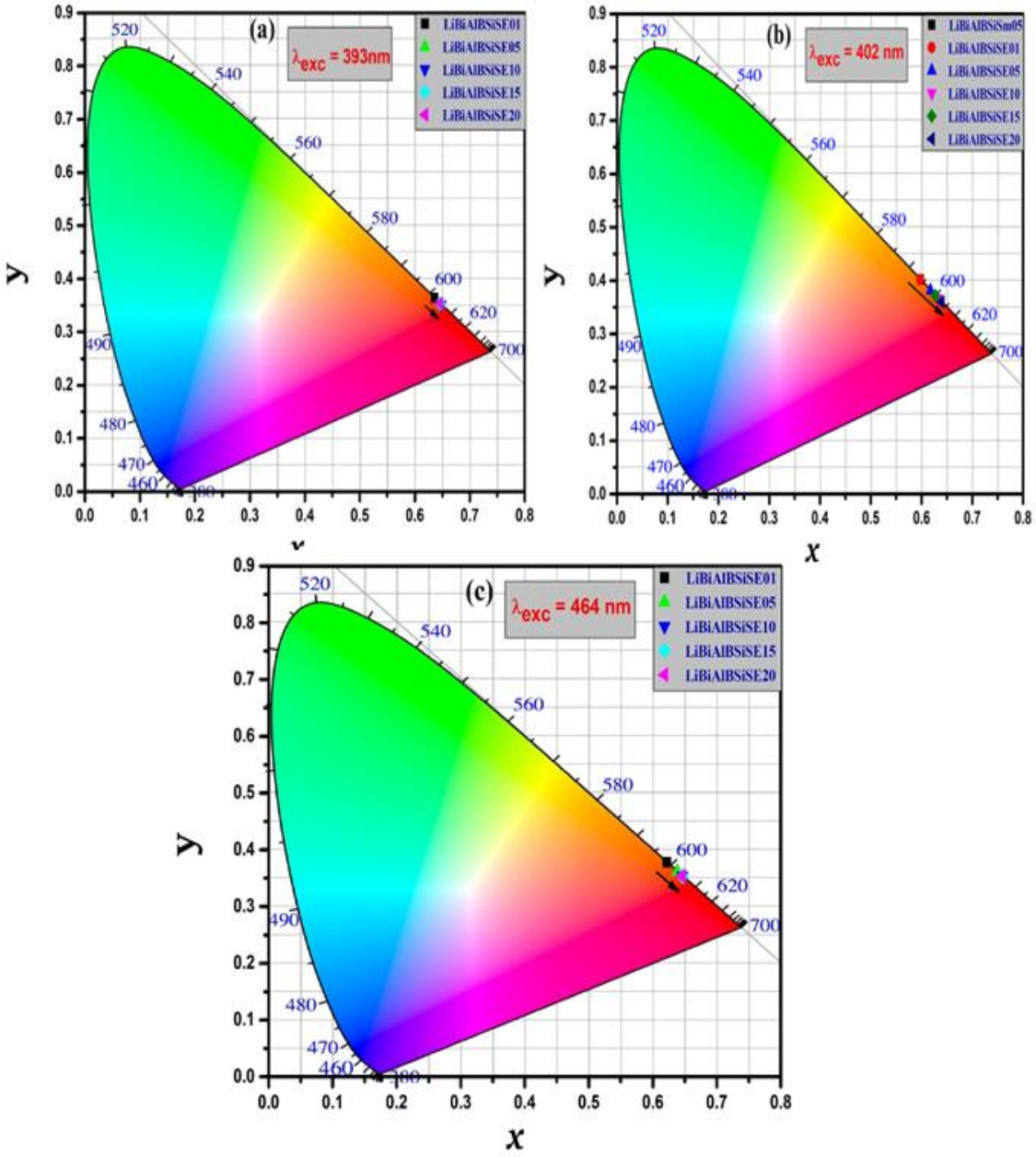

Fig. 5.11. CIE color coordinates Sm^{3+} and Sm^{3+}/Eu^{3+} co-doped LiBiAlBSi glasses under different excitation wavelengths (a) 393 nm (b) 402 nm and (c) 464 nm.

Therefore, it can be determined that the tunable emission attained from the reddish-orange to red region for Sm^{3+}/Eu^{3+} co-doped LiBiAlBSi glasses suggests that our glass system LiBiAlBSi codoped with Sm^{3+} and Eu^{3+} is an appropriate candidate for red emission element for white LEDs.

Table 5.2. Colorimetric properties of Sm^{3+}/Eu^{3+} co-doped LiBiAlBSi glasses for different excitation wavelengths.

Sample Name	CIE coordinates (*x*, *y*)		
	λ_{ex} =393 nm	λ_{ex} =402 nm	λ_{ex} =464 nm
LiBiAlBSiSm05	-	(0.5979, 0.4007)	-
LiBiAlBSiSE01	(0.6358, 0.3642)	(0.5972, 0.4021)	(0.6220, 0.3776)
LiBiAlBSiSE05	(0.6469, 0.3527)	(0.6177, 0.3818)	(0.6384, 0.3613)
LiBiAlBSiSE10	(0.6485, 0.3511)	(0.6323, 0.3671)	(0.6462, 0.3535)
LiBiAlBSiSE15	(0.6461, 0.3535)	(0.6274, 0.3720)	(0.6465, 0.3531)
LiBiAlBSiSE20	(0.6460, 0.3536)	(0.6397, 0.3599)	(0.6458, 0.3537)

5.3.7. TD-PL studies

The performance of white LEDs depends on temperature and so thermal stability is one of the vital factors to influence the PL performance (in terms of light output and color rendering index) of the materials used in fabricating white LEDs. To understand the effect of temperature on the PL intensity of the Sm^{3+}/Eu^{3+} co-doped optimized LiBiAlBSiSE10 glass, we have recorded the TD-PL spectra under 402 nm excitation wavelength over a temperature range from 303 to 473 K as depicted in Fig. 5.12 (a). From the figure, it can be noticed that the PL intensity steadily declines with the temperature showing thermal quenching. The emission intensity at 423 K holds about 71.23% of its initial intensity at 303 K as shown in Fig. 5.12 (b) which signifies that Sm^{3+}/Eu^{3+} co-doped optimized glass retains good thermal stability.

The thermal stability of the Sm^{3+}/Eu^{3+} co-doped optimized glass can be further verified by estimating the activation energy from the TD-PL spectral data using the Arrhenius equation given in chapter 1 (Equ. no.1.31) [192,193]. Fig. 5.12(c) shows a graph plotted for $\ln[(I_o/I_T)-1]$ versus $(1/K_BT)$ which is linearly fitted and the activation energy is estimated from the slope of the graph. The slope of this graph is -0.248 and correspondingly the activation energy is equal to 0.248eV. This obtained value of activation energy is relatively higher than the reported activation energy value (0.21eV) in the literature [192].

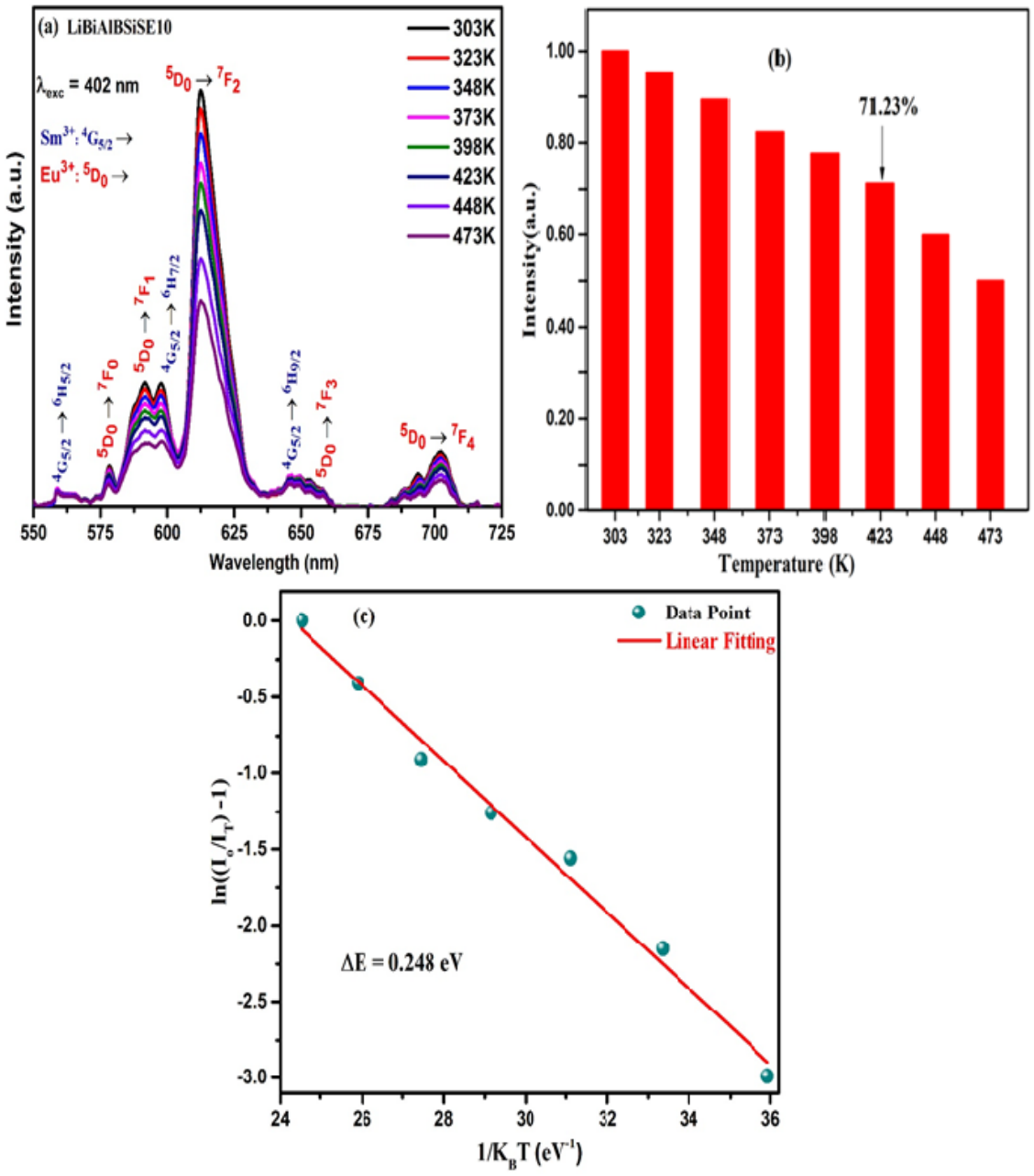

Fig. 5.12. (a) TD-PL spectra excited at 402 nm (b) PL intensity as a function of temperature. (c) Plot of $\ln((I_0/I_T)-1)$ versus $1/K_BT$ of Sm^{3+}/Eu^{3+} co-doped optimized LiBiAlBSiSE10 glass.

This relatively higher value of activation energy further suggests the thermal stability of the Sm^{3+}/Eu^{3+} co-doped optimized glass. Apart from the change in PL intensity with the change in temperature, the shape and peak position has not been changed confirming the good color retention of the optimized glass. Finally, the TD-PL studies allow us to contemplate that the Sm^{3+}/Eu^{3+} co-doped optimized LiBiAlBSiSE10 glass has relatively good thermal stability.

5.4. Summary

In this work, Sm^{3+}, Eu^{3+} single doped and Sm^{3+}/Eu^{3+} co-doped LiBiAlBSi glasses with varying concentrations of Eu^{3+} ions were formed via a melt quenching system. The excitation spectra recorded for Sm^{3+}/Eu^{3+} co-doped LiBiAlBSi glasses confirm the excitation of the titled glasses effectively by blue and n-UV light sources. In emission spectra, the dominant emission peaks for Sm^{3+} ions and Eu^{3+} ions are at 599 nm and 612 nm corresponding to $^4G_{5/2} \rightarrow {}^6H_{7/2}$ and $^5D_0 \rightarrow {}^7F_2$ transitions respectively. By using emission spectra, Dexter's ET formulation and Reisfeld's calculation approximation propose that the energy is shifted from sensitizer Sm^{3+} ions to activator Eu^{3+} ions in LiBiAlBSi glasses through non-radiative dipole-dipole interaction. The declination in PL decay lifetime observed for $^4G_{5/2}$ emitting level of Sm^{3+} ions with growing Eu^{3+} ions content suggests the ET process occurrence from Sm^{3+} to Eu^{3+} ions in LiBiAlBSi glasses. CIE coordinate measured for the as-prepared glasses under n-UV excitation shifted from orange to reddish-orange and then to the red region with the upsurge in Eu^{3+} concentration. The TD-PL studies show good thermal stability for the optimized LiBiAlBSiSE10 glass with a relatively high ΔE value (0.248 eV). The obtained results endorse that the optimized Sm^{3+}/Eu^{3+} co-doped LiBiAlBSiSE10 glass is an attractive and thermally stable potential candidate for synthesizing white LEDs with n-UV LED light chips in solid-state lighting and PV cells.

CHAPTER 6

Visible and NIR spectral analysis of Er^{3+} doped LiBiAlBSi glasses for laser applications

(The content of this chapter has been revised and communicated to "**Laser Physics (2023)")**

The LiBiAlBSi glasses incorporated with different concentrations (0.1 to 2 mol %) of Er^{3+} ions were formed through the melt quench technique. The study of their physical and spectroscopic properties by measuring the spectra of optical absorption, PL, and decay profiles. At excitation wavelength 378 nm, visible and NIR emission spectra were measured and showed intense green and NIR emission with respective transition $^4S_{3/2} \rightarrow {}^4I_{15/2}$ (547 nm) and $^4I_{13/2} \rightarrow {}^4I_{15/2}$ (1538 nm) respectively. The emission intensities of both visible and NIR spectra enhance up to 1.0 mol% doping of Er^{3+} amount in the host glass and after that decline due to the quenching effect. CIE coordinates for the visible spectra are revealed in the green region. Various parameters determined such as stimulated emission cross-section, optical gain, gain-bandwidth features and broadened emission spectra in the NIR region acclaim that the optimized LiBiAlBSiEr10 glass is an appropriate candidate for laser applications in visible and NIR regions.

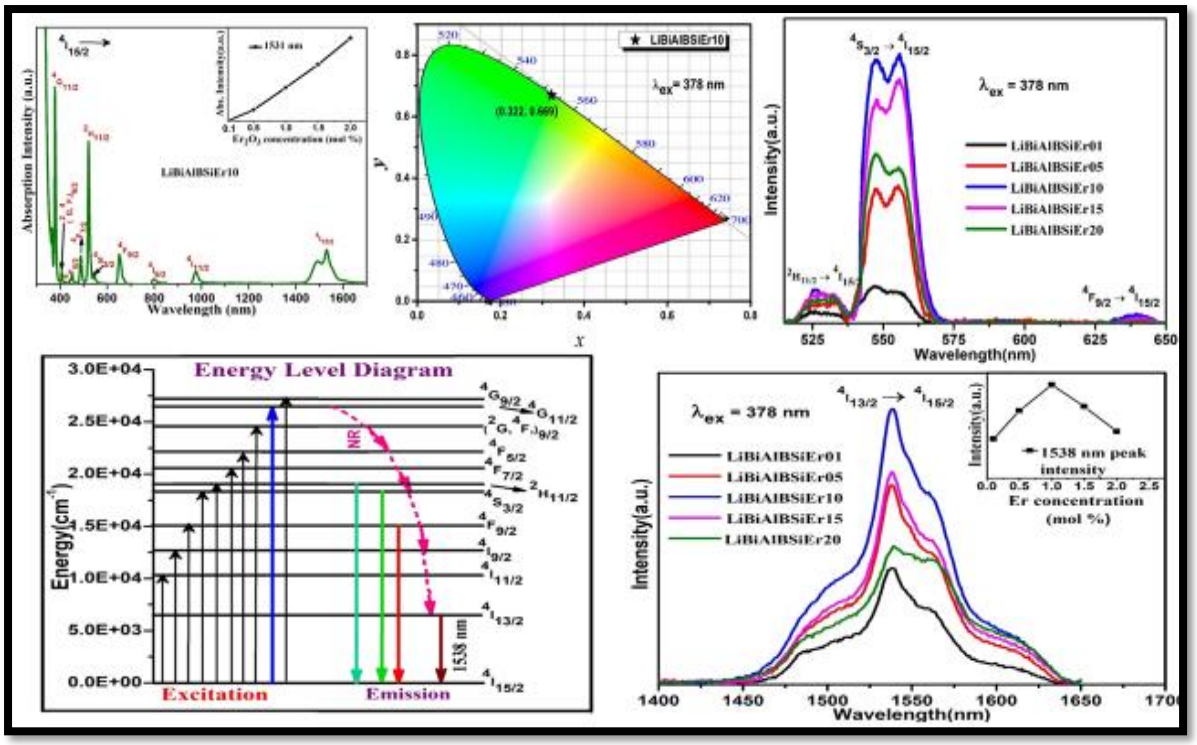

6.1. Introduction

Optically active luminescence glasses and phosphor materials attract the attention of scientists and researchers owing to their versatile applications in numerous fields such as telecommunication networks, SSL, LEDs, optical amplifiers, data storage devices, display monitors and sensors [194–197]. In several of the aforementioned applications, the optical properties of the materials are improved by integrating Rare Earth (RE) (optically active ions) with different host materials. The RE ions show optical absorption and PL features due to 4f-4f transitions shielded from surrounding ligands and external interaction. Among the RE ions, the sharp spectral emissions of trivalent erbium ions (Er^{3+}) from Near Infra-Red (NIR) to the visible region makes it suitable for several potential photonic applications such as gain media, eye-safe range visible lasers and near-infrared lasers, fiber amplifiers, temperature sensor, color displays, etc.[56,198,199]. The glasses doped with Er^{3+} ions play a vibrant role in the expansion & development of telecommunication networks. Er^{3+} ions can be relevant specifically for eye-safe lasers due to the numerous bands exhibited in the green, red and NIR regions [200]. Extensive studies on RE ions doped glasses have been done in visible and NIR regions.

In the present chapter, we investigate our glass system LiBiAlBSi doped with Er^{3+} ions to identify the optimized concentration of the Er^{3+} ions and find the physical and optical properties using absorption spectrum, excitation spectrum, visible-NIR emission spectra and decay spectra analysis. Consequently, the objective of this work is to prepare the glasses LiBiAlBSi incorporated with Er^{3+} ions and to investigate their appropriateness for laser applications in visible and NIR regions.

6.2. Experimental

A series of different concentrations (0.1 to 2 mol%) of Er^{3+} ions incorporated LiBiAlBSi glasses was formed through the melt quench technique wherein the composition is as follows: $20Li_2CO_3$-$7.5Bi_2O_3$-(7.5-x) Al_2O_3 - $45H_3BO_3$ - $20SiO_2$ - x Er_2O_3 (where x = 0.1 to 2.0 mol%). As per concentrations 0.1, 0.5, 1.0, 1.5, and 2.0 mol%, of Er^{3+} ions, the glasses are labelled as LiBiAlBSiEr01, LiBiAlBSiEr05, LiBiAlBSiEr10, LiBiAlBSiEr15, and LiBiAlBSiEr20, respectively. The AR grade raw materials Li_2CO_3, Bi_2O_3, Al_2O_3, H_3BO_3, and SiO_2 with high purity and 99.99% purity of Er_2O_3 are used According to series composition, constituent chemicals were weighed for 7g batch for each label as mentioned above and ground in agate mortar until a proper homogenous mixture was collected into silica crucible. Silica crucibles were kept in an electrical muffle furnace heated at 1150 °C for one hour and a uniform

melt was obtained. This uniform melt was poured and quenched in between the preheated plane brass plates. These obtained glasses were annealed in an electrical furnace for 4 hours at 350 °C to relieve air bubbles and strains.

The X-ray diffraction patterns were observed using the X-ray diffractometer Bruker-Model D8. Archimedes' principle was used to measure the density of prepared glasses and water was used as immersion liquid in the measurement. All spectral measurements were done under ambient conditions. The UV-Vis-NIR spectrophotometer with model no.V-670 of JASCO was utilized to record absorption spectra. The excitation and UV-Vis -NIR photoluminescence (PL) spectra were taken with a NIR spectrophotometer of Photon Technology International QM-51, and a Hitachi-F7000 fluorescence spectrophotometer. The decay profiles were measured with an Edinburgh FL920 fluorescence spectrometer which has an excitation source of a Xenon flash lamp.

6.3. Result and discussion

6.3.1. X-ray diffraction pattern study

The XRD patterns of un-doped glass LiBiAlBSi and Er^{3+} doped glass LiBiAlBSiEr10 are illustrated in Fig. 6.1. The XRD patterns do not present any narrow and sharp peak that suggests the absence of long-range order and supports an amorphous or non-crystalline nature of the prepared glasses [171,201].

6.3.2. UV–Visible and NIR absorption spectrum

To attain the optical transitions characteristic, the absorption spectra of the LiBiAlBSi glasses incorporated with trivalent Erbium ions were measured at ambient temperature in the range 350-1700 nm. Fig. 6.2 represents the absorption curve of the as-prepared glass sample LiBiAlBSiEr10 in UV–Visible and NIR region and obtained absorption band because of the interactions between electrostatic and spin orbits of the f–f energy level of Er^{3+} ions.

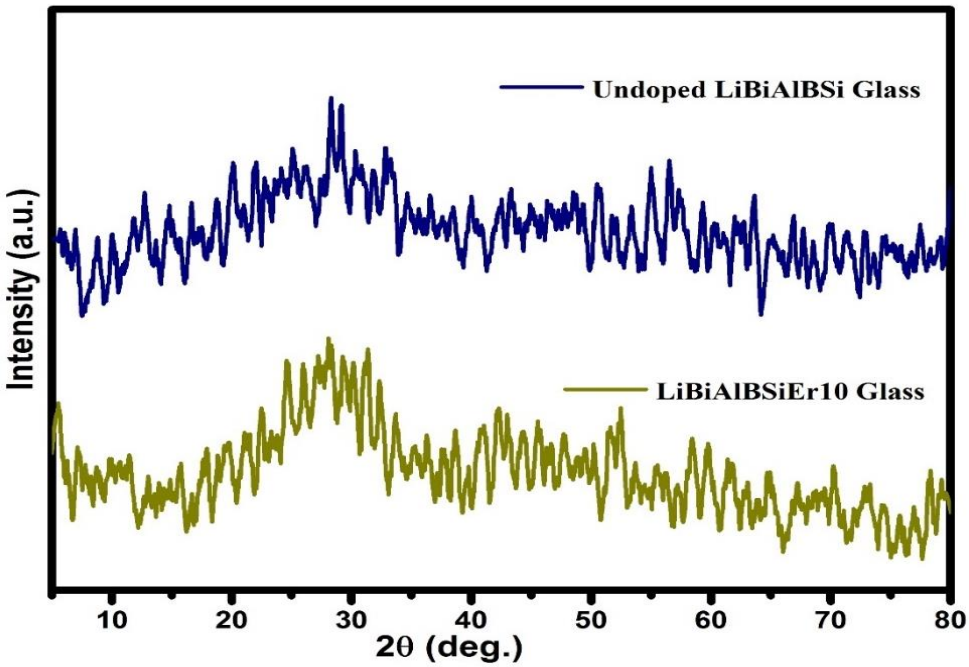

Fig. 6.1. XRD patterns of LiBiAlBSi and LiBiAlBSiEr10 glasses.

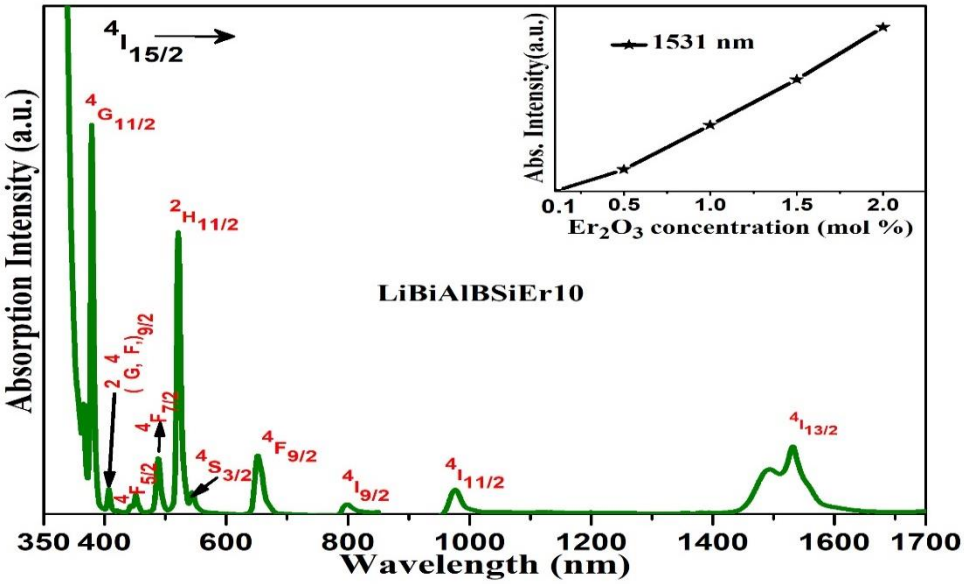

Fig. 6.2. The absorption spectrum of the Er^{3+} ions doped LiBiAlBSiEr10 glass. (Inset: dependence of absorption intensity at 1531 nm on the Er^{3+} ions concentration)

The absorption peaks were observed for the transitions from ground level $^4I_{15/2}$ to various exciting levels $^4G_{11/2}$ (378 nm), (^2G, $^4F)_{9/2}$ (408 nm), $^4F_{5//2}$ (453), $^4F_{7/2}$ (489 nm), $^2H_{11/2}$ (523 nm), $^4S_{3/2}$ (545 nm), $^4F_{9/2}$ (653 nm), $^4I_{9/2}$ (798 nm), $^4I_{11/2}$ (978 nm) and $^4I_{13/2}$ (1531 nm) of Er^{3+} ions and well-matched with data published by Carnall et al [21,22]. The obtained spectrum peaks position to be alike to the reported literature which reveals that Er^{3+} ions merge uniformly into

the prepared glass network. The absorption intensity for the transitions $^4I_{15/2} \rightarrow {}^2H_{11/2}$ (523 nm) and $^4I_{15/2} \rightarrow {}^4G_{11/2}$ (378 nm) are higher than other transitions in absorption spectra and follow $|\Delta J| \leq 2$, $|\Delta L| \leq 2$ and $|\Delta S| = 0$ selection rules. Therefore, these higher-intensity transitions are identified as hypersensitive transitions since these transitions are sensitive to the host environment [202]. The inset of Fig. 6.2 presents the relationship of absorption intensity at 1531 nm peaks with Er^{3+} ions concentration. The absorption intensity increases almost linearly from 0.1 mol% to 2.0 mol% concentration of Er^{3+} ions and the shape of absorption peaks at 1531 nm is not influenced by variation in Er^{3+} concentration. It means the crystal field in the host glass is controlled by the basic constituents of the host [203].

The bonding nature among doped RE ions and oxygen ligands in the matrix of host glass is predicted by the nephelauxetic ratio (β) and bonding parameters (δ). The plus or minus sign indicates the δ that predicts if the bond is covalent or ionic in nature. The β was estimated from all the attained transitions and the δ was estimated by using Eqn. no. 1.1 and 1.2 in Chapter 1 [91,204]. The calculated values of β and δ for glass LiBiAlBSiEr10 are 0.999968 and +0.00317 respectively. The positive value of δ ascribed to the Er^{3+} ions share a covalent bond with oxygen ligands in the host glass system.

6.3.2.1. Energy bandgap analysis

To obtain information on band structure and the related optical transitions, the rudimentary edge in the ultraviolet regime of absorption is helpful for both types of materials including crystalline and amorphous. Thus, the indirect optical energy bandgap (E_{opt}) was estimated by using the absorption spectra of Er^{3+} in LiBiAlBSi glasses. The fundamental absorption edge was used for the estimation of E_{opt} for LiBiAlBSi glasses incorporated with Er^{3+} ions by employing the equation of Davis and Mottas given in chapter 1 (equ. no.1.3) [88,205]. Generally, for oxide glasses, the indirect bandgap E_{opt} values were determined by the fitting of Tauc's plot in the linear region as represented in Fig.6.3 and values of E_{opt} given in Table 6.1. It is perceived that the indirect energy bandgap values are increasing (3.218 to 3.322 eV) with Er_2O_3 concentration in the present glasses. This observed rise in the values of the energy bandgap may because of the lessening of non-bridging oxygen (NBOs) in the glass matrix owing to oxygen binding variation. The reduction in NBO's lowers the valence band which leads to a surge in the values of E_{opt} [89].

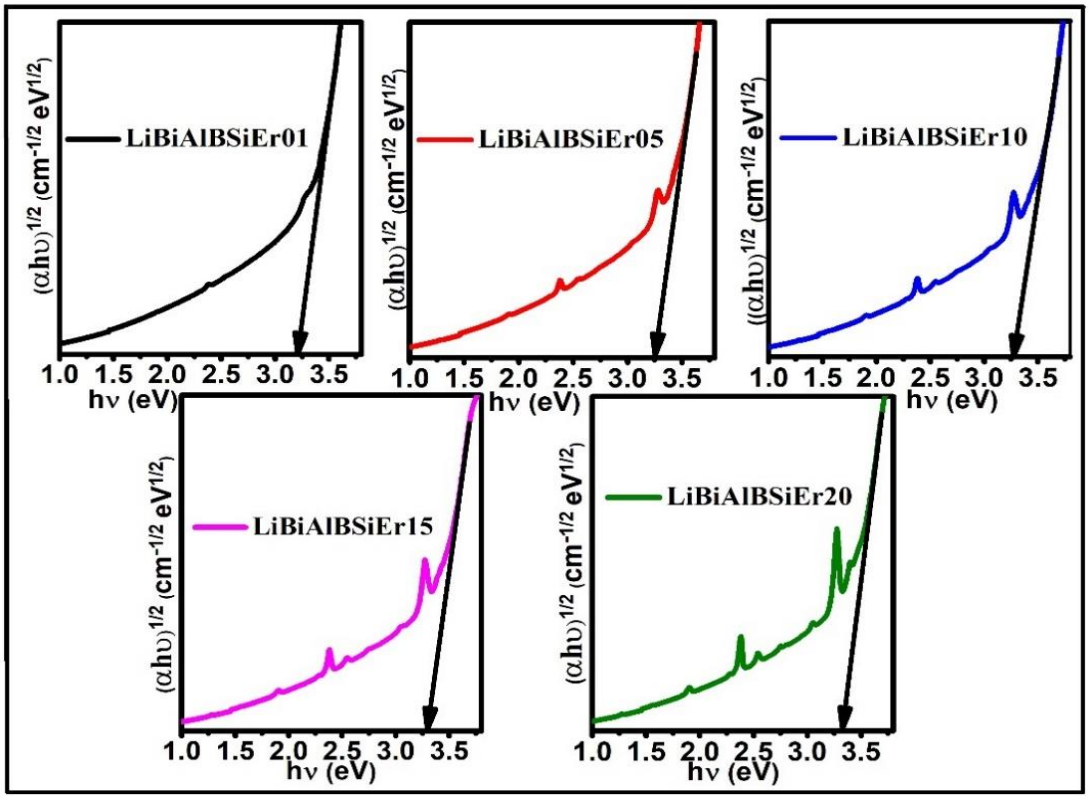

Fig. 6.3. Indirect bandgap plot of Er^{3+} ions doped LiBiAlBSi glasses.

6.3.2.2 Refractive index and physical properties analysis

The values of indirect E_{opt} were used for the estimation of the refractive index (n) for Er^{3+} doped LiBiAlBSi glasses by using Equ. no.4.1 given in chapter 4 [160,161]. The *n* values for LiBiAlBSi glasses doped with Er^{3+} ions prepared glasses are represented in Table 6.1. Some other physical parameters with the help of the refractive index were identified for the LiBiAlBSiEr10 glass by using the certain equation explained elsewhere [91]. In Table 6.2 estimated physical parameters are tabulated with other reported Er^{3+} doped glasses BiBTEr1.0 [201], BLFBEr1 [206] and ZnAlBiBEr10 [197].

It is observed from Table 6.2 that the physical properties of LiBiAlBSiEr10 glass and reported glasses are comparable. Density is the property for the study of the modification of geometric configurations, degree of structural compactness and changes in the coordination of glass networks. A refractive index is an effective tool for the investigation of optical materials. The solubility of RE ions is related to the field strength value and RE ions are highly soluble in the present glass host matrix as the calculated value of field strength is low. Molecular electronic polarizability is correlated to various properties such as dielectric properties, ionic refraction,

optical UV absorption and chemical stability. The chemical stability of material has an inverse relation with the value of molecular electronic polarizability [58,207,208]. The present glass system has a low value of molecular electronic polarizability which shows its good stability.

Table 6.1. The optical band gap (E_{opt}), for indirect allowed transitions along with the refractive index of Er^{3+} ions in LiBiAlBSi glasses.

Glass samples	Indirect E_{opt} (eV)	Refractive Index(n)
LiBiAlBSiEr01	3.218	2.341
LiBiAlBSiEr05	3.237	2.336
LiBiAlBSiEr10	3.261	2.330
LiBiAlBSiEr15	3.292	2.322
LiBiAlBSiEr20	3.322	2.315

Table 6.2. Physical properties of the LiBiAlBSiEr10 glass along with other reported glasses.

Physical properties	LiBiAlBSiEr10 [Present]	BiBTEr1.0 [201]	BLFBEr1 [206]	ZnAlBiBEr10 [197]
Density, d (g/cm^3)	3.634	3.777	3.47	3.904
Refractive index, n	2.330	1.741	1.781	1.816
Average molecular weight(g)	100.01	137.8	76.261	114.4
Dielectric constant(ϵ)	5.428	3.031	3.172	3.297
Optical dielectric constant (ϵ-1)	4.428	2.031	-	2.279
Polaron radius, $\mathbf{r_p}$ (Å)	1.44	1.582	5.035	1.187
Inter-atomic distance,$\mathbf{r_i}$ (Å)	3.575	3.927	12.497	2.945
Molecular electronic polarizability α (10^{-23} cm^3)	0.651	0.584	0.195	0.250
Field Strength, F (10^{15} cm^{-2})	14.456	11.976	2.37	21.28

6.3.2.3. Judd-Ofelt (J-O) analysis

J-O theory [42,43] has been recognized to evaluate the J-O intensity parameters($\Omega_2, \Omega_4, \Omega_6$) and various radiative properties of the glasses. The J-O parameters evaluated using oscillator strength determined experimentally were discussed thoroughly in chapter 1 [21]. The values of oscillator strength were estimated by describing the absorption spectral intensities of the f-f transitions of the LiBiAlBSi glasses doped with the Er^{3+} ions. The experimental oscillator strength (f_{exp}) was calculated with the help of the area of an absorption peak for the corresponding absorption transition by the equation described in the chapter 1 and the calculated oscillator strength (f_{cal}) was assessed by using the J-O theory [202]

The values of f_{exp} and f_{cal} oscillator strengths of absorption transitions in LiBiAlBSiEr10 glass are presented in Table 6.3 along with the transitions, transition energies, band positions and root mean square deviation (δ_{rms}) values. Relatively less value of the root means square deviation (δ_{rms}) shown in Table 6.3 predicts the better quality of fit between the experimental and calculated oscillator strengths and validity of J-O analysis. It is noticed from Table 6.3 that $^4I_{15/2} \rightarrow {}^4G_{11/2,}\ {}^2H_{11/2}$ transition show much higher values of oscillator strength when compared with other transitions. This is due to the enrichment of asymmetry nature which upsurges the possibility of emission in our prepared glasses and hence the numeral of electrons oscillates at greater transition strengths [209]. In general, the values of J-O intensity parameters are correlated with the local environment of around trivalent rare-earth ions which affect the radiative transition properties. J-O parameters were used to explain the symmetry, bonding nature, and rigidity of the present glass system.

Table 6.3. Transitions, transition energies (λ, nm), experimental (f_{exp}) and calculated (f_{cal}) oscillator strengths for LiBiAlBSiEr10 glass.

Transition from		**Oscillator strengths (× 10^{-6})**	
$^4I_{15/2}$	**λ (nm)**	f_{exp}	f_{cal}
$^4G_{11/2}$	378	17.1872	18.7624
$(^2G,{}^4F)_{9/2}$	408	0.623	2.0405
$^4F5/_2$	453	0.854	1.8015
$^4F7/_2$	489	2.1577	4.795
$^2H_{11/2}$	523	12.0396	10.5738
$^4S_{3/2}$	545	2.47	1.4817
$^4F_{9/2}$	653	3.1	2.8849
$^4I_{9/2}$	798	0.421	0.1272
$^4I_{11/2}$	978	1.28	1.6838
$^4I_{13/2}$	1531	4.0333	3.5712
δrms x 10^{-6}		± 1.264	

The J-O intensity parameters ($\Omega_{\lambda = 2, 4, 6}$) of LiBiAlBSiEr10 glass are represented in Table 6.4. The Ω_2 parameter is associated with the bonding nature and sensitivity towards the local environment among the surrounding ligand and the RE ions positions [202]. Table 6.4 also predicts the covalent characteristic between RE ions and ligand bonds for the as-prepared glass as it shows the higher value of the Ω_2. Other J-O parameters Ω_4 and Ω_6 are less sensitive to the local atmosphere and related to the viscosity and rigidity of the host glass matrix [197]. From Table 6.4, the less values of Ω_4 and Ω_6 are advantageous for good luminescence characteristics and the revealed trend $\Omega_2 > \Omega_6 > \Omega_4$ may predict the eminence quality of Er^{3+} ions doped LiBiAlBSiEr10 glass system for the applications of the optical device. The J-O parameters of the LiBiAlBSi Er10 glass and the other reported Er^{3+} ion-doped glasses BiBTEr1.0 [201], BLFBEr1 [206], LBTAFEr10 [199], PKAZFEr10 [195], and ZBLANP [210] are tabulated in Table 6.4, all show a similar trend $\Omega_2 > \Omega_6 > \Omega_4$.

Table 6.4. Judd-Ofelt Parameters (Ω_λ x 10^{-20}cm^2) of LiBiAlBSiEr10 glass along with reported values in literature.

Glass System	Ω_2	Ω_4	Ω_6	Trend	References
LiBiAlBSiEr10	3.94	0.21	2.04	$\Omega_2 > \Omega_6 > \Omega_4$	present work
BiBTEr1.0	11.99	2.22	3.54	$\Omega_2 > \Omega_6 > \Omega_4$	[201]
BLFBEr1	3.53	0.64	1.68	$\Omega_2 > \Omega_6 > \Omega_4$	[206]
LBTAFEr10	5.89	1.10	1.47	$\Omega_2 > \Omega_6 > \Omega_4$	[206]
PKAZFEr10	8.23	1.04	1.91	$\Omega_2 > \Omega_6 > \Omega_4$	[195]
ZBLANP	3.08	1.50	1.71	$\Omega_2 > \Omega_6 > \Omega_4$	[210]

6.3.3. PL and radiative properties analysis

6.3.3.1 Excitation spectrum analysis

In order to study PL characteristics of erbium-incorporated LiBiAlBSi glasses, the excitation spectrum of the LiBiAlBSiE10 glass sample has been observed in the wavelength range 200-1100 nm with emission wavelength 1538 nm and depicted in Fig. 6.4. The excitation spectra reveals the following peaks position at wavelength 368, 378, 407, 451, 489, 523, 546, 653, 804 and 980 nm with respective transitions of Er^{3+} ions from level $^4I_{15/2}$ (ground) to excited levels $^4G_{9/2}$, $^4G_{11/2}$, $(^2G, ^4F)_{9/2}$, $^4F_{5//2}$, $^4F_{7/2}$, $^2H_{11/2}$, $^4S_{3/2}$, $^4F_{9/2}$, $^4I_{9/2}$, and $^4I_{11/2}$ [135]. The highly intense observed transition ($^4I_{15/2} \rightarrow {}^4G_{11/2}$) among these transitions is at wavelength 378 nm

and therefore, it has been used as an excitation wavelength (λ_{ex}) for recording emission spectra for all Er^{3+} ions doped LiBiAlBSi glasses.

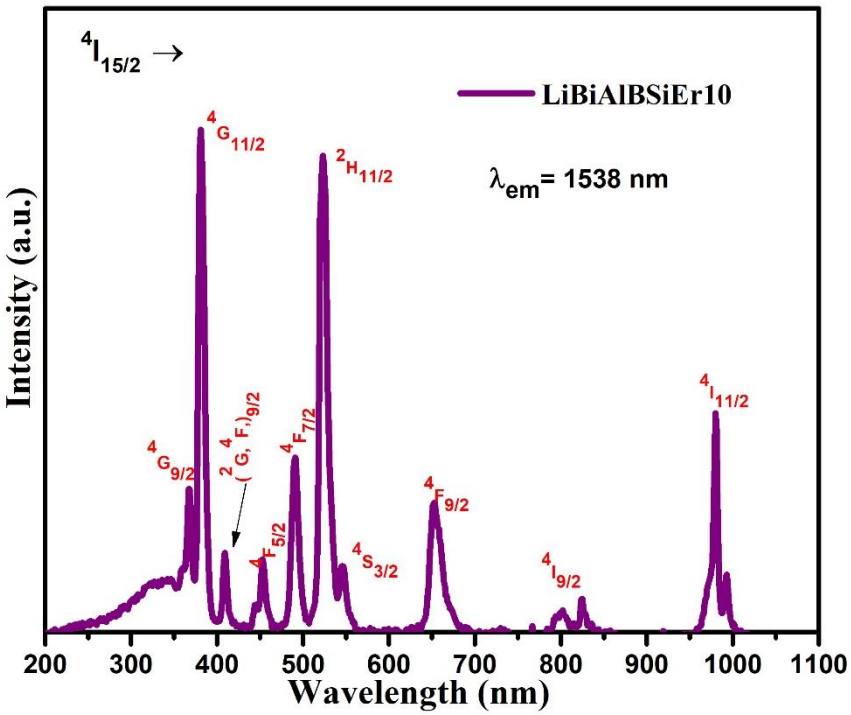

Fig. 6.4. The excitation spectrum of the Er^{3+} ions-doped LiBiAlBSiEr10 glass.

6.3.3.2. Visible emission spectral study

The visible emission spectra were measured under excitation 378 nm at room temperature in the visible range from 500 to 650 nm and shown in Fig. 6.5(a) for the above-mentioned glasses. The three emission peaks of Er^{3+} ions are exhibited in emission spectra and assigned with the transition as $^2H_{11/2} \rightarrow {}^4I_{15/2}$ (527 nm), $^4S_{3/2} \rightarrow {}^4I_{15/2}$ (547 nm) and $^4F_{9/2} \rightarrow {}^4I_{15/2}$ (639 nm). Among all the three transitions, the green region transition $^4S_{3/2} \rightarrow {}^4I_{15/2}$ (547 nm) is found to be more intense. The emission peak intensity rises till 1 mol % and after that intensity shows decrement due to the quenching effect. The inter-ionic distance decreases within adjacent Er^{3+} ions with an increment in the content of Er^{3+} ions which increase the possibility of non-radiative energy transfer through the mechanism of cross-relaxation, resultant of this is the diminishing emission intensity at higher concentration of Er^{3+} ions [24,201]. Judd-Ofelt (J-O) theory is a semi-empirical method that is used to evaluate the various spectroscopic radiative parameters as radiative branching ratio (β_R), transition probability (A), and radiative lifetimes (τ_R) of the exciting levels of RE ions doped glasses with the spectral data of absorption & emission measurements. The β_R is a significant parameter for emission transition to describe the lasing power and its value should be greater than 0.5 for potential laser application [63]. The radiative

parameters for LiBiAlBSiEr10 glass for the transition $^4S_{3/2} \rightarrow {}^4I_{15/2}$ are estimated by using the expression in the literature [57].

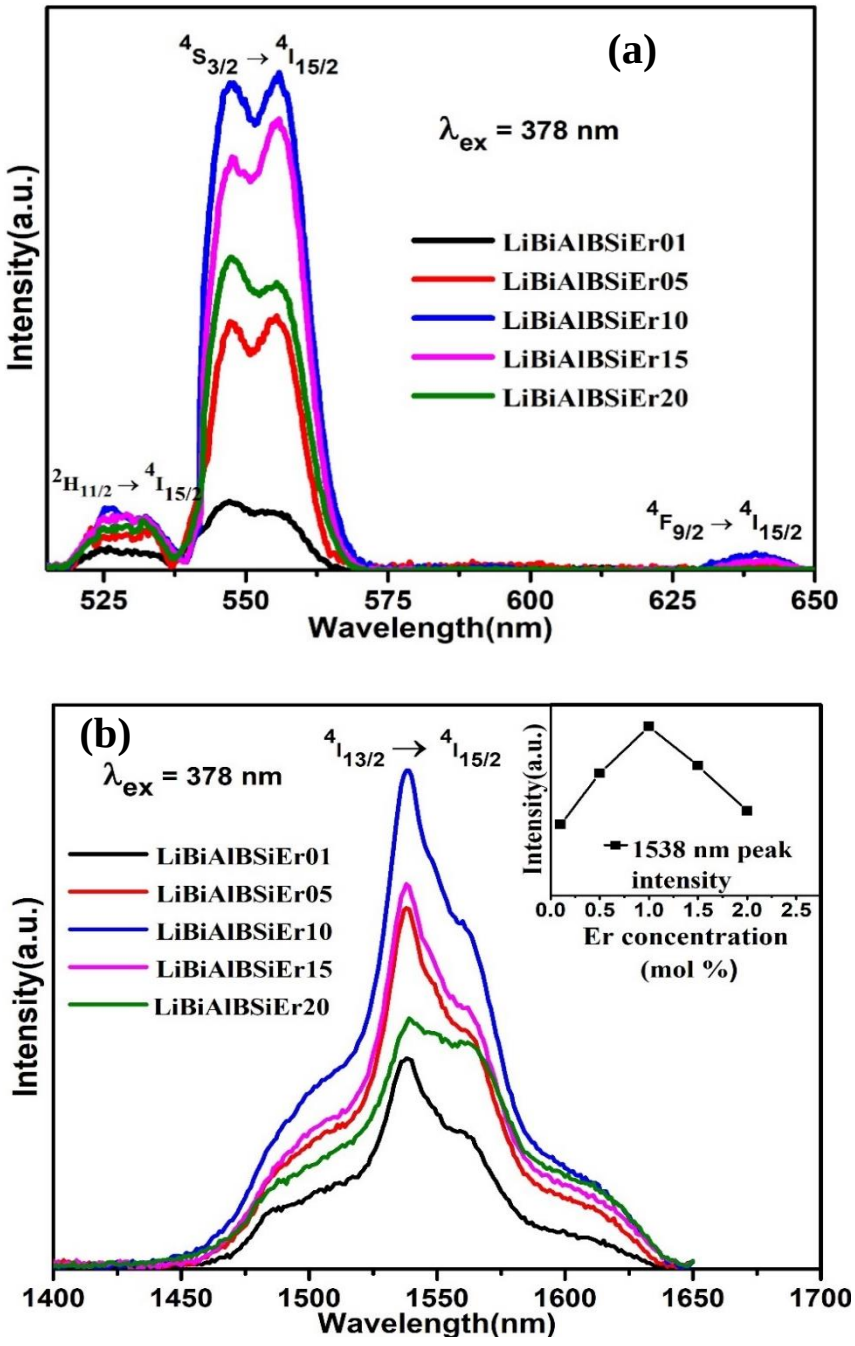

Fig. 6.5. Luminescence spectra of Er^{3+} ion doped LiBiAlBSi glasses in (a). Visible region (b). NIR region (inset: Variation of the emission intensity of transition $^4I_{13/2} \rightarrow {}^4I_{15/2}$ at 1538 nm with Er^{3+} ions concentration)

The values of A, τ_R and β_R of $^4S_{3/2} \rightarrow {}^4I_{15/2}$ transition is obtained as 7419.08 s^{-1}, 91 μs, and 0.676 respectively. The high luminescence intensity of transition, a large value of transition

probability, and branching ratio propose that our optimized LiBiAlBSiEr10 glass is an appropriate candidate for the applications of green laser action.

6.3.3.3. NIR emission spectral study

The emission spectra were recorded under excitation 378 nm in the NIR region from 1400 to 1650 and are shown in Fig. 6.5(b). The PL data for all Er^{3+} ions doped glasses samples provide the broad emission peak at 1538 nm wavelength respective characteristic features of Er^{3+} ions transition $^4I_{13/2} \rightarrow {}^4I_{15/2.}$ The transition $^4I_{13/2} \rightarrow {}^4I_{15/2}$ has significant attention because of its feasibility in infra-red laser, communication and range determination eye-safe laser applications [24]. The inset in Fig. 6.5(b) depicts the variation of emission intensity at 1538 nm with Er^{3+} concentration. As similar to the visible region emission intensity variation with dopant concentration, in the NIR region LiBiAlBSiEr10 glass has higher intensity and after that at the higher amount, the intensity declines due to concentration quenching. The quenching among the activator (Er^{3+}) beyond 1.0 mol% ions is observed owing to the non-radiative energy transfer mechanisms or multipole-multipole interaction [211].

To investigate the type of interaction mechanism, Dexter's theory applies to the emission spectral profile. According to Dexter's theory, three interaction mechanisms are liable for the type of inter-ionic interaction and are identified by the Equ.no. 4.2 in chapter 4 [39,105] Fig.6.6 depicts the graphs of log (I/x) versus log(x) and the parameter is attained from the slope of a linear fitted plot from experimental data.

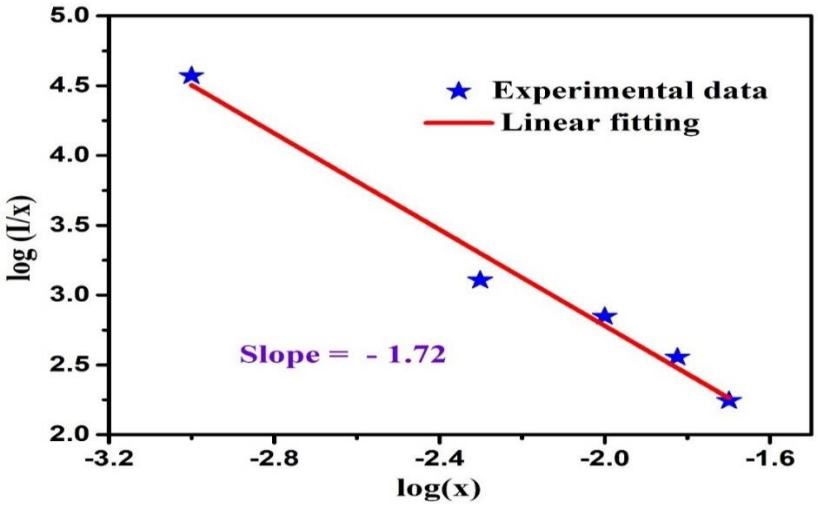

Fig. 6.6. Relation between log (I/x) and log (x) for different concentrations of Er^{3+}. Dexter model fitting is shown by the solid line.

From Fig. 6.6 it can be seen that the slope is 1.72 and the s value is calculated as 5.16, and this value is nearby 6. This result indicated that the interaction among Er^{3+} ions is dipole-dipole in

nature. The emission intensities decline above 1.0 mol% concentration of Er^{3+} ions may be due to the electric dipole-dipole interactions among the Er^{3+} ions.

From the NIR emission spectrum of optimized LiBiAlBSiEr10 glass for the $^4I_{13/2} \rightarrow {}^4I_{15/2}$ transition, the determined transition probability, branching ratio and radiative decay time are 745 s^{-1}, 1.0 and 1342 μs, respectively. The value of transition probability is much higher than the reported values. Another important factor in understanding the efficacy of the RE ions doped materials for laser application from the emission spectrum is stimulated emission cross-section (σ_{se}) and this parameter determines the amount of withdrawn energy from the lasing material. The σ_{se} value can be assessed by the given Equ.no. 1.15 in chapter 1 [212]. In Table 6.5, radiative parameters such as peak wavelength (λp), branching ratio (β), effective bandwidths ($\Delta\lambda p$), transition probability (A), stimulated emission cross-sections (σ_{se}), optical gain parameter ($\sigma_{se} \times \tau_R$) and gain bandwidth ($\sigma_{se} \times \Delta\lambda p$) of LiBiAlBSiEr10 for the NIR transition $^4I_{13/2} \rightarrow {}^4I_{15/2}$ (λp =1538 nm) are presented and compared with other glasses doped with Er^{3+} doped reported in the literature [24,201,213]. The optical gain ($\sigma_{se} \times \tau_R$) is an important parameter to evaluate the glass medium amplification for RE ions doped glasses. It is conspicuous from Table 6.5 that these radiative parameters have comparable values with reported values which specify that the optimized LiBiAlBSiEr10 glass is a possible applicant for optical amplifiers used in broadband.

Moreover, for all the LiBiAlBSi glasses incorporated with Er^{3+} ions, the NIR emission spectra show a wide-ranging emission (1.45–1.65 μm) with a peak position at 1.538 μm and it proposes the relevance of the present glass system in telecommunication window which covers optical communication bands such as Long (L), conventional (C) and short (S) [24,214].

Table 6.5. λp (nm), $\Delta\lambda$) (nm), β, A (s^{-1}), τ_R (μs), σ_{se} x 10^{-20} (cm^2), gain bandwidth ($\sigma_{se} \times \Delta\lambda p$ x 10^{-25}) (cm^3) and optical gain ($\sigma_{se} \times \tau_R$ x 10^{-23}) (cm^2 s) of 1.0 mol% Er^{3+} ions in LiBiAlBSi glass for the NIR emission transition $^4I_{13/2} \rightarrow {}^4I_{15/2}$ (λp =1538 nm) and compared with other reported glasses in literature for Er^{3+} doped glasses.

Transition	Parameters	LiBiAlBSiEr10 [Present]	MBSER10 Ref [24]	BiBTEr1.0 Ref[201]	SANSCEr10 Ref [213]
$^4I_{13/2} \rightarrow {}^4I_{15/2}$	λp	1538	1536	1572	1535
	$\Delta\lambda p$	49.29	67	80	53
	β	1	1	1	1
	A	745.01	371.2	441.05	193
	τ_R	1342	2690	2260	5180
	σ_{se}	2.07	1.578	1.472	0.98
	$\sigma_{se} \times \Delta\lambda p$	1.02	1.057	1.178	0.52
	$\sigma_{se} \times \tau_R$	2.78	0.425	3.34	0.378

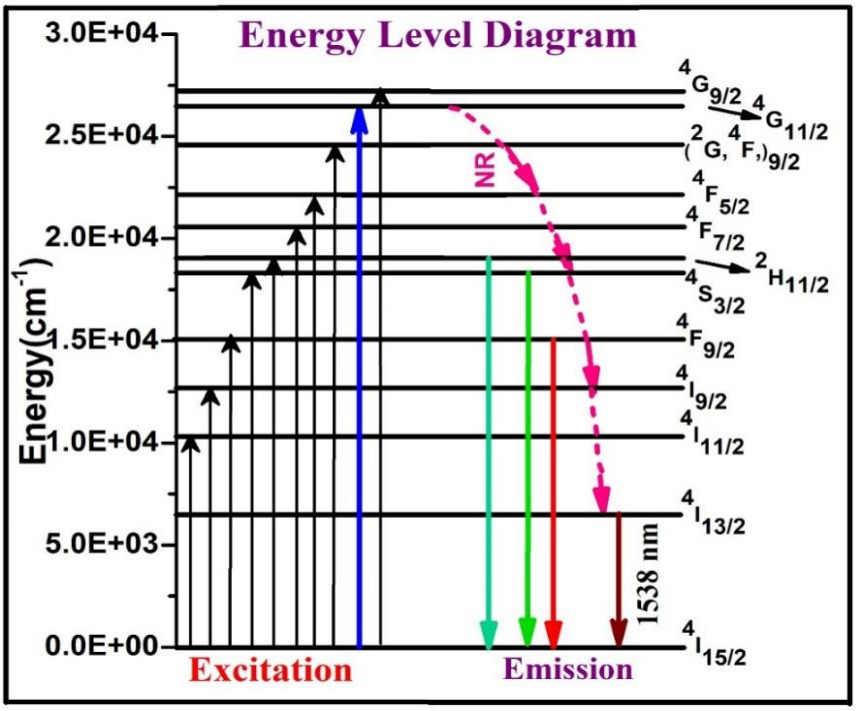

Fig. 6.7. Energy level diagram of 1.0 mol% Er^{3+} ions in LiBiAlBSi glasses.

To explain the inclusive mechanisms of excitation and emission, the partial energy level diagram of Er^{3+} doped glass LiBiAlBSiEr is shown in Fig. 6.7. When the glass was excited with 378 nm wavelength, the excitation of Er^{3+} ions from the level $^4I_{15/2}$ (ground) to higher excited state $^4G_{11/2}$ and such exciting Er^{3+} ions de-excites promptly via non-radiative (NR) relaxations they undergo prompt falling towards the levels $^2H_{11/2}$, $^4S_{3/2}$, $^4F_{9/2}$ and $^4I_{13/2}$ as shown in Fig. 6.7. The strong NIR emission transition ($^4I_{13/2} \rightarrow {}^4I_{15/2}$) is detected at 1538 nm whereas visible transitions are observed at the peak wavelengths 639 nm, 527 nm and 547 nm corresponding to the red, strong green and green emissions respectively.

6.3.4. Chromaticity color co-ordinates

For defining the colors, Commission Internationale de l'Eclairage (CIE) coordinates are a standard tool [57,171]. The human eye perceives the visible emission and color measures by CIE coordinates are evaluated. The visible emission spectra of LiBiAlBSi glasses incorporated with Er^{3+} ions are used for evaluation of the CIE coordinates under excitation wavelength 378 nm and tabulated in Table 6.6.

Table 6.6. CIE chromaticity coordinates of Er^{3+} ions in LiBiAlBSi glasses under 378 nm excitation wavelength and Experimental lifetimes (τ_{exp}) (μs) for $^4S_{3/2} \rightarrow {}^4I_{15/2}$ (548 nm) transition of Er^{3+} ions in LiBiAlBSi glasses.

Glass samples	x-coordinate	y-coordinate	τ_{exp}
LiBiAlBSiEr01	0.318	0.666	78.42
LiBiAlBSiEr05	0.316	0.677	76.67
LiBiAlBSiEr10	0.322	0.669	74.67
LiBiAlBSiEr15	0.332	0.659	69.17
LiBiAlBSiEr20	0.312	0.673	59.46

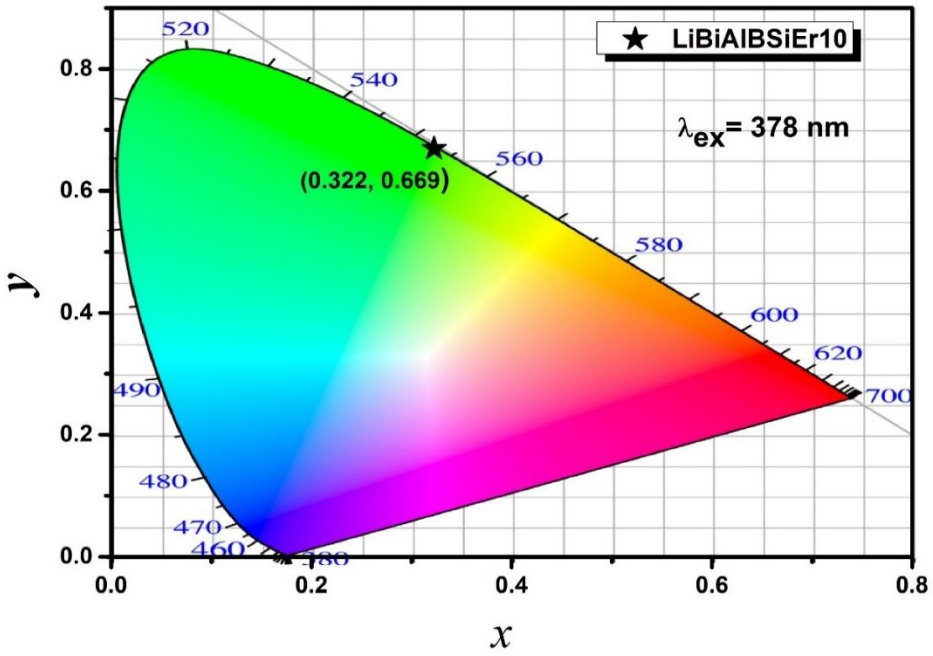

Fig. 6.8. CIE chromaticity coordinates of 1.0 mol% of Er^{3+} ions doped LiBiAlBSi glass.

In Fig. 6.8 show the CIE coordinates value of optimum glass LiBiAlBSiEr10 is (0.332, 0.669) in intense green region. Hence, optimum glass LiBiAlBSiEr10 is an appropriate candidate for photonic applications in visible green regions.

6.3.5. Visible Fluorescence decay analysis

For all the as-prepared glasses, decay profiles were measured under excitation and emission wavelengths 378 nm and 547 nm respectively. These decay profiles were recorded for characteristic green emission of Er^{3+} ions which initiates from excited level $^4S_{3/2}$ to lower level $^4I_{15/2}$ and a bi-exponential function is well fitted for decay profiles which are shown in Fig. 6.9. The bi-exponential equation and decay lifetimes average values (τ_{avg}) were estimated by using equ. no.1.19 and 1.20 given in chapter 1 [39,172]

Table 6.6 as an experimental lifetime (τ_{exp}) and their order in microseconds (μs). The values of τ_{exp} Table 6.6 decreases from 78.72 to 59.46 μs with Er^{3+} ions content from 0.1 to 2.0 mol%. The decline in lifetimes with an upsurge in the content of Er^{3+} ions is primarily due to the rise of energy transfer (ET) among neighbourhood Er^{3+} ions and ET from Er^{3+} ions to the impurities and other defects in the host.

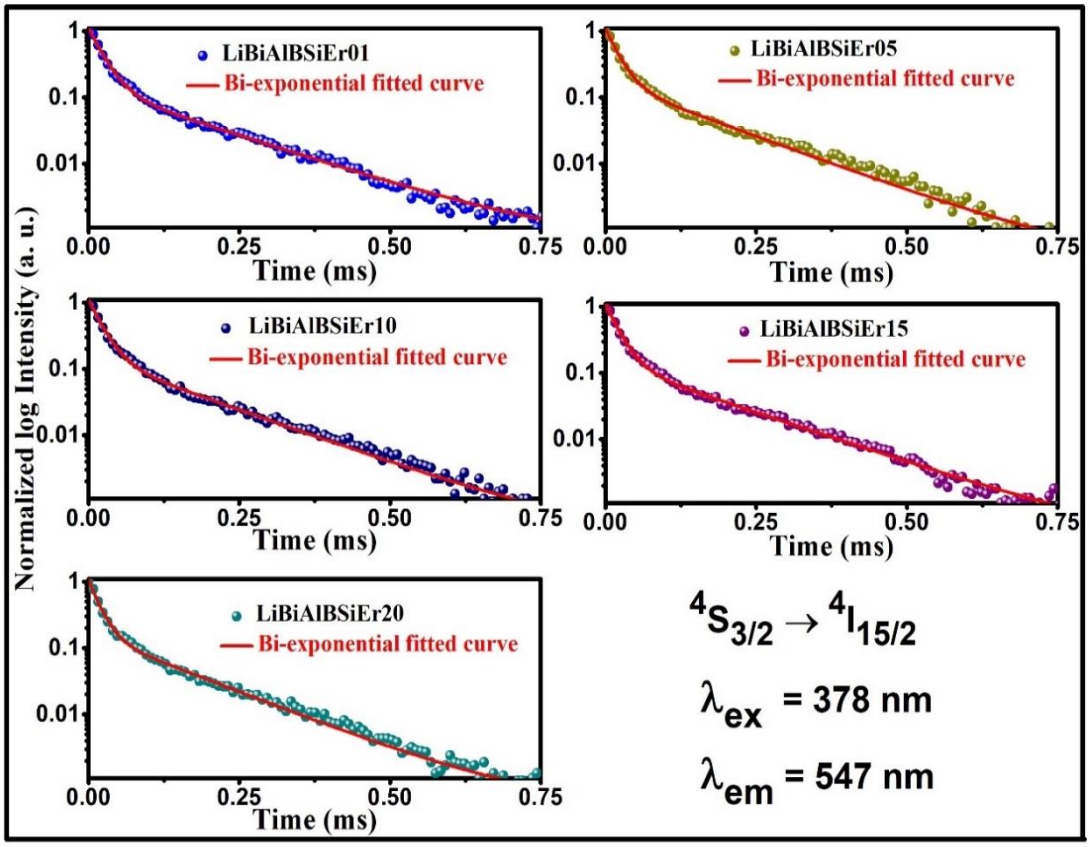

Fig. 6.9. Bi-exponential decay produced for $^4S_{3/2} \rightarrow {}^4I_{15/2}$ (547 nm) emission transition of Er^{3+} ions doped LiBiAlBSi glasses under 378 nm excitation.

6.4. Summary

The LiBiAlBSi glasses incorporated with different concentrations of Er^{3+} ions with good transparency and optical quality were synthesized via the melt quench method. The estimation of the bonding parameter, indirect bandgap and J-O investigation was executed based on the recorded absorption spectrum. The indirect energy bandgap values are increasing from 3.218 to 3.322 eV with Er_2O_3 concentration. The bonding parameter (δ) and trend $\Omega_2 > \Omega_6 > \Omega_4$ of J-O parameters indicate the predominance of covalent bonds between RE ions and ligand bonds. PL visible and strong NIR luminescence spectra were recorded under an excitation wavelength of 378 nm. The quenching effect is observed beyond 1.0 mol% of Er^{3+} ions which shows the optimized glass is LiBiAlBSiEr10 and the radiative parameters were estimated for assessing the lasing features of optimized glass. CIE color coordinates value of optimum glass LiBiAlBSiEr10 is (0.332, 0.669) in the visible green region. Relatively better values of radiative properties acclaim that an optimized glass system is suitable for applications such as laser and optical amplifiers applications in the NIR region.

CHAPTER 7

Conclusion and future scope of the work

7.1. Conclusion

Chapters 1 & 2, Discuss the objectives of the present thesis which were to synthesize good optical glasses doped with certain RE ions and optimize the conditions for a wide range of photonic applications. LiBiAlBSi glasses were successfully produced by melt quenching procedure doping with single and codoped RE ions such as (Sm^{3+}, Tb^{3+}, Sm^{3+}/$Eu^{+3,}$ and $Er^{3+)}$. The melt-quenching method and the different characterization procedures used in our studies were discussed in detail.

Chapter 3, explains in detail the preparation and characterization of Sm^{3+} ions doped LiBiAlBSi glasses. XRD pattern confirmed the amorphous nature of our glass system. FT-IR study was performed for un-doped glass to identify the involved network functional groups in the host glass. Numerous radiative properties for the prominent luminous levels of Sm^{3+} were estimated using absorption and emission spectra within the framework of the J-O theory. From the emission cross-sections, CIE coordinates, quantum efficiency, and branching ratios, it was suggested that 0.5 mol% of Sm^{3+} ion concentration is optimum in LiBiAlBSi glasses to improve the visible reddish-orange luminescent application.

In chapter 4, Tb^{3+} doped LiBiAlBSi glasses were prepared to investigate their suitability for visible green photonic applications. For these glasses, the indirect optical band gap was estimated in the 3.16-3.46 eV range. Four emission bands of Tb^{3+} ions showed in PL emission whereas an intense peak was observed in the green region and LiBiAlBSiTb15 (1.5 mol %) glass was optimized. Dexter's theory confirmed the dipole-dipole interaction among Tb^{3+} ions which is one reason for energy transfer and by this means concentration quenching. The optimized glass CIE coordinates (0.3128, 0.5764) are near to European Broadcasting Union illuminant specified intense green light coordinates. The relationship of τ_{exp} values with the PL spectra data used for the assessment of radiative properties. The thermal stability of the optimized glass was confirmed by the comparatively high activation energy value assessed from the TD-PL. All the above-mentioned studies along with thermal stability suggested the

suitability of the optimized glass for intense green photonic applications such as laser and tricolor white-LEDs as a green emission part.

In chapter 5, the single-doped Sm^{3+}, Eu^{3+} ions and Sm^{3+}/Eu^{3+} ions co-doped LiBiAlBSi glasses were prepared and studied the absorption, PL excitation, emission, and decay were performed to investigate their usefulness as red emission components for solid-state lighting and PV cells. Dexter's energy transfer scheme and Reisfeld's theory applied to emission spectra and confirmed the dipole-dipole nature of the mechanism of ET from Sm^{3+} ions to Eu^{3+} ions. The excitation spectrum for Sm^{3+}/Eu^{3+} co-doped LiBiAlBSi glasses of Eu^{3+} was extended by the incorporation of Sm^{3+} as a sensitizer. The CIE coordinate values shifted with the content of Eu^{3+} from reddish-orange to red region. The TD-PL of the optimized LiBiAlBSiSE10 glass shows its greater thermal stability. The above results of this chapter suggest the thermally stable $Sm^{3+/}Eu^{3+}$ co-doped optimized glasses are applicable as a potential candidate to fabricate white LEDs and PV cells via downshifting analysis.

In chapter 6, the Er^{3+} were successfully incorporated into the LiBiAlBSi glasses and their physical and spectroscopic properties by measuring the spectra of optical absorption, photoluminescence, and decay profiles. The indirect energy band gap values were calculated in the range of 3.218 to 3.322 eV. The bonding parameter (δ) and JO parameters tend $\Omega_2 > \Omega_6 > \Omega_4$ direct the occurrence of covalent bonds among RE ions and ligand bonds. Emission spectra were recorded for the Visible and NIR regions. The glass LiBiAlBSiEr10 was optimized and the radiative parameters were assessed for this. CIE color coordinates the value of optimum glass for visible spectra occurring in the green region. Comparatively better values of radiative properties suggest that an optimized glass system is appropriate for applications such as optical amplifiers and lasers in the NIR region.

All the aforesaid significant outcomes confirm that LiBiAlBSi glasses doped with RE ions direct their potential utility for photonic applications such as solid-state laser, LED lighting, PV cell, and optical amplifiers.

7.2. Scope for future work

Research works that will be carried out in the future are: -

- To enhance the luminescence properties of our glass host by varying the combination of different co-doped RE ions.
- To fabricate highly efficient w-LED using these glasses.
- Comparing the efficacy of the prepared materials with commercially available materials.
- To extend the utility of the as-synthesized glass for other possible applications such as temperature sensors, lasers, and optical fiber applications.

References

1. G. M. Barrow, "BOOKS: Introduction to Molecular Spectroscopy," McGraw-Hill, (1962).
2. J. S. Garcia', L. Bausia', and D. Jaque, *An Introduction to the Optical Spectroscopy* (John Wiley & Sons Ltd, 2005).
3. K. WILSON AND J. WALKER, *Principles and Techniques of Biochemistry and Molecular Biology, Cambridge University Press 2010* (n.d.).
4. C. N. Banwell, "Colin N. Banwell - Fundamentals of Molecular Spectroscopy-McGraw-Hill," (1983).
5. M. C. and J. B. Gupta, "The Handbook of Photonics," CRC Press (2019).
6. M. Gaft, R. Reisfeld, and G. Panczer, *Modern Luminescence Spectroscopy of Minerals and Materials* (2015).
7. C. R. Ronda, *Luminescence: From Theory to Applications* (n.d.).
8. Hans Bach Norbert Neuroth, *The Properties of Optical Glass* (1998), **29**(4).
9. E. Axinte, "Glasses as engineering materials: A review," Mater. Des. **32**(4), 1717–1732 (2011).
10. G. J. Copley, "New developments in glasses," Mater. Sci. Eng. **8**(1), 1–31 (1971).
11. A. Kitai, *Luminescent Materials and Application* (John Wiley & Sons Ltd, 2008).
12. B. C. G. G. Blasse, *Luminescent Materials* (2017).
13. K. Hirao, T. Mitsuyu, J. Si, and J. Qiu, *Active Glass for Photonic Devices* (2001), **7**.
14. T. P. Pearsall, "Photonics essentials: An introduction with experiments, McGraw-Hill," (2003).
15. Masayuki Yamane and Yohiyuki Asahara, *GLASSES FOR PHOTONICS, Cambridge University Press* (Cambridge University Press, 2000).
16. T. A. K. and D. W. Smith, F Graham, *Optics and Photonics : An Introduction Second Edition* (2007), **69**.
17. R. Nagaraj, P. Suthanthirakumar, R. Vijayakumar, and K. Marimuthu, "Spectroscopic properties of Sm^{3+} ions doped Alkaliborate glasses for photonics applications," Spectrochim. Acta - Part A Mol. Biomol. Spectrosc. **185**, 139–148 (2017).
18. R. S. Quimby, *Photonics and Lasers: An Introduction* (2006).
19. I. S. Amiri, S. R. Bin Azzuhri, M. A. Jalil, H. M. Hairi, J. Ali, M. Bunruangses, and P.

Yupapin, "Introduction to photonics: Principles and the most recent applications of microstructures," Micromachines **9**(9), (2018).

20. P. Yasaka and J. Kaewkhao, "Luminescence from lanthanides-doped glasses and applications: A review," Proc. - 2015 4th Int. Conf. Instrumentation, Commun. Inf. Technol. Biomed. Eng. ICICI-BME 2015 4–15 (2016).
21. M. Kumar and A. S. Rao, "Concentration-dependent reddish-orange photoluminescence studies of Sm^{3+} ions in borosilicate glasses," Opt. Mater. (Amst). **109**(June), 110356 (2020).
22. C. R. Kesavulu, H. J. Kim, S. W. Lee, J. Kaewkhao, N. Wantana, S. Kothan, and S. Kaewjaeng, "Optical spectroscopy and emission properties of Ho^{3+} -doped gadolinium calcium silicoborate glasses for visible luminescent device applications," J. Non. Cryst. Solids **474**(August), 50–57 (2017).
23. N. Deopa and A. S. Rao, "Spectroscopic studies of single near ultraviolet pumped Tb^{3+} doped Lithium Lead Alumino Borate glasses for green lasers and tricolour w-LEDs," J. Lumin. **194**(August 2017), 56–63 (2018).
24. A. Jose, S. Gopi, T. Krishnapriya, T. A. Jose, C. Joseph, N. V. Unnikrishnan, and P. R. Biju, "Spectroscopic investigations on 1.53 μm NIR emission of Er^{3+} doped multicomponent borosilicate glasses for telecommunication and lasing applications," Mater. Chem. Phys. **261**(December 2020), (2021).
25. N. Srisittipokakun, J. Kaewkhao, W. Chewpraditkul, and P. Limsuwan, "Comparative study of optical and spectroscopic properties of lead and bismuth on borosilicate glasses," Procedia Eng. **32**, 699–705 (2012).
26. K. Swapna, S. Mahamuda, A. S. Rao, M. Jayasimhadri, S. Shakya, and G. V. Prakash, "Tb^{3+} doped Zinc Alumino Bismuth Borate glasses for green emitting luminescent devices," J. Lumin. **156**, 180–187 (2014).
27. Y. B. Saddeek, M. S. Gaafar, and S. A. Bashier, "Structural influence of PbO by means of FTIR and acoustics on calcium alumino-borosilicate glass system," J. Non. Cryst. Solids **356**(20–22), 1089–1095 (2010).
28. M. I. Sayyed, F. Akman, M. R. Kaçal, and A. Kumar, "Radiation protective qualities of some selected lead and bismuth salts in the wide gamma energy region," Nucl. Eng. Technol. **51**(3), 860–866 (2019).
29. N. Deopa and A. S. Rao, "Spectroscopic studies of single near ultraviolet pumped Tb^{3+} doped Lithium Lead Alumino Borate glasses for green lasers and tricolour w-LEDs," J.

Lumin. **194**(September 2017), 56–63 (2018).

30. K. S. Rudramamba, D. V. Krishna Reddy, T. Sambasiva Rao, S. K. Taherunnisa, N. Veeraiah, and M. Rami Reddy, "Optical properties of Sm^{3+} doped strontium bismuth borosilicate glasses for laser applications," Opt. Mater. (Amst). **89**(January), 68–79 (2019).
31. T. Maeder, "Review of Bi_2O_3 based glasses for electronics and related applications," Int. Mater. Rev. **58**(1), 3–40 (2013).
32. M. Back, E. Trave, N. Mazzucco, P. Riello, and A. Benedetti, "Tuning the upconversion light emission by bandgap engineering in bismuth oxide-based upconverting nanoparticles," Nanoscale **9**(19), 6353–6361 (2017).
33. K. Swapna, S. Mahamuda, A. S. Rao, T. Sasikala, and L. R. Moorthy, "Visible luminescence characteristics of Sm^{3+} doped Zinc Alumino Bismuth Borate glasses," J. Lumin. **146**, 288–294 (2014).
34. J. E. Shelby, *Introduction to Glass Science and Technology 2nd Edition* (The Royal Society of Chemistry, 2005).
35. S. Singh, G. Kalia, and K. Singh, "Effect of intermediate oxide (Y_2O_3) on thermal, structural and optical properties of lithium borosilicate glasses," J. Mol. Struct. **1086**, 239–245 (2015).
36. N. S. Saetova, A. A. Raskovalov, B. D. Antonov, T. V. Yaroslavtseva, O. G. Reznitskikh, and N. I. Kadyrova, "The influence of lithium oxide concentration on the transport properties of glasses in the Li_2O-B_2O_3-SiO_2 system," J. Non. Cryst. Solids **443**, 75–81 (2016).
37. S. L. Brito, T. A. Lodi, R. F. Muniz, A. Steimacher, and F. Pedrochi, "Energy transfer investigation of Sm^{3+}/Eu^{3+} CaBAl glasses," J. Lumin. **219**(November 2019), 116947 (2020).
38. H. Kaur, M. Jayasimhadri, M. K. Sahu, P. K. Rao, and N. S. Reddy, "Synthesis of orange emitting Sm^{3+} doped sodium calcium silicate phosphor by sol-gel method for photonic device applications," Ceram. Int. **46**(16), 26434–26439 (2020).
39. M. Kumar and A. S. Rao, "Influence of Tb^{3+} ions concentration and temperature on lithium bismuth alumino borosilicate glasses for green photonic device applications," Opt. Mater. (Amst). **120**(July), 111439 (2021).
40. N. Deopa and A. S. Rao, "Spectroscopic studies of Sm^{3+} ions activated lithium lead alumino borate glasses for visible luminescent device applications," Opt. Mater. (Amst).

72, 31–39 (2017).

41. J. McKittrick and L. E. Shea-Rohwer, "Review: Down conversion materials for solid-state lighting," J. Am. Ceram. Soc. **97**(5), 1327–1352 (2014).
42. B. R. Judd, "Optical absorption intensities of rare-earth ions," Phys. Rev. **127**(3), 750–761 (1962).
43. G. S. Ofelt, "Intensities of Crystal Spectra of Rare-Earth Ions," J. Chem. Phys. **37**(3), 511–520 (1962).
44. M. C. Farries, P. R. Morkel, and J. E. Townsend, "Spectroscopic and lasing characteristics of samarium doped glass fibre," IEE proceedings. Part J, Optoelectron. **137**(5), 318–322 (1990).
45. C. K. Jayasankar, V. Venkatramu, P. Babu, T. Tröster, W. Sievers, G. Wortmann, and W. B. Holzapfel, "High-pressure fluorescence study of Sm^{3+} -doped borate and fluoroborate glasses," J. Appl. Phys. **97**(9), 5–12 (2005).
46. H. Largot, K. E. Aiadi, M. Ferid, S. Hraiech, C. Bouzidi, C. Charnay, and K. Horchani-Naifer, "Spectroscopic investigations of Sm^{3+} doped phosphate glasses: Judd-Ofelt analysis," Phys. B Condens. Matter **552**, 184–189 (2019).
47. B. Szpikowska-Sroka, N. Pawlik, T. Goryczka, M. Bańczyk, and W. A. Pisarski, "Influence of activator concentration on green-emitting Tb^{3+}-doped materials derived by sol-gel method," J. Lumin. **188**(January), 400–408 (2017).
48. Q. Chen, D. Valiev, S. Stepanov, J. Ding, L. Liu, C. Li, H. Lin, Y. Zhou, and F. Zeng, "Influence of the Tb^{3+} concentration on the luminescent properties of high silica glass," Opt. Mater. (Amst). **86**(September), 606–610 (2018).
49. S. N. S. Yaacob, M. R. Sahar, E. S. Sazali, Z. A. Mahraz, and K. Sulhadi, "Comprehensive study on compositional modification of Tb^{3+} doped zinc phosphate glass," Solid State Sci. **81**(January), 51–57 (2018).
50. M. K. Sahu, H. Kaur, B. V. Ratnam, J. S. Kumar, and M. Jayasimhadri, "Structural and spectroscopic characteristics of thermally stable Eu^{3+} activated barium zinc orthophosphate phosphor for white LEDs," Ceram. Int. **46**(16), 26410–26415 (2020).
51. K. Jha, M. Jayasimhadri, D. Haranath, and K. Jang, "Influence of modifier oxides on spectroscopic properties of Eu^{3+} doped oxy-fluoro tellurophosphate glasses for visible photonic applications," J. Alloys Compd. **789**, 622–629 (2019).
52. B. N. K. Reddy, B. D. Raju, K. Thyagarajan, R. Ramanaiah, Y. D. Jho, and B. S. Reddy, "Optical characterization of Eu^{3+} ion doped alkali oxide modified borosilicate glasses

for red laser and display device applications," Ceram. Int. **43**(12), 8886–8892 (2017).

53. M. R. Dousti, G. Y. Poirier, and A. S. S. De Camargo, "Structural and spectroscopic characteristics of Eu^{3+}-doped tungsten phosphate glasses," Opt. Mater. (Amst). **45**, 185–190 (2015).
54. A. Madhu, B. Eraiah, P. Manasa, and C. Basavapoornima, "Er^{3+}-ions doped lithium-bismuth-boro-phosphate glass for 1532 nm emission and efficient red emission up conversion for telecommunication and lasing applications," J. Non. Cryst. Solids **495**(March), 35–46 (2018).
55. F. Chen, T. Wei, X. Jing, Y. Tian, J. Zhang, and S. Xu, "Investigation of mid-infrared emission characteristics and energy transfer dynamics in Er^{3+} doped oxyfluoride tellurite glass," Sci. Rep. **5**(June), 1–11 (2015).
56. A. Miguel, R. Morea, J. Gonzalo, M. A. Arriandiaga, J. Fernandez, and R. Balda, "Near-infrared emission and upconversion in Er^{3+}-doped TeO_2-ZnO-ZnF_2 glasses," J. Lumin. **140**, 38–44 (2013).
57. M. S. Sajna, S. Thomas, K. A. Ann Mary, C. Joseph, P. R. Biju, and N. V. Unnikrishnan, "Spectroscopic properties of Er^{3+} ions in multicomponent tellurite glasses," J. Lumin. **159**, 55–65 (2015).
58. E. M. Ahmed, M. I. Youssif, and A. A. Elzelaky, "Structural, thermal and photoemission properties of erbium doped phosphate glass," Ceram. Int. **45**(18), 24014–24021 (2019).
59. A. K. Varshneya, *Fudamentals of Inorganic Glasses* (1993).
60. R. H. D. James F. Shackelford, *Ceramic and Glass Materials* (2008).
61. A. a El-kheshen, "Glass as Radiation Sensor," Curr. Top. Ioniz. Radiat. Res. 579–602 (1998).
62. A. S. L. Gomes, "Spectroscopy of Rare Earth Doped Glasses," (February), (2007).
63. C. Madhukar Reddy, B. Deva Prasad Raju, N. John Sushma, N. S. Dhoble, and S. J. Dhoble, "A review on optical and photoluminescence studies of RE^{3+} (RE=Sm, Dy, Eu, Tb and Nd) ions doped LCZSFB glasses," Renew. Sustain. Energy Rev. **51**, 566–584 (2015).
64. R. W. Douglas, "The use of glass in high-vacuum apparatus," J. Sci. Instrum. **22**(5), 81–87 (1945).
65. W. H. Zachariasen, "The atomic arrangement in glass," J. Am. Chem. Soc. **54**(10), 3841–3851 (1932).
66. M. H. Lewis, *Glasses and Glass-Ceramics* (1989).

67. Charles A. Harper, *HANDBOOK OF CERAMICS, GLASSES, AND DIAMONDS* (2001), **369**(1).
68. F. Gan and L. Xu, *Fuxi Gan • Lei Xu* (n.d.).
69. N. Ghobadi, "Band gap determination using absorption spectrum fitting procedure," Int. Nano Lett. **3**(1), 2–5 (2013).
70. D. W. Goodwin, "Optical Spectra of Transparent Rare Earth Compounds," Phys. Bull. **30**(12), 525–525 (1979).
71. G. H. Dieke, "Spectra and Energy Levels of Rare Earth Ions in Crystals," Phys. Bull. **20**(12), 525–525 (1969).
72. A. J. Freeman and R. E. Watson, "Theoretical investigation of some magnetic and spectroscopic properties of rare-earth ions," Phys. Rev. **127**(6), 2058–2075 (1962).
73. X. Huang, S. Han, W. Huang, and X. Liu, "Enhancing solar cell efficiency: The search for luminescent materials as spectral converters," Chem. Soc. Rev. **42**(1), 173–201 (2013).
74. J. C. Boyer, F. Vetrone, J. A. Capobianco, A. Speghini, and M. Bettinelli, "Variation of fluorescence lifetimes and judd-ofelt parameters between Eu^{3+} doped bulk and nanocrystalline cubic Lu_2O_3," J. Phys. Chem. B **108**(52), 20137–20143 (2004).
75. D. G. Karraker, "Hypersensitive Transitions of Six-, Seven-, and Eight-Coordinate Neodymium, Holmium, and Erbium Chelates," Inorg. Chem. **6**(10), 1863–1868 (1967).
76. B. R. Choppin, D. E. Henrie, and K. Buijs, "Environmental Effects on f-f Transitions. I. Neodymium(III)," Inorg. Chem. **5**(10), 1743–1748 (1966).
77. and L. E. Karl A. GSCHNEIDNER, Jr., "Handbook on the Physics and Chemistry of Rare Earths. vol. 1 Metals.," (1978).
78. W. T. Carnall, P. R. Fields, and K. Rajnak, " Electronic Energy Levels of the Trivalent Lanthanide Aquo Ions. IV. Eu^{3+} ," J. Chem. Phys. **49**(10), 4450–4455 (1968).
79. W. T. Carnall, P. R. Fields, and K. Rajnak, " Electronic Energy Levels of the Trivalent Lanthanide Aquo Ions. III. Tb^{3+} ," J. Chem. Phys. **49**(10), 4447–4449 (1968).
80. G. Liu and B. Jacquier, *Spectroscopic Properties of Rare Earths in Optical Materials* (n.d.).
81. Chr. Klixbüll Jørgensen and B.R.Judd, "Hypersensitive pseudoquadrupole transitions in lanthanides," Mol. Phys. **10113**(13), 1967–1976 (2003).
82. K. Binnemans, "Lanthanide-based luminescent hybrid materials," Chem. Rev. **109**(9), 4283–4374 (2009).

83. and L. E. Karl A. GSCHNEIDNER, Jr. and These, "Handbook on the Physics and Chemistry of Rare Earths,volume 25," Chem. Rev. **104**(12), 5785–5801 (2004).
84. F. Wang and X. Liu, "Recent advances in the chemistry of lanthanide-doped upconversion nanocrystals," Chem. Soc. Rev. **38**(4), 976–989 (2009).
85. D. F. De Sousa, L. F. C. Zonetti, M. J. V. Bell, R. Lebullenger, A. C. Hernandes, and L. A. O. Nunes, "Er^{3+}:Yb^{3+} codoped lead fluoroindogallate glasses for mid infrared and upconversion applications," J. Appl. Phys. **85**(5), 2502–2507 (1999).
86. D. D. Ramteke, A. Balakrishna, V. Kumar, and H. C. Swart, "Luminescence dynamics and investigation of Judd-Ofelt intensity parameters of Sm^{3+} ion containing glasses," Opt. Mater. (Amst). **64**, 171–178 (2017).
87. S. Mahamuda, K. Swapna, M. Venkateswarlu, A. Srinivasa Rao, S. Shakya, and G. Vijaya Prakash, "Spectral characterisation of Sm^{3+} ions doped Oxy-fluoroborate glasses for visible orange luminescent applications," J. Lumin. **154**, 410–424 (2014).
88. N. F. Mott and E. A. Davis, "Conduction In Non-crystalline Systems V. Conductivity, Optical Absorption and Photoconductivity In Amorphous Semiconductors," Philos. Mag. **22**(179), 903–922 (1970).
89. C. R. Kesavulu, A. C. Almeida Silva, M. R. Dousti, N. O. Dantas, A. S. S. De Camargo, and T. Catunda, "Concentration effect on the spectroscopic behavior of Tb3+ ions in zinc phosphate glasses," J. Lumin. **165**, 77–84 (2015).
90. R. Turki, M. Zekri, A. Herrmann, C. Rüssel, R. Maalej, and K. Damak, "Optical properties of peralkaline aluminosilicate glasses doped with Sm^{3+}," J. Alloys Compd. **806**, 1339–1347 (2019).
91. A. S. Rao, Y. N. Ahammed, R. R. Reddy, and T. V. R. Rao, "Spectroscopic studies of Nd^{3+}-doped alkali fluoroborophosphate glasses," in *Optical Materials* (1998), **10**(4), pp. 245–252.
92. C. K. J. C.S. Dwaraka Viswanath, "Photoluminescence, γ-irradiation and X-ray induced luminescence studies of Sm^{3+}-doped oxyfluorosilicate glasses and glass-ceramics," Ceram. Int. **44**(6), 6104–6114 (2018).
93. S. Tanabe, T. Ohyagi, N. Soga, and T. Hanada, "Compositional dependence of Judd-Ofelt parameters of Er^{3+} ions in alkali-metal borate glasses," Phys. Rev. B **46**(6), 3305–3310 (1992).
94. K. Maheshvaran, K. Linganna, and K. Marimuthu, "Composition dependent structural and optical properties of Sm^{3+} doped boro-tellurite glasses," J. Lumin. **131**(12), 2746–

2753 (2011).

95. Joseph R. Lakowicz, *Principles of Fluorescence Spectroscopy* (2006).
96. H. Y. William M. Yen Shigeo Shionoya, *Handbook of Phosphors 2nd Ed.* (2003), **23**(1).
97. M. K. Sahu, M. Jayasimhadri, K. Jha, B. Sivaiah, A. S. Rao, and D. Haranath, "Synthesis and enhancement of photoluminescent properties in spherical shaped Sm^{3+}/Eu^{3+} co-doped $NaCaPO_4$ phosphor particles for w-LEDs," J. Lumin. **202**(March), 475–483 (2018).
98. S. V Eliseeva and J.-C. G. Bünzli, "Lanthanide Luminescence for Functional Materials and Bio-Sciences Electronic Supporting Information," (2009).
99. W. Zheng, P. Huang, D. Tu, E. Ma, H. Zhu, and X. Chen, "Lanthanide-doped upconversion nano-bioprobes: Electronic structures, optical properties, and biodetection," Chem. Soc. Rev. **44**(6), 1379–1415 (2015).
100. N. Thejokalyani and S. J. Dhoble, "Novel approaches for energy efficient solid state lighting by RGB organic light emitting diodes - A review," Renew. Sustain. Energy Rev. **32**, 448–467 (2014).
101. N. Yeh, T. J. Ding, and P. Yeh, "Light-emitting diodes' light qualities and their corresponding scientific applications," Renew. Sustain. Energy Rev. **51**, 55–61 (2015).
102. S. Ye, F. Xiao, Y. X. Pan, Y. Y. Ma, and Q. Y. Zhang, "Phosphors in phosphor-converted white light-emitting diodes: Recent advances in materials, techniques and properties," Mater. Sci. Eng. R Reports **71**(1), 1–34 (2010).
103. F. Auzel, "Upconversion and Anti-Stokes Processes with f and d Ions in Solids," Chem. Rev. **104**(1), 139–173 (2004).
104. J. and L. E. Karl A. Gschneidner, "Handbook on the Physics and Chemistry of Rare Earths. vol. 9-North Holland (1987)," (n.d.).
105. D. L. Dexter and J. H. Schulman, "Theory of concentration quenching in inorganic phosphors," J. Chem. Phys. **22**(6), 1063–1070 (1954).
106. E. F. Schubert, *Light-Emitting Diodes 2nd Ed.* (2015), **7**(1).
107. C. S. McCamy, "Correlated color temperature as an explicit function of chromaticity coordinates," Color Res. Appl. **17**(2), 142–144 (1992).
108. B. Zhang, J. Zhang, Y. Guo, J. Wang, J. Xie, X. Li, W. Huang, L. Wang, and Q. Zhang, "Synthesis and photoluminescence of double perovskite $La_2LiSbO_6:Ln^{3+}$ (Ln= Eu, Tb, Tm, Sm, Ho) phosphors and enhanced luminescence of $La_2LiSbO_6:Eu^{3+}$ red phosphor via Bi^{3+} doping for white light emitting diodes," J. Alloys Compd. **787**, 1163–1172

(2019).

109. J. Zarzycki, "Glasses and amorphous materials," Science (80-.). **267**(5206), 1887 (1995).
110. R. A. Talewar, S. Mahamuda, K. Swapna, M. Venkateswarlu, and A. S. Rao, "Spectroscopic studies of Sm^{3+} ions doped alkaline-earth chloro borate glasses for visible photonic applications," Mater. Res. Bull. **105**(April), 45–54 (2018).
111. B. D. Cullity, "Elements of x-ray diffraction," Addison- Wesley Publ. Company, Inc, Philipp. (1958).
112. Eric Lifshin, *X-Ray Characterization of Materials* (WILEY-VCH, 1999).
113. J. A. D. H. P.R. Griffiths, *Fourier Transform Infrared Spectrometry 2nd Ed* (WILEY-INTERSCIENCE, 2007), **222**(4621).
114. D. Souri and K. Shomalian, "Band gap determination by absorption spectrum fitting method (ASF) and structural properties of different compositions of (60-x) V_2O_5-40TeO_2-xSb_2O_3 glasses," J. Non. Cryst. Solids **355**(31–33), 1597–1601 (2009).
115. X. Y. Sun, D. G. Jiang, W. F. Wang, C. Y. Cao, Y. N. Li, G. T. Zhen, H. Wang, X. X. Yang, H. H. Chen, Z. J. Zhang, and J. T. Zhao, "Luminescence properties of B_2O_3-GeO_2-Gd_2O_3 scintillating glass doped with rare-earth and transition-metal ions," Nucl. Instruments Methods Phys. Res. Sect. A Accel. Spectrometers, Detect. Assoc. Equip. **716**, 90–95 (2013).
116. V. Liepina, D. Millers, and K. Smits, "Tunneling luminescence in long lasting afterglow of $SrAl_2O_4$:Eu,Dy," J. Lumin. **185**(3), 151–154 (2017).
117. T. Jüstel, H. Nikol, and C. Ronda, "New developments in the field of luminescent materials for lighting and displays," Angew. Chemie - Int. Ed. **37**(22), 3084–3103 (1998).
118. C.-H. Kim, I.-E. Kwon, C.-H. Park, Y.-J. Hwang, H.-S. Bae, B.-Y. Yu, C.-H. Pyun, and G.-Y. Hong, "ChemInform Abstract: Phosphors for Plasma Display Panels," ChemInform **31**(49), no-no (2010).
119. S. B. Kolavekar, N. H. Ayachit, R. Rajaramakrishna, P. N G, and J. Kaewkhao, "Reddish-orange emission and Judd-Ofelt investigation of Sm^{3+} ions doped in zince-bismuth-phospho-tellurite glasses for solid lighting application," J. Lumin. **226**(June), (2020).
120. N. Yıldız Yorgun, "Gamma-ray shielding parameters of $Li_2B_4O_7$ glasses: undoped and doped with magnetite, siderite and Zinc-Borate minerals cases," Radiochim. Acta

107(8), 755–765 (2019).

121. K. Udaya Kumar, C. R. Kesavulu, P. Babu, and C. K. Jayasankar, "Investigation of modifier effect on the spectroscopic properties of Sm^{3+} ions in binary boro-bismuth glasses," J. Non. Cryst. Solids **505**(November 2018), 367–378 (2019).
122. S. P. Singh and B. Karmakar, "Bismuth oxide and bismuth oxide doped glasses for optical and photonic applications," Bismuth Charact. Prod. Appl. 229–249 (2012).
123. Y. B. Saddeek, K. A. Aly, and S. A. Bashier, "Optical study of lead borosilicate glasses," Phys. B Condens. Matter **405**(10), 2407–2412 (2010).
124. K. Bhargavi, M. Srinivasa Reddy, P. Raghava Rao, N. Narasimha Rao, M. Sundara Rao, V. Ravi Kumar, and N. Veeraiah, "The structural influence of aluminium ions on emission characteristics of Sm^{3+} ions in lead aluminium silicate glass system," Mater. Res. Bull. **47**(2), 267–273 (2012).
125. M. C. Eckersley, P. H. Gaskell, A. C. Barnes, and P. Chieux, "Structural ordering in a calcium silicate glass," Nature **335**(6190), 525–527 (1988).
126. D. HOU, X. PAN, J. LI, W. ZHOU, and X. YE, "Structure and luminescence properties of Sm^{3+} doped Y_2MoO_6 phosphor under near ultraviolet light excitation," J. Rare Earths **35**(4), 335–340 (2017).
127. K. Swapna, S. Mahamuda, A. Srinivasa Rao, S. Shakya, T. Sasikala, D. Haranath, and G. Vijaya Prakash, "Optical studies of Sm^{3+} ions doped Zinc Alumino Bismuth Borate glasses," Spectrochim. Acta - Part A Mol. Biomol. Spectrosc. **125**, 53–60 (2014).
128. G. Okada, S. Vahedi, B. Morrell, C. Koughia, G. Belev, T. Wysokinski, D. Chapman, C. Varoy, A. Edgar, and S. Kasap, "Examination of the dynamic range of Sm-doped glasses for high-dose and high-resolution dosimetric applications in microbeam radiation therapy at the Canadian synchrotron," Opt. Mater. (Amst). **35**(11), 1976–1980 (2013).
129. H. Kaur and M. Jayasimhadri, "Optimization of structural and luminescent properties with intense red emitting thermally stable Sm^{3+} doped $CaBiVO_5$ phosphors for w-LED applications," Opt. Mater. (Amst). **107**(May), 110119 (2020).
130. N. Deopa, A. S. Rao, A. Choudhary, S. Saini, A. Navhal, M. Jayasimhadri, D. Haranath, and G. Vijaya Prakash, "Photoluminescence investigations on Sm^{3+} ions doped borate glasses for tricolor w-LEDs and lasers," Mater. Res. Bull. **100**(September 2017), 206–212 (2018).
131. Rakpanich, "X-RAYS LUMINESCENCE, OPTICAL AND PHYSICAL STUDIES OF

BI_2O_3-B_2O_3-SM_2O_3 GLASSES SYSTEM," Phys. Int. **4**(1), 81–87 (2013).

132. K. Annapoorani, C. Basavapoornima, N. Suriya Murthy, and K. Marimuthu, "Investigations on structural and luminescence behavior of Er^{3+} doped Lithium Zinc borate glasses for lasers and optical amplifier applications," J. Non. Cryst. Solids **447**, 273–282 (2016).
133. I. Spectra, "I. Introduction," Acta radiol. **4**(S258), 5–6 (1966).
134. M. S. Dahiya, S. Khasa, and A. Agarwal, "Physical, thermal, structural and optical absorption studies of vanadyl doped magnesium oxy-chloride bismo-borate glasses," J. Asian Ceram. Soc. **3**(2), 206–211 (2015).
135. W. T. Carnall, P. R. Fields, and K. Rajnak, "Electronic energy levels of the trivalent lanthanide aquo ions. I. Pr^{3+}, Nd^{3+}, Pm^{3+}, Sm^{3+}, Dy^{3+}, Ho^{3+}, Er^{3+}, and Tm^{3+}," J. Chem. Phys. **49**(10), 4424–4442 (1968).
136. C. R. Kesavulu and C. K. Jayasankar, "Spectroscopic properties of Sm^{3+} ions in lead fluorophosphate glasses," J. Lumin. **132**(10), 2802–2809 (2012).
137. C. K. Jayasankar and E. Rukmini, "Optical properties of Sm^{3+} ions in zinc and alkali zinc borosulphate glasses," Opt. Mater. (Amst). **8**(3), 193–205 (1997).
138. R. C. Carter, "Measurement and analysis of excited-state decay kinetics and transitions of Sm^{3+} in chiroptical activity in the 6H trigonal Na," **51**, (1992).
139. M. Czaja, "Optical properties of Pr^{3+} , Sm^{3+} and Er^{3+} doped P_2O_5 – CaO – SrO – BaO phosphate glass," **32**, 547–553 (2010).
140. K. Gatterer, G. Pucker, H. P. Fritzer, and S. Arafa, "Hypersensitivity and nephelauxetic effect of Nd (III) in sodium borate glasses," **176**, 237–246 (1994).
141. L. R. Moorthy, "Judd ± Ofelt parametrization and radiative transitions analysis of Tm^{3+} doped alkali chloroborophosphate glasses," **12**, 0–6 (1999).
142. P. Van Do, V. P. Tuyen, V. X. Quang, L. X. Hung, L. D. Thanh, T. Ngoc, N. Van Tam, and B. T. Huy, "Investigation of spectroscopy and the dual energy transfer mechanisms of Sm^{3+}-doped telluroborate glasses," Opt. Mater. (Amst). **55**, 62–67 (2016).
143. O. Ravi, C. Madhukar Reddy, L. Manoj, and B. Deva Prasad Raju, "Structural and optical studies of Sm^{3+} ions doped niobium borotellurite glasses," J. Mol. Struct. **1029**, 53–59 (2012).
144. M. Jayasimhadri, E. J. Cho, K. W. Jang, H. S. Lee, and S. Il Kim, "Spectroscopic properties and Judd-Ofelt analysis of Sm^{3+} doped lead-germanate-tellurite glasses," J. Phys. D. Appl. Phys. **41**(17), (2008).

145. F. W. Billmeyer and M. Saltzman, "Principles of color technology. In: Color and Color Difference Measurement," 240 (1981).
146. J. C. G. Bünzli and C. Piguet, "Taking advantage of luminescent lanthanide ions," Chem. Soc. Rev. **34**(12), 1048–1077 (2005).
147. M. R. Babu, N. M. Rao, A. M. Babu, and L. Ramamoorthy, "Absorption and luminescence studies of Dy^{3+} doped Phosphate glass," **4**(11), 1–9 (2014).
148. T. O. Sales, R. J. Amjad, C. Jacinto, and M. R. Dousti, "Concentration dependent luminescence and cross-relaxation energy transfers in Tb^{3+} doped fluoroborate glasses," J. Lumin. **205**(February 2018), 282–286 (2019).
149. P. Abdul Azeem, M. Kalidasan, R. R. Reddy, and K. Ramagopal, "Spectroscopic investigations on Tb^{3+} doped lead fluoroborate glasses," Opt. Commun. **285**(18), 3787–3791 (2012).
150. X. Y. Sun, M. J. Zhou, C. Bin Deng, Q. M. Yang, and J. Zhong, "Glass forming regions and concentration-dependent luminescence properties of Tb^{3+}-activated tellurium-lutetium-tungsten glasses," J. Rare Earths **39**(2), 146–150 (2021).
151. S. Kaur, N. Deopa, A. Prasad, R. Bajaj, and A. S. Rao, "Intense green emission from Tb^{3+} ions doped zinc lead alumino borate glasses for laser and w-LEDs applications," Opt. Mater. (Amst). **84**(July), 318–323 (2018).
152. K. Marimuthu, R. T. Karunakaran, S. Surendra Babu, G. Muralidharan, S. Arumugam, and C. K. Jayasankar, "Structural and spectroscopic investigations on Eu^{3+}-doped alkali fluoroborate glasses," Solid State Sci. **11**(7), 1297–1302 (2009).
153. V. Venkatramu, D. Navarro-Urrios, P. Babu, C. K. Jayasankar, and V. Lavín, "Fluorescence line narrowing spectral studies of Eu^{3+}-doped lead borate glass," J. Non. Cryst. Solids **351**(10–11), 929–935 (2005).
154. J. F. M. Dos Santos, V. S. Zanuto, C. R. Kesavulu, G. Venkataiah, C. K. Jayasankar, L. A. O. Nunes, and T. Catunda, "Photothermal and spectroscopic characterization of Tb^{3+}-doped tungsten-zirconium-tellurite glasses," J. Appl. Phys. **128**(11), (2020).
155. M. R. Dousti, G. Y. Poirier, and A. S. S. de Camargo, "Tungsten sodium phosphate glasses doped with trivalent rare earth ions (Eu^{3+}, Tb^{3+}, Nd^{3+} and Er^{3+}) for visible and near-infrared applications," J. Non. Cryst. Solids **530**(November 2019), 119838 (2020).
156. G. Gao, A. Winterstein-Beckmann, O. Surzhenko, C. Dubs, J. Dellith, M. A. Schmidt, and L. Wondraczek, "Faraday rotation and photoluminescence in heavily Tb^{3+}-doped GeO_2-B_2O_3-Al_2O_3-Ga_2O_3 glasses for fiber-integrated magneto-optics," Sci. Rep. **5**, 1–6

(2015).

157. C. Zuo, Z. Zhou, L. Zhu, A. Xiao, Y. Chen, X. Zhang, Y. Zhuang, X. Li, and Q. Ge, "Luminescence properties of Tb^{3+}-doped borosilicate scintillating glass under UV excitation," Spectrochim. Acta - Part A Mol. Biomol. Spectrosc. **147**, 324–327 (2015).
158. J. F. M. Dos Santos, I. A. A. Terra, N. G. C. Astrath, F. B. Guimarães, M. L. Baesso, L. A. O. Nunes, and T. Catunda, "Mechanisms of optical losses in the $^5D_4$ and $^5D_3$ levels in Tb^{3+} doped low silica calcium aluminosilicate glasses," J. Appl. Phys. **117**(5), (2015).
159. H. Guo, Y. Wang, Y. Gong, H. Yin, Z. Mo, Y. Tang, and L. Chi, "Optical band gap and photoluminescence in heavily Tb^{3+} doped GeO_2-B_2O_3-SiO_2-Ga_2O_3 magneto-optical glasses," J. Alloys Compd. **686**, 635–640 (2016).
160. R. El-Mallawany, M. D. Abdalla, and I. A. Ahmed, "New tellurite glass: Optical properties," Mater. Chem. Phys. **109**(2–3), 291–296 (2008).
161. V. Dimitrov and S. Sakka, "Electronic oxide polarizability and optical basicity of simple oxides. I," J. Appl. Phys. **79**(3), 1736–1740 (1996).
162. F. Mohd Fudzi, H. M. Kamari, A. Abd Latif, and A. Muhammad Noorazlan, "Linear Optical Properties of Zinc Borotellurite Glass Doped with Lanthanum Oxide Nanoparticles for Optoelectronic and Photonic Application," J. Nanomater. **2017**, (2017).
163. N. S. Hussain, Y. P. Reddy, and S. Buddhudu, "Emission properties of Tb^{3+} -doped zinc boro-silicate glasses," (April), 303–308 (2001).
164. C. H. Kam and S. Buddhudu, "Photoluminescence properties of Eu^{3+}:ZrF_4–BaF_2–LaF_3–YF_3–AlF_3–NaF glasses," Phys. B Condens. Matter **344**, 182–189 (2004).
165. S. Kaur, A. S. Rao, M. Jayasimhadri, V. V. Jaiswal, and D. Haranath, "Tb^{3+} ion induced colour tunability in calcium aluminozincate phosphor for lighting and display devices," J. Alloys Compd. **826**, 154212 (2020).
166. M. Back, A. Massari, M. Boffelli, F. Gonella, P. Riello, D. Cristofori, R. Riccò, and F. Enrichi, "Optical investigation of Tb^{3+}-doped Y_2O_3 nanocrystals prepared by Pechini-type sol-gel process," J. Nanoparticle Res. **14**(4), (2012).
167. M. Jayasimhadri, K. Jha, B. V. Ratnam, H. J. Woo, K. Jang, A. S. Rao, and D. Haranath, "Single NUV band pumped PbO-GeO_2-TeO_2:Tb^{3+} yellowish green emitting glass material for tricolor white LEDs," J. Alloys Compd. **711**, 395–399 (2017).
168. X. Li, B. Chen, R. Shen, H. Zhong, L. Cheng, J. Sun, J. Zhang, H. Zhong, Y. Tian, and G. Du, "Fluorescence quenching of ^5D_J (J = 1, 2 and 3) levels and Judd-Ofelt analysis

of Eu^{3+} in $NaGdTiO_4$ phosphors," J. Phys. D. Appl. Phys. **44**(33), 2–8 (2011).

169. T. Yamashita and Y. Ohishi, "Concentration and temperature effects on the spectroscopic properties of Tb^{3+} doped borosilicate glasses," J. Appl. Phys. **102**(12), (2007).
170. F. HU, Z. ZHAO, F. CHI, X. WEI, and M. YIN, "Structural characterization and temperature-dependent luminescence of CaF_2:Tb^{3+}/Eu^{3+} glass ceramics," J. Rare Earths **35**(6), 536–541 (2017).
171. N. Deopa, M. K. Sahu, S. Kaur, A. Prasad, K. Swapna, V. Kumar, R. Punia, and A. S. Rao, "Enhanced visible green and 1.5 μm radiative emission of Er^{3+} ions in Li_2O-PbO-Al_2O_3-B_2O_3 glasses for photonic applications," J. Rare Earths **39**(5), 520–525 (2021).
172. M. K. Sahu and M. Jayasimhadri, "Conversion of blue emitting thermally stable $Ca_3Bi(PO_4)_3$ host as a color tunable phosphor via energy transfer for luminescent devices," J. Lumin. **227**(June), 117570 (2020).
173. Z. Wu, H. Wu, L. Tang, Y. Li, D. Xiaochun, and Y. Guo, "Fluorescence and energy transfer between Eu^{3+} and Sm^{3+} in single doped and co-doped borate glass," J. Non. Cryst. Solids **463**, 169–174 (2017).
174. S. B. Mallur, T. C. Khoo, S. Rijal, O. R. Huff, and P. K. Babu, "Peak stimulated emission cross sections and quantum efficiencies of Sm^{3+} and Sm^{3+}-Eu^{3+} co-doped bismuth boro-tellurite glasses," Mater. Chem. Phys. **258**(September 2020), 123886 (2021).
175. A. N. Meza-Rocha, A. Speghini, M. Bettinelli, and U. Caldiño, "Orange and reddish-orange light emitting phosphors: Sm^{3+} and Sm^{3+}/Eu^{3+} doped zinc phosphate glasses," J. Lumin. **167**, 305–309 (2015).
176. M. E. Alvarez-Ramos, R. C. Carrillo-Torres, R. Sánchez-Zeferino, U. Caldiño, and J. Alvarado-Rivera, "Co-emission and energy transfer of Sm^{3+} and/or Eu^{3+} activated zinc-germanate- tellurite glass as a potential tunable orange to reddish-orange phosphor," J. Non. Cryst. Solids **521**(June), 119462 (2019).
177. K. Jha and M. Jayasimhadri, "Effective sensitization of Eu^{3+} and energy transfer in Sm^{3+}/Eu^{3+} co-doped ZPBT glasses for CuPc based solar cell and w-LED applications," J. Lumin. **194**(July 2017), 102–107 (2018).
178. E. F. Huerta, O. Soriano-Romero, A. N. Meza-Rocha, S. Bordignon, A. Speghini, and U. Caldiño, "Lithium-aluminum-zinc phosphate glasses activated with Sm3+, Sm^{3+}/Eu^{3+} and Sm^{3+}/Tb^{3+} for reddish-orange and white light generation," J. Alloys Compd. **846**, (2020).

179. S. Nakamura, "Blue-green light-emitting diodes and violet laser diodes," MRS Bull. **22**(2), 29–35 (1997).
180. R. Wei, H. Zhang, F. Li, and H. Guo, "Blue-white-green tunable luminescence of Ce^{3+}, Tb^{3+} Co-doped sodium silicate glasses for white LEDs," J. Am. Ceram. Soc. **95**(1), 34–36 (2012).
181. D. R. N. Brito, M. N. Queiroz, M. J. Barboza, A. Steimacher, and F. Pedrochi, "Investigation of optical and spectroscopic properties of Sm^{3+} ions in CaBAl glasses," Opt. Mater. (Amst). **64**, 114–120 (2017).
182. M. A. K. Elfayoumi, M. Farouk, M. G. Brik, and M. M. Elokr, "Spectroscopic studies of Sm^{3+} and Eu^{3+} co-doped lithium borate glass," J. Alloys Compd. **492**(1–2), 712–716 (2010).
183. H. Y. Lin, Y. C. Fang, and S. Y. Chu, "Energy transfer $Sm^{3+}\rightarrow Eu^{3+}$ in potential red phosphor (Ca, Ba)$_3$(VO$_4$)$_2$:Sm^{3+}, Eu^{3+} for use in organic solar cells and white light-emitting diodes," J. Am. Ceram. Soc. **93**(11), 3850–3856 (2010).
184. M. A. K. El-Fayoumi and M. Farouk, "Structural properties of Li-borate glasses doped with Sm^{3+} and Eu^{3+} ions," J. Alloys Compd. **482**(1–2), 356–360 (2009).
185. H. Van Tuyen, M. Nogami, and L. X. Hung, "Reduction of Sm^{3+} and Eu^{3+} ions-co-doped Al_2O_3–SiO_2 glasses and photoluminescence properties," Opt. Mater. (Amst). **100**(November 2019), 109639 (2020).
186. R. Bajaj, A. S. Rao, and G. V. Prakash, "Linear and nonlinear photoluminescence from thermally stable KYF_4:Eu^{3+} cubic nanocrystals," J. Alloys Compd. **885**, 160893 (2021).
187. V. Naresh, B. H. Rudramadevi, and S. Buddhudu, "Crossrelaxations and non-radiative energy transfer from ($^4G_{5/2}$) Sm^{3+} → ($^5D^0$) Eu^{3+}: B_2O_3-ZnO glasses," J. Alloys Compd. **632**, 59–67 (2015).
188. S. Stojadinović and R. Vasilić, "Orange–red photoluminescence of Nb_2O_5:Eu^{3+}, Sm^{3+}coatings formed by plasma electrolytic oxidation of niobium," J. Alloys Compd. **685**, 881–889 (2016).
189. X. Min, Z. Huang, M. Fang, Y. Liu, C. Tang, and X. Wu, "Energy Transfer from Sm^{3+} to Eu^{3+} in Red-Emitting Phosphor $LaMgAl_{11}O_{19}$: Sm^{3+} , Eu^{3+} for Solar Cells and Near-Ultraviolet White Light-Emitting Diodes," Inorg. Chem. **53(12)**, 6060–6065 (2014).
190. J. Zheng, X. Wu, Q. Ren, W. Bai, Y. Ren, M. Wang, and O. Hai, "Investigation of luminescence properties and energy transfer in Sm^{3+} and Eu^{3+} co-doped $Sr_3Y(BO_3)_3$ red phosphors," Opt. Laser Technol. **122**(September 2019), 105857 (2020).

191. Y. R. Do and Y. D. Huh, "Optical Properties of Potassium Europium Tungstate Phosphors," J. Electrochem. Soc. **147**(11), 4385 (2000).

192. H. Guo, Q. Shi, K. V. Ivanovskikh, L. Wang, C. Cui, and P. Huang, "A high color purity red-emission phosphor based on Sm^{3+} and Eu^{3+} co-doped $Ba_3Bi(PO_4)_3$," Mater. Res. Bull. **126**(February), 110836 (2020).

193. M. Tian, P. Li, Z. Wang, X. Teng, Z. Li, J. Cheng, Y. Sun, C. Wang, and Z. Yang, "Synthesis, color-tunable emission, thermal stability, luminescence and energy transfer of Sm^{3+} and Eu^{3+} single-doped $M_3Tb(BO_3)_3$ (M = Sr and Ba) phosphors," CrystEngComm **18**(36), 6934–6947 (2016).

194. J. Rajagukguk, Fitrilawati, B. Sinaga, and J. Kaewkhao, "Structural and spectroscopic properties of Er^{3+} doped sodium lithium borate glasses," Spectrochim. Acta - Part A Mol. Biomol. Spectrosc. **223**, 117342 (2019).

195. V. B. Sreedhar, N. Vijaya, D. Ramachari, and C. K. Jayasankar, "Luminescence studies on Er^{3+} -doped zincfluorophosphate glasses for 1.53 μm laser applications," J. Mol. Struct. **1130**, 1001–1008 (2017).

196. G. R. Dillip, C. Madhukar Reddy, M. Rajesh, S. Chaurasia, B. Deva Prasad Raju, and S. W. Joo, "Green fluorescence of terbium ions in lithium fluoroborate glasses for fibre lasers and display devices," Bull. Mater. Sci. **39**(3), 711–717 (2016).

197. K. Swapna, S. Mahamuda, M. Venkateswarlu, A. Srinivasa Rao, M. Jayasimhadri, S. Shakya, and G. V. Prakash, "Visible, Up-conversion and NIR (∼1.5 μm) luminescence studies of Er^{3+} doped Zinc Alumino Bismuth Borate glasses," J. Lumin. **163**, 55–63 (2015).

198. I. V. Kityk, V. V. Halyan, V. O. Yukhymchuk, V. V. Strelchuk, I. A. Ivashchenko, Y. Zhydachevskyy, A. Suchocki, I. D. Olekseyuk, A. H. Kevshyn, and M. Piasecki, "NIR and visible luminescence features of erbium doped Ga_2S_3–La_2S_3 glasses," J. Non. Cryst. Solids **498**(December 2017), 380–385 (2018).

199. K. J. B.C. Jamalaiah, T. Suhasini, L. Rama Moorthy, K. Janardhan Reddy, Il-Gon Kim, Dong-Sun Yoo, "Visible and near infrared luminescence properties of Er^{3+}-doped LBTAF glasses for optical amplifier," Opt. Mater. (Amst). **34**, 861–867 (2012).

200. B. V. Padlyak, R. Lisiecki, and W. Ryba-Romanowski, "Spectroscopy of the Er-doped lithium tetraborate glasses," Opt. Mater. (Amst). **54**, 126–133 (2016).

201. Y. Anantha Lakshmi, K. Swapna, K. Siva Rama Krishna Reddy, M. Venkateswarlu, S. Mahamuda, and A. S. Rao, "Structural, optical and NIR studies of Er^{3+} ions doped

bismuth boro tellurite glasses for luminescence materials applications," J. Lumin. **211**(December 2018), 39–47 (2019).

202. F. Ahmadi, R. Hussin, and S. K. Ghoshal, "Spectral characteristics of Er^{3+} doped magnesium zinc sulfophosphate glasses," J. Alloys Compd. **711**, 94–102 (2017).
203. S. F. Li, Q. Y. Zhang, and Y. P. Lee, "Absorption and photoluminescence properties of Er-doped and Er/Yb codoped soda-silicate laser glasses," J. Appl. Phys. **96**(9), 4746–4750 (2004).
204. S. P. SINHA, "Complexes of the Rare Earths," Complexes Rare Earths 17–23 (1966).
205. R. Bajaj, A. Prasad, A. V. S. Yeswanth, P. Rohilla, S. Kaur, and A. S. Rao, "Down-shifting photoluminescence studies of thermally stable Dy^{3+} ions doped borosilicate glasses for optoelectronic device applications," J. Mater. Sci. Mater. Electron. (2022).
206. K. Mariselvam, R. Arun Kumar, and V. Rajeswara Rao, "Concentration-dependence and luminescence studies of erbium doped barium lithium fluoroborate glasses," Opt. Laser Technol. **118**(May 2018), 37–43 (2019).
207. S. A. Umar, M. K. Halimah, K. T. Chan, and A. A. Latif, "Physical, structural and optical properties of erbium doped rice husk silicate borotellurite (Er-doped RHSBT) glasses," J. Non. Cryst. Solids **472**(July), 31–38 (2017).
208. S. Mahamuda, K. Swapna, P. Packiyaraj, A. Srinivasa Rao, and G. Vijaya Prakash, "Lasing potentialities and white light generation capabilities of Dy^{3+} doped oxy-fluoroborate glasses," J. Lumin. **153**, 382–392 (2014).
209. K. Maheshvaran, S. Arunkumar, V. Sudarsan, V. Natarajan, and K. Marimuthu, "Structural and luminescence studies on Er^{3+}/Yb^{3+} co-doped boro-tellurite glasses," J. Alloys Compd. **561**, 142–150 (2013).
210. T. Xue, C. Huang, L. Wang, Y. Li, Y. Liu, D. Wu, M. Liao, and L. Hu, "Er^{3+}-doped fluorozirconate glass modified by PbF_2 with high stimulated emission cross-section," Opt. Mater. (Amst). **77**, 117–121 (2018).
211. C. Nageswara Raju, C. Adinarayana Reddy, S. Sailaja, H. J. Seo, and B. Sudhakar Reddy, "Spectroscopic investigations of Er^{3+}:CdO-Bi_2O_3-B_2O_3 glasses," Luminescence **27**(5), 334–340 (2012).
212. S. Hraiech, C. Bouzidi, and M. Férid, "Luminescence properties of Er^{3+}-doped phosphate glasses," Phys. B Condens. Matter **522**, 15–21 (2017).
213. G. Devarajulu, O. Ravi, C. M. Reddy, S. Z. Ali Ahamed, and B. D. P. Raju, "Spectroscopic properties and upconversion studies of Er^{3+}-doped SiO2-Al2O3-

Na_2CO_3-SrF_2-CaF_2 oxyfluoride glasses for optical amplifier applications," J. Lumin. **194**, 499–506 (2018).

214. A. D. Sontakke, K. Biswas, A. Tarafder, R. Sen, and K. Annapurna, "Broadband Er^{3+} emission in highly nonlinear Bismuth modified Zinc-Borate glasses," Opt. Mater. Express **1**(3), 344 (2011).

Optical Materials 109 (2020) 110356

Contents lists available at ScienceDirect

Optical Materials

journal homepage: http://www.elsevier.com/locate/optmat

Concentration-dependent reddish-orange photoluminescence studies of Sm^{3+} ions in borosilicate glasses

Mohit Kumar, A.S. Rao *

Department of Applied Physics, Delhi Technological University, Bawana Road, New Delhi, 110 042, India

ARTICLE INFO

Keywords:
Luminescence
Borosilicate glasses
Radiative properties
Emission cross-sections
Quantum efficiency

ABSTRACT

This paper elucidates the concentration-dependent photoluminescence properties of samarium ions in Lithium bismuth alumino borosilicate (LiBiAlBSi) glasses using XRD, FT-IR, absorption, excitation, emission & decay to quantify the luminescence properties of the titled glasses. XRD and FT-IR spectral data ascertain the non-crystalline nature and vibrational energies in host glass respectively. The intense excitation band observed at 400 nm in near UV region (under $\lambda_{em} = 600$ nm) is employed to read the emission spectra. Under 400 nm intense excitation wavelength, the titled glasses show intense visible reddish-orange emission at 600 nm. From the emission spectra, it is observed that 0.5 mol% of Sm^{3+} ions concentration in LiBiAlBSi glass is optimum for reddish-orange emission. The CIE coordinates estimated for LiBiAlBSi glasses are in good proximity with the reddish-orange emission coordinates specified by Nichia Corporation. Branching ratios, emission cross-sections, quantum efficiency, and CIE coordinates estimated finally reveals the aptness of the LiBiAlBSi glasses for reddish-orange optoelectronic device applications.

1. Introduction

The steady growth in the field of luminescence exhibited by rare earths (RE)/transition metal (TM) activated materials fascinated the scientists because of their remarkable applications in up & down-converting lasers and photonics devices. The transitions produced within the electronic states of these ions in host matrix play a substantial role in the aforementioned applications [1–8]. Especially RE doped glasses are having certain interesting features like broad inhomogeneous bandwidths, the capacity to accept high concentration of RE ions, low production cost, good thermal stability and easy manufacturing process [1–6]. Glass lasers have high fluorescence lifetimes, high gain and can be easily made into the required shape. A host matrix with relatively low phonon energy can give high quantum efficiency by reducing the non-radiative relaxation process. Materials with low phonon energies are very much needed to design optical fiber amplifiers and lasers [7,9,10]. Borates and silicates are the two well-known glass formers with scientific merits such as low melting point, high degree of transparency, good RE ions solubility, high thermal stability, high field strength, less cation size, and high chemical durability. A combination of B_2O_3 and SiO_2 produces a significant glass network known as borosilicate glasses which have a lower thermal expansion coefficient, less melting temperatures, high softening temperature, good mechanical strength, high thermal stability, and highly resistant to corrosion. Such characteristic features of borosilicate glasses may be helpful for many industrial applications like photovoltaic cells, displays, MEMs, etc. Borosilicate glasses possess relatively high phonon energy and cannot reduce non-radiative decay losses [11–15]. Nevertheless, such redundant and unwanted high phonon energies existing in borosilicate glasses can be curbed effectively by supplementing them suitably with heavy metal oxides (HMOs) such as bismuth oxide (Bi_2O_3) and lead oxide (PbO). High density & atomic numbers of HMOs added to a glass helps them to act robustly in providing shielding to the radioactive radiations. Low concentration of PbO amends the network of borosilicate glasses due to lead structural unit [PbO_4]. Further increase in PbO content, makes it to partially play the role of a glass former. This dual role of lead can also enhance radiative emission properties of the host glass. But at the same time, use of lead creates several issues due to hazardous effects on the environment and health. Bi_2O_3 plays a similar kind of role in glasses hosts as PbO due to their identical electronic properties without hazardous effects. Glasses containing bismuth have higher infrared transparency, large index of refraction, large dielectric constant, and high density. As Bi^{3+} ions are prone to give low field strengths, stand-alone, Bi_2O_3 can't portrait the role of network former. However, in

* Corresponding author.
E-mail addresses: drsrallam@gmail.com, drsrallam@gmail.com (A.S. Rao).

https://doi.org/10.1016/j.optmat.2020.110356
Received 19 June 2020; Received in revised form 15 August 2020; Accepted 19 August 2020
Available online 13 September 2020

Optical Materials 120 (2021) 111439

Contents lists available at ScienceDirect

Optical Materials

journal homepage: www.elsevier.com/locate/optmat

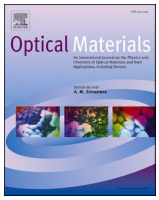

Research Article

Influence of Tb^{3+} ions concentration and temperature on lithium bismuth alumino borosilicate glasses for green photonic device applications

Mohit Kumar, A.S. Rao *

Department of Applied Physics, Delhi Technological University, Bawana Road, New Delhi, 110 042, India

ARTICLE INFO

Keywords:
Photoluminescence
Glasses
Terbium ions
Emission cross sections
CIE coordinates

ABSTRACT

Lithium bismuth alumino borosilicate (LiBiAlBSi) glasses doped with various concentrations of trivalent terbium (Tb^{3+}) ions were prepared to explore their physical, optical, and photoluminescence (PL) characteristics features. Diffraction pattern recorded for an undoped as well as doped (1.5 mol% of Tb^{3+}) LiBiAlBSi glass ascertained the amorphous nature. Absorption spectra reveal several peaks in n-UV and blue regions. The indirect optical band gap for Tb^{3+} doped LiBiAlBSi glasses was found in the 3.16-3.46 eV range. PL measurements such as emission (under 378 nm excitation) and excitation (under 542 nm emission) were recorded to study the usage of the as-prepared glasses for green photonic device applications. PL emission spectra reveal four emission bands of Tb^{3+} ions originating from the excited level of $^5D_4$ to $^7F_{J\ (=3,4,5,6)}$ levels. The intensity of the emission peak observed in the green region at 542 nm ($^5D_4 \rightarrow {}^7F_5$) escalates up to 1.5 mol% of Tb^{3+} ion concentration and declines beyond due to concentration quenching. Dexter theory applied to the PL emission spectral features reveals dipole-dipole interaction among Tb^{3+} ions responsible for the transfer of energy and thereby concentration quenching. The CIE coordinates and CCT values calculated for the as-prepared glasses are closure to the values of intense green emission given by the European Broadcasting Union illuminant. The experimental lifetime values (τ_{exp}) measured for the intense green emission ($^5D_4 \rightarrow {}^7F_5$) are reducing with the upsurge in the content of Tb^{3+} ions in the titled glasses. Correlation of τ_{exp} values with the PL emission spectral data facilitate the estimation of radiative properties. Relatively high activation energy value estimated from the temperature-dependent PL show the thermal stability of the optimized glass. The PL (excitation, emission, decay, temperature-dependent) studies along with colorimetric studies confirm the aptness of the LBiAlBSiTb15 glass for photonic applications such as laser and tricolour w-LEDs as a green emitting component.

1. Introduction

In recent years, the scientific community has made a great effort in exploring the spectral behaviour of rare-earth (RE) ions doped glasses for various photonic device applications. The unique spectroscopic features such as narrow emission bands, possessing many fluorescing states, relatively longer lifetimes, and a large number of excited states for optical pumping of RE ions prompted the scientists to explore the applications of RE doped materials in solid-state lasers, light-emitting diodes (LEDs), flat-panel displays, optical amplifiers, solar cells, and optical fibre amplifiers [1–4]. For the fabrication of advanced optical devices, the knowledge of the optical characteristics of RE ions activated materials such as transition positions, transition probabilities, quantum efficiency, branching ratios, non-radiative and radiative decay rates are required [4,5]. The outcome of the visible emission transitions of RE ions noticed within their 4f shells. These transitions were unresponsive to the surrounding environment owing to the shielding outcome of outer electrons of 5s and 5p orbitals. Due to the special property, RE ions doped glasses have been preferred as significant luminescent materials and found to be employed for the aforesaid applications. The RE ions activated luminescent glass materials possess several remarkable characteristics such as relatively easy fabrication with low cost, longer lifetime, environmental friendliness and higher reliability [1,5–10]. Nowadays, LEDs are replacing conventional light sources in the lighting industry. The RE ions doped glasses are the most appropriate candidates for w-LEDs fabrication because of the prime reason of non-usage of epoxy resin while constructing an LED. This automatically results in no aging effects and subsequently longer life span when compared with LEDs prepared by using crystalline phosphors in which epoxy is must [11,12]. In addition to the above, an inhomogeneous broadening of

* Corresponding author.
E-mail address: drsrallam@gmail.com (A.S. Rao).

https://doi.org/10.1016/j.optmat.2021.111439
Received 10 June 2021; Received in revised form 19 July 2021; Accepted 30 July 2021
Available online 7 August 2021

Chemical Physics Letters 788 (2022) 139303

Contents lists available at ScienceDirect

Chemical Physics Letters

journal homepage: www.elsevier.com/locate/cplett

Downshifting analysis of Sm^{3+}/Eu^{3+} co-doped LiBiAlBSi glasses for red emission element of white LEDs

Mohit Kumar, A.S. Rao *, Sumandeep Kaur

Department of Applied Physics, Delhi Technological University, Bawana Road, New Delhi 110 042, India

ARTICLE INFO

Keywords:
Photoluminescence
Energy transfer
Lifetime
Optical glasses
Thermal stability
White LED
PV cells

ABSTRACT

The Sm^{3+}, Eu^{3+} single doped, and Sm^{3+}/Eu^{3+} co-doped lithium bismuth alumino borosilicate (LiBiAlBSi) glasses were prepared by using the melt quenching method and studied photoluminescence (PL) excitation, PL emission, and PL decay to have a better insight into their utility as red emission element for white LEDs. Sm^{3+} doped LiBiAlBSiSm05 glasses exhibit admirable emission features in the reddish-orange region under n-UV excitation (402 nm). Sm^{3+}/Eu^{3+} co-doped LiBiAlBSi glasses can be adeptly excited by the blue and n-UV region which is confirmed from the excitation spectrum. In the Sm^{3+}/Eu^{3+} co-doped LiBiAlBSi glasses, the PL decay lifetime for the Sm^{3+} emitting level ($^4G_{5/2}$) declines and the energy transfer efficiency increases with an upsurge in Eu^{3+} ion content, which suggests the energy transfer (ET) process occurs from Sm^{3+} to Eu^{3+} ions. The ET process from Sm^{3+} to Eu^{3+} ions is also suggested by Dexter's ET method and Reisfeld's approximation by using emission spectra due to non-radiative dipole-dipole (d-d) interaction. The calculated values of CIE chromaticity coordinate for the as-prepared glasses under n-UV excitation shifted from reddish-orange to the red spectral part with the upsurge in Eu^{3+} concentration. The temperature-dependent PL studies of the optimized LiBiAlBSiSE10 glass revealed its superior thermal stability. All the results obtained finally suggest that, the Sm^{3+}/Eu^{3+} co-doped LiBiAlBSi glass with 0.5 mol% of Sm^{3+} ions and 1.0 mol% of Eu^{3+} ions is a thermally stable candidate to produce intense red color needed to fabricate white LEDs under n-UV and blue excitation through the downshifting process.

1. Introduction

Over the years, the assimilation of rare earth (RE) ions into glass systems have revolutionary changes in diverse fields such as solid-state lighting (SSL), waveguides, optical fiber, flat-panel display, optical converters, solid-state lasers, optical information processing, and photovoltaic (PV) cells [1-4]. In the field of SSL, white light-emitting diodes (LEDs) show recognized remarkable attention as compared to conventional sources of light and their several uses are flat-panel display, cellular phone illumination, automotive displays, and traffic signals, etc. White LEDs have numerous prominent characteristics such as long-serving lifetime, high luminous efficiency, small size, energy conservation, high brightness, fast switching, and being environment friendly. Despite these advantages, white LEDs have some weaknesses in practical applications, such as high color temperature because of the deficiency in red emission characteristics [1,5,6]. Presently, two diverse approaches have been purposeful to acquire white light using LED chips. The first method is a combination of separate red, green and blue releasing LED sources to attain white light and is called the RGB method. In the second method, for the fabrication of white LEDs, single(yellow)/multiple (RGB) phosphor materials are used with n-UV/blue sources of excitation [7,8]. The first commercial technique to fabricate the phosphor-converted white LEDs uses the yellow emitting phosphor which is basically cerium doped yttrium aluminium garnet (YAG: Ce^{3+}) with a blue LED chip. This method has numerous drawbacks like poor color rendering index, thermal quenching, and halo effect because of the separation of yellow-blue color. For better white light attainment with an improved color rendering index, a combination of RGB phosphors and an excitation source (n-UV LED chip) is required. Nonetheless, in this method, red phosphor shows very weak efficiency as compared to blue and green phosphors [2,9,10]. In both methods, phosphor is used in the form of powder and encapsulated in an epoxy resin. This epoxy resin gets deteriorated at high energy light sources of excitations, high power, and high temperatures which affects the luminous efficacy of phosphor. Therefore, RE ions doped glasses are preferred over phosphor because they satisfy both purposes of the wavelength converter and epoxy resin-

* Corresponding author.
E-mail address: drsrallam@gmail.com (A.S. Rao).

https://doi.org/10.1016/j.cplett.2021.139303
Received 6 October 2021; Received in revised form 8 December 2021; Accepted 20 December 2021
Available online 24 December 2021